



ΕΘΝΙΚΟ ΚΑΙ ΚΑΠΟΔΙΣΤΡΙΑΚΟ ΠΑΝΕΠΙΣΤΗΜΙΟ ΑΘΗΝΩΝ

ΣΧΟΛΗ ΘΕΤΙΚΩΝ ΕΠΙΣΤΗΜΩΝ

ΤΜΗΜΑ ΓΕΩΛΟΓΙΑΣ ΚΑΙ ΓΕΩΠΡΙΒΑΛΛΟΝΤΟΣ

ΤΟΜΕΑΣ ΙΣΤΟΡΙΚΗΣ ΓΕΩΛΟΓΙΑΣ - ΠΑΛΑΙΟΝΤΟΛΟΓΙΑΣ

**Multiproxy paleoenvironmental and paleoclimatic analysis in biota-rich
sediments of North and South Aegean Sea during the last 21 ka**

Χριστίνα Γιαμαλή

A.M.: 173

ΔΙΔΑΚΤΟΡΙΚΗ ΔΙΑΤΡΙΒΗ

ΑΘΗΝΑ 2021



NATIONAL AND KAPODISTRIAN UNIVERSITY OF ATHENS
SCHOOL OF SCIENCES
DEPARTMENT OF GEOLOGY AND GEOENVIRONMENT
SECTION OF HISTORICAL GEOLOGY – PALAEOLOGY

**Multiproxy paleoenvironmental and paleoclimatic analysis in biota-rich
sediments of North and South Aegean Sea during the last 21 ka**

Christina Giamali

PhD thesis

Athens 2021

Τριμελής συμβουλευτική επιτροπή

Καθηγήτρια Ε. Κοσκερίδου
(Επιβλέπουσα), ΕΚΠΑ

Ομότιμος Καθηγητής Β. Καρακίτσιος,
ΕΚΠΑ

Καθηγήτρια Α. Αντωνάρακου, ΕΚΠΑ

Επταμελής εξεταστική επιτροπή –

Καθηγήτρια Ε. Κοσκερίδου
(Επιβλέπουσα), ΕΚΠΑ

Καθηγήτρια Α. Αντωνάρακου, ΕΚΠΑ

Ομότιμος Καθηγητής Β. Καρακίτσιος,
ΕΚΠΑ

Καθηγητής Γ. Αναστασάκης ΕΚΠΑ

Καθηγήτρια Χ. Ντρίνια ΕΚΠΑ

Διευθυντής Ερευνών. Α.Π.
Καραγεώργης ΕΛΚΕΘΕ

Διευθυντής Ερευνών Γ. Ρουσάκης
ΕΛΚΕΘΕ

Advisory Committee

Prof. E. Koskeridou (Head of the
Advisory Committee), NKUA

Prof. Emer. V. Karakitsios, NKUA

Prof. A. Antonarakou, NKUA

Assessment Committee

Prof. E. Koskeridou, NKUA

Prof. Emer. V. Karakitsios, NKUA

Prof. A. Antonarakou, NKUA

Prof. G. Anastasakis, NKUA

Prof. C. Drinia, NKUA

Research Director A.P. Karageorgis,
HCMR

Research Director G. Rousakis,
HCMR

I declare that I am the owner of the copyrights of this work and as far as I am concerned this dissertation does not insult other persons or infringes the copyright of third parties.

Part of this work was done at the Hellenic Survey of Geology and Mineral Exploration (H.S.G.M.E.) in the frame of YPOTHER project, and at the National and Kapodistrian University of Athens.

Any part of this thesis has not been submitted in any previous application for a higher degree or any other qualification at this University or any other institution.

All figures are by the author unless otherwise stated.

The approval of this doctoral thesis by the department of Geology and Geoenvironments of the National and Kapodistrian University of Athens does not imply acceptance of the author's opinions (N.5343/1932, Άρθρο 202 παρ.2).

*This work is dedicated to all those who take
the long journey in achieving their goals.*

Acknowledgements

I would like to thank my supervisor Prof. Efterpi Koskeridou for her endless support and her believing in me and my choices. The same stands for Prof. Assimina Antonarakou, who supported me and guided me into a new world for me at that moment, the world of planktonic foraminifera. The encouragement and patience that I received from both of them helped me in accomplishing my goal. Furthermore, the same encouragement and support I received from Prof. Vasileios Karakitsios, who is also cordially thanked. In addition, I would like to thank the rest of the seven-member assessment committee Prof. George Anastasakis, Prof. Chara Drinia, Dr. Aristomenis P. Karageorgis and Dr. Grigoris Rousakis for their advices and constructive comments.

This thesis became real, after my collaboration with the Hellenic Survey of Geology and Mineral Exploration (H.S.G.M.E.) in the frame of YPOTHER project whose scientific responsible was Dr. Chryssanthi Ioakeim. Her encouragement and support in accomplishing this thesis were essential. I would like also to thank the department of General Geology & General Cartography of H.S.G.M.E. who allowed me to use the material I examined during the YPOTHER project, for my thesis. Special thanks go to the Hellenic Center of Marine Research (HCMR) who collaborated in the frame of YPOTHER project, the captain and crew of R/V Aegaeo (HCMR) for their technical assistance during the YPOTHER cruises, and Mrs. A. Androni (HCMR) for the organic carbon analysis for the cores of the North Aegean Sea.

I would also like to heartfully thank Dr. George Kontakiotis. His endless support and constructive discussion and comments made this research possible. In addition, professors and colleagues (Prof. G. Theodorou, D. Thivaïou, V. Mitsopoulou, M. Dagla, Dr. K. Agiadi, Dr. S. Zarkogiannis) from the Section of Historical Geology and Palaeontology are thanked for the constructive discussions and support during all these years. Stelios Petrakis from the Section of Physical Geography & Oceanography is thanked for providing the data for the production of maps constructed in GIS. Dr. Panagiotis Karkanis and Dr. Dimitris Michailidis from the Wiener Laboratory of the American School of Classic Studies (ASCSA; Athens)

are cordially thanked for the assistance that they provided with the Scanning Electron Microscope.

Moreover, I would like to thank my colleagues from the Goulandris Natural History Museum, and especially Dr. E. Vardala – Theodorou. Without their support and flexibility this thesis would have been difficult to be completed. In this part, I should point out, that quarantine during COVID-19 pandemic allowed me to finish the research.

Last but not least, I would like to thank my family and my friends (Dimitris G., Varvara G., Vassiliki G., Maria G., Mimika G., Maria M., Margarita D., Votsalakis, Vassilis N., and my team Φυσalis) that were by my side during all these years supporting me in any way possible and understanding me.

Abstract

Aspects of paleoclimatic and paleoceanographic evolution of the north Aegean Sea through the late Quaternary are revealed by the study of quantitative variations in planktonic foraminiferal, and pteropodal assemblages (including multivariate statistical approach; principal component analysis (PCA)), the isotopic composition of planktonic foraminifera ($\delta^{18}\text{O}$ and $\delta^{13}\text{C}$); and hydrographic-related indices (planktonic paleoclimatic curve (PPC), productivity (E-index), stratification (S-index), upwelling (U-index), seasonality), extracted from three high-sedimentation rate cores from the North and South Aegean Sea (North Aegean Trough and the submarine area between Kimolos and Sifnos islands). Based on the statistical analysis, besides sea surface temperature (SST), which shows the highest explanatory power for the distribution of the analyzed fauna, primary productivity, water column stratification, and seasonality also control the planktonic foraminifera and pteropod communities during the late Quaternary. Pteropod fauna during the Holocene and especially the sapropel deposition were recorded for the first time in the Aegean Sea.

Focusing on last ~21 calibrated thousands of years before present (ka BP), cold and eutrophicated conditions were identified during the Late Glacial period (21.1–15.7 ka BP) and were followed by warmer and wetter conditions during the deglaciation phase. The beginning of the Holocene was marked by a climatic amelioration and increased seasonality. The more pronounced environmental changes were identified during the deposition of the sapropel layer/sublayers, with extremely warm and stratified conditions S1a (9.4–7.7 ka BP) and S1b (6.9–6.4 ka BP) in the south Aegean Sea and warm and humid phase at the north Aegean Sea (9.6–6.1 ka BP).

The Holocene climatic instability of the study area is further supported by six episodes of brief cooling in the North Aegean (NAEGC6–NAEGC1) centered at 9.30, 8.05, 7.05, 4.55, 3.55, and 2.05 ka BP, and two in the south Aegean Sea (SAEGC2–SAEGC2) centered at 7.35 and 5.35 ka BP, reflected by significant faunal changes and oxygen isotope enrichments. These cold/arid events are coeval with equivalent cooling events that have been described in different basins of the Mediterranean Sea, while signal similarities with equivalent changes in the intensity of the Siberian high suggest a climatic link between the studied area and the high-latitude areas.

Περίληψη

Στην παρούσα διδακτορική διατριβή μελετήθηκαν οι πανίδες των πλαγκτονικών τρηματοφόρων και πτεροπόδων σε ιζήματα του Ανώτερου Τεταρτογενούς από τρεις πυρήνες βαρύτητας του Αιγαίου Πελάγους, με στόχο την παλαιοπεριβαλλοντική και παλαιοκλιματική ανασύνθεση. Συγκεκριμένα επιλέχθηκαν προς μελέτη δύο πυρήνες από την Τάφρο του Βορείου Αιγαίου και ένας από την υποθαλάσσια περιοχή μεταξύ των νήσων Κιμώλου και Σίφνου. Οι περιοχές αυτές επιλέχθηκαν καθώς παρουσιάζουν υψηλούς ρυθμούς ιζηματογένεσης και ιδιαίτερες φυσιογεωγραφικές και υδρολογικές συνθήκες, καθιστώντας δυνατή την μελέτη των παλαιοκλιματικών διακυμάνσεων.

Για την επίτευξη της διατριβής έγιναν μικροπαλαιοντολογικές αναλύσεις των συναθροίσεων των πλαγκτονικών τρηματοφόρων και πτεροπόδων που συλλέχθηκαν από τους πυρήνες. Για πρώτη φορά έγινε καταγραφή των κάτω Πλειστοκαινικών και Ολοκαινικών συναθροίσεων των πτεροπόδων για το Αιγαίο Πέλαγος. Επιπλέον έγιναν ισοτοπικές αναλύσεις σε κελύφη των πλαγκτονικών τρηματοφόρων τόσο για την χρονολόγηση των πυρήνων (^{14}C) όσο και για την παροχή πληροφοριών για τις κλιματικές μεταβολές ($\delta^{18}\text{O}$ & $\delta^{13}\text{C}$). Στη συνέχεια έγινε στατιστική επεξεργασία των συναθροίσεων (πολυπαραγοντική ανάλυση) με στόχο τον εντοπισμό των περιβαλλοντικών παραγόντων που ελέγχουν την εξάπλωση των πανίδων.

Οι συναθροίσεις των πτεροπόδων του Ανώτερου Τεταρτογενούς περιλαμβάνουν 13 είδη πτεροπόδων (*H. inflatus*, *L. bulimoides*, *L. retroversa*, *L. trochiformis*, *C. acicula*, *Creseis* sp., *B. chierchiae*, *H. striata*, *S. Subula*, *C. pyramidata*, *C. cuspidata*, *Cavolinia* sp.) εκ των οποίων τα 11 είναι κοινά και για τις δύο περιοχές. Οι διαφορές που εντοπίζονται στην πανίδα (*L. bulimoides* και *C. cuspidata*) οφείλονται στις διαφορετικές φυσικογεωγραφικές και κλιματικές συνθήκες μεταξύ βορείου και νοτίου Αιγαίου. Με βάση τα οικολογικά χαρακτηριστικά των πτεροπόδων δημιουργήθηκε ένας δείκτης για την στρωματοποίηση της υδάτινης στήλης (λόγος Επιπελαγικών – Μεσοπελαγικών ειδών [E\M]). Από την πολυπαραγοντική ανάλυση που έγινε στις πανίδες των πλαγκτονικών τρηματοφόρων και πτεροπόδων, διαπιστώθηκε πως η επιφανειακή θαλάσσια θερμοκρασία παίζει τον κύριο ρόλο στην εξάπλωσή τους. Ωστόσο, η παραγωγικότητα των υδάτων, ο βαθμός στρωματοποίησης της υδάτινης στήλης, τα ανοδικά ρεύματα και η εποχικότητα είναι επίσης παράγοντες που ελέγχουν την κατανομή τόσο των πλαγκτονικών τρηματοφόρων όσο και των πτεροπόδων. Βάση της πολυπαραγοντικής ανάλυσης που έγινε, διαπιστώθηκε επίσης και ο βαθμός που επηρεάζει κάθε παράγοντας τις διαφορετικές πανίδες στις διαφορετικές περιοχές.

Η συσχέτιση και ο συνδυασμός των παραπάνω μεθόδων παρείχαν σημαντικές πληροφορίες για την παλαιοπεριβαλλοντική και παλαιοκλιματική εξέλιξη της ανατολικής Μεσογείου. Κατά το τέλος της Παγετώδους Περιόδου (21.1–15.7 ka BP), ψυχρές και ευτροφικές συνθήκες επικρατούσαν, οι οποίες ακολουθούνται από θερμότερες και πιο υγρές κατά την περίοδο της αποπαγοποίησης. Το Ολόκαινο

χαρακτηρίζεται από καλυτέρευση των κλιματικών συνθηκών. Οι πιο έντονες περιβαλλοντικές μεταβολές αυτή την περίοδο εντοπίστηκαν κατά τα διαστήματα απόθεσης του σαπροπηλού S1 (νότιο Αιγαίο: S1a 9.4–7.7 ka BP και S1b 6.9–6.4 ka BP, βόρειο Αιγαίο: S1 9.6–6.1 ka BP), όπου θερμές συνθήκες σε συνδυασμό με έντονη στρωματοποίηση της υδάτινης στήλης καταγράφονται.

Τέλος, με βάση τις πανιδικές μεταβολές και τα ισότοπα οξυγόνου ($\delta^{18}\text{O}$) αναγνωρίστηκαν έξι (6) ψυχρά επεισόδια στο βόρειο Αιγαίο (NAEGC6–NAEGC1) με ηλικιακό επίκεντρο τα 9.30, 8.05, 7.05, 4.55, 3.55, και 2.05 ka BP, και δύο (2) στο νότιο Αιγαίο (SAEGC2–SAEGC2) με επίκεντρο τα 7.35 και 5.35 ka BP. Αυτά τα ψυχρά/ξηρά επεισόδια συμπίπτουν με παρόμοια επεισόδια που έχουν περιγραφεί από άλλες θέσεις της δυτικής, κεντρικής και ανατολικής Μεσογείου, και συνδέονται επίσης με άλλα υψηλότερων γεωγραφικών πλατών.

Contents

1. Introduction.....	10
2. Regional Oceanographic Setting.....	14
2.1. The Mediterranean Sea and water masses circulation	14
2.2. The Aegean Sea and water masses circulation	18
2.3. Studied sites	22
2.3.1. The NAT	22
2.3.2. The submarine depression between Kimolos and Sifnos islands.....	24
3. Material and Methods	26
3.1. Material.....	26
3.2. Methods.....	27
3.2.1. Preparation of samples and Micropalaeontological analyses.....	27
3.2.2. Biogeochemical analyses	28
3.2.3. Time stratigraphic framework.....	30
3.2.4. Statistical analysis	30
3.2.5. Palaeoenvironmental indices.....	31
4. Results.....	32
4.1. Lithostratigraphy of Gravity Cores	32
4.2. Identification Criteria of the fauna, Classification and Ecological features.....	35
4.2.1. Planktonic foraminifera.....	35
4.2.2. Holoplanktonic Gastropods – Pteropoda	41
4.3. Planktonic Foraminifera Distribution Pattern	51
4.4. Pteropod Distribution Pattern.....	56
4.5. Total Organic Carbon and Stable Isotopes	60
5. Age Model	64
6. Multivariate statistical analyses	77
6.1. Q-mode Cluster Analysis.....	77
6.2. Principal Component Analysis (PCA)	84
6.2.1. Planktonic Foraminifera.....	84
6.2.2. Pteropoda	90
6.3. Differences in pteropod fauna between the South and North Aegean Sea	99

6.4.	North versus South Aegean.....	100
6.4.1.	Planktonic Foraminifera.....	100
6.4.2.	Pteropoda	102
6.5.	Foraminifera versus Pteropoda	104
7.	Palaeoclimate and Palaeoenvironment.....	105
7.1.	Paleoenvironmental Indices – Temperature, Productivity and Stratification	105
7.2.	Palaeoenvironmental Reconstruction.....	111
7.3.	Holocene climate variability and its relationship to large-scale climatic changes.....	119
7.3.1.	Abrupt Holocene cooling events and their impact on eastern Mediterranean hydrologic regime.	122
8.	Conclusions.....	128
9.	References.....	131
10.	Appendix.....	164

1. Introduction

Over the last decades, there has been considerable interest in the role of the subtropical oceans in climate change and, in particular, oceanic sub-basins and marginal seas. These settings are often more responsive to paleoceanographic and paleoclimatic changes than global oceans because of their smaller size and partial isolation. As an example, the relatively small volume of the Mediterranean Sea causes changes in its climatic forcing to be recorded virtually instantaneously in paleoceanographic proxy data, such as stable isotope and other geochemical ratios, and in microfossil abundances (Kontakiotis, 2012). Specifically, the signals registered by changes in abundance and distribution of fossil microorganisms, provide a reliable and well-documented record at both global and local scales (e.g. Antonarakou et al., 2015, 2019; Bonfardeci et al., 2018; Cacho et al., 2001; Drinia et al., 2016; Kontakiotis et al., 2019; Koskeridou et al., 2017; Kouli et al., 2012; Lirer et al., 2014; Sbaffi et al., 2004; Siani et al., 2013; Siani et al., 2010; Triantaphyllou et al., 2009b; Wall-Palmer et al., 2014). The basin's limited communication with the open ocean implies that any climatic signals will be recorded in an amplified fashion in Mediterranean properties, such as temperature, salinity, and specific elemental concentrations (Casford et al., 2002; Kontakiotis, 2016; Louvari et al., 2019; Marino et al., 2009).

The Aegean Sea is an ideal archive to investigate climatic evolution at both global and local scale because of its intermediate position between the higher- and lower-latitude climate systems (Giorgi and Lionello, 2008; Rohling et al., 2009; Zervakis et al., 2004), high sedimentation rate marine records compared to the open Mediterranean Sea (Aksu et al., 1995; Geraga et al., 2010; Kontakiotis, 2016; Roussakis et al., 2004), as well as paleo-latitude and land-locked configuration (Lykousis et al., 2002; Poulos, 2020). Such marginal Seas are often more responsive to paleoceanographic and paleoclimatic changes than global oceans, with climatic signals to be recorded in an amplified fashion in Mediterranean properties such as temperature, salinity and specific elemental concentrations, because of their smaller size and partial isolation (Kontakiotis, 2012), and therefore can be considered as miniature oceans. In addition to interactions with the Black Sea, northern Aegean, and Levantine basins with remote and local atmospheric forcing (Poulos et al., 1997; Zervakis et al., 2000), the south Aegean Sea is characterized by intense biogeochemical contrasts in its hydrology in response to a climatic gradient from mid-latitude to subtropical regimes that appears to be very sensitive to climate

changes. However, most of the current paleoclimatic and paleoceanographic studies are still limited to deep marine records (Geraga et al., 2005, 2010; Giamali et al., 2019; Kotthoff et al., 2008a; Kuhnt et al., 2007) and consequently little is known about continental shelf and/or coastal areas within this marginal Sea (Antonarakou et al., 2018; Drinia et al., 2016; Koutrouli et al., 2018; Louvari et al., 2019; Triantaphyllou et al., 2009a,b).

Marine sediment cores are good archives of past oceanic developments, due to their often long time series of more or less uninterrupted sediment sequences that potentially store information about past climatic and oceanographic developments in physical, chemical and biological parameters. Environmental changes related to the different water column characteristics can be recorded virtually instantaneously in palaeoceanographic proxy data, such as stable isotope and other geochemical ratios (Antonarakou et al., 2015; Bazzicalupo et al., 2020; Kontakiotis et al., 2011, 2016; Le Houedec et al., 2020), and micro-fossil abundances, such as planktonic foraminifera and pteropods (Giamali et al., 2019; Karakitsios et al., 2017; Kontakiotis et al., 2019). This makes them extremely valuable for both stratigraphic correlations and paleoenvironmental/paleoclimate reconstructions (Antonarakou et al., 2019; Casford et al., 2007; Checa et al., 2020; Comeau et al., 2010; Giamali et al., 2019; Karakitsios et al., 2017; Kontakiotis et al., 2013, 2016, 2019; Lirer et al., 2014; Margaritelli et al., 2018, 2020; Tsiolakis et al., 2019; Vasiliev et al., 2019).

Planktonic foraminifera apart from being excellent biostratigraphical indicators, they have been proofed an excellent tool for the palaeoenvironmental and palaeoclimate reconstruction (Pujol and Vergnaud-Grazzini, 1995). Their significance in the study of modern and past marine ecosystems in the Mediterranean Sea is well underlined (Antonarakou et al., 2018; Berger et al., 1982; Fhlaithearta et al., 2010; Geraga et al., 2005; Hemleben et al., 1989; Kontakiotis, 2016; Lirer et al., 2014; Perez-Folgado et al., 2003; Pujol and Vergnaud-Grazzini, 1995; Sbaffi et al., 2001; Sbaffi et al., 2004; Triantaphyllou et al., 2009a,b; Zarkogiannis et al., 2019b, 2020) and it is due to their widespread occurrence in modern oceans, with rather clearly defined faunal provinces for many species, and the fact that they produce calcitic shells that contribute substantially to the micro-fossil faunal record. Indeed, they provide one of the most continuous and clearly interpretable fossil records used in reconstructing the climatic, ecological and geological history of the earth. Particularly, they are used as indicators of temperature, salinity,

and nutrient content making it possible to identify past circulation through the sedimentary record (Casford et al., 2002, 2003; Giamali et al., 2019; Kontakiotis, 2016; Zarkogiannis et al., 2019a; Zarkogiannis et al., 2019b) and detect long- and short-term paleoclimatic and paleoceanographic changes in the study area (Casford et al., 2003; Geraga et al., 2005, 2010; Giamali et al., 2019, 2020; Howes et al., 2017; İşler et al., 2016; Kontakiotis, 2012; Triantaphyllou et al., 2009a).

Pteropods are widespread and abundant in the global ocean and entirely adapted to a pelagic life cycle (Hunt et al., 2008; Lalli and Gilmer, 1989). Owing to their aragonite nature of their shells that increase their weight as settling particles and hence their sinking speed (Lochte and Pfannkuche, 2003), their deposition is expected to be close to their habitat (Vinogradov, 1961). Particularly in the Mediterranean Sea, preservation of pteropods shells is excellent as a result of the relatively shallow water, high bottom water temperatures, and probably the limited number of mud feeders (Herman, 1971). A considerable number of studies (e.g., Almogi-Labin et al., 1991, 1998, 2008, 2009; Bhattacharjee, 1997; Buccheri, 1984; Buccheri et al., 2002; Singh et al., 2005; Wall-Palmer et al., 2014) have shown that late Quaternary pteropod assemblages and their distribution pattern in the world oceans, changes with temperature and the overall climatic conditions that also affect the aragonite compensation depth (ACD). Recent studies (Johnson et al., 2020) have shown that modern eastern Mediterranean pteropod communities are found to be more abundant than in those at western Mediterranean Sea. Their abundances are positively correlated with the aragonite saturation state (Ω_{ar}), O_2 concentration, pH, salinity and temperature, and negatively correlated with nutrient concentrations (Howes et al., 2015; Johnson et al., 2020). However, pteropod assemblages and their distribution in the Aegean Sea during late Quaternary are poorly documented (Giamali et al., 2019, 2020). Studying the past distribution of these organisms is important so as to give insights on how environmental factors and especially stressors such as hypoxia or anoxia influence them. The difficulty in maintaining pteropods in culture for extended periods (Manno et al., 2017), couple the need to investigate their response in the natural laboratory and especially during sapropel layers.

The overall objective of this thesis is to reconstruct palaeoclimate and palaeoceanographic conditions and further extend our knowledge of the climatic variability in the north and south Aegean (eastern Mediterranean Sea) during the late Quaternary. In order to advance the

understanding of the spatial and temporal variability of observed climatic and paleoceanographic changes, planktonic foraminifera and pteropods were collected and analyzed from three gravity cores (KIM-2A, AEX-15, and AEX-23). Apart from the well-studied in Aegean Sea, planktonic foraminifera, this thesis aims to provide new insights on pteropods diversity and distribution, as they are studied for the first time in late Quaternary records of the Aegean Sea and especially within the sapropel layers. In order to investigate the environmental factors that control their distribution, multivariate statistical analysis is performed in both faunal groups. In addition, the micro-palaeontological and geochemical data retrieved from the records, are used so as to investigate differences between the fauna and among the factors affecting the north and the south Aegean. Finally, the high-resolution paleoclimatic data that revealed from their distribution patterns coupled with variations of oxygen and carbon isotopic signals, helped to identify short-term cold events during the Holocene. These events were further compared with previously published circum-Mediterranean and global climate records (Bond et al., 2001; Cacho et al., 2001; Combourieu-Nebout et al., 2009, 2013; Desprat et al., 2013; Emeis et al., 2000, 2003; Frigola et al., 2007; Geraga et al., 2008; Incarbona and Sprovieri, 2020; Mayewski et al., 2004).

2. Regional Oceanographic Setting

2.1. The Mediterranean Sea and water masses circulation

The Mediterranean Sea occupies an elongated area of about 2.5 million km² between Europe and Africa. It has a restricted communication with the world ocean through the narrow and shallow Strait of Gibraltar. A submarine ridge between Sicily and African coast (Sicilian Channel) divides the Mediterranean Sea into two main basins, the eastern Mediterranean (EMS) and the western (WMS) (Figure 1). The western part is subdivided into three principal submarine basins. The Alborán Basin is east of Gibraltar, between the coasts of Spain and Morocco. The Algerian (sometimes called the Algero-Provençal or Balearic) Basin, east of the Alborán Basin, is west of Sardinia and Corsica, extending from off the coast of Algeria to off the coast of France. The Tyrrhenian Basin, that part of the Mediterranean known as the Tyrrhenian Sea, lies between Italy and the islands of Sardinia and Corsica.

The EMS is subdivided into four basins. The Ionian Basin lies to the south of Italy and Greece, where the deepest sounding in the Mediterranean, about 4.900 m, has been recorded. The Levantine Basin, which is separated by the Ionian Basin by a submarine ridge between the western end of Crete and Cyrenaica (Libya), and is extended to the south of Anatolia (Turkey). The Aegean Sea which extends north of the island of Crete and is bounded on the west and north by the coast of Greece and on the east by the coast of Turkey. The Adriatic Sea, northwest of the main body of the eastern Mediterranean Sea, is bounded by Italy to the west and north and by Slovenia, Croatia, Bosnia and Herzegovina, Montenegro, and Albania to the east (Figure 1).

Because of its relatively small size, its geographical location, and its semi-land-locked nature, the Mediterranean Sea is very sensitive and responds quickly to atmospheric forcings and/or anthropogenic influences. It is a region where major oceanic processes occur, though on smaller scales than those occurring in the world ocean (Schroeder et al., 2012).

Three major water masses predominate in the Mediterranean Sea (Figure 2). The most important is that of Atlantic Water (AW), which is composed by the Atlantic Surface Water and the North Atlantic Central Water (Schroeder et al., 2012), as it derives from the only connection with the world ocean, the Gibraltar Strait. The AW flows parallel to the African coast and through the Sicily strait reaches the eastern Mediterranean. In the Levantine basin, this water mass, it is

branching into cyclonic and anticyclonic gyres. The salinity of this water mass is increasing towards the eastern part due to evaporation (Malanotte-Rizzoli and Robinson, 1988).

In the Levantine basin, the Levantine Intermediate Water mass (LIW) is being formed. This formation is the outcome of the cold and arid winds which influence the surface water masses. The LIW inflows into the Aegean, Adriatic and Tyrrhenian basins and finally outflows from Gibraltar Strait. Its salinity is higher than 38.5‰ and it flows in depths of 200 – 600 m (Garzoli and Maillard, 1979; Millot et al., 2006).

The third water mass is referred to the Deep Water masses (MDW) which are formed in the northern part of the Iberian Sea (Liguro – Provençal), in the northern part of Adriatic Sea, in the north Aegean Sea and in Cretan Sea (Lykousis et al., 2002; Zervakis et al., 2000). Depth, temperature and salinity of the MDW are differentiated due to their formation in different sub-basins.

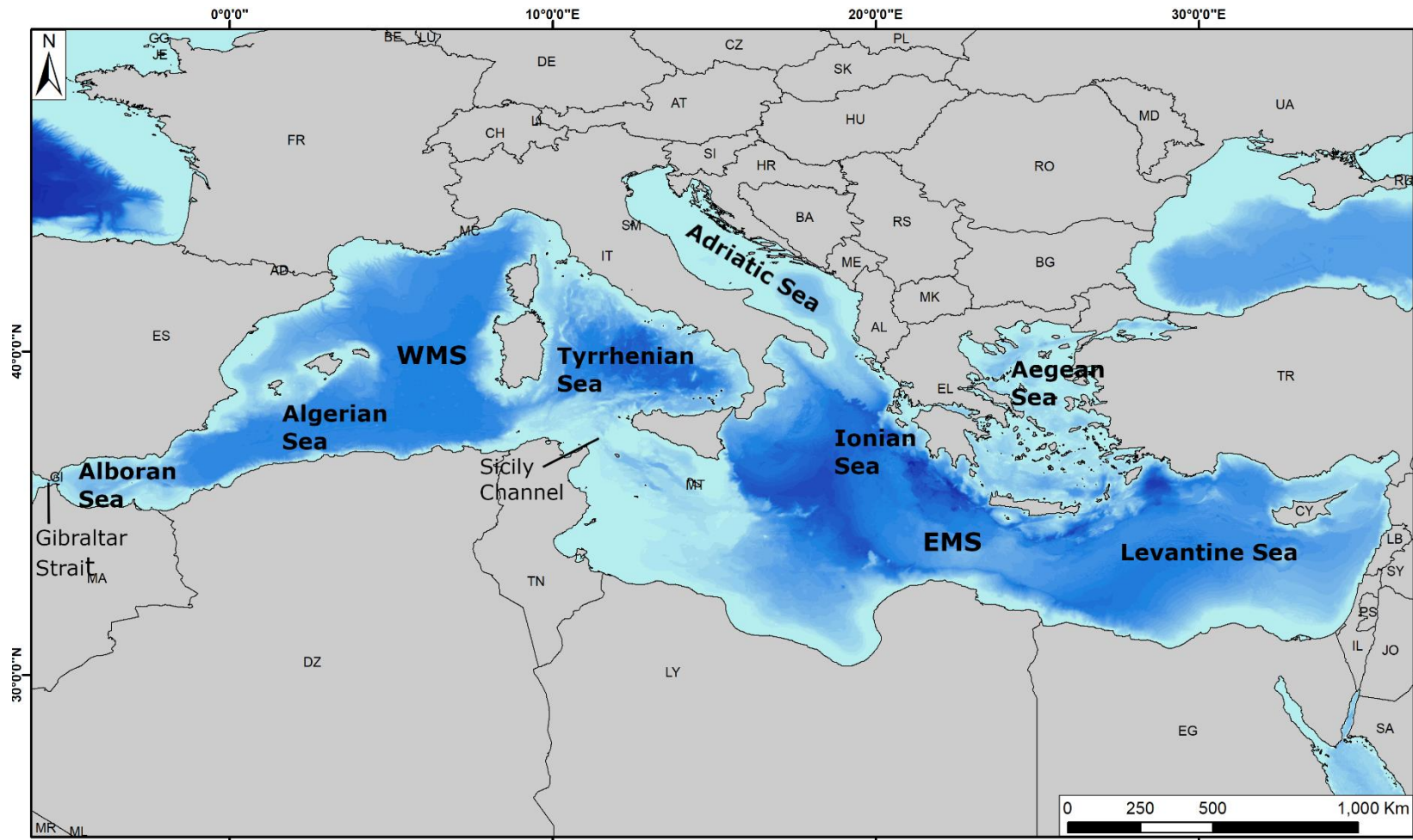


Fig. 1. Map of the Mediterranean Sea with names of sub-basins (WMS: Western Mediterranean Sea and EMS: Eastern Mediterranean Sea). Map available via GIS, bathymetry is after (Ioc, 2003) country names are given by © EuroGeographics for the administrative boundaries (Eurostat).

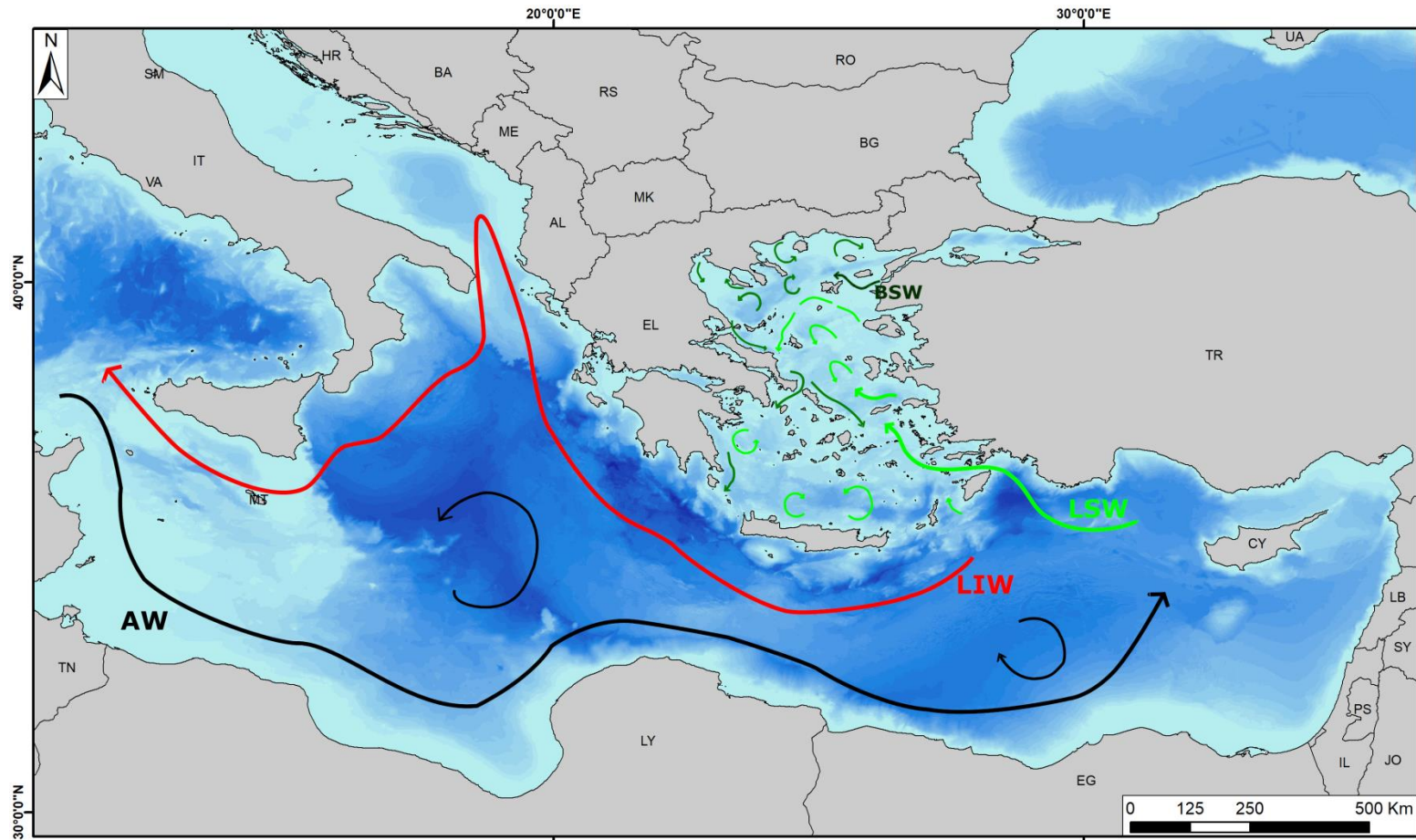


Fig. 2. Simplified schematic of the surface circulation system and water masses pathways in the eastern Mediterranean Sea. The main flows of the surface Atlantic Water (AW: black arrow) and the Levantine Intermediate Water (LIW: red arrow), along with the surface circulation of the Aegean Sea (green and light green arrows; LSW: Levantine Surface Water and BSW: Black Sea Water) are shown based upon (Karageorgis et al., 2008; Lykousis et al., 2002; Poulos, 2009; Zervakis et al., 2005a). Map available via GIS, bathymetry is after (Ioc, 2003) country names are given by © EuroGeographics for the administrative boundaries (Eurostat).

2.2. The Aegean Sea and water masses circulation

The Aegean Sea is situated between Turkey and Greece (Figure 3) and is one of the largest basins in the Eastern Mediterranean (water capacity of $8.1 \times 10^{13} \text{ m}^3$) with a mean depth that of 450 m (Velaoras and Lascaratos, 2005). It's connected with the Black and Marmara Seas through the Dardanelles and Bosphorus Straits, and with the open eastern Mediterranean (Levantine Sea) through the Cretan Straits. The complex topography is a feature of the Aegean Sea due to the great variability of its shores and bottom relief (Zervakis et al., 2000). Geographically, it is divided into the South, Central, and North Aegean, and it turns out that this division can be extended also to the hydrographic characteristics of the sub-basins of the sea.

The South Aegean (extend in between 35N and 37N) consists mainly of the Cretan and the shallow shelf of the Cyclades Plateau, along with the Myrtoan Sea at the NW part of the region (Figure 3). The Central Aegean consist of the northern shelf of the Cyclades islands and the Chios and Ikaria basins and extends between 37N and 38 40' N. Finally, the North Aegean (lying north of 38 40' N) is characterized by an alternation of deep trenches and troughs, shallow shelves and sills. In general, the deep basins of the North Aegean are oriented in a SW-NE direction. The North Sporades and Athos basins reaching depths of 1468 and 1149 m respectively are separated by a 500 m deep sill from the 1550 m deep Limnos basin. All three of them form the North Aegean Trough (NAT; Figure 3) and are separated by a 350 m sill from the North Skyros basin and from the broader Chios basin, lying to their south.

According to (Lykousis et al., 2002) and (Poulos, 2009), the upper part of the water column (50-100 m) is composed by the following water masses: a) the Black Sea Water (BSW) flowing into the Aegean Sea from the Dardanelles Strait, b) the Levantine Surface Water (LSW) entering the Aegean from the Cretan Arc Straits, c) the Modified Atlantic Water (MAW) deriving from the Ionian Sea and d) the Cretan Surface Water (CSW) that is observed north of Crete (Figure 2). In depths of about 250 – 300 m at the south Aegean and 350 – 400 m at the central and north Aegean the Levantine Intermediate Water (LIW) is encountered. Moreover, in the south Aegean Sea at depths of 300 – 700 m a cold and dense water mass is observed being known as “Transitional Mediterranean Waters” (TMW). The TMW derives from the mid-depths of the Eastern Mediterranean through the eastern and western Cretan Arc Straits. Finally, in the deepest/ bottom parts the Cretan Deep Water (CDW) formed locally and/or in the surrounding

shelf areas. In the deepest parts of the central and north Aegean Sea the dense North Aegean Deep Water is encountered (Figure 2).

The oceanography of the Aegean Sea is controlled by: 1) the climate contrasts between more humid conditions in the north and semiarid conditions in the south and (Kuhnt et al., 2007) and 2) the exchange of water masses with the Levantine Sea, Ionian Sea, and Black Sea. Particularly, the cooler (9–22°C) and of lower salinity (24–28 psu) Black Sea outflow waters flows along the east coast of Greece to reach the southwest Aegean Sea, and, due to their high nutrient contents, fuel productivity in the North Aegean Sea (Lykousis et al., 2002). The warm (16°C in winter; 25°C in summer) and saline (39.2–39.5 psu) Levantine surface waters flow northward along the eastern Aegean to the Dardanelles Straits (Zervakis et al., 2000, 2004). Several rivers discharge into the Aegean Sea, mostly from the north Hellenic coast and from the east coast of Turkey. Together, Black Sea outflow waters and river inputs both supply the Aegean with freshwater (Poulos et al., 1997).

The Aegean Sea is characterized, in general, by a cyclonic water circulation, although the most active dynamic features are the mesoscale cyclonic and anticyclonic eddies (Lykousis et al., 2002) either permanent and/or recurrent. Thus, the Levantine waters, entering the Aegean through the eastern Cretan Straits, travel northwards along the eastern Aegean coast. When they reach the Black Sea outflow, in the vicinity of Limnos Island, they get subducted below the very light Black Sea waters. Subsequently, Levantine waters move westwards and eventually southwards along the east coast of the Hellenic Peninsula; the latter is associated with a very strong, permanent return flow along the east coast of the island of Evvoia. A branch of this flow is directed towards the northeastern edge of the Cyclades Plateau feeding, partially, the cyclone of Chios Basin, whilst a small branch of it crosses the strait between the SE end of Evvoia and the Andros Island and flowing south-westward enters the Myrtoan Sea where it feeds a recurrent cyclone (Poulos, 2009). Moreover, dense water formation has been reported over the Limnos and Samothraki plateau by Theocharis and Georgopoulos (1993) due to the mixing of surface brackish waters (BSW plus river outflows) with more saline waters of Levantine origin, possibly induced by local cold atmospheric conditions. In addition, part of the low-salinity water mass (BSW) is arrested occasionally by a permanent anticyclone flowing around the island of Samothraki. Besides, the low-salinity surface waters of the Samothraki Plateau form a

thermohaline front with higher salinity waters along the Athos-Limnos Strait. This front, under certain conditions, ‘breaks’ and a cyclone is formed off the Athos peninsula, moving southwards from the plateau, while waters of higher salinity flow northwards passing west of Limnos island. The North Sporades basin is characterized, generally, by a variable meso-scale circulation and the recurrence of a cyclone over the deep basin.

The circulation pattern of the South Aegean Sea, including the Cretan arc passages, is characterized by intense mesoscale variability incorporating a succession of transient and/or recurrent cyclonic and anticyclonic eddies (Lykousis et al., 2002; Theocharis et al., 1993, 1999a,b). Both of these features induce an overall water transport from the west to the east along the southern part of the Cretan Sea (Figure 2).

The water circulation in the Aegean Sea undergoes small variability at a synoptic scale, as a response to the atmospheric variability. However, on a seasonal time-scale, there is a major change in the Aegean Sea circulation pattern, which may be playing a significant role, not only in influencing its longer-term hydrographic properties, but also in affecting its ecosystem (Zervakis et al., 2005b). This seasonal change, that takes place annually in the Aegean Sea, is the coastal upwelling of intermediate waters, evident every summer along the eastern Aegean, as a response to the persistence of the Etesian northerly winds during the summer period. The importance of this coastal upwelling is small, in comparison to coastal upwelling sites in the open ocean, due to the oligotrophic character of the Aegean Sea (Skiriris et al., 2010).

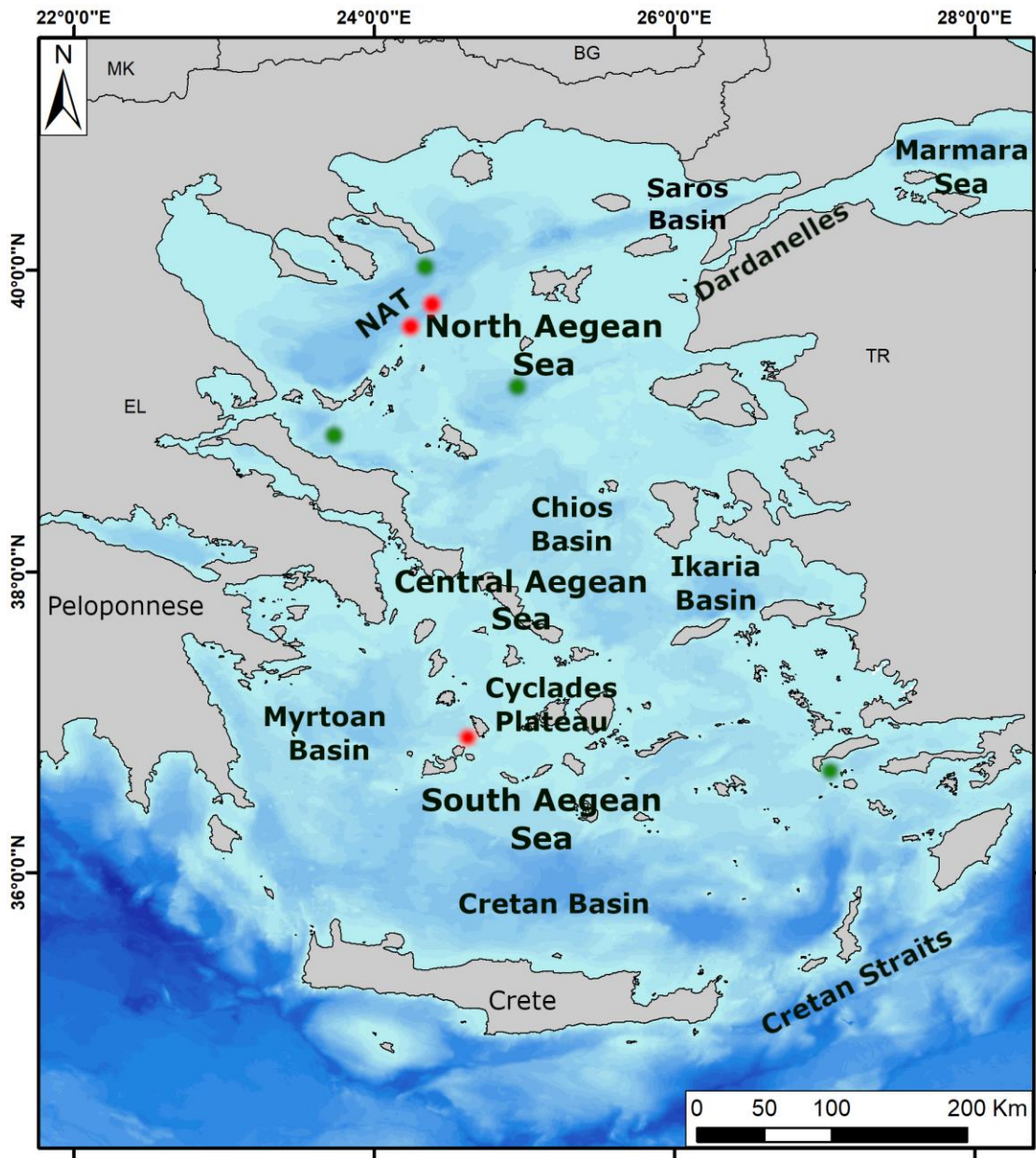


Fig. 3. North, Central and South Aegean Sea along with the major basins in there. Red dots represent the location of studied cores and green dots, the location of nearby cores used in the subsequent age model. Map available via GIS, bathymetry is after (Ioc, 2003) country names are given by © EuroGeographics for the administrative boundaries (Eurostat).

2.3. Studied sites

The three gravity cores studied in this thesis are collected from two distinct areas from north and south Aegean, each one unique for its own geological characteristics. The vicinity of these areas with major geological structures as well as the sea level changes during the last 21 kyr, render these gravity cores as special tool for investigating spatial and temporal variability of climatic and oceanographic changes.

2.3.1. The NAT

Two studied cores presented here (AEX-15 and AEX-23) have been collected from Athos Basin. Athos Basin, north Sporades Basin and Lemnos Basin are the three deep basins of the North Aegean Trough (NAT; Figure 4) which is a NE-SW trending deep depression situated in northern Aegean Sea. Athos basin reaches depths of approximately 1200 m (Roussakis et al., 2004; Zervakis et al., 2000). The morphologic differentiation of the NAT is strongly related with the North Anatolian Fault (NAF) (Mascle and Martin, 1990), as it is one of the three major fault zones that NAF splits. All of the fault zones appear to accommodate a comparable amount of deformation (Koukouvelas and Aydin, 2002). The NE-SW to E-W striking NAT fault zone takes up the dextral – slip motion on the NAF at its western termination.

Apart from deformation that is taking place in the NAT, the oceanographic aspects in this area are of paramount importance. The main characteristic of the north Aegean is that the fluvial freshwater inputs from the Black Sea and the river runoff from Greek and Turkish mainland dilute the highly saline waters from Levantine and south – central Aegean. In there, three major water masses can be recognized; the superficial nutrient-rich and less saline Black Sea Water (BSW; Figure 2), the Levantine Intermediate Water (LIW; Figure 2) with higher salinity, and the North Aegean Deep Water (DW) which is the outcome of the buoyancy loss of the Aegean Intermediate Water (which derives from the LIW). The extent to which this basin supplies dense deep water and oxygen to the whole Mediterranean it is controlled by the antagonistic influences of freshwater influx on the one hand and winter cooling on the other (Zervakis et al., 2000).

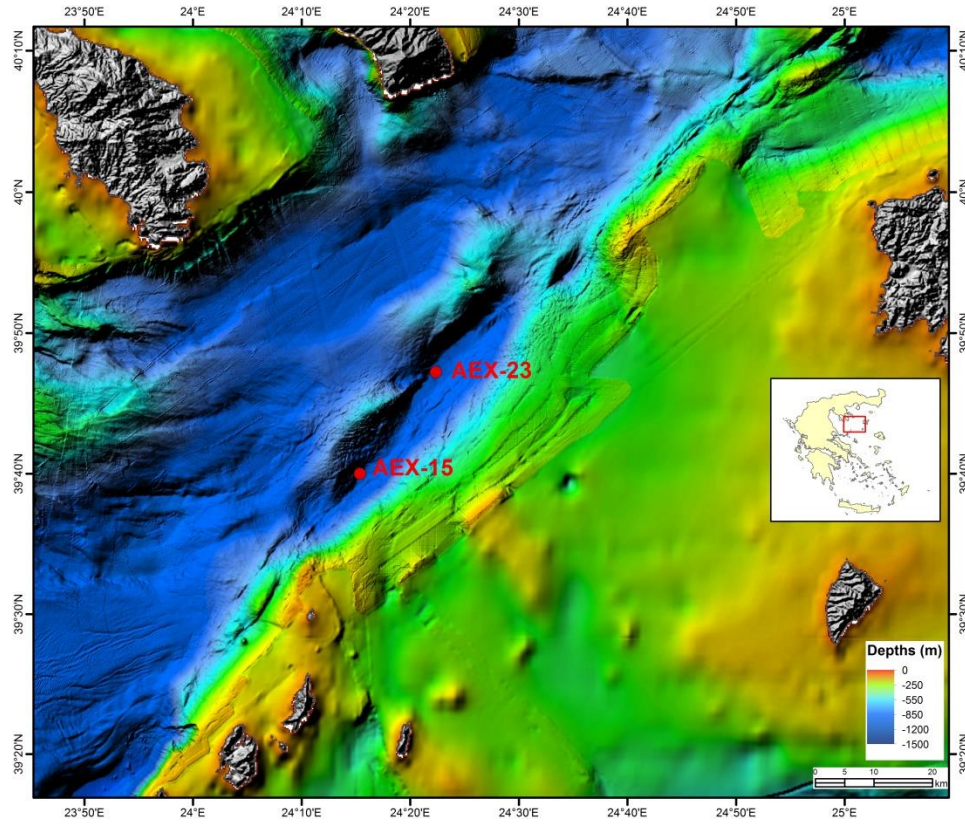


Fig. 4. North Aegean Trough (NAT) and location of the gravity cores AEX-15 and AEX-23. Figure provided by HCMR.

2.3.2. The submarine depression between Kimolos and Sifnos islands

Milos and Kimolos islands lie in the westernmost sector of the Cyclades plateau. Both islands are part of the South Aegean Volcanic Arc; one of the most important geological structures of the Aegean Sea. The submarine area between Kimolos and Sifnos Islands is characterized by a rather complex relief as it is related to the volcanic arc (Figure 5). Its sedimentary and Quaternary tectonic evolution have been studied previously by (Piper and Perissoratis, 2003) and the submarine geomorphology and sediment properties were subject of the YPOTHER/Aegean Exploration project. In this context multi-beam bathymetry, seismic profiling, and remotely operated vehicle dives were utilized to provide information on this peculiar geomorphological feature.

Karageorgis et al. (2016) analyzing the results of the survey separated the submarine depression into three parts; the southern, the eastern and the northern respectively (Figure 5). The southern part includes the highly irregular submarine slopes of Kimolos Island. The eastern part comprises of the smooth west-south shelf and slope of Sifnos Island. The northern part occupies the southern part of the sedimentary basin which has developed north of Kimolos volcanic province and west of Sifnos metamorphic province. Unlike most flat sedimentary basins, it displays a peculiar relief with local depressions and structural highs spatially alternating. The authors recognized six noticeable depressions which have been labelled with numbers (Figure 5). Depression number 1 (Nr.1) is the deepest one with depths up to 743 m surrounded by steep slopes. The second depression (Nr.2) is at the north of Kimolos slope with maximum depth of 378 m. The depressions Nr. 3, 4, 5 are shallower and are located in the basin north of Kimolos. The last depression Nr. 6 marks the narrowest point of the strait between Kimolos volcanic province and Sifnos metamorphic province. The gravity core KIM-2A was collected north of the depression Nr.1 in a water depth of 600 m.

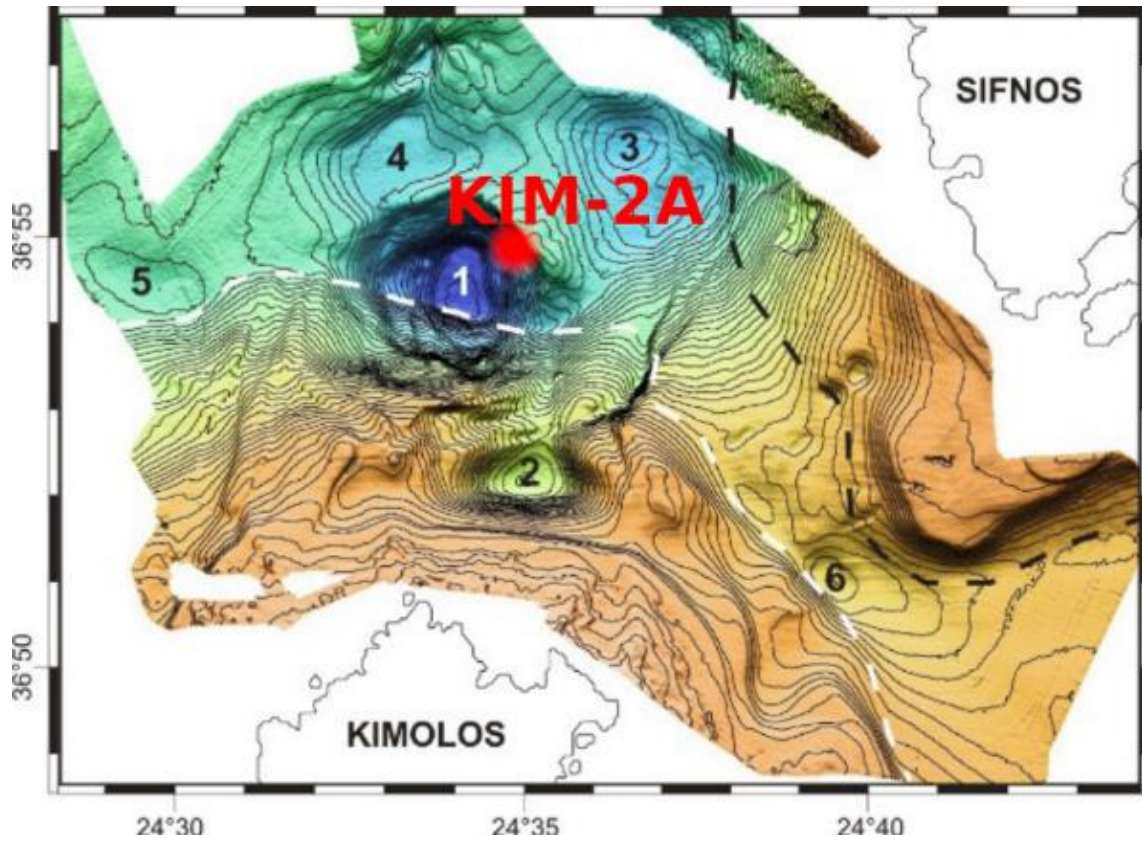


Fig. 5. Submarine area between Sifnos and Kimolos islands along with the six depressions recognized by Karageorgis et al., (2016) and the location of core KIM-2A (modified by Karageorgis et al., 2016).

3. Material and Methods

3.1. Material

For the present study three gravity cores from the north and south Aegean Sea were analyzed. Two cores (AEX-15, AEX-23) were collected from a relatively isolated elongated sub-basin of the north Aegean Sea, oriented NE–SW, with dimensions of approximately 42×7 km and a maximum depth of 1290 m. Core AEX-15 ($39^{\circ}39.900'N$, $24^{\circ}15.369'E$; 1242 m water depth, length 178 cm) was recovered from the southern sector of the basin, and core AEX-23 ($39^{\circ}49.464'N$, $24^{\circ}22.354'E$; 1226 m water depth, length 322 cm) was recovered near the depocenter of the basin (Figure 4). The third core (KIM-2A) was collected from the south Aegean area, from a submarine depression located north of Kimolos Island (Figure 5; $36^{\circ}95.464'N$, $24^{\circ}06.354'E$; 640 m water depth, length 200 cm) (Table 1). The totality of the cores was recovered during several R/V Aegaeo cruises from 2013 to 2015 (Table 1) in the frame of “YPOTHER” project (Submarine Geological Researches in Aegean Sea) of H.S.G.M.E. in collaboration with HCMR.

All studied cores contain distinct organic-rich dark intervals representing the regional expression of the most recent sapropel S1. All samples taken were used for palaeontological (planktonic foraminifera and pteropods) and geochemical (oxygen and carbon isotopes) analyses. Details on the location of the cores are reported in Table 1.

Table 1. Coordinates, length, depth, number of samples and Expedition journey of the three studied gravity cores.

Gravity Core	Location	Coordinates		Length (cm)	Depth (m)	No of Samples	Expedition
KIM-2A	South Aegean	36 95.464'	24 06.354'	200	640	58	R/V Aegaeo - 3/05/2014
AEX-15	North Aegean	39 39.900'	24 15.369'	178	1242	115	R/V Aegaeo - 28/09/2013
AEX-23	North Aegean	39 49.464'	24 22.354'	322	1226	46	R/V Aegaeo - 29/09/2013

3.2. Methods

The methods are based on high resolution micro- palaeontological and geochemical data ($\delta^{18}\text{O}$ and $\delta^{13}\text{C}$ isotopes, AMS ^{14}C datings, Corg content, Ba/Al). In particular, planktonic foraminifera and pteropods were identified for each sample of every core. Stable carbon and oxygen isotopes were measured in all samples and eight (8) Accelerator Mass Spectrometry (AMS) radiocarbon (^{14}C) datings were performed. Determination of organic carbon (Corg) was performed in the totality of the cores. For the cores from north Aegean major elements (Al) and barium (Ba) were performed on selected sediment samples.

3.2.1. Preparation of samples and Micropalaeontological analyses

The first step of the analysis took place at the laboratory of sedimentology of Hellenic Centre for Marine Research (HCMR) during several phases of the YPOTHER project. Multi logger and lithological description were performed for each core. The recognition of sedimentological units in color level was based on Munsell soil color chart (2000) (U.S. Department of Agriculture, Handbook 18 – Soil Survey Manual). Dense sampling (every 1 cm) followed the discrete units of each core (sapropel layers) whereas the rest of the sediments were sampled with 1 cm, 2 cm or 5 cm resolution. The sampling preparation took place at HCMR and was performed by Dr. Chr. Ioakim.

All samples were prepared following standard micropaleontological procedures of the HyPerCal protocol (Zarkogiannis et al., 2020). Approximately 3 cm³ of dried sediment was washed and sieved through 63 and 125 μm sieves, and residues were dried in an oven at 50⁰C. Qualitative and quantitative analyses have been performed on the planktonic foraminiferal assemblages for the >125 μm fraction, split into aliquots each containing at least 300 specimens. All the shells were picked, identified and counted in each sample and then converted into percentages of the total number of planktonic foraminifera, based on the extrapolation of a counted split (Annex D). Planktonic foraminiferal taxonomy follows the work of Hemleben et al., (1989) with additional updates from Aurahs et al., (2009; 2011), Numberger-Thuy et al., (2009) and Kontakiotis et al., (2017). All morphotypes of *G. ruber* (“Normal,” “Platys,” “Elongate,” and “Twin” types; Kontakiotis et al., 2017) were plotted together, distinguishing only the “alba” and “rosea” varieties because of different ecological characteristics. Planktonic species with phylogenetic

affinities and similar ecological characteristics were counted together and grouped to better interpret distribution patterns. Thus, *Globigerina bulloides* group includes the species *G. bulloides* and *Globigerina falconensis*, the *Globigerinoides sacculifer* group includes *Globigerinoides trilobus* and *G. sacculifer*, and the *Globigerinella siphonifera* group includes the species *Globigerinella aequilateralis*, *Globigerina calida*, and *Globigerina digitata*. The species *Globigerinita glutinata* includes the morphotypes with and without bulla. Within the group of Neogloboquadriniids, two types were discerned: *Neogloboquadrina pachyderma* and *Neogloboquadrina dutertrei*.

For the malacological analysis holoplanktonic gastropods (specifically the Order Pteropoda; Suborder Euthecosomata) were handpicked from the whole residual material of the >125 µm fraction. All the shells were picked, identified, counted, and then converted into percentages of the total number of pteropods. The identification in species level follows the works of Di Geronimo (1970), Van der Spoel (1976), Panchang et al. (2007), Janssen (2012), Janssen et al., (2019), Wall-Palmer et al. (2014) and Rampal (2017). Raw data were transformed into percentages of the total abundance and relative percentage abundance curves were plotted, after exclusion of rare species (<3%) (Annex I).

Finally, species of particular interest of both taxa were treated under Scanning Electron Microscope Analysis (SEM) at Wiener Laboratory of the American School of Classic Studies (ASCSA; Athens). All the identified specimens were stored in chapman slides, at the Hellenic Survey of Geology and Mineral Exploration (H.S.G.M.E.) laboratory of palaeontology.

3.2.2. Biogeochemical analyses

Stable Isotopes

For stable oxygen and carbon isotope measurements ($\delta^{18}\text{O}$, $\delta^{13}\text{C}$), 30 specimens of the planktonic species *Globigerinoides ruber* f. *alba* were picked from the 250–300 µm size fraction. In particular, the morphotype “Normal” of Kontakiotis et al., (2017) (usually represented to *G. ruber* sensu stricto) was exclusively used in order to minimize potential morphotype-specific differential responses in stable isotope compositions (Antonarakou et al., 2015; Wang et al.,

2000). This size fraction limitation was used to minimize ontogenetic and growth rate effects on shell geochemistry (Spero et al., 2003). The analyses were carried out at the Laboratory of Geology and Geophysics at Edinburgh University. Foraminiferal $\delta^{18}\text{O}$ and $\delta^{13}\text{C}$ data were calibrated to National Bureau of Standards -19 (NBS19), and the isotope values are reported in ‰ relative to Vienna Pee Dee belemnite scale. The external standard errors of the stable carbon and oxygen isotope analyses are $<0.06\text{‰}$ and 0.08‰ , respectively.

Organic Carbon content, Al and Ba

In core KIM-2A Organic Carbon (C_{org}) was determined by the $\text{K}_2\text{Cr}_2\text{O}_7\text{-Fe}(\text{NH}_4)_2 \cdot 6\text{H}_2\text{O}$ titration based on the (Walkley and Black, 1934) methodology with the (Angelova et al., 2014) adaptation at the Laboratory of the Hellenic Survey of Geology and Mineral Exploration (H.S.G.M.E.).

In cores AEX-15 and AEX-23 determination of organic carbon (C_{org}), major elements (Al) and barium (Ba) were performed on selected sediment samples in order to detect the depth where the onset and termination of S1 deposition occurred (e.g., Martínez-Ruiz et al., 2003, and references therein). C_{org} was determined in a Fisons Instruments EA-1108 CHNS analyzer. The operating parameters were very similar to those reported by Cutter and Radford-Knoery (1991), Nieuwenhuize et al. (1994), and Verardo et al. (1990). The precision of the method is within 5%. A detailed description of the analytical procedure is given by Karageorgis et al. (2009). Major element concentrations were determined on fused beads using an X-ray fluorescence spectrometer (Panalytical PW-2400) at the biogeochemical laboratory of the Hellenic Centre for Marine Research, which is accredited according to ELOT EN ISO/IEC 17025:2005. Aluminum and barium were determined as oxides following the procedure described in Karageorgis et al. (2005). In addition, barium excess (Ba_{ex}) that represents marine barite, and thus enhanced productivity (Martínez-Ruiz et al., 2003), was estimated according to Karageorgis et al. (2005). The analytical precision is 5–10% on the basis of duplicate runs of standards and unknowns, whereas accuracy was assessed using the international reference material PACS-2.

3.2.3. Time stratigraphic framework

The chronostratigraphy of the cores is based on eight Accelerator Mass Spectrometry radiocarbon datings (AMS ^{14}C) that were originally performed on *Globigerinoides ruber* tests at Beta Analytics laboratories. Apart from the AMS ^{14}C datings, the chronostratigraphy was supplemented by the detected additional control points, as defined by Ba, Al, and organic carbon measurements and well-dated correlation horizons from nearby north and south Aegean cores (Figure 3; green dots). Conventional ^{14}C ages were calibrated by means of the Calib version 7.0.2 software (Stuiver and Reimer, 1993) and the Marine13 data set with a regional reservoir age correction (ΔR) of 139 ± 40 years for the S1 sapropel interval (Facorellis and Maniatis, 1998) and of 58 ± 85 yr outside the sapropel S1 interval (Reimer et al., 2013). Hereafter, ages in this study are reported in calibrated thousands of years before present, notated ka BP.

3.2.4. Statistical analysis

Multivariate statistical analyses

Q-mode cluster analysis was used to determine the overall statistical similarity between samples, following the algorithms of Davis (1988) using the correlation coefficient matrix. Q-mode analysis was performed after exclusion of rare species (< 3%) and grouping of species that have a discontinuous, scattered distribution at generic level. The results of cluster analysis were reported and arranged in two-dimensional hierarchical dendrograms, wherein locations were presented along the Y-axis while similarity level is plotted on the X-axis.

Principal Component Analyses (PCA) is used to reduce the dimensionality of a multivariate data set to a few principal factors that determine the distributions of species. For this analysis all raw data for the totality of the samples and specimens were used. Raw data were processed using PAST (2.17) multivariate statistical software package of Hammer et al., (2001). The resulting factor scores show the contribution of each factor in every sample and therefore the down-core contribution of each factor. The total number of factors was defined by minimizing the remaining “random” variability and by the possibility to relate the factors to modern hydrographic conditions and planktonic foraminiferal and pteropod ecology.

3.2.5. Palaeoenvironmental indices

Planktonic Palaeoclimatic Curve

The planktonic foraminiferal relative distributions are used as a first-order estimate of Sea Surface Temperature (SST) variations. An index of the SST variations was constructed based on the down-core variation of planktonic foraminiferal abundances, and it was referred to as Planktonic Paleoclimatic Curve (PPC). The PPC was obtained by the formula $(w - c) * 100 / (w + c)$, where w represents the warm water indicators (*G. ruber*, *O. universa*, *G. sacculifer*, *B. digitata*, *G. rubescens*, *G. aequilateralis*, *G. calida*) and c the cold water indicators (*G. inflata*, *T. quinqueloba*, *G. truncatulinoidea*, *G. glutinata*, *G. scitula*) (Rohling et al., 1993b).

Productivity – Stratification – SPRUDTS

The Eutrophication index (E-index; Kontakiotis, 2016) was estimated using the sum of the eutrophic (*Neogloboquadrina pachyderma*, *Neogloboquadrina dutertrei*, *Globigerina bulloides*, *Turborotalita quinqueloba*, *Globoconella inflata*) species versus the sum of the eutrophic plus oligotrophic (*Globigerinoides ruber alba*, *Globigerinoides ruber rosea*, *Globoturborotalita rubescens*, *Globigerinoides sacculifer*, *Orbulina universa*, *Globigerina siphonifera*) species.

The down-core ratio between *G. bulloides* and *G. ruber* was estimated showing the degree of the stratification of the upper water column (S-index; Kontakiotis, 2016; Sbaffi et al., 2004). The percentage of *G. bulloides* was estimated as an upwelling index (U-index; Kontakiotis, 2016). The species *G. siphonifera* gr., *G. rubescens*, *O. universa*, and *G. sacculifer* gr. are referred as SPRUDTS group, following the ecological characteristics of Rohling et al., (1993b).

4. Results

4.1.Lithostratigraphy of Gravity Cores

The lithological description for each core is given right below. The description and sampling took place at the laboratory of HCMR after multi logger processes. The recognition of the colors of the different lithological units was based on the color table of (Oyama and Takehara, 1970) “Revised standard soil color charts Munsell notation and color names”.

KIM-2A

Lithologically, this core contains a distinct organic-rich dark interval, divided into two separate sub-units (S1a and S1b respectively), representing the regional expression of the most recent sapropel S1 (Anastasakis and Stanley, 1984; Mercone et al., 2000) (Figure 6a). From the bottom up to 87.5 cm, light gray clay can be observed (Munsell soil color 5Y 7/1). The following 24 cm are of gray color (5Y 5/1) and correspond to the lower sub-unit (S1a) of the sapropel. Between 63.5 cm and 52 cm light gray clay (5Y 7/1) can be observed, indicative of the sapropel interruption (S1i). From 52 cm to 40 cm mud of gray color (5Y 5/2) characterizes the upper sapropel sub-unit (S1b). The clay continues up to 13.5 cm with a light gray clay (5Y 7/1) color. From this point to the top of the core watery clay of light-yellow color (5Y 7/4) can be observed (Figure 6a).

AEX 15

Core AEX-15 is of 178 cm length. From the bottom up to 165 cm mud of grayish olive color is observed (Munsell soil color 7.5 6/2). The following 43 cm consists of mud with gradient in color from dark olive gray (2.5GY 4/1) to olive gray (5Y 6/2) and grayish olive (7.5 5/2). This interval corresponds with the sapropel layer S1. From 122 cm to 87 cm olive yellow (5Y 6/2) mud with rare darker laminae is observed, and is followed by 66 cm of grayish olive (5Y 6/2) mud with dense darker laminae. The interval between 21 cm to 14 cm consists of dull yellow (2.5Y 6/4) mud and the one between 14 to 12 cm of yellowish brown (2.5Y 5/3) mud with shell debris. From 12cm to the top of the core mud with gradient in color and in water content is observed (Figure 6b).

AEX 23

AEX-23 is the longest core of this study and consists of 320 cm of pelagic-hemipelagic sediments. Specifically, from the bottom to 292 cm a sapropel layer of 2,5GY 4/1 (Munsell soil color) dark olive gray color is observed. Lens of mud rich in organic matter are following for 6 cm with dark olive gray color (2,5GY 4/1 & 2,5GY 3/1). From 286 cm to 40 cm the core is composed by mud of greyish olive color (5Y 6/2). In the top 40 cm the mud is becoming rich in water content and of olive yellow color (7,5Y 6/3) (Figure 6c).

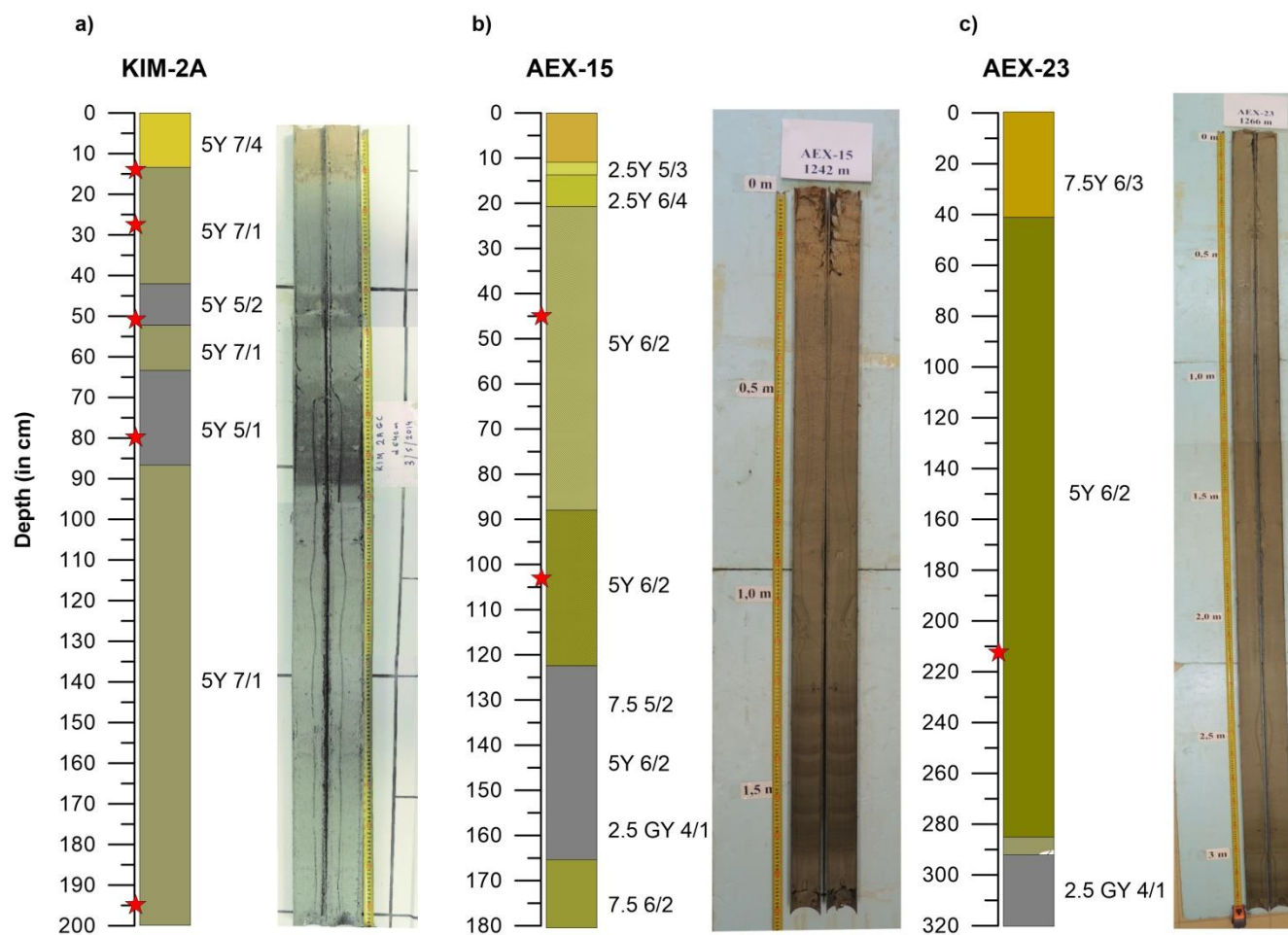


Fig. 6. Lithologic log and photos of the studied cores along with the color code of the lithological units; a) Core KIM-2A, b) Core AEX-15, c) Core AEX-23. Red stars represent the exact point that AMS datings were done.

4.2. Identification Criteria of the fauna, Classification and Ecological features

As this study focuses on micro- and macro-biota (planktonic foraminifera and pteropods), it is essential to provide their taxonomical and ecological features. Both groups consist of water column dwellers which can be used as palaeoenvironmental and palaeoceanographic indicators. Properties of water masses affect the tests of these planktonic taxa as well as their distribution and therefore their presence or absence from the sedimentary archive and/or their geochemical imprint. In this way, planktonic foraminifera and pteropods are useful for unraveling the palaeoenvironment and the palaeoceanographic circulation. For the taxonomical analysis of the fauna a baseline must be followed for all samples that will be tracked during the identifications and interpretation. Therefore, it is crucial to describe the criteria that were used in this thesis. All the groups referred below were formed considering their morphological aspects, palaeoenvironmental and ecological features as well as biostratigraphic ranges.

4.2.1. Planktonic foraminifera

Foraminifera are single-celled eukaryotic organisms that live both in marine and fresh water environment. They range in size from 100µm – 15cm in length. Foraminifera are classified primarily by the composition and morphology of their tests. Tests can be made of organic compounds, sand grains, and other particles cemented together (agglutinated), or secreted calcium carbonate (CaCO₃). Many groups are commonly made of a number of chambers, added during growth. The arrangement of these chambers and the position and shape of apertures are important for taxonomic classification.

Foraminifera exhibit both benthic (epifaunal or infaunal) and planktonic (passive floating) lifestyles. There are approximately 40 species of planktonic foraminifera in the ocean today. This comprises about 1% of the extant species of foraminifera. In the open marine environment, benthic foraminifera are usually much more diverse yet occur in lower abundances than planktonic foraminifera (Dowsett, 2007).

Planktonic foraminifera apart from being excellent biostratigraphical indicators, they have been proved an excellent tool for the palaeoenvironmental and palaeoclimate reconstruction. Species identified in the cores' sediments are presented in the classification below. Furthermore, planktonic species with phylogenetic affinities and similar ecological characteristics were

counted together and grouped to better interpret distribution patterns. Ecological significance based on numerous references for each species or group is also given below.

Classification

Kingdom CHROMISTA

Phylum FORAMINIFERA

Class GLOBOTHALAMEA

Subclass ROTALIANA

Order ROTALIIDA

Suborder GLOBIGERININA

Superfamily GLOBIGERINITOIDEA

Family Globigerinitidae Bermúdez, 1961

Subfamily Globigerinitinae Bermúdez, 1961

Genus *Globigerinita* Brönnimann, 1951

Species *Globigerinita glutinata* (Egger, 1893)

Superfamily GLOBIGERINOIDEA

Family Globigerinidae Carpenter et al., 1862

Subfamily Globigerininae

Genus *Beella* Banner & Blow, 1960

Species *Beella digitata* (Brady, 1879)

Genus *Globigerina* d'Orbigny, 1826

Species *Globigerina bulloides* d'Orbigny, 1826

Genus *Globigerinella* Cushman, 1927

Species *Globigerinella calida* (Parker, 1962)

Species *Globigerinella siphonifera* (d'Orbigny, 1839)

Genus *Globigerinoides* Cushman, 1927

Species *Globigerinoides ruber* (d'Orbigny, 1839)

Genus *Globoturborotalita* Hofker, 1976

Species *Globoturborotalita rubescens* (Hofker, 1956)

Genus *Trilobatus* Spezzaferri, Kucera, Pearson, Wade, Rappo, Poole, Morard & Stalder, 2015

Species *Trilobatus sacculifer* (Brady, 1877)

Genus *Turborotalita* Blow & Banner, 1962

Species *Turborotalita quinqueloba* (Natland, 1938)

Subfamily Orbulininae Schultze, 1854

Genus *Orbulina* d'Orbigny, 1839

Species *Orbulina universa* d'Orbigny, 1839

Superfamily GLOBOROTALIOIDEA

Family Globorotaliidae Cushman, 1927

Genus *Globoconella* Bandy, 1975

Species *Globoconella inflata* (d'Orbigny, 1839)

Genus *Globorotalia* Cushman, 1927

Species *Globorotalia scitula* (Brady, 1882)

Species *Globorotalia truncatulinoidea* (d'Orbigny, 1839)

Genus *Neogloboquadrina* Bandy, Frerichs & Vincent, 1967

Species *Neogloboquadrina dutertrei* (d'Orbigny, 1839)

Species *Neogloboquadrina pachyderma* (Ehrenberg, 1861)

Globigerinita glutinata: it is a cosmopolitan species preferring shallow waters (~75m) (Reiss et al., 2000) and a diatom feeder (Hemleben et al., 1989) normally associated with the spring bloom, triggered by the newly available nutrients at the end of winter mixing and increased solar radiation. Its diet allows the species to survive in both oligotrophic surface and eutrophic deeper waters (Hemleben et al., 1989; Schiebel and Hemleben, 2005; Schiebel et al., 2001). It has a short reproductive cycle (Hemleben et al., 1989) and its occurrence may also be an opportunistic response to any increase in number in nutrient availability. Usually absent in the sapropel S1 deposition throughout the Aegean (Casford et al., 2002).

Globigerina bulloides group: includes the species *Globigerina falconensis* as well as the poorly preserved specimens of small size. The latter is not possible to be identified whether it belongs to *G. bulloides* or *G. falconensis*.

Globigerina bulloides: lives in the surface or subsurface waters withstanding large fluctuations in temperature, salinity and density of the water column (Rohling et al., 1993b). It is an eutrophic species, indicative of sub-polar water masses highly dependent on enhanced food levels; upwelling, strong seasonal mixing or freshwater inputs (Reiss et al., 1999; Rohling et al., 2004). This species can survive at the end of phyto- and zooplankton blooms, when oxygen had been rapidly consumed (Principato et al., 2003).

Globigerinella siphonifera group: under this group the species *G. aequilateralis*, *G. calida* and *Beella digitata* and *G. siphonifera* are summarized due to their similar habitats and ecological characteristics. *G. siphonifera* gr. is a representative of warm oligotrophic waters (Kontakiotis, 2016), member of the SPRUDTS group and it displays peak abundances in winter (Rohling et al., 2004).

Globigerinoides ruber: All morphotypes of the species *Globigerinoides ruber* (*G. elongatus*, *G. pyramidalis*, *G. gomitulus*, *G. extremus*) were classified under the *G. ruber*, as they have been proved to be morphological varieties of the same species. Within the morphospecies of *G. ruber*, two variations in shell color are recognized, *G. ruber* “white” and *G. ruber* “pink”. These variations were counted and plotted separately in all cores due to their different ecological preferences.

This species is considered as indicative of warm and oligotrophic surface waters (Pujol and Vergnaud-Grazzini, 1995; Thunell, 1978), with minimum temperature required at ~14°C (Bijma et al., 1990a,b; Hemleben et al., 1989; Reiss et al., 1999). The high abundance of *G. ruber* during the late Glacial and Holocene periods has been observed all throughout the Mediterranean Sea (Buckley et al., 1982; Hayes et al., 1999; Kontakiotis, 2016; Antonarakou et al., 2015; Giamali et al., 2019, 2020). *G. ruber* exhibits two varieties, a pink (*rosea*) and a white (*alba*) forma. It is considered that the pink forma prefers warmer waters than the white which prefers lower temperatures (Hemleben et al., 1989).

Globorotalita rubescens: Based on (Capotondi et al., 1999) the species *Globorotalita rubescens* and *Globigerinoides tenellus* can be summarized under the label *G. rubescens* due to their similar habitats. *G. rubescens* occurs in warm through temperate waters (Hemleben et al., 1989).

Globigerinoides sacculifer group: is a minor warm planktonic indicator representative of warm oligotrophic waters and it has been related to the occurrence of a surface pycnocline during the S1 (Kontakiotis, 2016; Principato et al., 2003). Is an euryhaline species which withstands salinities in a range of 24-47‰ and tolerates temperature of 14-31°C (Hemleben et al., 1989). The specimens of *Globigerinoides sacculifer* and *Globigerinoides trilobus* were grouped under the species *G. sacculifer* gr.

Turborotaliita quinqueloba: is considered as indicative of cool waters (Lourens et al., 1992; Thunell, 1978), but is also tolerant to fairly low salinity and/or enhanced fertility in surficial waters (Rohling et al., 1997).

Orbulina universa: is member of the SPRUDTS group, prefers warm oligotrophic conditions. Lives in temperature range 12-31°C, and although its photosynthetic symbionts show a dominant habitat in shallower waters, with sufficient light penetration, it can be found down to 250 m (Hemleben et al., 1989).

Globoconella inflata: is regarded as indicative of deep seasonal mixing (in association with winter mixing) (Hemleben et al., 1989; Pujol and Vergnaud-Grazzini, 1995; Rohling et al., 1995). This species in the Mediterranean is associated with cool and deep mixed waters (Pujol and Vergnaud-Grazzini, 1995; Thunell, 1978). The rapid and temporal increase of *G. inflata* after the end of the sapropel S1 is documented in almost all the cores from the eastern

Mediterranean and is attributed to deep water ventilation (Casford et al., 2002; De Rijk et al., 1999; Geraga et al., 2000).

Globorotalia scitula: is shown living at depth and is tolerant of low temperatures (Hemleben et al., 1989; Lourens et al., 1992; Thunell, 1978). It reflects a cool, homogeneous, and relatively eutrophic winter mixed layer (Reiss et al., 1999; Rohling et al., 2004).

Globorotalia truncatulinoides: its presence/ absence is controlled by the winter convection and vertical mixing (Pujol and Vergnaud-Grazzini, 1995).

Neogloboquadrina pachyderma: is shown living at depth, and is known to thrive at or just above the base of the euphotic zone and generally prefers stable stratified environments (Hemleben et al., 1989; Reiss et al., 1999; Rohling et al., 1993b, 1995). This species is known to prevail in stable stratified settings with a well-developed deep chlorophyll maximum (DCM) (Hemleben et al., 1989; Reiss et al., 1999; Rohling et al., 1993b) in a water mass isolated from the surface water system (Casford et al., 2002). It is considered to thrive in colder waters (Pujol and Vergnaud-Grazzini, 1995).

Neogloboquadrina dutertrei: Neogloboquadrinid species are indicative of cool and eutrophicated waters associated with the formation of a Deep Chlorophyll Maximum (DCM) layer (Fairbanks and Wiebe, 1980). Neogloboquadrinids are intermediate water dwellers and may suggest shoaling of the pycnocline into the base of the euphotic layer to create a distinct deep chlorophyll maximum.

Both neogloboquadrinids identified in this work (*N. dutertrei*, *N. pachyderma*) are separated to dextral and sinistral forms due to their different oceanographic preferences. For instance, *N. pachyderma* dextral is considering preferring warmer water conditions than the sinistral one.

SPRUDTS: The species *G. sacculifer*, *G. trilobus*, *G. rubescens*, *Orbulina universa*, *B. digitata*, *G. tenellus*, *G. siphonifera* are typical of warm water and of stratified water column (Rohling et al., 1997) and they consist SPRUDTS group (Rohling et al., 1993a).

4.2.2. Holoplanktonic Gastropods – Pteropoda

As holoplanktonic gastropods are poorly studied in the Aegean Sea, it is essential to provide details on their taxonomy, way of life, preservation, and habitats.

Pteropoda (or commonly pteropods) are planktonic gastropods, which have evolved wings from the foot, structure that characterizes animals in the class Gastropoda. These wings are uniquely adapted to enable the animals to live their entire lives as a planktonic form (Bé and Gilmer, 1977) and they are, therefore, termed holoplanktonic.

Pteropods are widespread and abundant in the global ocean and entirely adapted to a pelagic life cycle (Hunt et al., 2008; Lalli and Gilmer, 1989). Are divided into three suborders, the Euthecosomata, Pseudothecosomata (shelled pteropods), and Gymnosomata (naked pteropods), which differ in their morphology, behavior and trophic position. The species classification in the suborder of Euthecosomata is based on their shell morphology whereas for shell-less Gymnosomata species it is based on the anatomical features of the feeding apparatus (Lalli and Gilmer, 1989; Van der Spoel, 1976).

In Euthecosomata two superfamilies are distinguished: Limacinoidea and Cavolinoidea. The latter consists of four extant families (Cavoliidae, Cliidae, Creseidae, Hyalocylidae) whereas the former from three (Heliconoididae, Limacinidae, Thieleidae). The suborder Pseudothecosomata contains one superfamily: Cymbulioidea consisting of three families (Cymbuliidae, Desmopteridae, Peraclidae). Representatives of the families Cymbuliidae and Peraclidae though they have been identified in genera level in this work, they are not included as this thesis is focusing on Euthecosomata.

Shell structure

Pteropods are one of only a few taxa that make their shells out of aragonite a polymorph of calcium carbonate. The biogeochemical importance of aragonite production by pteropods has been shown in a number of studies (Acker and Byrne, 1989; Berner and Honjo, 1981). On a global scale, aragonite production by pteropods might constitute at least 12% of the total carbonate flux worldwide (Bednaršek et al., 2012a; Bednaršek et al., 2012b; Berner and Honjo, 1981). Their aragonite shell not only contributes to the transfer of organic and inorganic material into the deep ocean (Tréguer et al., 2003) but also increases the weight of pteropods as settling

particles and hence their sinking speed (Lochte and Pfannkuche, 2003). For that reason, deposition close to their habitat is to be expected (Vinogradov, 1961).

Owing to their aragonite nature of their shells, pteropods are more susceptible to solution than other marine macrofossils. The state of aragonite shell preservation depends on the degree of organic matter combustion in the sediments and their transport and removal by currents (Herman, 1971). Well preserved shells occur in sediments, where the supply of organic matter is limited and O₂ levels are high. Preservation deteriorates with increased supply of organic carbon, O₂ consumption and increased production of CO₂ (Almogi-Labin et al., 1986). Particularly in the Mediterranean Sea, preservation of pteropods shells is excellent as a result of the relatively shallow water, high bottom water temperatures, and probably the limited number of mud feeders. Furthermore, as a result of rapid rates of sedimentation, seas offer higher resolution of Quaternary events than do ocean basins (Herman, 1971). Nowadays, Pteropoda abundances are known to be higher in the eastern Mediterranean than in the western, as the higher aragonite saturation state and their unique method of feeding is fulfilled (Johnson et al., 2020).

Way of life-habitats

Eutecosomata are usually phytophagous organisms, occasionally feeding on floating organic particles (Trégouboff and Rose, 1957). They perform diurnal vertical migration, descending in day and rising to the surface at night. The important factors controlling the vertical distribution are light, pressure, temperature, oxygen content and salinity (Herman and Rosenberg, 1969). Due to their vulnerability (nature of the shell) and the restricted tolerance to changes in the above-mentioned factors, they can be useful indicators of past environment as it has been shown before (e.g., Herman, 1971; Herman, 1989; Singh et al., 2005; Wall-Palmer et al., 2014).

Because of their migratory life style, Eutecosomata can be characterized either as epipelagic (shallow-water dwellers: 0 – 200 m) or as mesopelagic (deeper-water dwellers: 200 – 1000 m). Some species are bathypelagic and live in water depths of 1000 m and more. Mesopelagic species are sensitive to the degree of water column stratification and to the extent of the oxygen minimum zone (OMZ) (Almogi-Labin et al., 2008). Most species show preference for warmer environments and are distributed in tropical and subtropical realms. In colder water the species

diversity is reduced, but individuals frequently occur in dense populations (Janssen and Peijnenburg, 2014).

Classification

Kingdom ANIMALIA

Phylum MOLLUSCA

Class GASTROPODA

Subclass HETEROBRANCHIA

Infraclass EYTHYNEURA

Subterclass TECTIPLEURA

Order PTEROPODA

Suborder EUTHECOSOMATA

Superfamily CAVOLINIOIDEA

Family Cavoliniidae Gray, 1850 (1815)

Genus *Cavolinia* Abildgaard, 1791

Species *Cavolinia inflexa* (Lesueur, 1813)

Species *Cavolinia* sp.

Genus *Diacria* J.E. Gray, 1840

Species *Diacria trispinosa* (Blainville, 1821)

Family Cliidae Jeffreys, 1869

Genus *Clio* Linnaeus, 1767

Species *Clio pyramidata* Linnaeus, 1767

Species *Clio cuspidata* (Bosc, 1801)

Family Creseidae Rampal, 1973

Genus *Boasia* Dall, 1889

Species *Boasia chierchiae* (Boas, 1886)

Genus *Creseis* Rang, 1828

Species *Creseis acicula* (Rang, 1828)

Species *Creseis* sp.

Genus *Styliola* Gray, 1847

Species *Styliola subula* (Quoy & Gaimard, 1827)

Family Hyalocylidae A. W. Janssen, 2020

Genus *Hyalocylis* Fol, 1875

Species *Hyalocylis striata* (Rang, 1828)

Superfamily LIMACINOIDEA

Family Heliconoididae Rampal, 2019

Genus *Heliconoides* d'Orbigny, 1836

Species *Heliconoides inflatus* (d'Orbigny, 1835)

Family Limacinidae Gray, 1840

Genus *Limacina* Bosc, 1817

Species *Limacina bulimoides* (d'Orbigny, 1835)

Species *Limacina retroversa* (J. Fleming, 1823)

Species *Limacina trochiformis* (d'Orbigny, 1835)

Cavolinia genus is not separated into species. As shells of *Cavolinia* are fragile, only protoconchs are able to be found and identified into genera level. The only exception of non-fragmented specimens encountered is that of *Cavolinia inflexa*. In this species two formae (or subspecies) have been recognized (Janssen, 2012; Rampal, 2002) but as the non-fragmented specimens are no more than five, it has been considered of none significance to treat this species separately. Thus, all the unrecognized species along with the few *C. inflexa* were grouped under *Cavolinia* spp.. However, ecological features of *C. inflexa* are given.

Cavolinia inflexa: It lives between the surface and 250m (Bé and Gilmer, 1977) and its temperature span is 16°C-28°C. The salinity tolerance is that between 35.5‰-36.6‰ (Van der Spoel, 1976). Herman (1981) interpreted this species as a temperate water species with a wide depth range distribution, abundant in the western basins, reaching peak abundances in the Ligurian and Provençal basins, decreasing in abundance in the Tyrrhenian and Adriatic, and even being rare in the Ionian and Levantine basins.

Diacria trispinosa group: includes various formae based on several authors (e.g., Bontes and van der Spoel, 1998; Hilgersom and Van der Spoel, 1987; Rampal, 2002; Van der Spoel, 1976). Janssen (2012) accepts two separate species in the *D. trispinosa*-group, viz. *D. trispinosa* and *D. major* (Boas, 1886) with the latter not recorded in the Mediterranean. In the material studied for the present thesis this species is represented predominantly by protoconchs and fragments of the teleoconch, and thus are assigned as *D. trispinosa*. This species is a warm – water, mesopelagic species typical of Atlantic influenced waters (Biekart, 1989; Buccheri et al., 2002) most abundant in depths of 300 to 400 m (Jung, 1973). Herman (1971, 1981) and Corselli and Grecchi (1990) summarized western Mediterranean occurrences, concluding on introduction into the Mediterranean by currents from the Atlantic.

Genus *Clio* was separated into two species; *C. cuspidata* and *C. pyramidata*. The main feature for the identification of the species is the protoconch. *C. pyramidata* is further separated into three formae; *lancelota*, *pyramidata* and *tyrrhenica* (Janssen, 2012). The difference among these three is lay upon the straight or curved sidelines of this triangular species. As the majority of the material studied here, contains fragmented specimens or solely protoconchs it was difficult the separation into formae. Regarding their environmental aspect, *C. pyramidata* f. *lancelota* is considering to prefer warm environments than the North Atlantic Ocean dweller *C. pyramidata* f. *pyramidata*. *C. pyramidata* f. *tyrrhenica* though, it has been introduced by Janssen (2012) as a cold water dweller, slightly different morphologically from f. *pyramidata* encountered in the Mediterranean. This new forma of *Clio pyramidata* has no formal taxonomic status as infrasubspecific names are not recognized by the ICZN rulings. Therefore, no further identifications of formae were possible in this work and the species *C. pyramidata* is ascribed to *C. pyramidata* sensu lato.

Clio pyramidata: is a mesopelagic, temperate species (Buccheri et al., 2002), though it has been also recognized as sub-tropical and cold-tolerant by Chen and Bè, (1964). Temperatures ranges based on (Van der Spoel, 1976) are between 4 and 28°C, whereas temperature and salinity ranges given by (Jung, 1973) are 7.0 to 27.8°C and 36.1 to 36.5‰ respectively. Its greatest abundance is met in depths of 200 to 400 meters, based on the same author. Herman (1971) describing it as ‘a bathypelagic species collected in 2000 m deep tows in the Ionian Sea’.

Clio cuspidata: (Herman, 1971; Herman, 1981) characterized *Clio cuspidata* as ‘a bathypelagic species which is present in all basins (of the Mediterranean) at low frequencies, reaching peak abundancies in the cool Alboran, Liguria and Provençal basins’. Its temperatures range between 15.3-23.0°C.

Boasia chierchiaie: This species is synonymous with *Creseis chierchiaie* and in this work findings correspond to the forma *constircta*. Herein it will be referred to as *Boasia chierchiaie* in order to be consistent with WoRMS nomenclature. *B. chierchiaie* is an epipelagic species occurring in the mixed layer. It can tolerate minimum salinity of 29.92‰ and maximum temperature of 31.35°C (Singh et al., 2005). A close relationship between abundance of this species and bathymetric conditions has been documented in the southern part of the western Indian shelf (Singh et al., 1998). *B. chierchiaie* is known to proliferate in low (Rottman, 1980) as well as high salinity (Almogi-Labin et al., 1991) shallow waters. It has been documented a better preservation for this species in anoxic bottom conditions (Singh et al., 2005).

Creseis genus has concerned many authors due to its species synonyms and formae. In the material examined here one species was able to be recognized; *Creseis acicula*. Due to the long debate on synonyms of this species it has been considered suitable to use the nomenclature of WoRMS (Horton et al., 2021; Janssen, 2018). Thus, *C. acicula* is a synonym of *C. clava*. Due to the long debate on the other species of *Creseis* (e.g., *virgula*, *conica*), other species encountered in the studied material were assigned to *Creseis* sp.

Creseis acicula: it is an epipelagic subtropical – tropical species (Buccheri et al., 2002). It prefers the shallowest depth habitat amongst all epipelagic pteropods (Frontier, 1973; Rottman, 1980; Wormelle, 1962). Van der Spoel (1976) recorded salinity and temperature ranges of this taxon as 35.5–36.7‰ and 10–27.9°C, respectively. Sakthivel (1969) and Rottman (1980) found abundant

occurrences of this species in low salinity waters of the Bay of Bengal and the South China Sea, respectively. Thus, *C. acicula* has tolerance to a wide range of salinity (30–55‰) (Singh et al., 2005). Almogi-Labin et al., (2008) based on the above-mentioned remarks, refers to this species as the most euryhaline among all pteropods. Singh et al., (2005) found that this species is preserved best in anoxic bottom conditions, whereas it is poorly preserved where oxygen concentration is high enough to cause dissolution of these delicate species.

Hyalocyclis striata: This tropical sub-surface/epipelagic water species is present all over the Mediterranean but is clearly more common in the eastern than in more western parts of the basin (Buccheri et al., 2002; Herman, 1971). Its temperature and salinity ranges are 13.8-27.8°C and around 36.2‰ respectively (Jung, 1973).

Styliola subula: it is considered as a mesopelagic warm water species preferring high salinity (steno-haline) (Almogi-Labin et al., 2008; Buccheri et al., 2002; Singh et al., 2005) and more abundant in oxygen-rich water (Sakthivel, 1973). Its temperature range is 13.8-27.8°C (Jung, 1973). Rampal (2011) referred to this species as very common in the southwestern and eastern Mediterranean. Its disappearance on the palaeontological record has been attributed to fluctuations in the intensity of the OMZ (Almogi-Labin et al., 2000, 2008; Singh et al., 2005).

Heliconoides inflatus: It is considered as a mesopelagic subtropical species (Bé and Gilmer, 1977; Buccheri et al., 2002; Van der Spoel, 1976). It lives at a depth ranging from 200-1000 m (Almogi-Labin and Reiss, 1977), tolerates temperature oscillations between 14-28°C (Jung, 1973; Van der Spoel, 1976) and it is tolerant to a wide range of salinity (32-40‰; Singh et al., 2005). This species is known to proliferate in the present-day Oxygen Minimum Zone (OMZ), with a minimum concentration of c. 0.5 ml O₂ l⁻¹ in the Red Sea (Weikert, 1982; Weikert and Cederbaum, 1987). It is most common in areas known to be oligotrophic (Bé and Gilmer, 1977; McGowan, 1989; Sijinkumar et al., 2010). It is a fact that this migratory species adopts a variable depth habitat during its growth stages (veligers, juveniles and adults). Adults of *H. inflatus* migrate much deeper in the water column and, therefore, are more susceptible to the low oxygen concentration in the OMZ. Smaller forms appear to be restricted in their vertical migration, preferring to live in the upper part of the water column (Almogi-Labin et al., 1988) and so may not be affected much by the intensified OMZ (Singh et al., 2005). Living populations of this

species are present in the eastern Mediterranean, but the species is far more common in the western part of the basin.

Limacina retroversa: it is an epipelagic, typical of cold-water regions species (Buccheri et al., 2002; Herman, 1971). It lives at a depth of 150 m (Van der Spoel, 1976) and it vertical migrates on a daily and seasonal basis (Bé and Gilmer, 1977). The recorded temperature range is 2-19°C (Bé and Gilmer, 1977), the salinity range is 31-36‰ (Van der Spoel, 1976). Froget (1967) stresses the importance of the taxon as an indicator of northern Atlantic climatic conditions.

Limacina trochiformis: is an epipelagic, tropical species, bearing temperature changes between 13.8-27.9°C and salinity oscillations between 35.5-36.8‰ (Jung, 1973; Van der Spoel, 1976), though it can stand reduced surface salinities (Buccheri et al., 1998; Buccheri and Torelli, 1981). It lives at depths of 99-165 m (Van der Spoel, 1976). It is associated with the mixed layer in the water column (Almogi-Labin et al., 1988; Bé and Gilmer, 1977; Wormuth, 1981) thriving in upwelling conditions (Bé and Gilmer, 1977; Sakthivel, 1969). It has been noted that this species prefers eutrophic conditions and reduced surface salinities (Buccheri et al., 2002; Di Donato et al., 2009).

Limacina bulimoides: Is a migratory /mesopelagic pteropod species that lives in a well-ventilated water column (Almogi-Labin et al., 1988) and typical of Atlantic influenced waters (Buccheri et al., 2002). In the Atlantic the recorded temperature range is 13.8-27.8°C and the salinity range 35.5‰-36.7‰ (Jung, 1973). Herman (1971) interpreted the species as a ‘low salinity (36‰) Atlantic water indicator, present at low frequencies in all basins’ (of the Mediterranean). Corselli and Grecchi (1990) including *L. bulimoides* among the ‘specie accidentali’ (=accidental species), refer to the few observations of living western Mediterranean specimens and to the abundant occurrence of this species in cores from the eastern Mediterranean, considering it especially common during the Holocene. Results of (Johnson et al., 2020) are consistent with (Corselli and Grecchi, 1990). Almogi-Labin et al., (2008) uses its maximum abundance in Red Sea as an indicator of arid conditions.

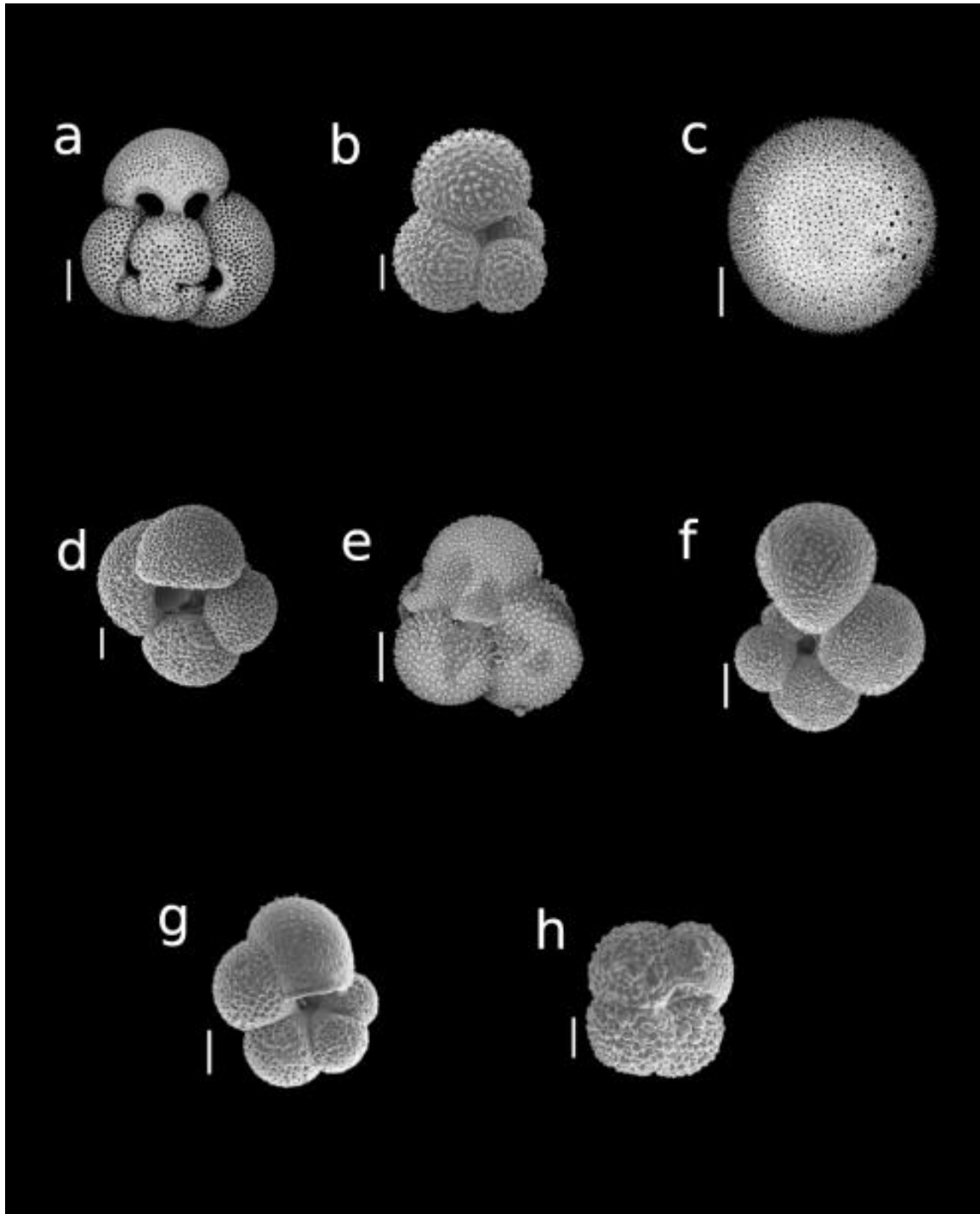


Fig. 7. SEM photographs of selected planktonic foraminifera species; a. *Globigerinoides ruber* f. *alba*, b. *Globigerina falconensis* c. *Orbulina universa*, d. *Globigerina bulloides*, e. *Globigerinita glutinata*, f. *Globigerinella calida*, g. *Turborotalita quinqueloba*, h. *Neogloboquadrina pachyderma* [d]. Scale bars: 100 μm (a, c, f); 50 μm (b, d, e, g, h).

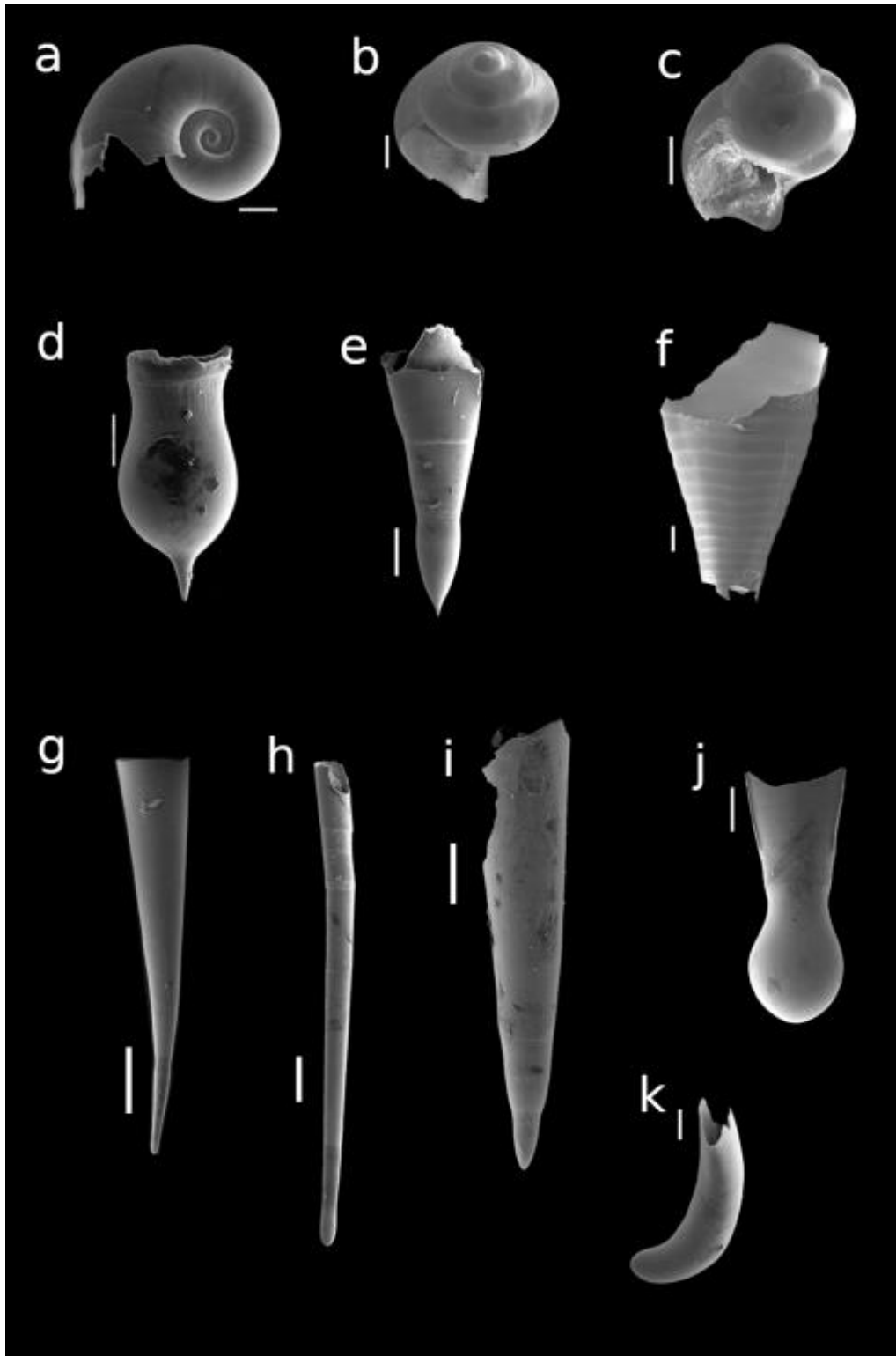


Fig. 8. SEM photographs of selected pteropod species; a. *Heliconoides inflatus*, b. *Limacina retroversa*, c. *Limacina trochiformis*, d. *Clio cuspidata* protoconch, e. *Clio pyramidata*, f. *Hyalocyclis striata*, g. *Boasia chierchiaie*, h. *Creceis acicula*, i. *Styliola subula*, j. *Diacria trispinosa*, k. *Cavolinia* sp. embryonic part. Scale bars: 500 μ m (g); 200 μ m (a, e, h, i); 100 μ m (b, c, d, f, j, k).

4.3. Planktonic Foraminifera Distribution Pattern

The qualitative analysis of the cores revealed 19 planktonic foraminiferal species lumped into 15 groups: *G. ruber* f. *alba*, *G. ruber* f. *rosea*, *G. sacculifer* group, *G. bulloides* group, *G. siphonifera* group, *G. scitula*, *G. truncatulinoides*, *G. inflata*, *O. universa*, *T. quinqueloba*, *G. glutinata*, *G. rubescens*, *G. conglobatus*, *N. pachyderma*, *N. dutertrei*. The down-core stratigraphic distributions of their relative abundance are described below and are depicted in figures 9, 10 and 11.

KIM-2A

From the bottom of the core up to 153 cm, the fauna is characterized by high relative abundances of the species *G. ruber* f. *alba* (22–34%), *N. pachyderma* (10–40%), *T. quinqueloba* (3–30%), and *G. bulloides* gr. (8–33%). Additional components of the fauna are *N. dutertrei*, *G. glutinata*, and *G. scitula*. After the 153 cm, an abrupt decline in Neogloboquadrinids and *T. quinqueloba* can be observed, while *G. bulloides* follows an opposite trend with relative abundance of 33%. From that point up to 127 cm *N. pachyderma* and *N. dutertrei* reach their maximum abundances (45% and 15% respectively), whereas *T. quinqueloba* is still present but with low percentages (up to 10%). The relative abundance of *G. bulloides* gr. does not exceed 16% and *G. ruber* f. *alba* is also present but with equally low frequency (lower than 20%). Between 127 cm and 100 cm the fauna is characterized by the dominance of *G. bulloides*, *N. pachyderma*, *N. dutertrei*, *G. ruber* f. *alba*, *G. glutinata*, and *G. rubescens*. Additional components, with lower percentages, are the species *T. quinqueloba* and *G. inflata*. The interval between 100 cm and 41.5 cm is characterized by a shift in fauna. Most of the species dominating the previous interval are decreasing or becoming absent (*T. quinqueloba*, Neogloboquadrinids, *G. glutinata* and *G. inflata*). Prevailing species of this interval are *O. universa* (44%), *G. ruber* f. *rosea* (38%), *G. bulloides* gr. (27%), *G. siphonifera* gr. (20%), and *G. sacculifer* gr. (14%). In the final segment of the core, from 41.5 cm to the top, the sampling presents poor resolution, but certain significant changes can be observed. The *G. ruber* f. *alba*, *G. inflata* and *G. truncatulinoides* present a peak (57%, 31%, and 7% respectively) and the relative abundances of *G. ruber* f. *rosea*, *O. universa*, and *G. siphonifera* gr. are decreasing. *N. pachyderma*, *G. inflata*, and *G. glutinata* are re-appearing, but with low percentages (Figure 9).

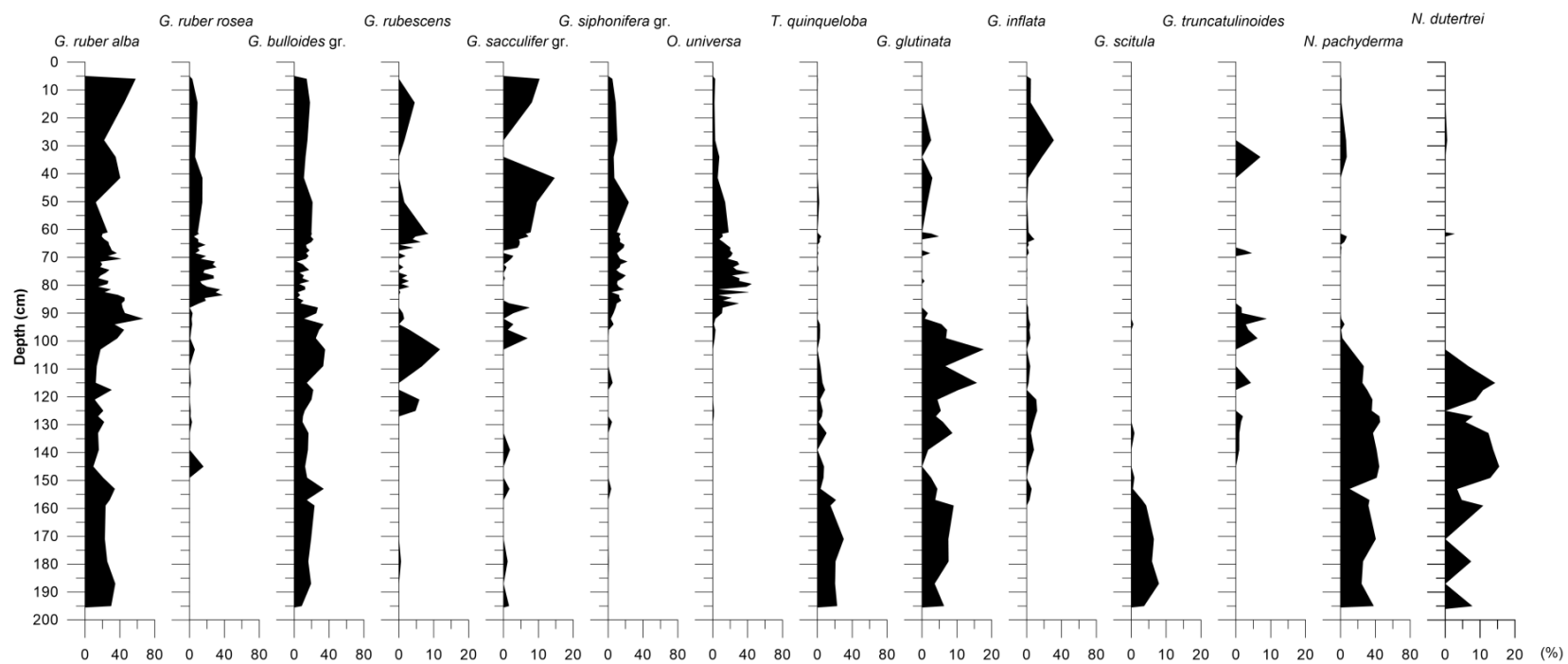


Fig. 9. Frequency curves of the most indicative planktonic foraminiferal species versus depth (in cm) in core KIM-2A.

Core AEX-15

From the bottom to 165.5 cm the assemblage is dominated by *G. ruber* f. *alba* with percentages up to 35%, along with *T. quinqueloba* (34%) and *G. bulloides* (29%). Present with low percentages in this interval are the species *G. glutinata* (12%), *G. rubescens* (13%) and *O. universa* (11%). Between 165 cm and 120 cm (AEX-15), the warm subtropical species (*G. ruber* f. *rosea* and *O. universa*) are abundant with percentages up to 25%, and the species *T. quinqueloba* and *G. bulloides* present their maximum percentages (~68% and 48%, respectively). At the same interval Neogloboquadrinids occur sporadically and with very low percentages (<2%), and *G. inflata* is totally absent (Figure 10). The relative abundance curves of *G. sacculifer* group, *G. siphonifera* group, and *O. universa* display highly variable down-core patterns, occasionally reaching significant percentages (10–30%). *G. ruber* f. *alba* and *G. rubescens* are continuously present but in small percentages. The interval between 120 cm and 107 cm is characterized by the increase of *G. inflata* (32%) and *N. pachyderma* (16%) percentages. Furthermore, *G. bulloides*, *O. universa* and *T. quinqueloba* are decreasing, whereas *G. ruber* f. *alba* relative abundance has an increasing trend. Additional components of the fauna are the *G. sacculifer*, *G. glutinata*, and *G. rubescens* with low percentages, while *G. siphonifera* gr. presents relatively the same pattern as before. From 107 cm to the top of the core the distribution pattern of these species is limited, with the exception of the upper part of the core, which is marked by a sharp increase of *N. pachyderma*. During this interval, *G. ruber* f. *alba* reaches maximum abundances (up to 65%). *G. ruber* f. *rosea* (~10–15%) and *T. quinqueloba* (~15–30%) are still present but less abundant, whereas *O. universa* decreases dramatically (Figure 10). Increasing percentages of *G. rubescens* (~15–30%) and *G. glutinata* (~5%) are also recorded.

AEX-15

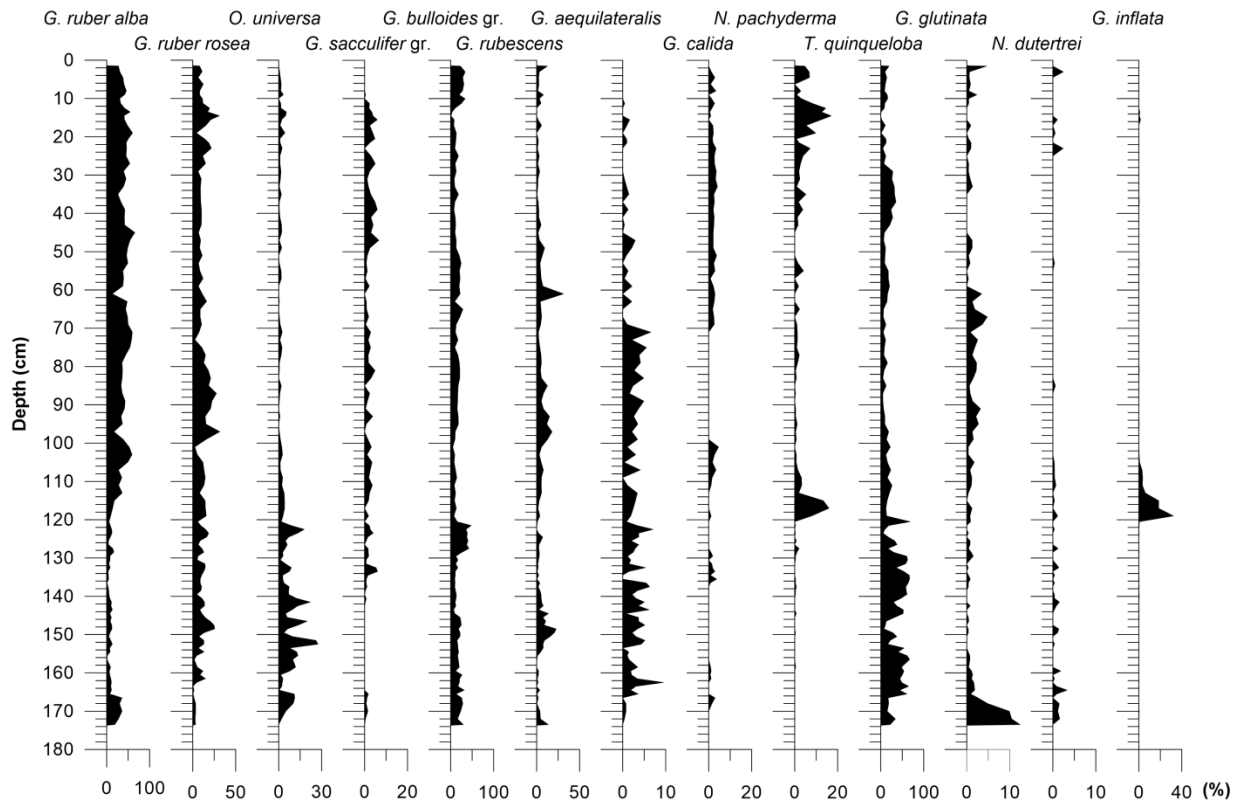


Fig. 10. Frequency curves of the most indicative planktonic foraminiferal species versus depth (in cm) in core AEX-15.

Core AEX-23

The interval between 320 cm to 291 cm of the core presents high relative abundances of the species *T. quinqueloba* (~64%), *G. bulloides* (~45%), *G. ruber* f. *rosea* (15%) and *O. universa* (11%). Additional components of the fauna are species *G. ruber* f. *alba*, *G. sacculifer*, *G. glutinata*, and *G. rubescens* with low percentages (<10%). At 291 cm a sharp increase in the abundance of *G. inflata* (23%) and *N. pachyderma* (5%) is observed. From 291 cm to the top of the core, the dominant species are the *T. quinqueloba* (59%), *G. ruber* f. *alba* (reaching 41%), *G. bulloides* (reaching 20%) and *G. rubescens* (14%). *O. universa* decreases gradually from 291 cm to 202.5 cm, whereas afterwards its relative abundance does not exceed 1%. *G. inflata* present peak at 272.5 cm (23%) and after 242.5 cm is becoming very rare or absent (Figure 11).

AEX-23

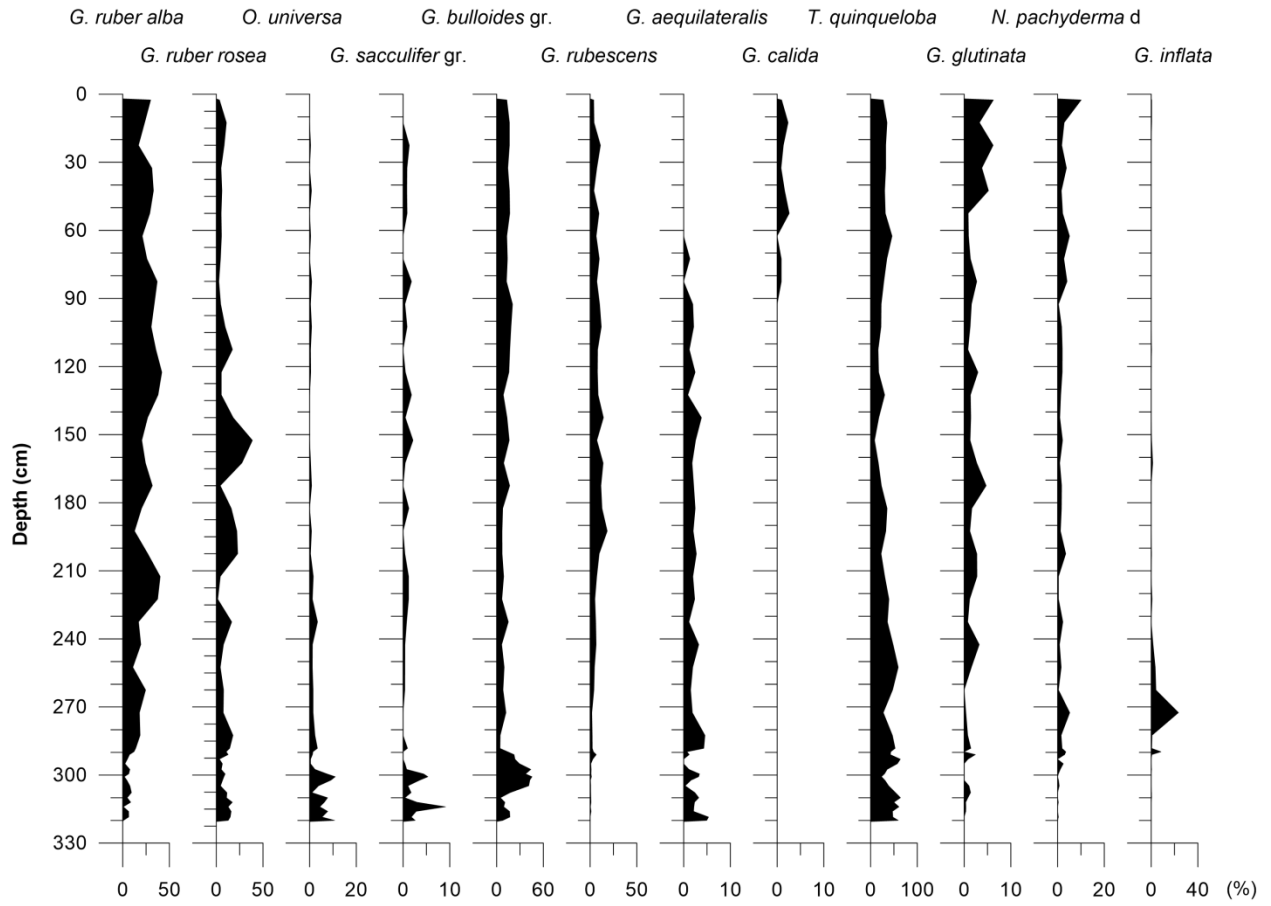


Fig. 11. Frequency curves of the most indicative planktonic foraminiferal species versus depth (in cm) in core AEX-23.

4.4.Pteropod Distribution Pattern

All samples also include aragonitic pteropods which indicate an excellent preservation regime along with the strong carbonate preservation potential of the eastern Mediterranean basin (Antonarakou et al., 2019; Schneider et al., 2007). A total of 13 species of Euthecosomata (*Heliconoides inflatus*, *Limacina trochiformis*, *Limacina bulimoides*, *Limacina retroversa*, *Creseis acicula*, *Creseis* sp., *Boasia chierchiae*, *Hyalocyclis striata*, *Styliola subula*, *Clio pyramidata* s.l., *Clio cuspidata*, *Diacria trispinosa*, *Cavolinia* spp.) were identified. Adult specimens, when present, were fragmented (*Cavolinia* spp., *C. pyramidata*, *C. trispinosa*). The protoconchs (*Clio*, *Diacria* and *Cavolinia*) made the identification of certain species and genera possible, as they were the only residue left. The down-core variation of their abundance is presented below.

KIM-2A

Within the basal part of the core sequence, the fauna is composed almost exclusively of the pteropod *L. retroversa*. An additional component is the species *C. pyramidata*, but with very low percentages (<3.5%). Between 153 cm to 127 cm the pteropodal fauna becomes more diverse with the species *H. inflatus*, *D. trispinosa*, *C. acicula*, and *B. chierchiae* appearing in the fauna. The relative abundance of *C. pyramidata* gradually increases (up to 45%), in contrast to the decline of *L. retroversa* (drops to ~40%). The latter disappears completely from the fauna at 105 cm. Between 109 cm and 85 cm the pteropod fauna consists mainly of *H. inflatus*, *C. acicula*, *C. pyramidata*, and *D. trispinosa*, with *L. bullimoides* appearing for the first time at 109 cm. The species *C. pyramidata* and *D. trispinosa* are decreasing up until the top of the core. In the last 85 cm of the core, *Cavolinia* spp. appears in the fauna, reaching its maximum abundance (58%) at 41.25 cm and 85.5 cm, with the species *H. inflatus* and *B. chierchiae* (15–58% and 3–40% respectively) as additional components. At 65.5 cm, *L. trochiformis* presents a short occurrence and between 65 cm and 60 cm *Creseis* sp. presents its maximum relative abundance (36%). Towards the top of the core *L. trochiformis* and *S. subula* present their highest percentages (~6% and 15% respectively) (Figure 12).

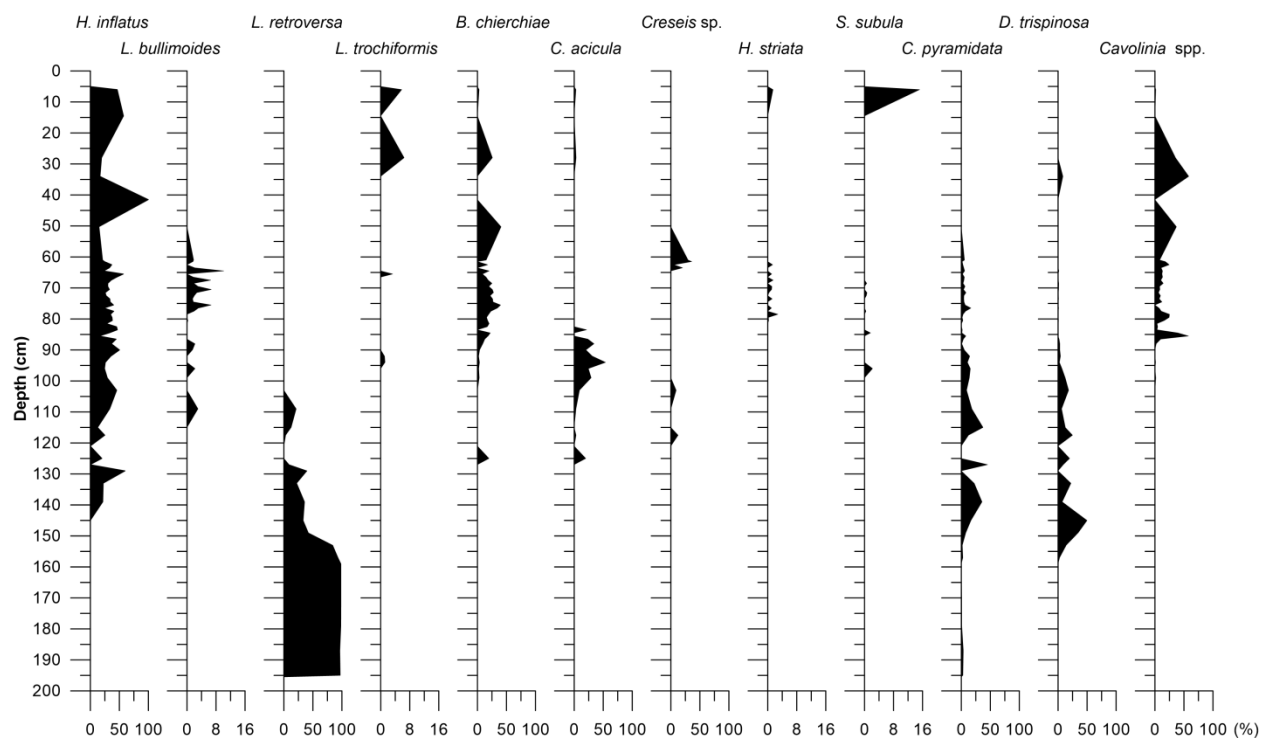


Fig. 12. Frequency curves of the pteropod species versus depth (in cm) in core KIM-2A.

Core AEX-15

In the interval between 173.5 cm to 164.5 cm of AEX-15 the pteropods *C. acicula*, *D. trispinosa*, *H. inflatus*, and *C. pyramidata* are present with high relative abundances. Low percentages of the species *B. chierchiae* (5%) and *Cavolinia* spp. (5%) are observed towards the end of this interval. Between 164.5 cm and 120 cm, the fauna is characterized by the high relative abundances in *H. inflatus* (79%), *B. chierchiae* (58%), and *Cavolinia* spp (22%). The species *C. pyramidata* and *D. trispinosa* decrease dramatically (0-6% and 0-11% respectively), while *C. acicula* after 156.5 cm is almost absent. From 120 cm to the top of the core, the pteropod fauna is more diverse. *H. inflatus*, *Cavolinia* spp., *B. chierchiae*, *C. clava*, and *C. pyramidata* present a continuous record. The species *L. trochiformis*, *S. subula* and *C. cuspidata* are the new components of the fauna. In five samples of the upper part of the core few specimens of the species *L. retroversa* are observed (Figure 13).

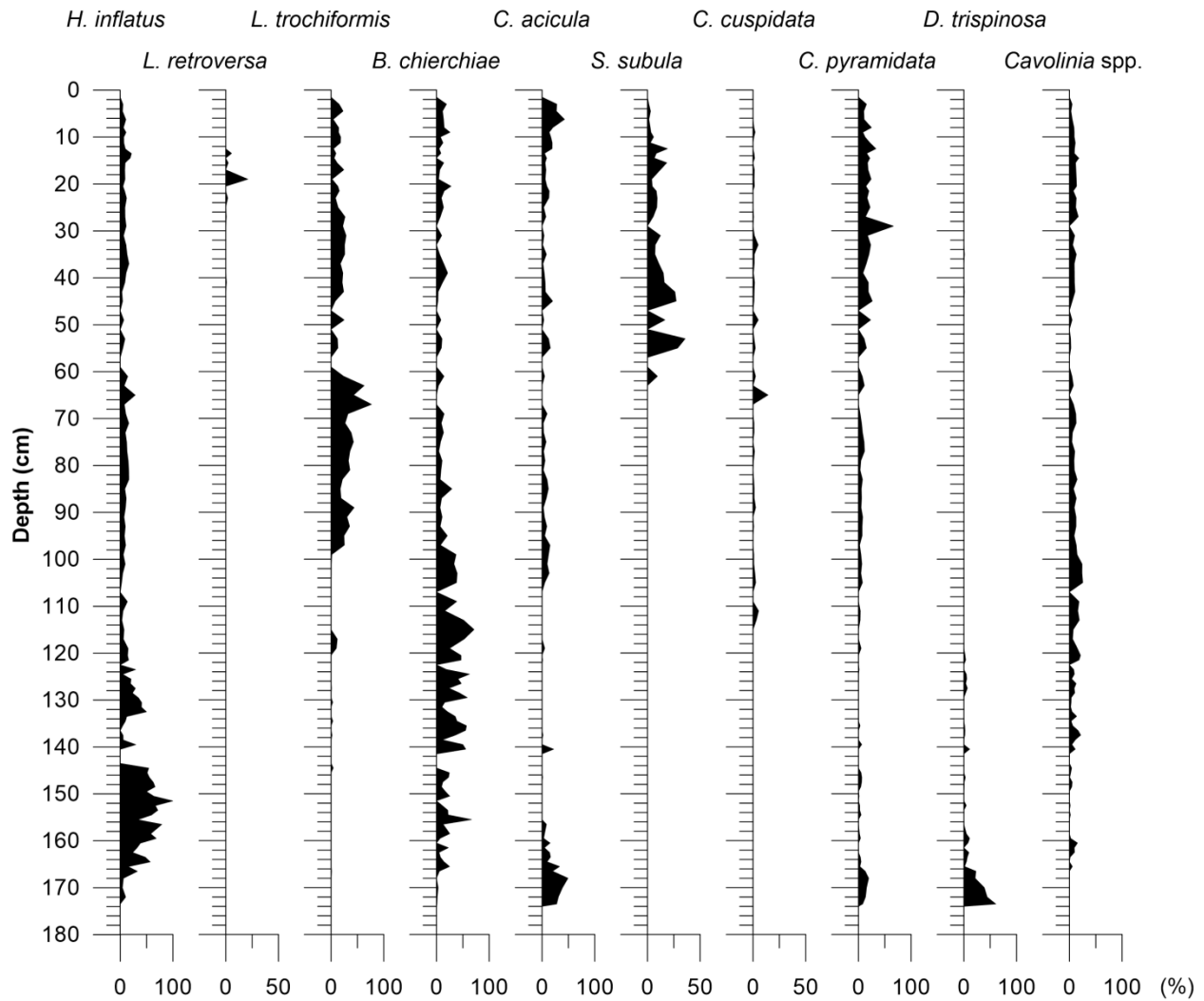


Fig. 13. Frequency curves of the pteropod species versus depth (in cm) in core AEX-15.

Core AEX-23

The down-core variation of the pteropod species of AEX-23 resembles that of the core AEX-15. Specifically, in the interval between 320 cm to 291 cm, which represent a part of the sapropel S1 layer, the fauna is similar with that of the equivalent interval of AEX-15 (approximately 130-120 cm). It consists of high percentages of *B. chierciae* (47%), *H. inflatus* (46%), and *Cavolinia* spp. (24%). Low relative abundances of the species *D. trispinosa* (14%), *L. trochiformis* (6%) are also recorded. From 291 cm to the top the fauna is more diverse. The species *B. chierciae*, *H. inflata*, *Cavolinia* spp., prevail with a continuous character. *C. acicula* presence is interrupted for 20 cm (272.5 – 252.5 cm), while the species *C. pyramidata*, and *C. cuspidata* are entering the fauna with a short delay and their percentages remain low (15% and 1.5% respectively). *L.*

trochiformis and *S. subula* are becoming components of the fauna much later (212.5 cm and 112.5 cm respectively). Here as well, few specimens of *L. retroversa* are observed at 142.5 – 112.5 cm, at 72.5 cm and 32.5 cm (Figure 14).

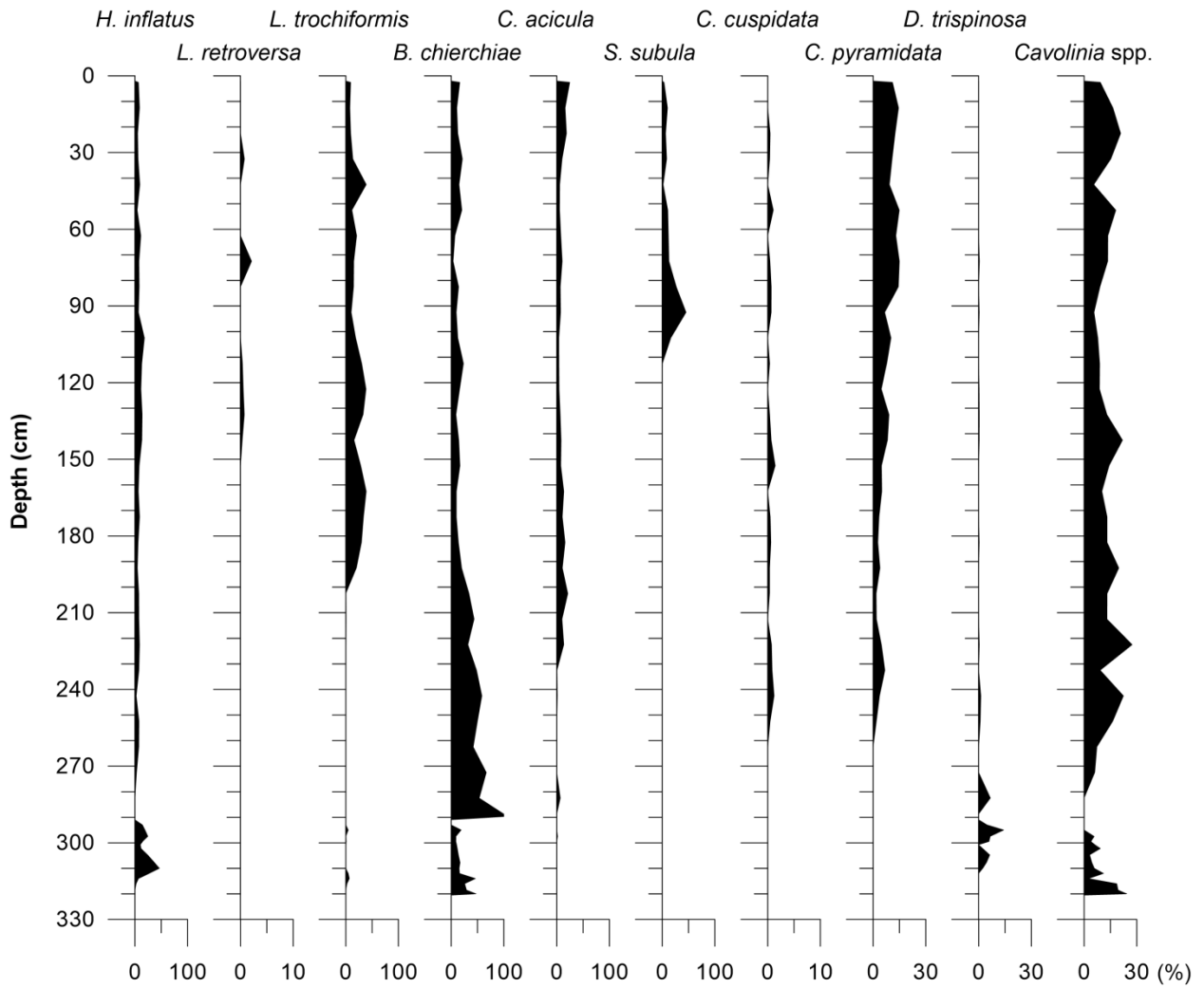


Fig. 14. Frequency curves of the pteropod species versus depth (in cm) in core AEX-23.

4.5. Total Organic Carbon and Stable Isotopes

KIM-2A

The organic carbon concentration (C_{org}) in KIM-2A generally exhibits values around 1% (Figure 15a). This pattern is interrupted in two intervals related to the sapropel sub-units deposition. The first interval (S1a; 89–64 cm) is characterized by high C_{org} concentration, ranging from 1.5% to 3.4%, and in the second interval (S1b; 52.5–40 cm), C_{org} concentration ranges from 1.8% to 2.4% (Figure 15a). Thus, the deposition of S1 sapropel layer started at 89 cm and terminated at 40 cm. The interruption of sapropel S1 layer (S1i) is detected between 64 cm and 52.5 cm, as suggested by the decline of the C_{org} content (~1.3%).

As shown in Figure 15a, between 196 cm and 159 cm, $\delta^{18}O_{G. ruber}$ values range from +2.9 to +3.2‰. From 157 cm to 115 cm, a depletion in $\delta^{18}O_{G. ruber}$ values is observed (up to +0.9‰) and persists until the 34 cm with even lower values. More precisely, the depleted values were recorded from two intervals (88.5–65.5 cm and 50.25–34 cm) with an average value of –0.08‰ and +0.25‰ respectively. In the interval corresponding to 66.5–61 cm, slightly heavier $\delta^{18}O_{G. ruber}$ values were observed (+0.6 to –0.1‰). In the final unit of the core, from 28 cm until the top, a core enrichment in $\delta^{18}O_{G. ruber}$ is recorded. The $\delta^{13}C_{G. ruber}$ values of KIM-2A core exhibit more scatter than the $\delta^{18}O$ records. In the basal part of the core (200 – 88 cm) values range between +1.3 to +0.2‰. In the interval between 88 cm and 61 cm the $\delta^{13}C_{G. ruber}$ ranges between 0.3 and 0.9‰ with the exception of three high-positive peaks at 80.5 cm, 73.5 cm, and 71.5 cm with values of 1.4‰, 1.2‰, and 1.3‰ respectively. From 50.25 cm to the top of the core, $\delta^{13}C_{G. ruber}$ exhibits heavier values with an average of +1.29‰ (Figure 15a).

AEX-15

In core AEX-15 C_{org} values range between 0.8% and 1.6% in the interval from 160 cm to 113 cm (Figure 16). In the rest of the samples C_{org} content does not exceed 0.5%. In the same core, from sample 172 cm to 130 cm, Ba_{ex} and Ba/Al ratio, exhibit a similar trend towards heavier values. From sample 130 cm up to 109 cm, Ba_{ex} values are decreasing. The same pattern follows Ba/Al ratio, from sample 120 cm to 109 cm. Towards the top of the analyzed interval the reduction in values of both curves is interrupted by heavier values in sample 107 cm (Figure 16).

Oxygen and carbon isotopic values are presented in Figure 15b. Oxygen isotopic values of *G. ruber* display considerable scatter in the intervals between 173.5 cm and 120 cm. Less variable and rather light values are observed in the part toward the top of the core. More explicitly, $\delta^{18}\text{O}_{G. ruber}$ values range from -2.86‰ to + 4.15‰ between 173.5 cm and 120 cm (Figure 15b), with the most significant enrichments to be recorded at 160.5 cm (3.24‰) and at 158.5 cm (4.15‰). At about 146 cm, a shift to heavier $\delta^{18}\text{O}$ values is observed (from 0.2‰ to 0.8‰) and is followed by a recovery of light values. The same pattern is observed again at 141 cm with $\delta^{18}\text{O}_{G. ruber}$ ranging from 0.1‰ to 0.9‰. Towards the top of the core, $\delta^{18}\text{O}_{G. ruber}$ is relatively stable (values around zero), with the only exceptions of three peaks (a negative -2.8‰ at 111 cm and two positives at 89 cm [+ 1.8‰] and at 43 cm [+ 1.29‰]).

The carbon isotope analyses ($\delta^{13}\text{C}_{G. ruber}$) exhibit more scatter (Figure 15b) than the $\delta^{18}\text{O}$ records, especially in the lower part of the core. Values of $\delta^{13}\text{C}_{G. ruber}$ show a gradual decrease up to 120 cm, culminating in a minimum at about 142.5 cm. The only exceptions in this interval are the following positive peaks: 160.5 cm (+1.2‰), 158.5 cm (+1.6‰), and 144.5 (+2.4‰). From 120 cm to the top of this core, the general trend shows values ranging from approximately + 0.3‰ to + 1‰ with two distinct negative excursions at 41 cm (-1.2‰) and at 111 cm (-1.1‰) along with a positive one at 45 cm (+2.2‰).

AEX-23

In core AEX-23 C_{org} values range between 0.6% to 1.6% in the interval from 320 cm to 272.5 cm (Figure 16). In the rest of the samples, C_{org} content does not exceed 0.6%. Ba_{ex} and Ba/Al ratio exhibit a similar increasing trend from sample 320 cm to 293 cm. From sample 293 cm up to 242.5 cm, Ba_{ex} values and Ba/Al ratio are decreasing. The same pattern continues towards the top of the analyzed interval with the exception of samples 232.5 cm and 202.5 cm.

Values of $\delta^{18}\text{O}$ present slight enrichment (-0.1‰ to + 1‰) between samples 320 cm and 291 cm. From this point on, $\delta^{18}\text{O}_{G. ruber}$ is relatively stable around zero, with the only exceptions of two positive peaks (+1.07‰ at 62.5 cm and + 1.34‰ at 2.5 cm) (Figure 15c). Between 320 cm and 291 cm $\delta^{13}\text{C}_{G. ruber}$ is depleted (from -0.6‰ to + 0.3‰). The interval between 288 cm and

212.5 cm is characterized by heavier values (average + 0.6‰). From 212.5 cm to the top, $\delta^{13}C_{G. \text{ruber}}$ exhibits slightly lighter values with a negative peak at 202.5 cm (-0.2‰) (Figure 15c).

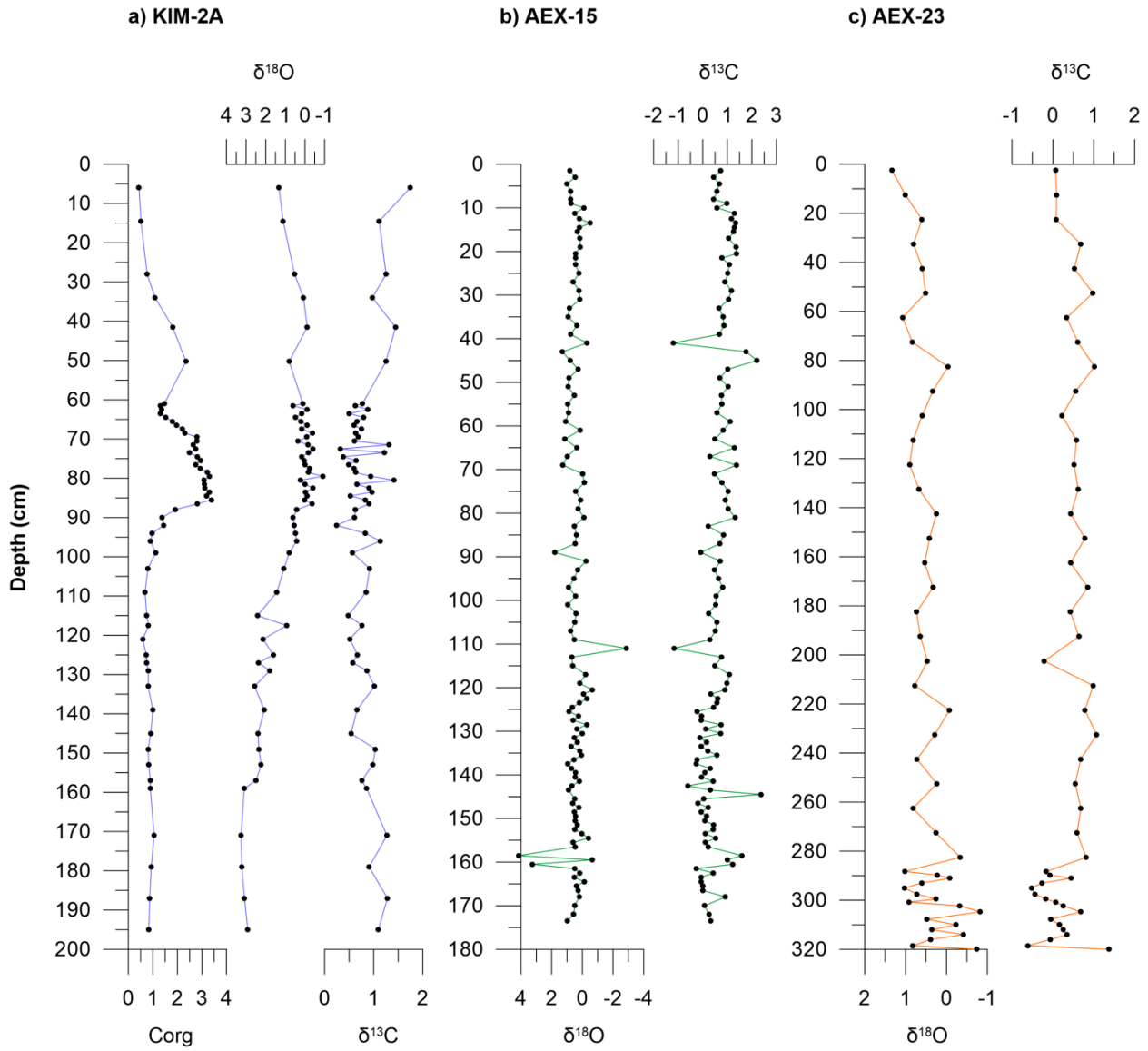


Fig. 15. C_{org} concentrations for KIM-2A, oxygen isotope record ($\delta^{18}O$) and carbon isotope ($\delta^{13}C$) in a) KIM-2A, b) AEX-15 c) AEX-23

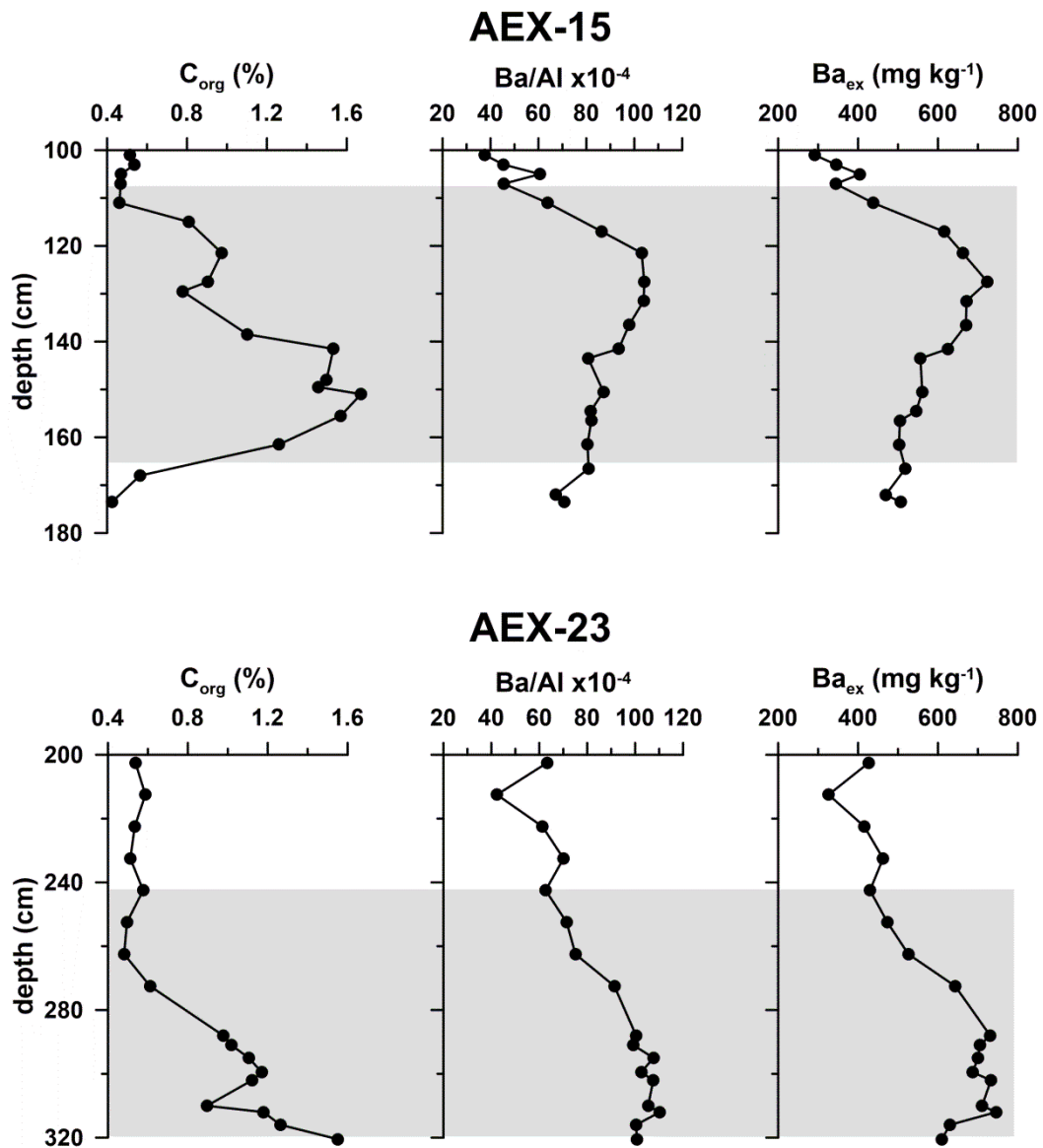


Fig. 16. C_{org} and Ba_{ex} concentrations and Ba/Al ratios for AEX-15 and AEX-23.

5. Age Model

In order to proceed in the time stratigraphic framework apart from the AMS ^{14}C datings, chronostratigraphic control points were used. Specifically, the planktonic foraminifera distribution pattern allowed identification of the biozone Ia/Ib, Ib/Ic, Ic/II and II/III boundaries of (Jorissen et al., 1993) which are useful chronologic standards for dating late Quaternary marine sequences in the central and eastern Mediterranean (including the Aegean Sea - Casford et al., 2002; Geraga et al., 2010; Kontakiotis, 2016; Zachariasse et al., 1997) due to their Mediterranean-wide applicability and synchronicity (Capotondi et al., 1999; Casford et al., 2001; Hayes et al., 1999). Furthermore, correlations are also suggested by variations of organic carbon (Corg) and major elements (Al) and barium (Ba), as they allowed the identification of the onset and termination of S1 layers (e.g., Casford et al., 2007; De Lange et al., 2008).

Identification of Biozone boundaries & Bioevents

In the south Aegean core KIM-2A, the interval between 196 cm and 153 cm is characterized by the dominance of *N. pachyderma*, *T. quinqueloba*, *G. scitula* and *G. glutinata* with additional components the species *G. ruber* f. *alba* and *G. bulloides* (Figure 17). This glacial fauna corresponds to biozone III and it has been recognized throughout the Mediterranean Sea (e.g., Casford et al., 2002; Geraga et al., 2010). The interval between 153 cm and 109 cm corresponds to biozone II and is characterized by high relative abundances of Neogloboquadrinids and *G. glutinata* and the presence of and *G. inflata* (Figure 17). In the lower part of this interval *G. ruber* f. *rosea* appears for the first time. Subzone Ic (109–40 cm) was identified by the warm subtropical species (*G. ruber* f. *rosea*, *G. siphonifera* gr. and *O. universa*). In addition, it includes abundant *G. bulloides* and *G. rubescens* specimens. The sharp increase in the abundance of *G. inflata* at 41.5 cm is inferred to mark the onset of the Ib subzone. The Ia/Ib boundary (at 20 cm) is marked by the decrease of the latter species along with the decrease in the *N. pachyderma* abundance (Figure 17). In this core the Bioevent “Start of $\delta^{18}\text{O}_{G. ruber}$ depletion T1a” of (Casford et al., 2002), was also detected at 159 cm.

In the north Aegean cores AEX-15 and AEX-23, subzone Ic (173 cm–120 cm, AEX-15) was identified by the warm subtropical species (*G. ruber* f. *rosea*, and *O. universa*) as well as by *T. quinqueloba* and *G. bulloides* (Figure 18a,b). The sharp increase in the abundance of *G. inflata*

and *N. pachyderma* at 120 cm in AEX-15 and at 291 cm in AEX-23 is inferred to mark the onset of the Ib subzone, whereas the Ia/Ib boundary is marked by their decrease (107 cm in AEX-15; Figure 18a, and 242.5 cm in AEX-23; Figure 18b). This subzone is also characterized by the maximum abundances of *G. ruber* f. *alba* and the sharp increase of *N. pachyderma* at the upper part. The re-entrance event of the pteropod *S. subula* at 61 cm in AEX-15 and at 112.5 cm in AEX-23 was also used (Buccheri et al., 2002; Giamali et al., 2019).

Determination of Sapropel Layers

Organic carbon content (C_{org}) in KIM-2A generally exhibits values around 1% (Figure 15a). This pattern is interrupted in two intervals related to the sapropel sub-units deposition. The first interval (S1a; 89–64 cm) is characterized by high C_{org} concentration, ranging from 1.5% to 3.4%, and in the second interval (S1b; 52.5–40 cm), C_{org} concentration ranges from 1.8% to 2.4% (Figure 15a). Thus, the deposition of S1 sapropel layer started at 89 cm and terminated at 40 cm. The interruption of sapropel S1 layer (S1i) is detected between 64 cm and 52.5 cm, as suggested by the C_{org} (~1.3%) (Figure 17).

In core AEX-15, although the onset of sapropel S1 (at 165 cm) is clearly depicted in organic carbon content (C_{org} sharp increase from background values, Figure 16), its termination is obscured by oxidation processes. In this case, Ba is a more reliable proxy to record the original thickness of the sapropel layer (De Lange et al., 2008). Therefore, the vertical distribution of C_{org} with respect to Ba/Al and Baex shows that sapropel S1 deposition commenced at 165 cm and terminated at 107 cm, with the sediments between 107 and 120 cm representing the oxidized sapropel (Figure 18a). In core AEX-23, elemental profiles corroborate termination at 242.5 cm, while the oxidation zone extends up to 291 cm, and the onset of S1 deposition is not reached in the core (Figure 18b).

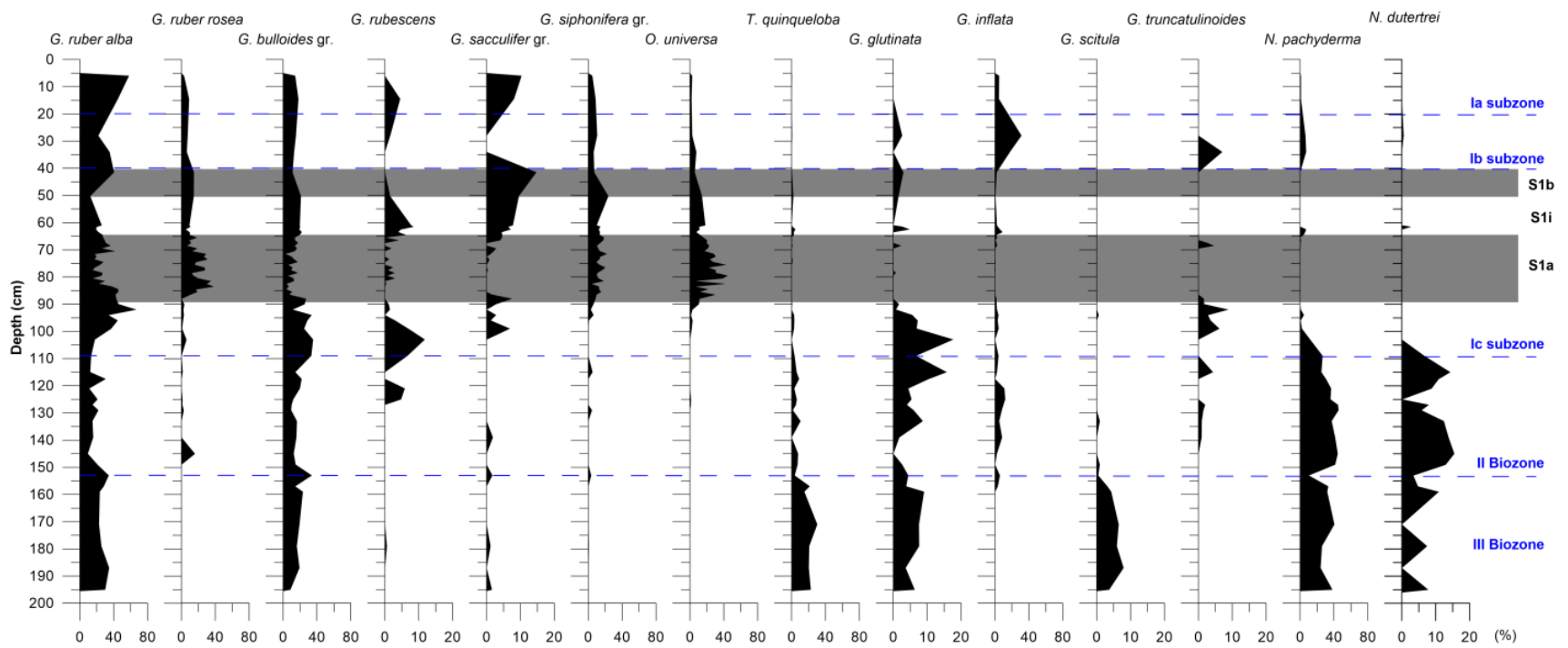


Fig. 17. Frequency curves of the most indicative planktonic foraminiferal species in core KIM-2A. The dashed blue lines represent the Ia/Ib, Ib/Ic, Ic/II and II/III boundaries, whereas the gray bands the sapropel S1 sublayers.

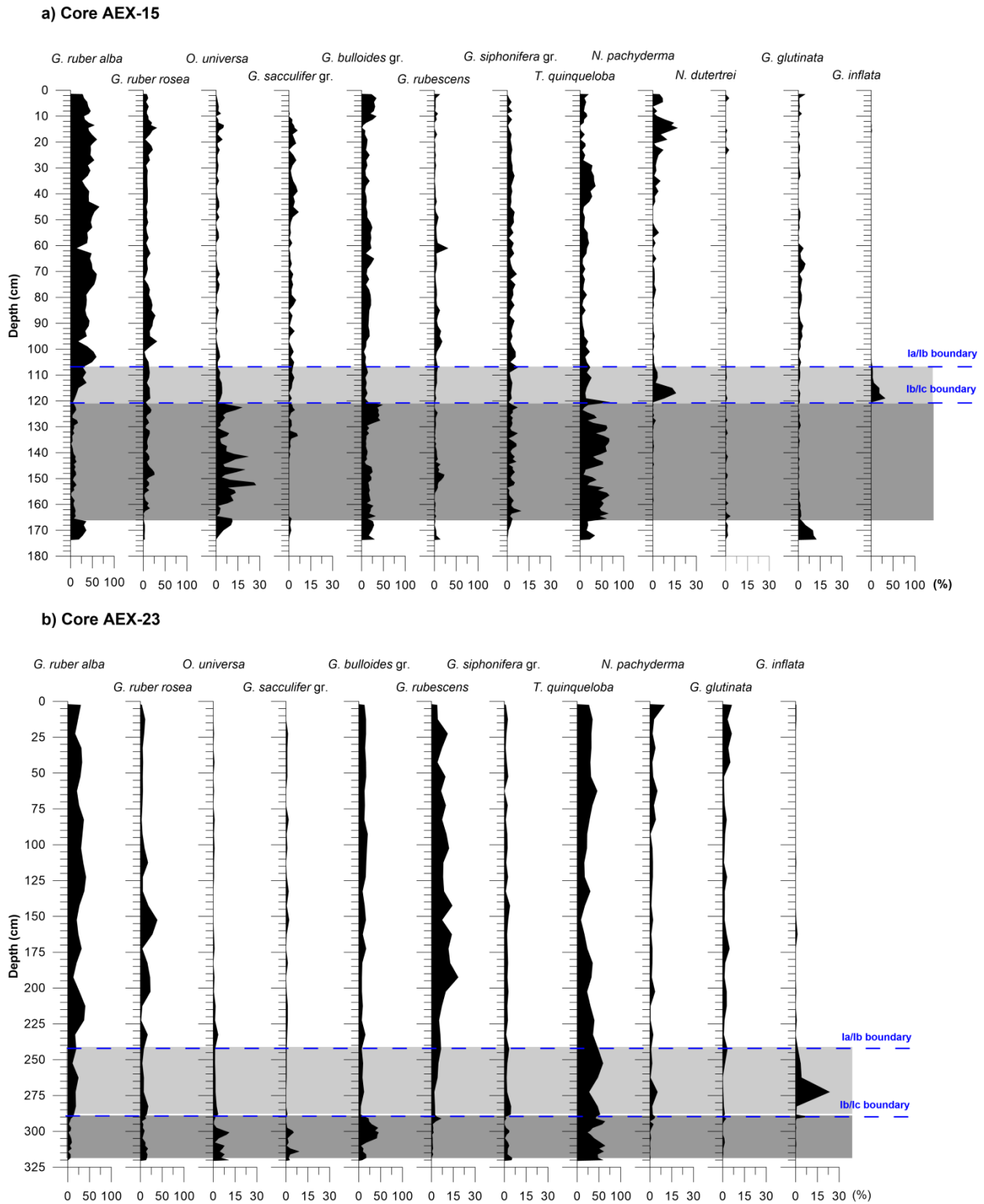


Fig. 18. Frequency curves of the most indicative planktonic foraminiferal species in core a) AEX-15 and b) AEX-23. The dashed blue lines represent the Ia/Ib and Ib/Ic boundaries and the gray and light gray bands the sapropel S1 layer and its oxidized part respectively.

Chronology

Chronology adopted in the core KIM-2A derived from a polynomial fit through the five AMS ^{14}C datings and the time markers correlative to the start and end of sapropel deposition, as well as the planktonic foraminiferal biozone Ia/Ib, Ib/Ic, Ic/II and II/III boundaries of Jorissen et al., (1993) (Table 2). The resulting age model is illustrated in figure 19 and is consistent with the multi-proxy chronological framework of (Casford et al., 2007) for the Aegean sediment cores, thus supporting the robustness of the chronology. For the ages of the onset and termination of sapropel deposition, the relevant ages from the nearby core NS-14 is used (Kontakiotis, 2016; Triantaphyllou et al., 2009a; Triantaphyllou et al., 2009b).

Table 2. Calibrated radiocarbon dates (AMS ^{14}C) and chronostratigraphic control points' dates for core KIM-2A. Control points' dates are after: a: (Jorissen et al., 1993); b: (Kontakiotis, 2016); c: (Triantaphyllou et al., 2009a); d: (Casford et al., 2002)

KIM-2A					
AMS & Chronostratigraphic Control Points	Depth (cm)	Conventional Radiocarbon Age (BP)	Two Sigma Calibrated Age Range (BP)	Mean Calibrated Age (ka BP)	References
Beta—425634	14.5	4890+/-30	4845–5325	5.08	
Ia/Ib boundary	20			5.2	a
Beta—425635	28	5320+/-30	5444–5855	5.65	
S1b top	40			6.4	b, c
Beta—425636	50.25	6790+/-30	7036–7292	7.16	
S1b base	52.5			7.3	b, c
S1a top	65.5			7.9	b, c
Beta—425637	79.5	8320+/-30	8532–8883	8.71	
S1a base	89			10	b, c
Ic/II boundary	109			11.3	a
II/III boundary	153			15.5	a
$\delta^{18}\text{O}_{G. ruber}$ depletion	159			15.9	d
Beta—425638	195	18890+/-70	21962–22508	22.24	

According to our proposed age model (Figure 19), the sedimentary horizons sampled in this study span the interval from the late glacial period, and the subsequent transition (Termination 1; T1) to the middle Holocene (Northgrippian stage) (i.e., ~5–21 ka BP). The average sedimentation rate is 11.86 cm/ka, and is in good agreement to those reported in the marginal Aegean basin (Aksu et al., 1995; Casford et al., 2002; Kontakiotis, 2016; Kuhnt et al., 2007). These sedimentation rates were derived from the age model, assuming that the sediment

accumulation has been moderately consistent throughout each interval. In particular, the average sedimentation rates are 8.10 cm/ka for the late glacial, 10.30 cm/ka for the Termination T1, and 16.46 cm/ka for the Holocene.

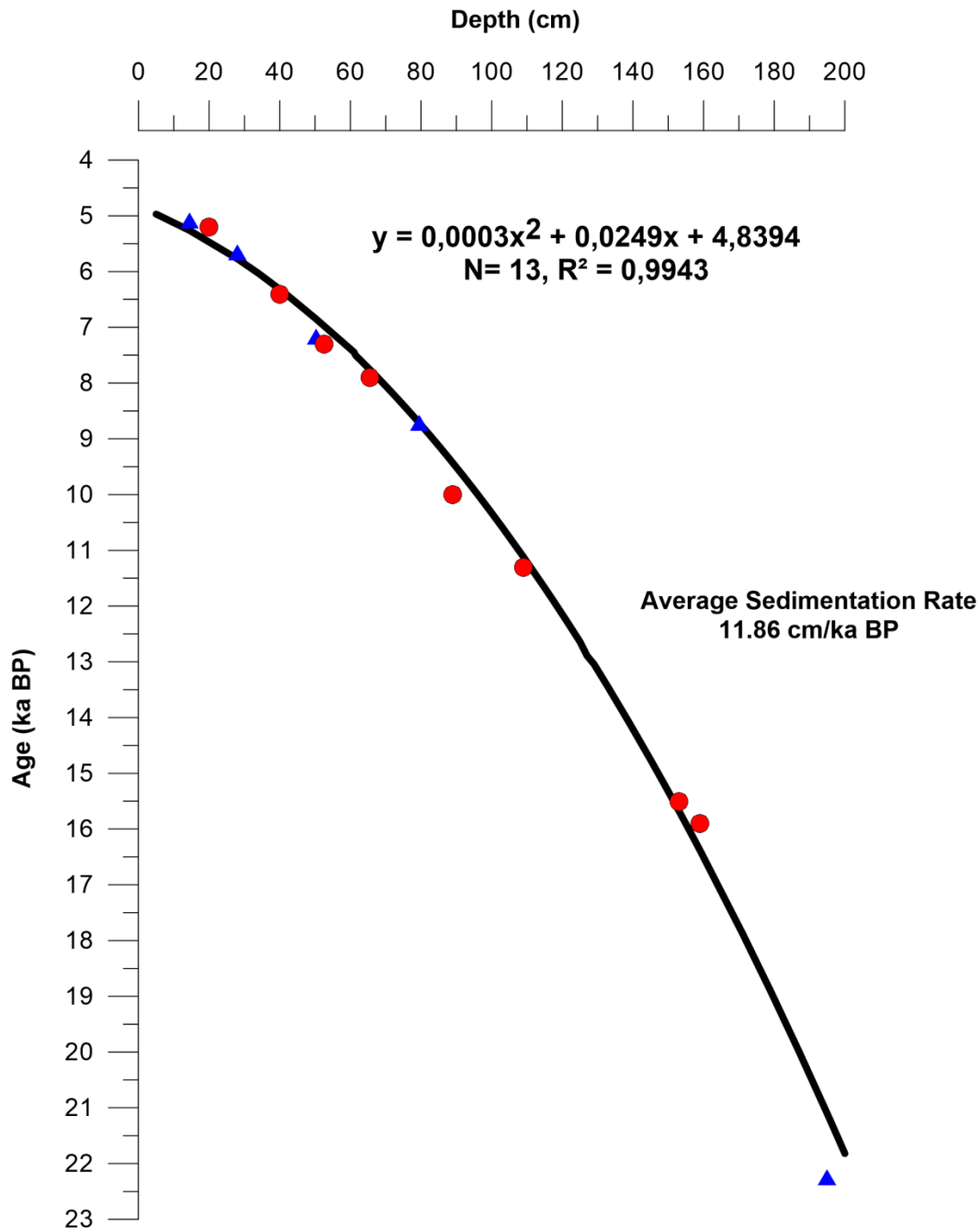


Fig. 19. Time stratigraphic framework of the core KIM-2A; blue triangles represent AMS ¹⁴C datings, whereas red dots represent control points and bio-litho-stratigraphic horizons used as stratigraphic markers.

Chronology adopted in the cores AEX-15 and AEX-23 is established by linear interpolation between all dating points. In addition to the AMS ^{14}C dates, the biostratigraphic control provides two well-dated correlation horizons, the biozone Ia/Ib and Ib/Ic boundaries of (Casford et al., 2002). For the ages of the onset of sapropel deposition, we have used the relevant ages from the nearby core (Geraga et al., 2010; Herrle et al., 2018; Kotthoff et al., 2008a) (Tables 3 and 4).

Table 3. Calibrated radiocarbon dates (AMS ^{14}C) and chronostratigraphic control points' dates for core AEX-15. a: (Buccheri et al., 2002); b (Casford et al., 2002); c: (Casford et al., 2007); d: (Kotthoff et al., 2008a); e: (Geraga et al., 2010); and f: (Herrle et al., 2018)

AEX-15					
AMS & Chronostratigraphic Control Points	Depth (cm)	Conventional Radiocarbon Age (BP)	Two Sigma Calibrated Age Range (BP)	Mean Calibrated Age (ka BP)	References
Beta—425626	45	2580+/-30	1940–2393	2.2	
<i>Styliola subula</i> re-entrance event	61			3.3	a
Beta—425627	103	5170+/-30	5276–5645	5.5	
Ia/Ib & top of Ba anomaly	107			6.1	b, c
Ib/Ic	120			7.0	b
Onset of S1	165			9.6	d, e, f

Table 4. Calibrated radiocarbon dates (AMS ^{14}C) and chronostratigraphic control points' dates for core AEX-23. Control points' dates are after: a: (Buccheri et al., 2002); b (Casford et al., 2002); c: (Casford et al., 2007)

AEX-23					
AMS & Chronostratigraphic Control Points	Depth (cm)	Conventional Radiocarbon Age (BP)	Two Sigma Calibrated Age Range (BP)	Mean Calibrated Age (ka BP)	References
<i>Styliola subula</i> re-entrance event	112.5			3.3	a
Beta—425628	212.5	4890+/-30	4811–5264	5.1	
Ia/Ib & top of Ba anomaly	242.5			6.1	b, c
Ib/Ic	291			7.0	b

Based on the adopted chronostratigraphic framework, sediment levels used in this study span the last 10.1 ka BP for core AEX-15 and 7.5 ka BP for AEX-23, with an average sedimentation rate of 17.3 and 42.8 cm/ka, respectively (Figure 20). These rates assume that the sediment accumulation has been consistent throughout each interval, and they are in good agreement to

those reported in the north Aegean Sea (>20 cm/ka; (Kontakiotis, 2016; Kotthoff et al., 2008a; Kotthoff et al., 2008b; Kuhnt et al., 2007; Zachariasse et al., 1997). The differing rates between the two cores expresses the heterogeneity of sedimentation rates previously documented in the north Aegean Sea (Roussakis et al., 2004), resulting from large seafloor topographic contrasts and variable sedimentary processes in the study area. In particular, the higher sedimentation rate of core AEX-23 is explained by the adjacent slope that transports sedimentary inputs by deep bottom currents.

The age model was applied in the downcore graphs for both faunal groups, in order to proceed in the interpretation of our results in respect with time. Thus, the downcore distribution of pteropods and planktonic foraminifera for the totality of the cores, it is shown in Figures 21 – 26.

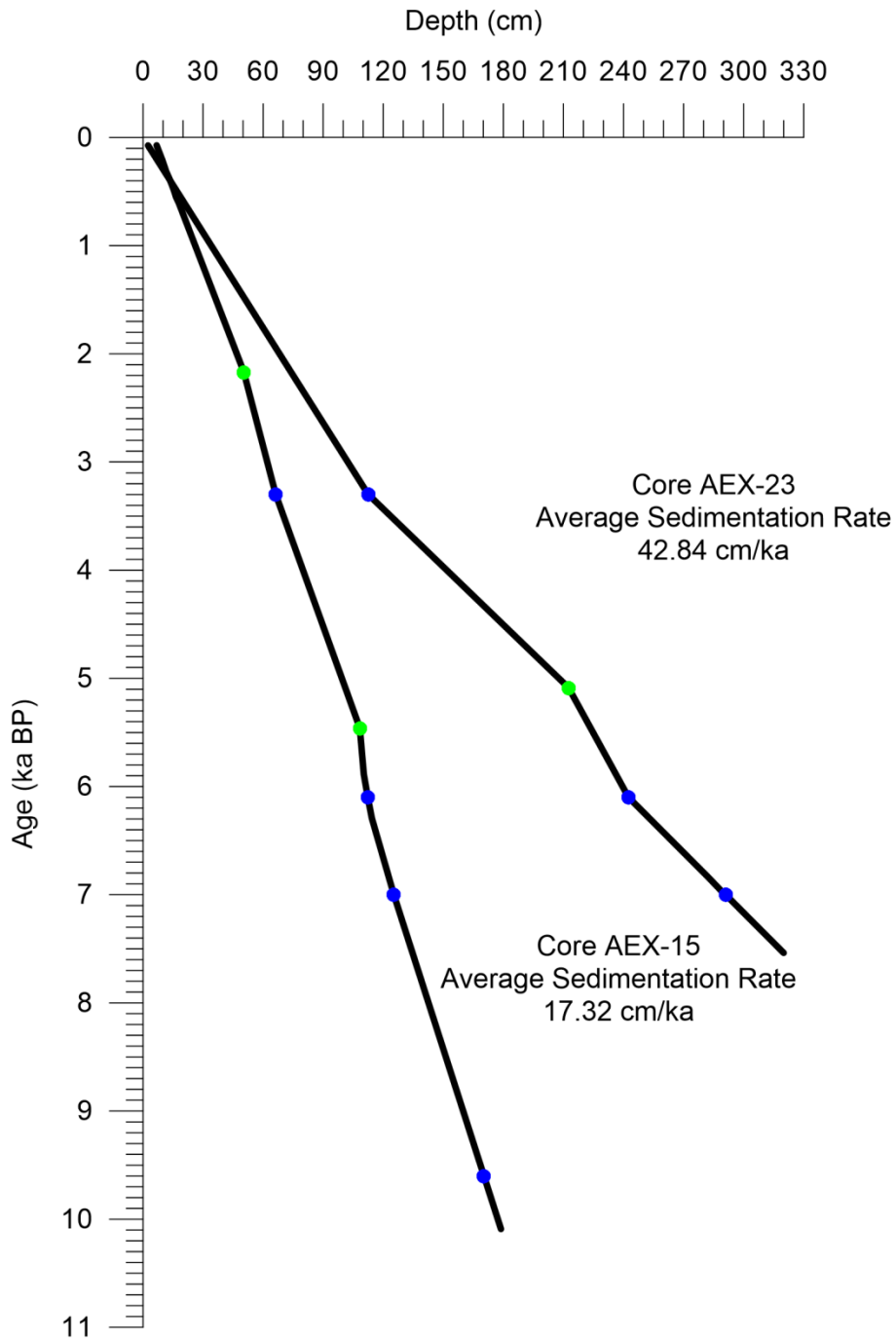


Fig. 20. Time stratigraphic framework (age model and mean sedimentation rates) of the cores AEX-15 and AEX-23. Blue dots represent control points and bioevents, whereas green dots represent accelerator mass spectrometry (AMS) ¹⁴C datings.

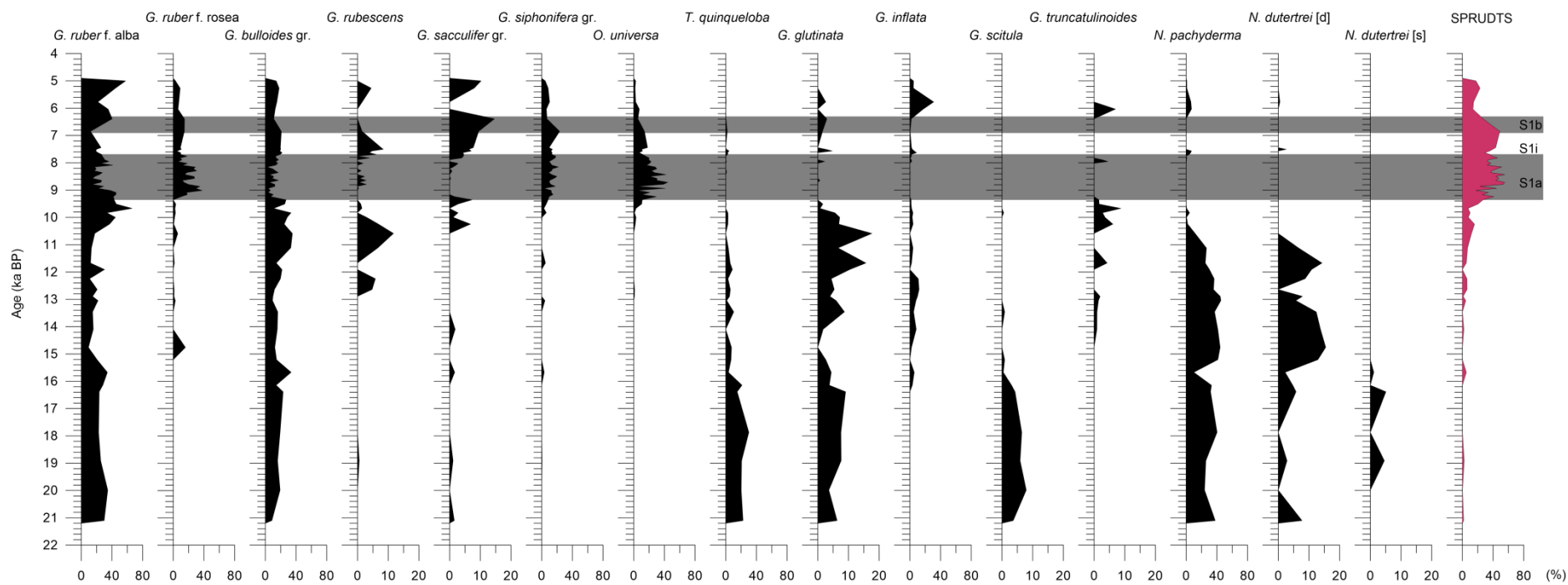


Fig. 21. Downcore variation of selected planktonic foraminifera in core KIM-2A versus age in ka BP. Gray bands represents the sapropel S1 sublayers.

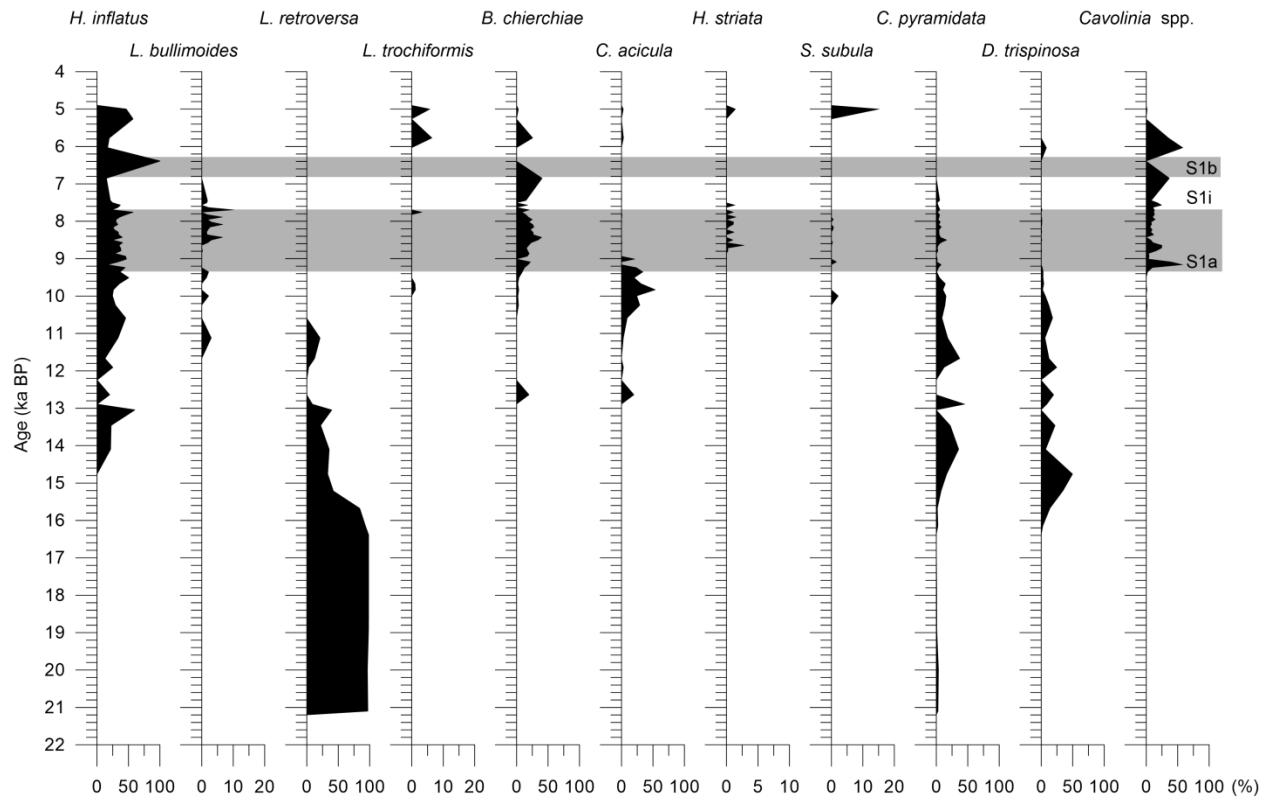


Fig. 22. Downcore variation of pteropods in core KIM-2A versus age in ka BP. Gray bands represents the sapropel S1 sublayers.

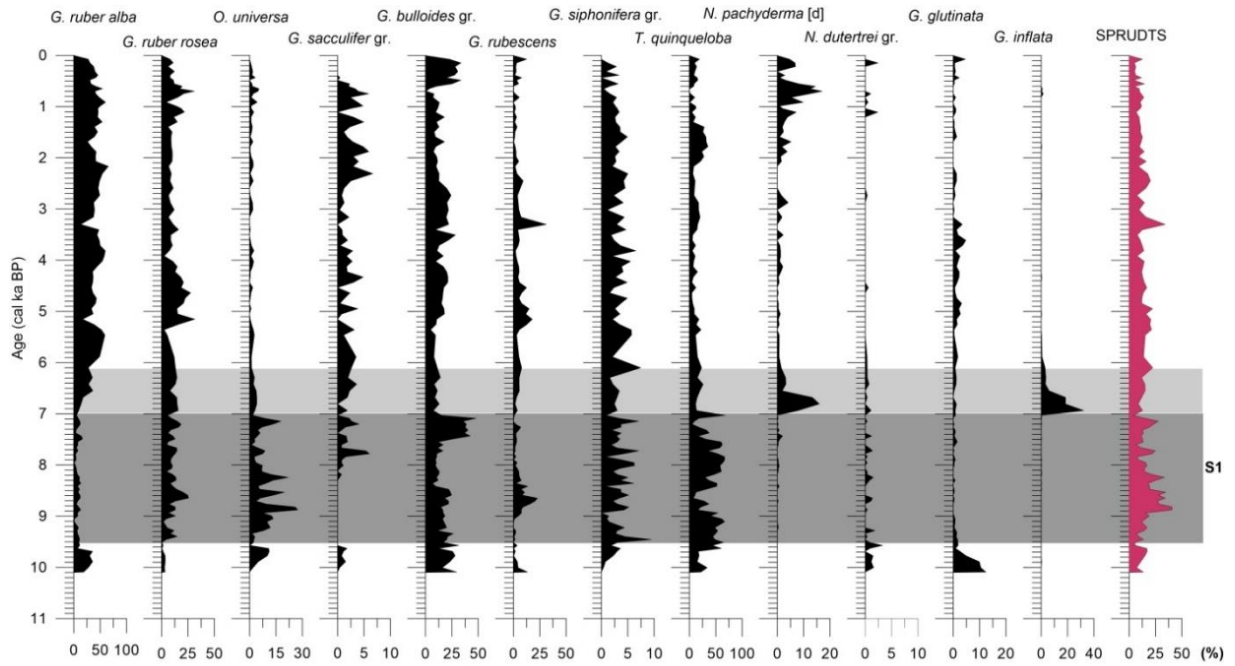


Fig. 23. Downcore variation of selected planktonic foraminifera in core AEX-15 versus age in ka BP. Gray and light gray bands represent the sapropel S1 layer and its oxidized part respectively.

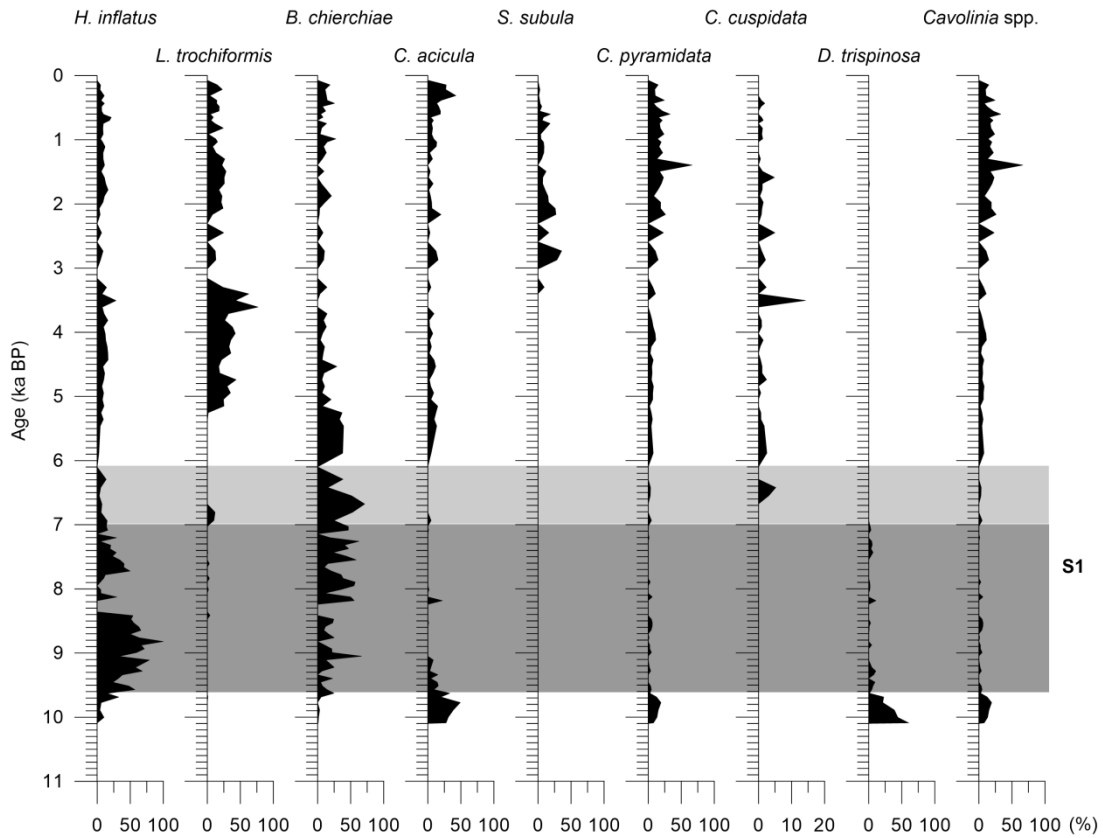


Fig. 24. Downcore variation of pteropods in core AEX-15 versus age in ka BP. Gray and light gray bands represent the sapropel S1 layer and its oxidized part respectively.

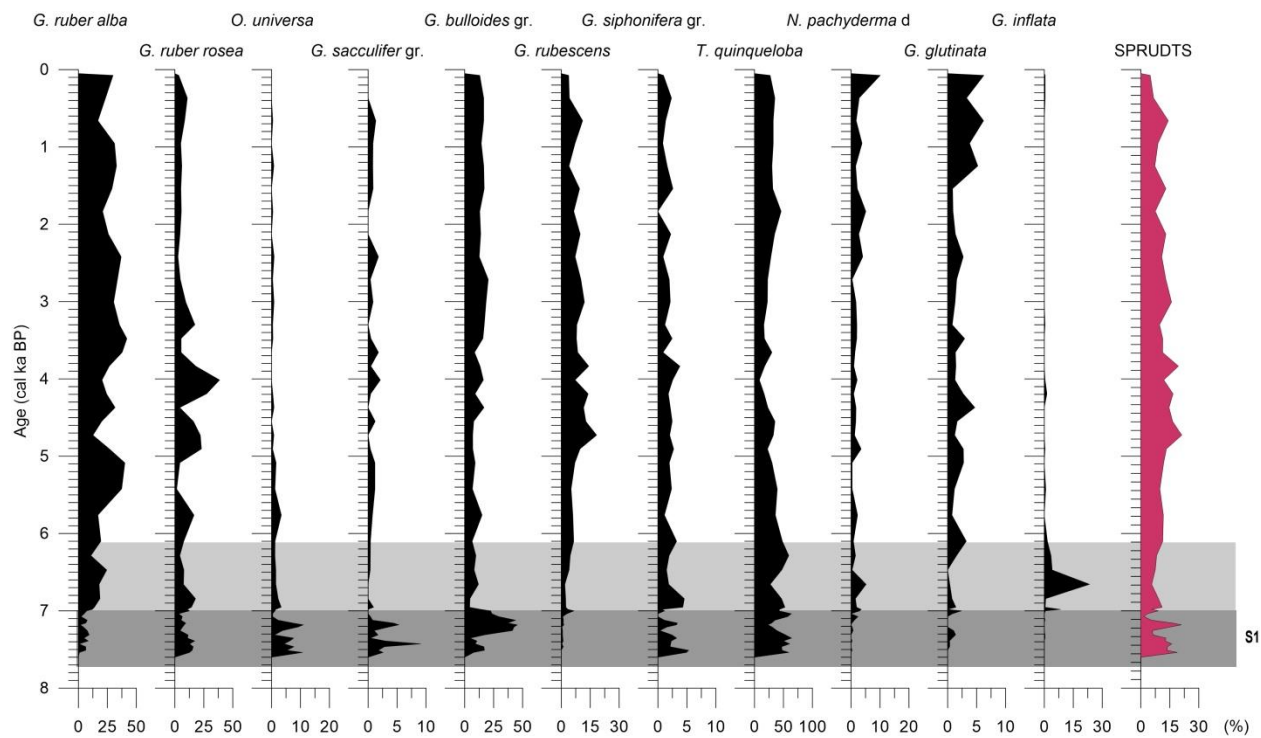


Fig. 25. Downcore variation of selected planktonic foraminifera in core AEX-23 versus age in ka BP.

Gray and light gray bands represent the sapropel S1 layer and its oxidized part respectively.

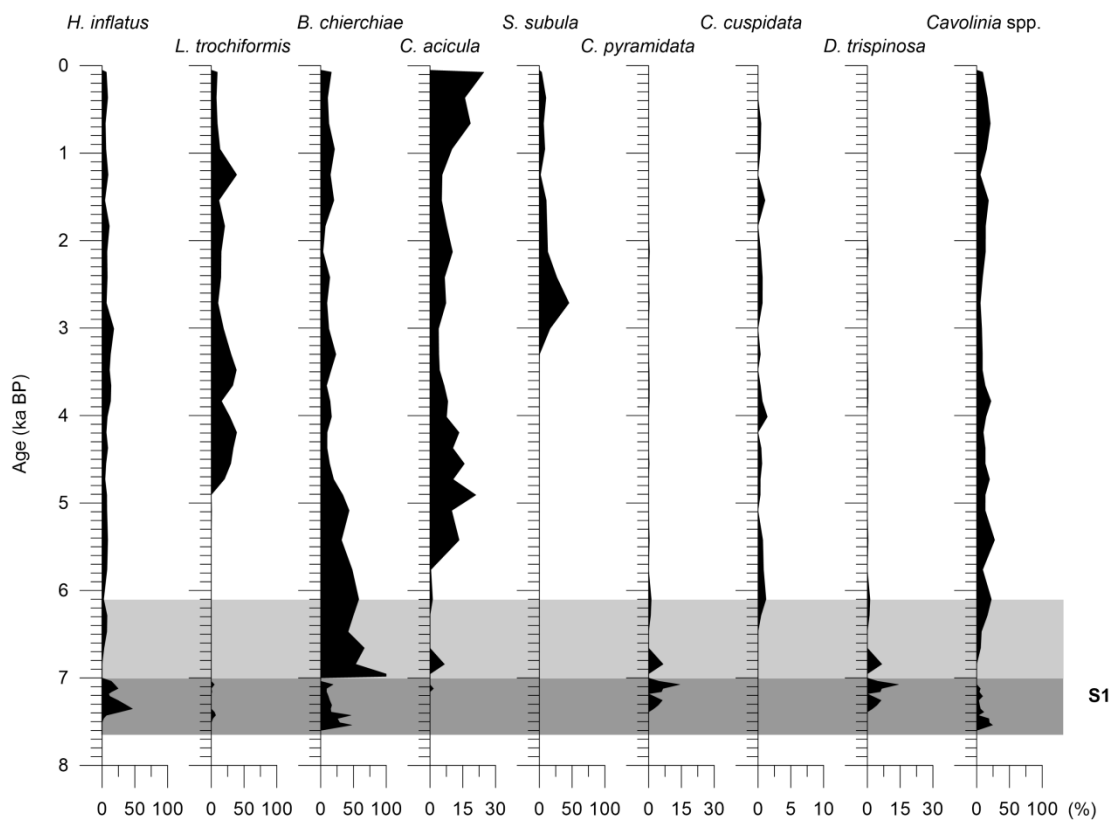


Fig. 26. Downcore variation of pteropods in core AEX-15 versus age in ka BP. Gray and light gray bands represent the sapropel S1 layer and its oxidized part respectively.

6. Multivariate statistical analyses

From the row data of the micropalaeontological analysis, multivariate statistical analyses were performed, in order to detect factors controlling the planktonic foraminifera and pteropod assemblages. Q-mode cluster analysis was used to determine the overall statistical similarity between samples, following the algorithms of (Davis, 1988) using the correlation coefficient matrix. The results of cluster analysis were reported as Euclidean, Gower distances (KIM-2A, AEX-23 respectively) and Moristita similarity (AEX-15), and arranged in two-dimensional hierarchical dendrograms, wherein locations were presented along the Y-axis while similarity level is plotted on the X-axis. Principal Component Analyses (PCA) is used to reduce the dimensionality of a multivariate data set to a few principal factors that determine the distributions of species. The resulting factor scores show the contribution of each factor in every sample and therefore the down-core contribution of each factor. The total number of factors was defined by minimizing the remaining “random” variability and by the possibility to relate the factors to modern hydrographic conditions and planktonic foraminiferal ecology.

6.1.Q-mode Cluster Analysis

Two and three distinct assemblages of planktonic foraminifera were identified by Q-mode cluster analysis in the south and north Aegean respectively, reflecting different biotopes during the late Quaternary. Each assemblage is characterized by the dominant species and named after it.

South Aegean (KIM-2A)

Biotope I (assemblage *N. pachyderma*): it contains 18 samples (from 103 cm to 195 cm; Figure 27) which represent the lower part of the core that corresponds to the deglaciation period. This assemblage is dominated by *N. pachyderma* (up to 44%) and can be separated into two sub-assemblages Ia and Ib based on the *T. quinqueloba* percentages. Ia sub-assemblage contains nine samples (115 cm and 121 – 149 cm; Figure 27) and corresponds to the T1. Besides *N. pachyderma* the species *G. ruber alba* (20%), *G. bulloides* (19%), *N. dutertrei* (15%), *G. inflata* (11%), *T. quinqueloba* (< 10%) and *G. glutinata* (8%) occur, indicating the existence of eutrophic, low-salinity, well-stratified environment (Geraga et al., 2010; Kontakiotis, 2016; Rohling et al., 1993b; Vergnaud-Grazzini et al., 1977). Ia sub-assemblage consists of a well-developed DCM layer, in which enhanced production can be realized by shoaling of the

thermocline to a depth that falls well within the euphotic layer. Ib sub-assembly consists of seven samples (sample 117.5 cm and 157 cm to 195 cm; Figure 27) and corresponds to the late glacial period. In this sub-assembly apart from the high abundance of *N. pachyderma*, *T. quinqueloba* plays a significant role (20-30%). *Neogloboquadrina pachyderma* in particular, is associated with a well- developed Deep Chlorophyll Maximum (DCM) in regions where the shallow nutricline favors its formation at the base of the euphotic zone (Fairbanks and Wiebe, 1980). Both species of this sub-assembly (Ib) characterize cold water conditions and together with other typical cold – water species (e.g., *G. glutinata*, *G. scitula*) reflect the presence of particularly cold and eutrophic water masses in the south Aegean Sea (Casford et al., 2002; Geraga et al., 2005).

Biotope II (assembly *G. ruber alba*): it contains 40 samples that represent the upper part of the core (sample 153 cm, samples between 6 cm – 99 cm; Figure 27) in which *G. ruber alba* is dominant. Biotope II can be separated into three sub-assemblies depending on the relative abundances of species involved. The sub-assembly IIa corresponds to the pre- and post-sapropel intervals containing 12 samples (Samples: 6 cm, 14.5 cm, 28 cm, 34 cm, 41.5 cm, 88 – 99 cm, 153 cm; Figure 27). Apart from *G. ruber alba* which is the dominant species, *G. bulloides*, *G. inflata* and SPRUDTS group are also present indicating an oligotrophic to mesotrophic environment. A seasonal pattern is detected as species indicative of stratified water column (*G. ruber alba*, SPRUDTS) coexist with species indicative of homogenous water column (*G. bulloides* and *G. inflata*). The branch IIb corresponds to the sapropel S1a and S1b layers with 28 samples being involved (Samples: 50.25 cm, and 61 cm – 86.5 cm; Figure 27). This sub-assembly is characterized by high percentages of both varieties of the species *G. ruber*. Species of the SPRUDTS group are also abundant with *O. universa* as its main component (up to 44%). All these species suggest a warm oligotrophic environment with a highly stratified water column. The presence of the mesotrophic to eutrophic *G. bulloides* (~15%) into this sub-assembly could be attributed to the increased riverine inputs in the surficial waters (Geraga et al., 2005, 2008, 2010; Rohling et al., 1997; Zachariasse et al., 1997).

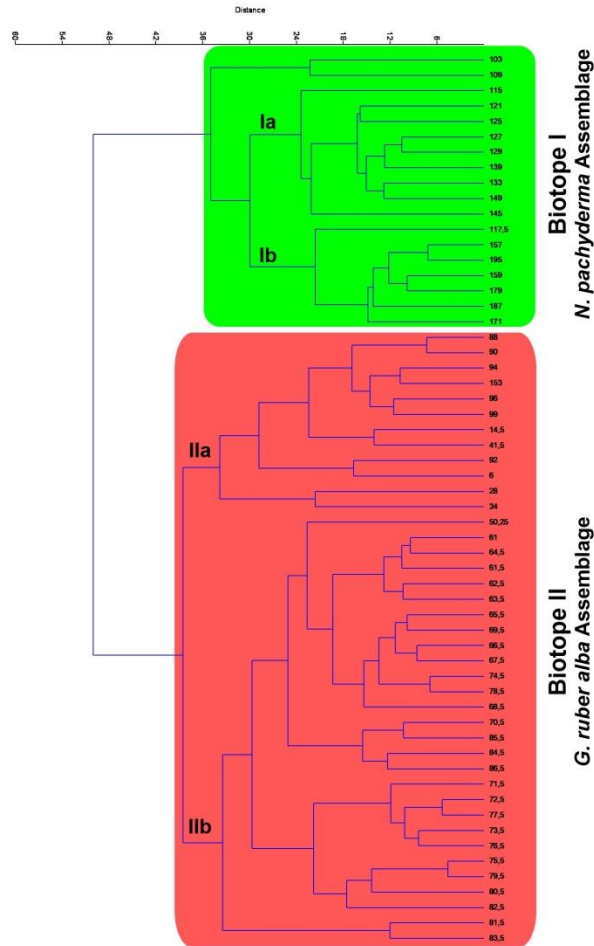


Fig. 27. Dendrogram resulting from Q-mode cluster analysis and the biotopes identified in core KIM-2A.

North Aegean AEX-15 & AEX-23

Biotope I (Assemblage *T. quinqueloba*): In the core AEX-15 it contains 48 samples (samples 61 cm, 97 cm and samples between 120 cm to – 166 cm; Figure 28). Apart from samples 61 and 97, the rest 45 samples correspond to the sapropel S1 layer. The same pattern is observed in core AEX-23. It contains 16 samples (samples between 293 cm – 320 cm and the samples 282.5 cm and 288.95 cm; Figure 29) 14 of which correspond to the sapropel S1 layer and the other two, to its oxidized part. This assemblage is dominated by *T. quinqueloba* (average 43% in AEX-15 and average 47% in AEX-23), an eutrophic species preferring low salinities. In the eastern Mediterranean it has been recorded to thrive in sapropelic layers, attributed to low salinity and

perhaps high fertility of the surficial waters (De Rijk et al., 1999; Geraga et al., 2010; Rohling et al., 1997; Zachariasse et al., 1997). In this assemblage *G. bulloides* also occur with high percentages (50% in AEX-15 and 45% in AEX-23). This species lives in the surface or subsurface waters withstanding large fluctuations in temperature, salinity and density of the water column and is associated to seasonal upwellings (Rohling et al., 1993b). In north Aegean though, it has been documented that *G. bulloides* along with *T. quinqueloba* into the S1 are related to low salinity and high fertility of the surficial waters (Kontakiotis, 2016; Rohling et al., 1997; Zachariasse et al., 1997), possibly due to the larger river inflows draining the north Aegean land. In additions, the warm oligotrophic *G. ruber rosea* and SPRUDTS group occur abundantly. Their abundance is mainly controlled (beyond temperature) by the stratification of the water column (Rohling et al., 1997). They occur close to the surface, where solar radiation is maximized, and in the low fertility mixed layer, characterized by a strong vertical stratification of surface waters during the summer months (Hemleben et al., 1989). Thus, Biotope I can be interpreted as an environment with increased riverine inputs that supply nutrients and making the surficial water less saline.

Biotope II (assemblage *G. inflata*): in core AEX-15 this biotope contains 3 samples (115 cm, 117 cm, 119 cm; Figure 28) whilst in AEX-23 only one (272.5 cm; Figure 29). The dominant component of this assemblage is *G. inflata* (32% in AEX-15 and 23% in AEX-23). *Globorotalia inflata* is temperate species indicative of homogenous water column that prefers to live at the bottom of thermocline depths (Hemleben et al., 1989). Additional components of this assemblage are the species *N. pachyderma*, *G. ruber alba*, *G. ruber rosea*, *T. quinqueloba* and *G. bulloides* (percentages around 13% each). *Neogloboquadrina pachyderma* thrives in cool water close to or below the thermocline. Its abundance is related to the development of a DCM (Fairbanks and Wiebe, 1980). This biotope represents an environment with seasonal contrast as warm species (*G. ruber* f. *alba*, *G. ruber* f. *rosea*) are found along with cold ones (*N. pachyderma*, *T. quinqueloba*) with a deep mixed layer that lies above a well – developed DCM.

Biotope III (Assemblage *G. ruber alba*): in core AEX-15 this biotope contains 65 samples (from 113 cm -1.5 cm and from 166.6-173.5 cm; Figure 28) whilst in AEX-23 it contains 29 (262.5 cm to 2.5 cm and samples 289.75 cm and 291 cm; Figure 29). In both cases this assemblage corresponds mostly to the post sapropel S1 interval apart from the samples between 166.5 cm –

173.5 cm of AEX-15, which derive from the pre-sapropel interval. This assemblage is characterized by the predominance of the warm, oligotrophic *G. ruber alba* (an average percentage of 40% in AEX-15 and 30% in AEX-23). Next in abundance are the eutrophic *G. bulloides* and *T. quinqueloba* the former being more abundant in AEX-15 whereas the latter in AEX-23. *Globigerinoides ruber rosea*, *G. rubescens* and *N. pachyderma* [d] are also present in both cores but with significantly lower percentages. In this biotope simultaneously occur oligotrophic species (*G. ruber alba*, *G. ruber rosea*, and *G. rubescens*) and eutrophic (*G. bulloides*, *T. quinqueloba* and *N. pachyderma*) indicating a seasonal contrast in productivity probably related to the food availability. Seasonality is also reinforced by the continuous presence of *G. glutinata* (average 1.1% in AEX-15 2.2% in AEX-23), since this species can survive both in oligotrophic surface, and in more eutrophic waters by changing its diet from diatoms to crysophytes (Hemleben et al., 1989). Moreover, the findings suggest a seasonal contrast in temperature as warm species (*G. ruber alba*, *G. ruber rosea*, and *G. rubescens*) coexist with the cool ones (*T. quinqueloba* and *N. pachyderma*).

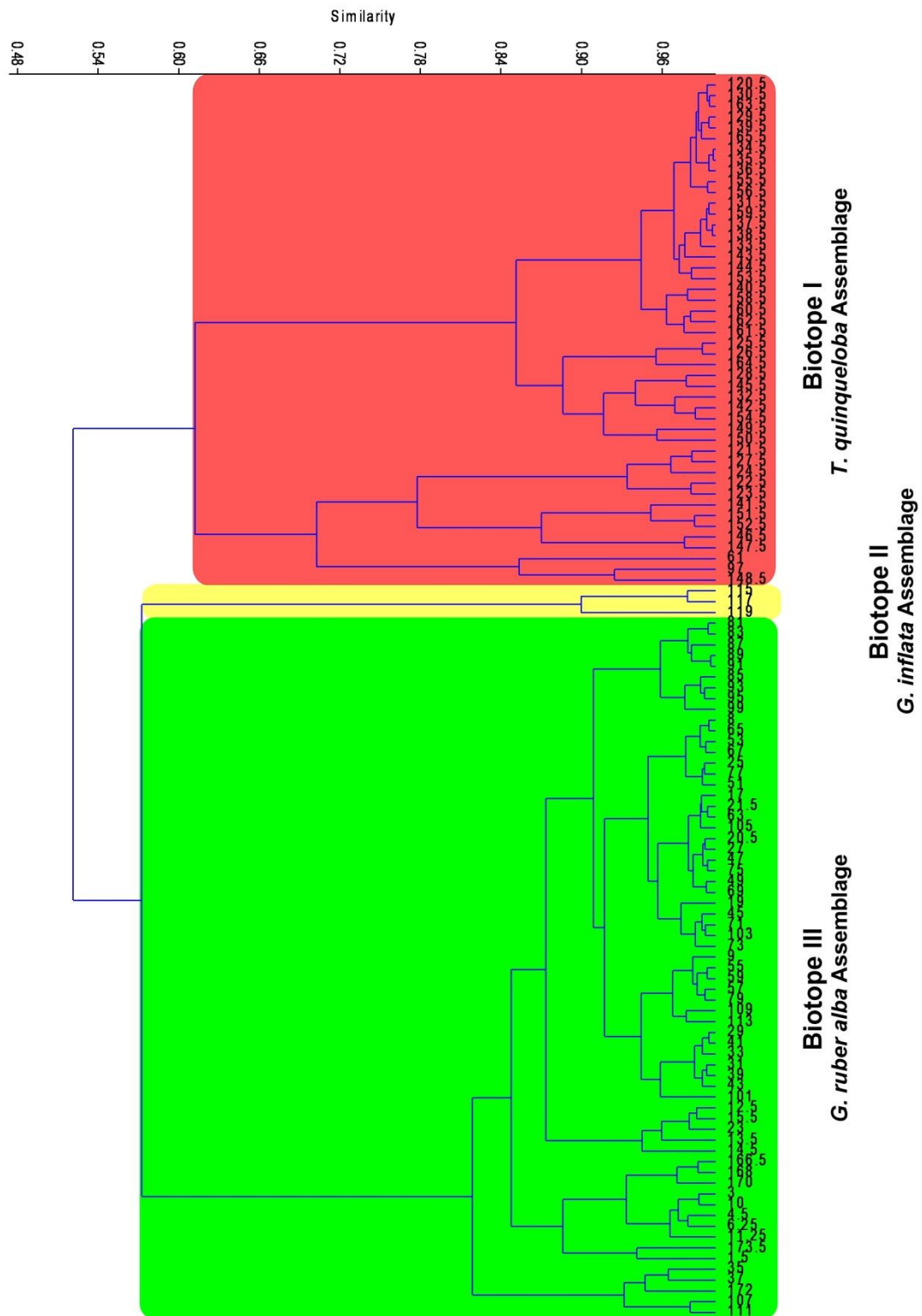


Fig. 28. Dendrogram resulting from Q-mode cluster analysis and the biotopes identified in core AEX-15.

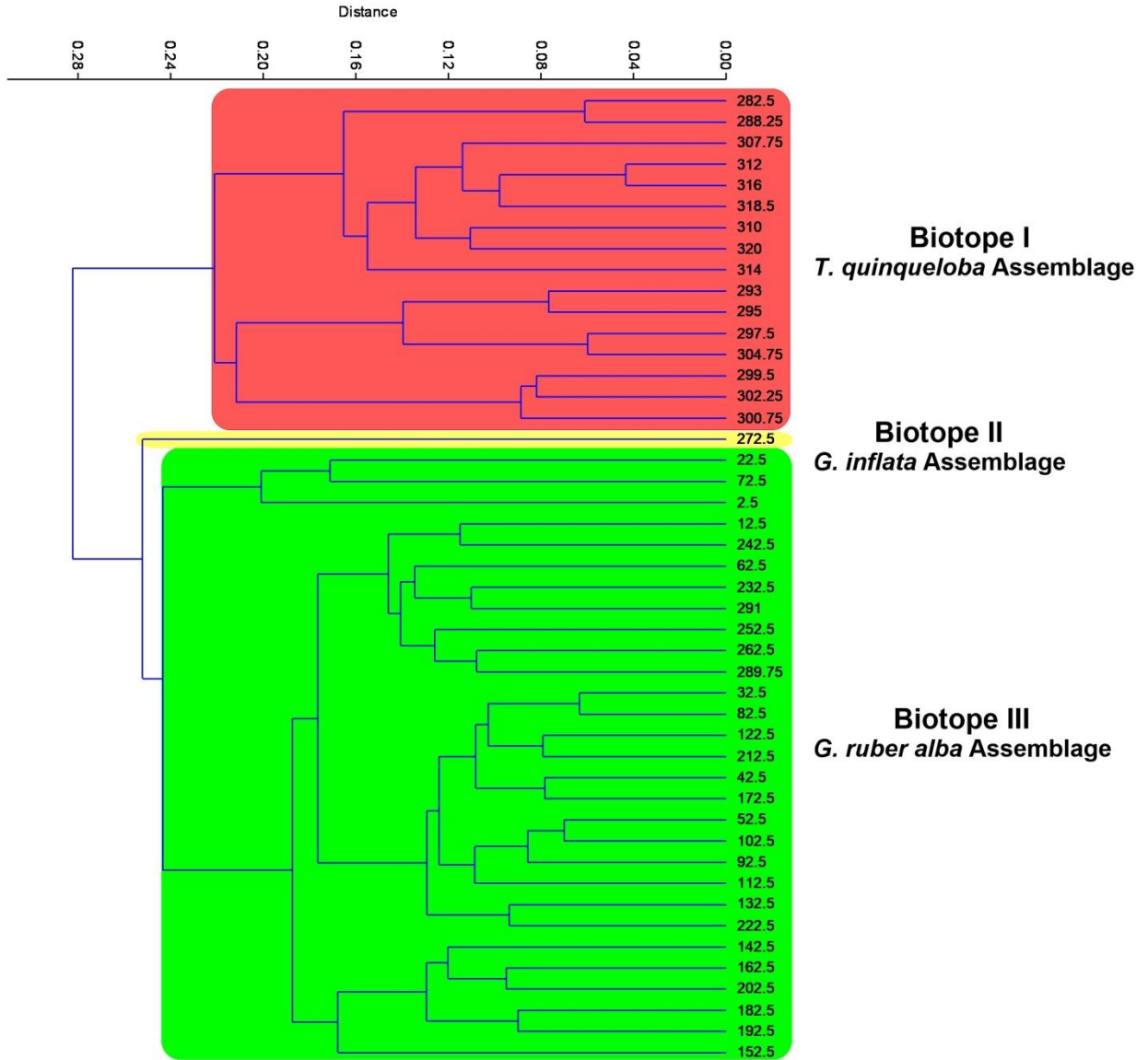


Fig. 29. Dendrogram resulting from Q-mode cluster analysis and the biotopes identified in core AEX-23.

6.2. Principal Component Analysis (PCA)

A standardized principal component analysis (PCA) was carried out on the total data set using the varimax method, in order to determine the impact of various environmental parameters on the planktonic distribution. The application of this statistical analysis yielded a three-factor model for both planktonic foraminiferal and pteropod communities in north and south sub-basins. The interpretation of the three components in each case was based on the screen plots of eigen values, and the factor loadings of the planktonic foraminiferal and pteropod species respectively. The distinguished factors with their factor loadings showing the contribution of each factor in every sample and therefore the down-core contribution of each factor (Figures 30–32). In the case of a bipolar factor, which has extremes of positive and negative loadings, high positive factor scores are related to the positive pole and high negative scores to the negative pole, respectively. They account for 81.57% and 82.81%, of the total variance in the south (KIM-2A) for the planktonic foraminiferal and pteropod respectively, 90.94% and 79.46% for the north Aegean core AEX-15 and 92.25% and 85.46% for north Aegean core AEX-23 (planktonic foraminiferal and pteropod respectively) (Tables 5,7,9,11,13,15). Finally, a comparison between the two planktonic groups was made, in order to investigate whether factors controlling pteropod distribution differ from planktonic foraminifera.

6.2.1. Planktonic Foraminifera

South Aegean – KIM-2A

Table 5. PCA factors based on planktonic foraminifera and their percentages of the total variability for core KIM-2A.

KIM-2A			
PCA factors	Eigenvalue	% variance	Cumulative % of the total variance
1	432.137	50.256	50.256
2	193.038	22.449	72.705
3	76.2131	8.8632	81.568
4	53.3399	6.2032	87.771
5	38.4841	4.4755	92.247
6	24.4952	2.8487	95.096
7	15.5611	1.8097	96.905
8	7.97016	0.92689	97.832

9	7.63218	0.88759	98.720
10	5.03693	0.58577	99.306
11	2.88765	0.33582	99.641
12	2.25794	0.26259	99.904
13	0.666282	0.077486	99.981
14	0.159802	0.018584	100.000

The first varimax factor (PCA1) accounts for 50.26% of the total variance (Table 5) and is interpreted as **Temperature** factor (Figure 30a). In detail, the species with positive loadings (*N. pachyderma*, *T. quinqueloba*, *N. dutertrei*, *G. glutinata*, *G. inflata*, *G. bulloides*, and *G. scitula*; Table 6) thrive in cold – water masses, while the species with negative loadings (*O. universa*, *G. ruber rosea*, *G. siphonifera* gr., and *G. ruber alba*; Table 6) in warm – water conditions. Factor PCA2 accounts for 22.5% of the total variance (Table 5) with positive loadings being expressed by species living in a highly stratified water column (*O. universa*, *G. ruber rosea* and neogloboquadrinids; Table 6) (Hemleben et al., 1989; Rohling et al., 1997). The main representative species of the negative pole are *G. ruber alba* and *G. bulloides* gr., and are species typical of weak development of these conditions. *G. bulloides* is associated with warm water and oligotrophic conditions and is indicative of upwelling, strong seasonal mixing or fresh water inputs (Rohling et al., 1993b). Therefore, the second varimax factor (PCA2) is referred to as the **Stratification** factor (Figure 30b). The third varimax factor (PCA3) describes 8.9% of the total variance (Table 5), and also display a bipolar character, with its positive pole to be represented mainly by *G. ruber* f. *alba* and *N. pachyderma* and the negative pole by *G. bulloides* (Table 6). The above species that characterize the PCA3 factor are the main exponents of the seasonal contrasts governing planktonic foraminiferal assemblages in the Mediterranean Sea during the last glacial cycle (Goudeau, 2015; Wilke et al., 2009; Wit et al., 2010). Thus, the third varimax factor (PCA3; Figure 30c) is referred to as a **Seasonality** factor.

Table 6. Ranking of the planktonic foraminiferal species and their factor loadings along the PCA factors in core KIM-2A. Bold data indicate the most important factor loadings in each factor (red for negative; black for positive values).

Species	Factor 1	Factor 2	Factor 3
<i>O. universa</i>	-0.511	0.363	0.194
<i>G. ruber alba</i>	-0.158	-0.776	0.443
<i>G. ruber rosea</i>	-0.375	0.302	0.101
<i>G. sacculifer</i>	-0.028	-0.091	-0.122
<i>G. siphonifera</i> gr.	-0.251	0.099	-0.152
<i>G. inflata</i>	0.079	-0.020	-0.136
<i>G. bulloides</i>	0.094	-0.199	-0.691
<i>G. rubescens</i>	0.008	-0.012	-0.209
<i>N. pachyderma</i>	0.643	0.320	0.305
<i>N. dutertrei</i>	0.155	0.100	0.051
<i>T. quinqueloba</i>	0.197	0.001	0.258
<i>G. truncatulinoides</i>	0.007	-0.060	0.004
<i>G. glutinata</i>	0.129	-0.014	-0.110
<i>G. scitula</i>	0.032	-0.009	0.064

Core AEX-15

Table 7. PCA factors based on planktonic foraminifera and their percentages of the total variability for core AEX-15.

AEX-15			
PCA factors	Eigenvalue	% variance	Cumulative % of the total variance
1	622.458	67.949	67.949
2	142.717	15.579	83.528
3	67.9386	7.4164	90.944
4	27.039	2.9517	93.896
5	22.7885	2.4877	96.384
6	17.852	1.9488	98.333
7	6.21708	0.67867	99.011
8	3.39922	0.37107	99.382
9	2.74832	0.30001	99.682
10	1.76144	0.19228	99.875
11	0.784001	0.085584	99.960
12	0.342134	0.037348	99.998
13	0.0172397	0.0018819	99.999

The first varimax factor (PCA1) accounts for 67.95% of the total variance (Table 7) and it exhibits a bipolar character with the negative pole dominated by the eutrophic species *T. quinqueloba* (Lourens et al., 1992; Thunell, 1978), while the positive pole is dominated by the oligotrophic *G. ruber* f. *alba* (Table 8). Therefore, this factor is interpreted as **Productivity** indicator (Figure 31a). The second factor (PCA2) explains 15.58% of the total variance (Table 7). It is characterized by positive values of the surface dwellers *G. ruber* f. *alba* and *T. quinqueloba*. The latter is tolerant to fairly low salinity and/or enhanced fertility in surficial waters (Rohling et al., 1993b), whereas the former is also indicative of stratified water column (Kontakiotis, 2016). Negative loadings are dominated mainly by the species *G. bulloides* gr., which is highly dependent on enhanced food levels; upwelling, strong seasonal mixing or freshwater inputs (Lourens et al., 1992; Reiss et al., 1999; Rohling et al., 2004). Thus, the PCA2 factor is referred to as the **Stratification** factor (Figure 31b). The third varimax factor (PCA3) accounts for the 7.4% of the total variance (Table 7) and is interpreted as **Upwelling** indicator

(Figure 31c). This is due to its main positive representative, *G. bulloides* (Table 8), which is directly associated with seasonal upwelling (Rohling et al., 1993b). On the other hand, the negative loadings are represented mainly by the species *G. ruber* f. *rosea*, a warm subtropical species, whose abundance is mainly controlled by the stratification of the water column (Rohling et al., 1997).

Table 8. Ranking of the planktonic foraminiferal species and their factor loadings along the PCA factors in core AEX-15. Bold data indicate the most important factor loadings in each factor (red for negative; black for positive values).

Species	Factor 1	Factor 2	Factor 3
<i>O. universa</i>	-0.084	-0.170	-0.137
<i>G. ruber alba</i>	0.670	0.569	0.256
<i>G. ruber rosea</i>	0.077	-0.209	-0.515
<i>G. sacculifer</i>	0.027	0.033	-0.027
<i>G. inflata</i>	0.002	-0.044	-0.183
<i>G. bulloides</i>	-0.024	-0.536	0.734
<i>G. rubescens</i>	0.011	-0.158	-0.155
<i>G. aequilateralis</i>	-0.002	0.001	-0.023
<i>G. calida</i>	0.006	0.032	0.000
<i>N. pachyderma</i>	0.050	-0.004	-0.155
<i>N. dutertrei</i>	-0.003	-0.006	-0.001
<i>T. quinqueloba</i>	-0.731	0.536	0.159
<i>G. glutinata</i>	0.008	-0.005	0.063

Core AEX-23

Table 9. PCA factors based on planktonic foraminifera and their percentages of the total variability for core AEX-23.

AEX-23			
PCA factors	Eigenvalue	% variance	Cumulative % of the total variance
1	297.508	52.429	52.429
2	148.072	26.094	78.523
3	77.9132	13.73	92.253
4	16.8919	2.9768	95.230
5	11.6111	2.0462	97.276
6	7.02929	1.2387	98.515
7	4.3437	0.76547	99.280
8	1.62484	0.28634	99.567
9	1.26568	0.22305	99.790
10	0.797468	0.14053	99.930
11	0.357763	0.063047	99.993
12	0.039244	0.0069158	100.000

The first factor (PCA1) accounts 52.43% of the total variance (Table 9) with positive loadings defined mainly by the eutrophic surface dweller *T. quinqueloba* which is indicative of cool waters (Pujol and Vergnaud-Grazzini, 1995) and secondary by the species *G. bulloides* gr., *O. universa*, and *G. sacculifer* (Table 10). The presence of species such as *T. quinqueloba* and *G. bulloides* indicates that the surface mixed layer became more eutrophic, and can be attributed to the shoaling of the pycnocline due to winter mixing and upwelling. On the contrary, the negative loadings are defined mainly by *G. ruber* f. *alba*, followed by *G. rubescens*, *G. ruber* f. *rosea*, and *G. glutinata*, indicative of warm oligotrophic surface waters (Pujol and Vergnaud-Grazzini, 1995; Thunell, 1978). Thus, the first factor PCA1 is interpreted as **Productivity** indicator (Figure 32a). The second factor (PCA-2) accounts 26.09% for the total variance (Table 9). Positive pole is mainly represented by *G. bulloides* gr., a eutrophic species associated with seasonal upwelling (Rohling et al., 1993b). Species representing negative loadings are mainly the *T. quinqueloba*

and *G. ruber alba* (Table 10). Thus, the PCA2 factor is referred to as the **Upwelling** indicator (Figure 32b).

The third factor (PCA3) accounts 13.73% for the total variance (Table 9). The positive loading species (*G. ruber rosea*, SPRUDTS) indicate a warm and strongly stratified water column, which characterizes most of the Holocene, and especially the sapropel S1. Their abundance is mainly controlled by the thermal stratification of the water column (Rohling et al., 1997). The negative loadings in contrast, include species typical of the weak development of the stratified conditions (main species: *G. ruber* f. *alba*, *G. bulloides* gr., and *T. quinqueloba*; Table 10). Henceforth, PCA3 is referred to as the **Stratification** factor (Figure 32c).

Table 10. Ranking of the planktonic foraminiferal species and their factor loadings along the PCA factors in core AEX-15. Bold data indicate the most important factor loadings in each factor (red for negative; black for positive values).

Species	Factor 1	Factor 2	Factor 3
<i>O. universa</i>	0.096	0.091	0.049
<i>G. ruber alba</i>	-0.623	-0.343	-0.416
<i>G. ruber rosea</i>	-0.043	-0.008	0.811
<i>G. sacculifer</i>	0.031	0.041	0.028
<i>G. inflata</i>	0.000	-0.021	0.012
<i>G. bulloides</i>	0.091	0.827	-0.292
<i>G. rubescens</i>	-0.184	-0.076	0.106
<i>G. siphonifera</i> gr.	0.007	-0.016	0.055
<i>N. pachyderma</i>	-0.041	-0.021	-0.036
<i>N. dutertrei</i>	-0.009	-0.003	-0.015
<i>T. quinqueloba</i>	0.744	-0.425	-0.252
<i>G. glutinata</i>	-0.045	-0.028	-0.035

6.2.2. Pteropoda

As in planktonic foraminifera, here as well, a standardized principal component analysis (PCA) was carried out on the total data set, in order to determine the impact of various environmental parameters on pteropod distribution, and furthermore to examine whether similar or dissimilar hydrographic conditions prevailed in the two aforementioned Aegean sub-basins. This analysis yielded a three-factor model in north and south sub-basins. The distinguished factors were

considered that account for 82.81%, 79.46% and 85.46% of the total variance in the south (KIM-2A) and north (AEX-15 and AEX-23) Aegean respectively (Tables 11,13,15).

South Aegean – KIM-2A

Table 11. PCA factors based on pteropods and their percentages of the total variability for core KIM-2A.

KIM-2A			
PCA Factors	Eigenvalue	% variance	Cumulative % of the total variance
1	1209,14	58,663	58,663
2	273,91	13,289	71,952
3	223,817	10,859	82,811
4	104,846	5,0867	87,898
5	100,727	4,8869	92,785
6	63,5077	3,0812	95,866
7	53,2518	2,5836	98,449
8	23,7844	1,1539	99,603
9	4,32791	0,20997	99,813
10	2,86233	0,13887	99,952
11	0,755953	0,036676	99,988
12	0,236728	0,011485	100,000

The first varimax factor (PCA1) accounts 58.66% of the total variance (Table 11) and is interpreted as **Temperature** factor (Figure 30d). Negative loadings consist of the warm – water species *H. inflatus*, whereas positive loadings consist mainly of the subarctic species *L. retroversa* (Table 12). The second factor (PCA2) describes 13.29% of the total variance (Table 11) with its positive pole represented mainly by the mesopelagic oligotrophic *H. inflatus* and the negative one by the epipelagic *Cavolinia* sp., and *B. chierchiaie* (Table 12). Particularly, the down-core scores of this factor coincide with the $\delta^{13}\text{C}$, indicating that variations in primary productivity have an impact on pteropod abundances. Even though nutrient concentrations are not a limited factor for their distribution (Johnson et al., 2020), our data suggest that fluctuations in nutrients and salinity due to the increased freshwater inputs during the sapropel deposition favor the flourishing of some species (*Cavolinia* spp., *B. chierchiaie*; Figure 22) (Giamali et al., 2020). Therefore, PCA2 is interpreted as **Productivity** factor (Figure 30e). The third varimax factor (PCA3), accounts for 10.27% of the total variance (Table 11). The negative loadings consist

mainly of the mesopelagic *C. pyramidata*, *D. trispinosa* and the shallow epipelagic and tolerant to low salinities species, *C. acicula* (Table 12). The mesopelagic species of this pole are indicative of a well ventilated water column (Sijinkumar et al., 2010). The epipelagic *C. acicula*, present in the negative pole, can be explained by its state of preservation, which is related to the oxic or anoxic conditions of the bottom. Positive loadings of this factor consist of the species *H. inflatus*, which is mesopelagic and the epicpelagic species *Cavolinia* sp., *L. retroversa* and *B. chierchiae* (Table 12). Epipelagic species are favored in a more intense and expanded OMZ. The fact that the mesopelagic *H. inflatus* takes part in the positive pole of this factor can be explained due to its dual character. This species adopts a variable depth habitat during its growth stages (veligers, juveniles and adults) and also is tolerant to low oxygen concentration of the OMZ (Singh et al., 2005). Thus, the third factor (PCA3) is referred to as a **Stratification** factor (Figure 30f), as the degree of stratified water column is linked to the intensity and expansion of the OMZ.

Table 12. Ranking of the pteropod species and their factor loadings along the PCA factors in core KIM-2A. Bold data indicate the most important factor loadings in each factor (red for negative; black for positive values).

Species	Axis 1	Axis 2	Axis 3
<i>H. inflatus</i>	-0,387	0,693	0,453
<i>L. bulimoides</i>	-0,015	-0,012	0,010
<i>L. retroversa</i>	0,895	0,175	0,304
<i>L. trochiformis</i>	-0,005	0,000	0,008
<i>B. chierchiae</i>	-0,154	-0,334	0,286
<i>C. acicula</i>	-0,064	0,227	-0,328
<i>Creseis</i> sp.	-0,027	-0,031	-0,038
<i>H. striata</i>	-0,004	-0,002	0,008
<i>S. subula</i>	-0,006	0,015	0,004
<i>C. pyramidata</i>	0,009	-0,024	-0,437
<i>D. trispinosa</i>	0,051	-0,020	-0,420
<i>Cavolinia</i> sp.	-0,131	-0,570	0,380

Table 13. PCA factors based on pteropods and their percentages of the total variability for core AEX-15.

AEX15			
PCA Factos	Eigenvalue	% variance	Cumulative % of the total variance
1	494,862	37,764	37,764
2	362,476	27,662	65,426
3	183,956	14,038	79,464
4	95,0715	7,2552	86,7192
5	78,8895	6,0203	92,7395
6	35,6337	2,7193	95,4588
7	29,4056	2,244	97,7028
8	24,0161	1,8327	99,5355
9	3,7509	0,28624	99,82174
10	2,33109	0,17789	99,99963

The first varimax factor (PCA1) explains 37.76% of the total variance (Table 13), with the positive loadings expressed by the species *H. inflatus* and *B. chierchiae* (Table 14). *H. inflatus* adopts a variable depth habitat during its growth stages (veligers, juveniles and adults) and also is tolerant to low oxygen concentration of the OMZ (Singh et al., 2005). *B. chierchiae* is favored in a more intense and expanded OMZ. Both species are primary components of the sapropel fauna of this core. In contrast negative loadings are expressed mainly by *L. trochiformis* and *C. pyramidata*, species indicative of a well-ventilated water column (Bé and Gilmer, 1977; Singh et al., 2005). Thus, PCA1 can be explained as a **Stratification** factor (Figure 31d). The second factor (PCA2) explains the 27.66% of the total variance (Table 13). Its positive pole is represented mainly by the mesopelagic oligotrophic *H. inflatus* and the negative one by the epipelagic *B. chierchiae* (Table 14). The distribution of the latter species proliferates by changes in salinity and it seems that nutrient fluctuations during S1 favor its flourishing (Giamali et al., 2020; Singh et al., 2005). Therefore, PCA2 is interpreted as **Productivity** factor (Figure 31e). The third factor (PCA3) describes 14.04% of the total variance (Table 13). The main representative of the positive pole, *L. trichiformis* (Table 14), is characterized as typical

upwelling species (Bé and Gilmer, 1977). Thus, the PCA3 can be interpreted as an **Upwelling** factor (Figure 31f).

Table 14. Ranking of the pteropod species and their factor loadings along the PCA factors in core AEX-15. Bold data indicate the most important factor loadings in each factor (red for negative; black for positive values).

Species	Axis 1	Axis 2	Axis 3
<i>H. inflatus</i>	0,8659	0,3801	0,1618
<i>L. retroversa</i>	-0,0056	0,0056	-0,0114
<i>L. trochiformis</i>	-0,3639	0,3003	0,7328
<i>B. chierchiae</i>	0,2175	-0,8421	0,2444
<i>C. acicula</i>	-0,1332	0,0705	-0,4481
<i>S. subula</i>	-0,1005	0,0618	-0,0169
<i>C. cuspidata</i>	-0,0145	0,0104	0,0277
<i>C. pyramidata</i>	-0,1896	0,1655	-0,0882
<i>D. trispinosa</i>	-0,0110	0,0350	-0,3942
<i>Cavolinia</i> spp.	-0,0792	-0,1367	0,1093

AEX-23

Table 15. PCA factors based on pteropods and their percentages of the total variability for core AEX-23.

AEX-23			
PCA Factors	Eigenvalue	% variance	Cumulative % of the total variance
1	575,776	59,257	59,257
2	166,624	17,148	76,405
3	88,0575	9,0626	85,4676
4	62,2565	6,4073	91,8749
5	41,4792	4,2689	96,1438
6	22,5672	2,3226	98,4664
7	8,19763	0,84368	99,31008
8	4,5734	0,47068	99,78076
9	1,88562	0,19406	99,97482
10	0,101273	0,010423	99,98524
11	0,096186	0,009899	99,99514
12	0,040206	0,004138	99,99928

The first varimax factor (PCA1) of core AEX-23 explains the 59.26% of the total variance (Table 15) and is mainly defined positively by *B. chierchiae* (Table 16). The distribution of this epipelagic, warm-water species is affected by nutrient and salinity fluctuations (Giamali et al., 2020; Singh et al., 2005). Therefore, PCA1 of this core is interpreted as **Productivity** factor (Figure 32d). The second varimax factor (PCA2) explains the 17.15% of the total variance (Table 15) with the positive loadings expressed mainly by the epipelagic typical upwelling species *L. trochiformis* (Bé and Gilmer, 1977). In contrast, negative loadings are mainly expressed by the mesopelagic oligotrophic *H. inflatus* (Table 16). Hence, PCA2 is referred to as **Upwelling** indicator (Figure 32e). Finally, the third factor (PCA3) accounts 9.1% of the total variance (Table 15) with positive loadings mainly represented by the stenohaline mesopelagic species *S. subula* (Buccheri et al., 2002). Negative loadings of this factor are expressed mainly by the epipelagic *L. trochiformis* (Table 16), which is associated with the mixed layer and with upwelling conditions (Almogi-Labin et al., 1988; Bé and Gilmer, 1977; Singh et al., 2005) and the mesopelagic *L. inflata*. The latter adapts a variable depth habitat and also is tolerant to low oxygen concentration of the OMZ (Singh et al., 2005). Thus, the third factor PCA3 can be explained as stratification indicator (Figure 32f).

Table 16. Ranking of the pteropod species and their factor loadings along the PCA factors in core AEX-23. Bold data indicate the most important factor loadings in each factor (red for negative; black for positive values).

Species	Axis 1	Axis 2	Axis 3
<i>H. inflatus</i>	-0,146	-0,440	-0,448
<i>L. retroversa</i>	-0,003	0,006	0,001
<i>L. trochiformis</i>	-0,266	0,764	-0,525
<i>B. chierchiae</i>	0,939	0,211	-0,105
<i>C. acicula</i>	-0,082	0,259	0,219
<i>H. striata</i>	-0,003	0,004	0,015
<i>S. subula</i>	-0,096	0,113	0,595
<i>C. cuspidata</i>	-0,001	0,011	0,010
<i>C. pyramidata</i>	-0,087	0,214	0,220
<i>D. trispinosa</i>	-0,007	-0,121	-0,066
<i>Cavolinia</i> spp.	-0,050	0,193	0,241

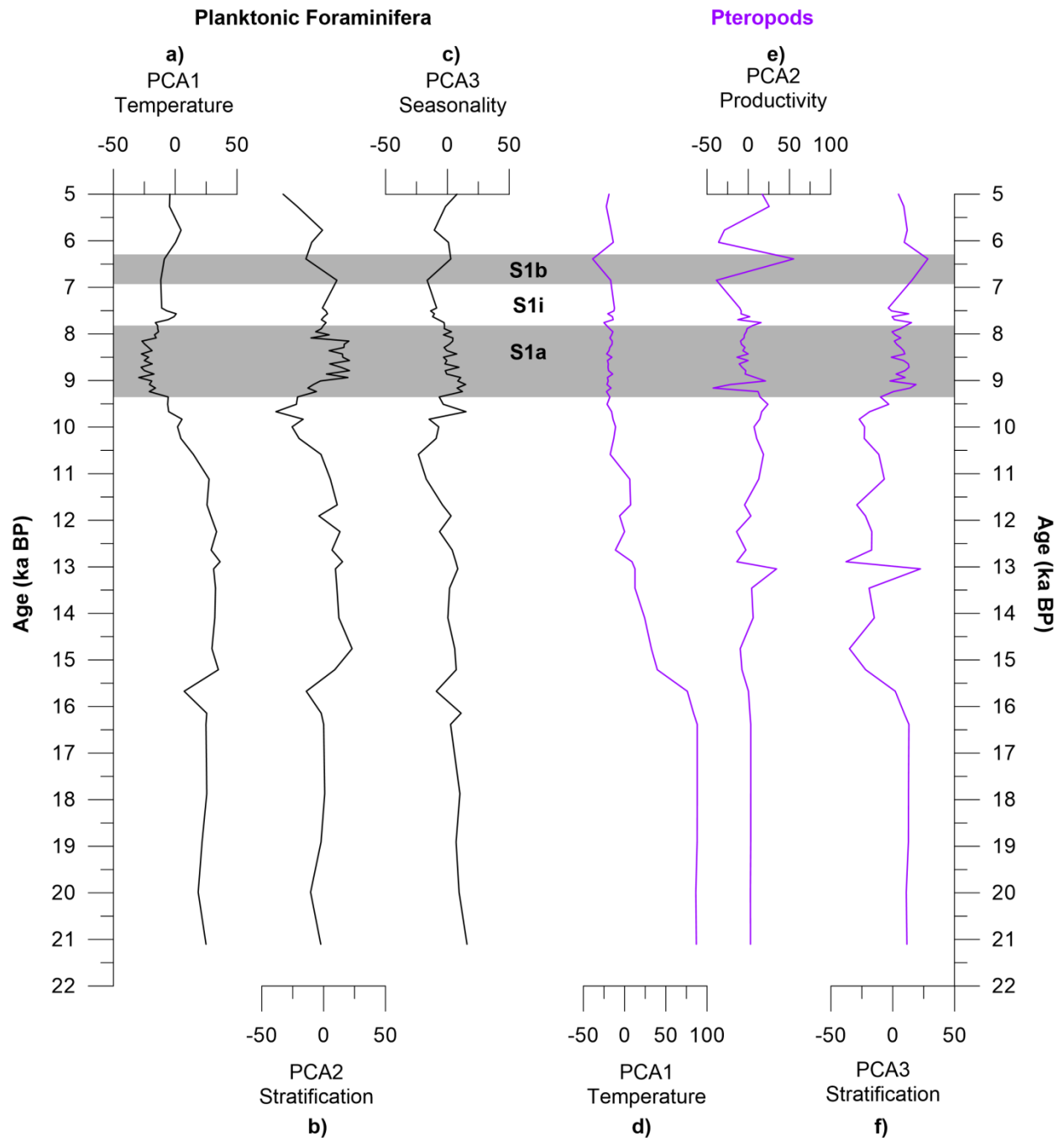


Fig. 30. Score plots of the Factors revealed from PCA analysis of core KIM-2A.

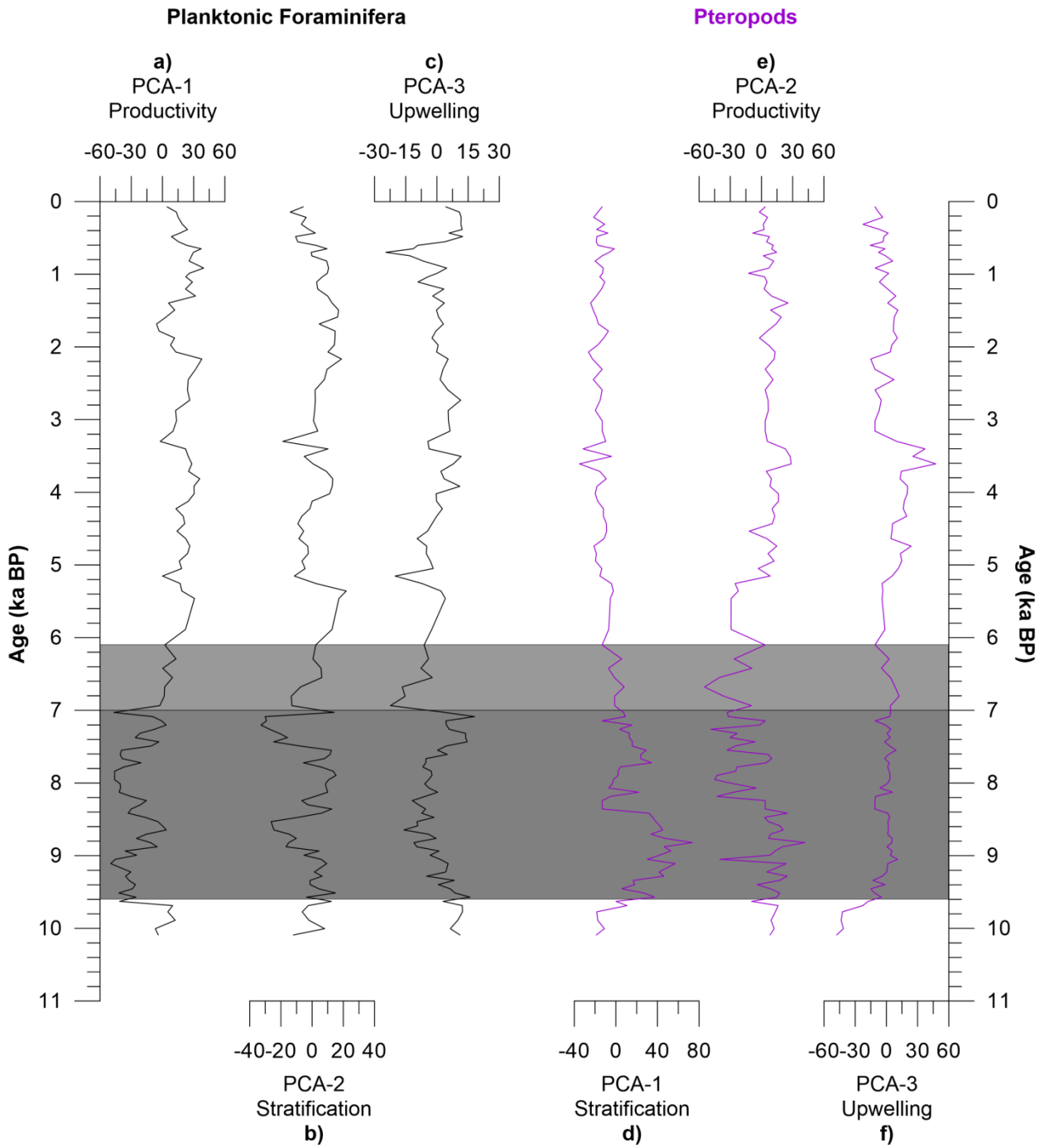


Fig. 31. Score plots of the Factors revealed from PCA analysis of core AEX-15.

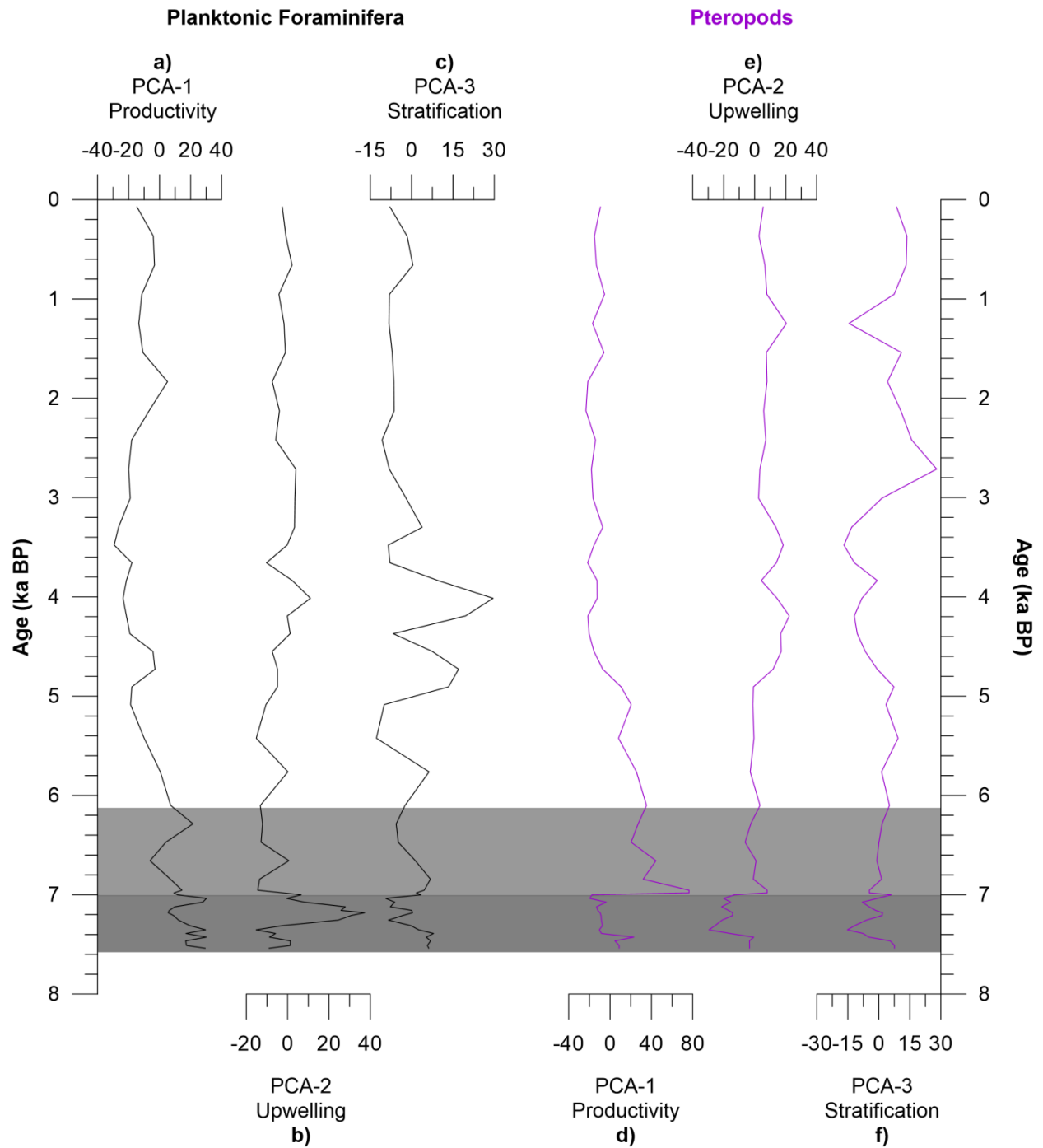


Fig. 32. Score plots of the Factors revealed from PCA analysis of core AEX-23.

6.3. Differences in pteropod fauna between the South and North Aegean Sea

Although pteropod fauna seems quite similar in both the study areas, few differences can be observed. Specifically, in south Aegean pteropod fauna includes 12 species, one of which is not encountered in the north Aegean. The same pattern is observed in north Aegean Sea, with one of the 12 species of the pteropod fauna not encountered in the south.

As knowledge on pteropod late Quaternary records is limited for the Aegean Sea, it is crucial to understand and explain these differences, based on their ecological characteristics and the factors described above, controlling their distribution. To do so, it is essential to focus on the two species differentiating the faunal pattern (Table 20). Those are the following: *Limacina bulimoides* and *Clio cuspidata*.

Limacina bullimoides it is a mesopelagic species that is considered as indicator of arid conditions (Almogi-Labin et al., 2008). Thus, its absence in the north Aegean Sea, can be explained by the different hydrographic characteristics and the climate contrasts between more humid conditions in the north and semi-arid conditions in the south Aegean Sea (Lykousis et al., 2002).

Clio cuspidata is a bathypelagic pteropod. Bathypelagic pteropods are found below 1000 m depth. Thus, its absence in the south Aegean Sea must be attributed to the bathymetry of the Kimolos submarine depression (maximum depth 743m; Figure 5; Karageorgis et al., 2016).

Table 20. Pteropod species in south and north Aegean Sea. Species in bold represent those that encounter only in one of the two regions.

Pteropod Fauna	
South Aegean	North Aegean
<i>H. inflatus</i>	<i>H. inflatus</i>
<i>L. bulimoides</i>	<i>L. retroversa</i>
<i>L. retroversa</i>	<i>L. trochiformis</i>
<i>L. trochiformis</i>	<i>B. chierchiaie</i>
<i>B. chierchiaie</i>	<i>Creseis</i> sp.
<i>Creseis</i> sp.	<i>C. acicula</i>

<i>C. acicula</i>	<i>S. subula</i>
<i>S. subula</i>	<i>H. striata</i>
<i>H. striata</i>	<i>C. pyramidata</i>
<i>C. pyramidata</i>	<i>C. cuspidata</i>
<i>D. trispinosa</i>	<i>D. trispinosa</i>
<i>Cavolinia</i> spp.	<i>Cavolinia</i> spp.

6.4. North versus South Aegean

PCA performed on planktonic foraminifera and pteropod data, was used to interpret the environmental factors controlling their distribution in north and south Aegean. This analysis has dual character; that of spatial (north versus south Aegean) and of temporal variability, as south Aegean core covers the last 21 ka BP and cores from north Aegean the last 10 ka BP. Particularly, core KIM-2A provides information for Late Glacial, deglaciation and early to mid-Holocene, in contrast with the cores of north Aegean, whose analyses provide information on factors concerning the Holocene period. Specifically, for the north Aegean both cores were chosen for the PCA in order to focus better on environmental parameters of the entire Holocene (AEX-15 almost entire Holocene, including S1; AEX-23 as a tool to focus on the Northgrippian and Meghalayan stages).

6.4.1. Planktonic Foraminifera

As shown in previous studies concerning late Quaternary, SST is the dominant factor controlling the biogeography of planktonic foraminifera at both global and local scale (Kontakiotis, 2016; Kontakiotis et al., 2011; Kucera et al., 2005). However, particularly in the Aegean Sea, additional factors controlling planktonic foraminifera distribution are primary productivity and seasonality; factors that are linked with water column stratification (Kontakiotis, 2016). Nowadays, in the Mediterranean Sea, modern planktonic foraminifera communities are mainly controlled by nutrient concentration, temperature and salinity (Zarkogiannis et al., 2020; Kontakiotis et al., 2021; Avnaim-Katav et al., 2020; Gregg and Casey, 2007; Mallo et al., 2017; Schiebel et al., 2004; Thunell, 1978).

Table 17. Factors extracted from PCA analysis on planktonic foraminifera for the totality of the cores.

Factors	South Aegean	North Aegean	
		AEX-15	AEX-23
PCA1	Temperature	Productivity	Productivity
PCA2	Stratification	Stratification	Upwelling
PCA3	Seasonality	Upwelling	Stratification

This study reveals differences in factors controlling north and south Aegean Sea (Table 17). This fact can be explained primary because of the age of the cores (KIM-2A spans the last 22 ka, AEX-15 & AEX-23 span the last 10 ka), and secondary due to the significantly different hydrographic characteristics between these two basins (Lykousis et al., 2002), with the north Aegean being more humid in contrast with the semi-arid south Aegean. Consequently, the main controller of planktonic foraminifera distribution in south Aegean is SST (PCA1 in KIM-2A; Giamali et al., 2020). During late Quaternary, SST shows the highest explanatory power, as it has been showed before from other records of the Mediterranean (e.g., Geraga et al., 2010; Kontakiotis, 2016). In contrast, the main factor (PCA1 in AEX-15 & AEX-23) controlling north Aegean planktonic foraminifera distribution is SSP (productivity; Table 17). This variation between the PCA1 of north and south Aegean can be explained by the two parameters mentioned above. Particularly, the freshwater influx from the Black Sea and surrounding rivers draining into the north Aegean, and the presence of cyclonic and anticyclonic eddies and thus to the development of down- and upwellings enriched on nutrients (Geraga et al., 2010; Lykousis et al., 2002) have as a result the increased eutrophication of the north Aegean compared to that of the south.

Apart from SST and SSP the planktonic foraminifera distribution is controlled by the degree of the vertical stratification of the water column (PCA2 in KIM-2A & AEX-15, PCA3 in AEX-15; (Table 17). Stratified water conditions contribute to the formation of sapropels (De Lange et al., 2008) and can be triggered by lower surface-water salinity and relatively warm winter conditions that lead to the restriction of deep-water formation (Rohling et al., 2015), as well as enhanced nutrient inputs by the borderlands' rivers (Mélières et al., 1997; Rohling, 1991; Rossignol-Strick, 1995) that result in higher primary productivity. Stratification factor, as shown by the PCA, controls both north and south Aegean faunal compositions, though, in AEX-23 in lower grade

(13%) than in the other two cores (22% in KIM-2A, 15% in AEX-15). This slight difference in percentages can be attributed to the age that cores' sediments span. Specifically, cores KIM-2A and AEX-15 contain the entire sapropel S1 layer(s), whereas, AEX-23 includes only the upper part of it. Stratification is also linked to seasonality (Kontakiotis, 2016); factor that the results of this study suggest that also controls south Aegean planktonic foraminifera distribution (PCA3 in KIM-2A). Seasonal fluctuation in foraminifera composition follows seasonal changes in hydrographic conditions (Schiebel and Hemleben, 2005; Wilke et al., 2009). In contrast, seasonality seems to be a less influencing factor in assemblages of north Aegean Sea. The third PCA factor for this region (PCA3 in AEX-15 & PCA2 in AEX-23; Table 17) indicates that upwellings contribute in planktonic foraminifera distribution. Upwellings control food availability and foraminifera reproductive cycles (Hemleben et al., 1989) and are directly correlated with the seasonal fluctuations (Fraile et al., 2009; Wilke et al., 2009). The fact that upwelling seems to contribute in higher percentages in AEX-23 (26%) than in AEX-15 (7.5%) can be attributed in the age that cores' sediments span.

6.4.2. Pteropoda

A considerable number of studies (e.g., Bhattacharjee, 1997; Buccheri, 1984; Gaby and Sengupta, 1985) have shown that late Quaternary pteropod assemblages and their distribution pattern in the world oceans, changes with temperature and the overall climatic conditions that also affect the aragonite compensation depth (ACD). Recent studies (Johnson et al., 2020) have shown that modern eastern Mediterranean pteropod communities are found to be more abundant than in western Mediterranean Sea. Their abundances are positively correlated with the aragonite saturation state (Ω_{ar}), O_2 , pH, salinity and temperature, and negatively correlated with nutrient concentration (phosphate and nitrate concentrations) (Howes et al., 2015; Johnson et al., 2020).

Table 18. Factors extracted from PCA analysis on pteropods for the totality of the cores.

Factors	South Aegean	North Aegean	
		AEX-15	AEX-23
PCA1	Temperature	Stratification	Productivity
PCA2	Productivity	Productivity	Upwelling
PCA3	Stratification	Upwelling	Stratification

The data analyzed in this work suggest a temperature control of pteropoda distribution when looking at the past 21 ka (PCA1 in KIM-2A; Table 18). This main factor is also in agreement with records from all over the world (Buccheri, 1984; Herman, 1971, 1981; Pierrot-Bults and Peijnenburg, 2015) and is observed only the south Aegean Sea. However, when focusing on the Holocene period, pteropod composition seems to be affected by other factors such as productivity (PCA2 in KIM-2A, PCA2 on AEX-15 & PCA1 in AEX-23), the extent and strength of the OMZ which is related to the stratification of the water column (PCA3 in KIM-2A, PCA1 in AEX-15 and PCA3 in core AEX-23), and upwelling conditions (PCA3 of AEX-15 & PCA2 of AEX-23) (Table 18). The latter factor, though, as depicted by PCA, appears to be affecting only the north Aegean pteropod fauna.

Particularly, the down-core scores of the Productivity factor (PCA2 in KIM-2A, PCA2 in AEX-15 and PCA1 in AEX-23) coincide with the $\delta^{13}\text{C}$ and E-index values, indicating that variations in primary productivity have an impact on pteropod abundances. Even though nutrient concentrations are not a limited factor for their distribution (Johnson et al., 2020) our data suggest that fluctuations in nutrients and salinity due to the increased freshwater inputs during the sapropel deposition favor the species-specific flourishing (*Cavolinia* spp., *B. chierchiae*; Figures 24 and 26). Additionally, the stratification factor (PCA3 in KIM-2A, PCA1 in AEX-15 and PCA3 in AEX-23; Table 18) suggests that oxygen concentration, and thus the intensity of the oxygen minimum zone (OMZ), are parameters that affect pteropod distribution and particularly the mesopelagic species (Almogi-Labin et al., 2008). OMZ alterations are climatically controlled, with humid and milder climates favoring a strong and well developed OMZ, whereas cooler and/or arid periods are characterized by a more aerated OMZ (Almogi-Labin et al., 1998; Sijinkumar et al., 2010). This parameter could explain well the distribution pattern of pteropods during sapropel S1 deposition, which remain unknown up to now.

Finally, the third factor affecting pteropod distribution in north Aegean Sea seems to be the upwellings (PCA3 in AEX-15 & PCA2 in AEX-23). The participation of this factor in Holocene records of north Aegean is explained by the presence of cyclonic and anticyclonic eddies and thus to the development of down- and upwellings of the organic matter (Geraga et al., 2010; Lykousis et al., 2002), seems to be responsible for the higher nutrient levels in the water, and thus for an increase in productivity of the north Aegean Sea.

6.5. Foraminifera versus Pteropoda

Both faunal groups seem to be reliable indicators for past paleoceanographic and palaeoclimatic changes, as shown by the PCA performed. The differences relay up on the extent that each factor affects the fauna. Specifically, the factor of temperature seems to be the dominant factor that affects equally both groups. Upwelling, though is not the dominant factor, it affects both groups. On the other hand, productivity and stratification are factors that exist in both areas for both taxa, but with different intensity. In the south Aegean Sea, planktonic foraminifera seem to express better the Stratification factor than pteropods (Table 19). This is due to the lower number of species of pteropods that are affected from stratified conditions in comparison with the planktonic foraminifers (e.g., *H. inflatus* that survives in such conditions by changing its habitat). In contrast, at core AEX-15 in the north Aegean Productivity factor is expressed more intensified in planktonic foraminifera fauna than in pteropods, and the opposite is observed with the Stratification factor (Table 19). This can be explained by the planktonic foraminifera species *T. quinqueloba* and *G. bulloides* indicative of cold and humid conditions, that render the role of productivity as main factor and especially in the more humid and eutrophicated north Aegean region (Geraga et al., 2010; Lykousis et al., 2002). The only factor that does not affect pteropod fauna, based on the PCA, is that of Seasonality. This is due to the low influence of seasonal factor, on the temperate and tropical pteropod species (Manno et al., 2017). The fact that in core AEX-23 all factors affect equally both groups can be explained by the time spanning of this core.

Table 19. Total factors extracted from PCA for both taxa and both regions.

Factors	South Aegean KIM-2A		North Aegean AEX-15		North Aegean AEX-23	
	Foraminifera	Pteropoda	Foraminifera	Pteropoda	Foraminifera	Pteropoda
PCA1	Temperature	Temperature	Productivity	Stratification	Productivity	Productivity
PCA2	Stratification	Productivity	Stratification	Productivity	Upwelling	Upwelling
PCA3	Seasonality	Stratification	Upwelling	Upwelling	Stratification	Stratification

7. Palaeoclimate and Palaeoenvironment

7.1. Paleoenvironmental Indices – Temperature, Productivity and Stratification

The late Quaternary palaeoenvironmental evolution and the main palaeoceanographic changes of the north and south Aegean Sea was reconstructed using high resolution micropalaeontological and geochemical data ($\delta^{18}\text{O}$ and $\delta^{13}\text{C}$ isotopes, AMS ^{14}C datings, C_{org} content). In particular, micropalaeontological interpretations were based on the downcore variations of planktonic organisms (foraminifera and pteropoda) and indices extracted by the aforementioned organisms. Planktonic foraminifera indices (PPC, E-index, U-index, SPRUDTS) that were used in this study are explained in detail in the material and methods chapter and are based in a number of studies (e.g., Geraga et al., 2005, 2010; Hemleben et al., 1989; Kontakiotis, 2016; Rohling et al., 1993a; Sbaffi et al., 2004; Triantaphyllou et al., 2009a).

Concerning pteropods, indices that have been used in literature are based mainly in Quaternary records from the Red Sea, the Caribbean Sea, the Gulf of Aden, the Gulf of Aqaba, the Arabian Sea and the Mediterranean Sea (Almogi-Labin, 1982; Almogi-Labin et al., 1986, 1991, 1998; Deuser et al., 1976; Edelman-Furstenberg et al., 2009; Herman, 1968, 1971, 1981; Herman and Rosenberg, 1969; Ivanova, 1985; Johnson et al., 2020; Reimer et al., 2013; Reiss et al., 1980; Singh et al., 2005; Wall-Palmer et al., 2012, 2014; Winter et al., 1983). Previous studies have used pteropods in order to extract information mainly on depth, state of preservation, the strength of OMZ and palaeoclimate. A brief description of these indicators is following.

Herman (Herman and Rosenberg, 1969) suggested the ratio of *Creseis* spp./*H. inflatus* as bathymetric indicator due to the species restricted depth ranges. The converse ratio has also been used as the degree of the stratification of water column (Almogi-Labin et al., 1991, 1998; Singh et al., 2001). Another palaeo-application concerning variations in pteropod shells, is the *Limacina* Dissolution Index (LDX) (Gerhardt et al., 2000; Gerhardt and Henrich, 2001; Wall-Palmer et al., 2012, 2013). This method was originally developed to detect post-depositional dissolution, but latter has been used in studies of shell dissolution on living pteropods due to low carbonate saturation in the surface water (Manno et al., 2017). The pteropod diversity (number of pteropod species per sample) is long being used and correlated to glacial and interglacial stages and thus to temperature (Almogi-Labin et al., 1998, 2008; Janssen and Peijnenburg, 2014; Wall-

Palmer et al., 2014), as species richness is high during interglacial stages, intermediate during glacial, and very low during extreme glacial maximum conditions. Furthermore, the relative abundances of epipelagic and mesopelagic species are widely used in order to indicate the strength and extent of the oxygen minimum zone (OMZ) and the degree of the stratification of the water column (Almogi-Labin et al., 1998, 2008; Edelman-Furstenberg et al., 2009). In addition, the abundance of epipelagic species, it has also been used as an indicator for humid or arid periods (Almogi-Labin, 2010), with high relative percentages suggesting humid periods, whereas low percentages indicating arid periods. Another indicator of arid conditions that has been proposed is the relative abundance of *L. bulimoides* (Almogi-Labin et al., 1998; Edelman-Furstenberg et al., 2009). A number of studies (e.g., Blanc-Vernet et al., 1969; Buccheri, 1984; Buccheri et al., 2002; Carboni and Esu, 1987; Torelli and Buccheri, 1983) concerning Mediterranean records are dedicating in constructing palaeoclimatic curve. This curve is mainly based on the occurrence of the species *Limacina retroversa*, which is frequently found to be present in large numbers in Pleistocene bottom samples and is considered to be characteristic for colder intervals, by comparing its numerical abundance to warm-water species like *H. inflatus*, *L. trochiformis*, *C. inflexa*, and/or *D. trispinosa*.

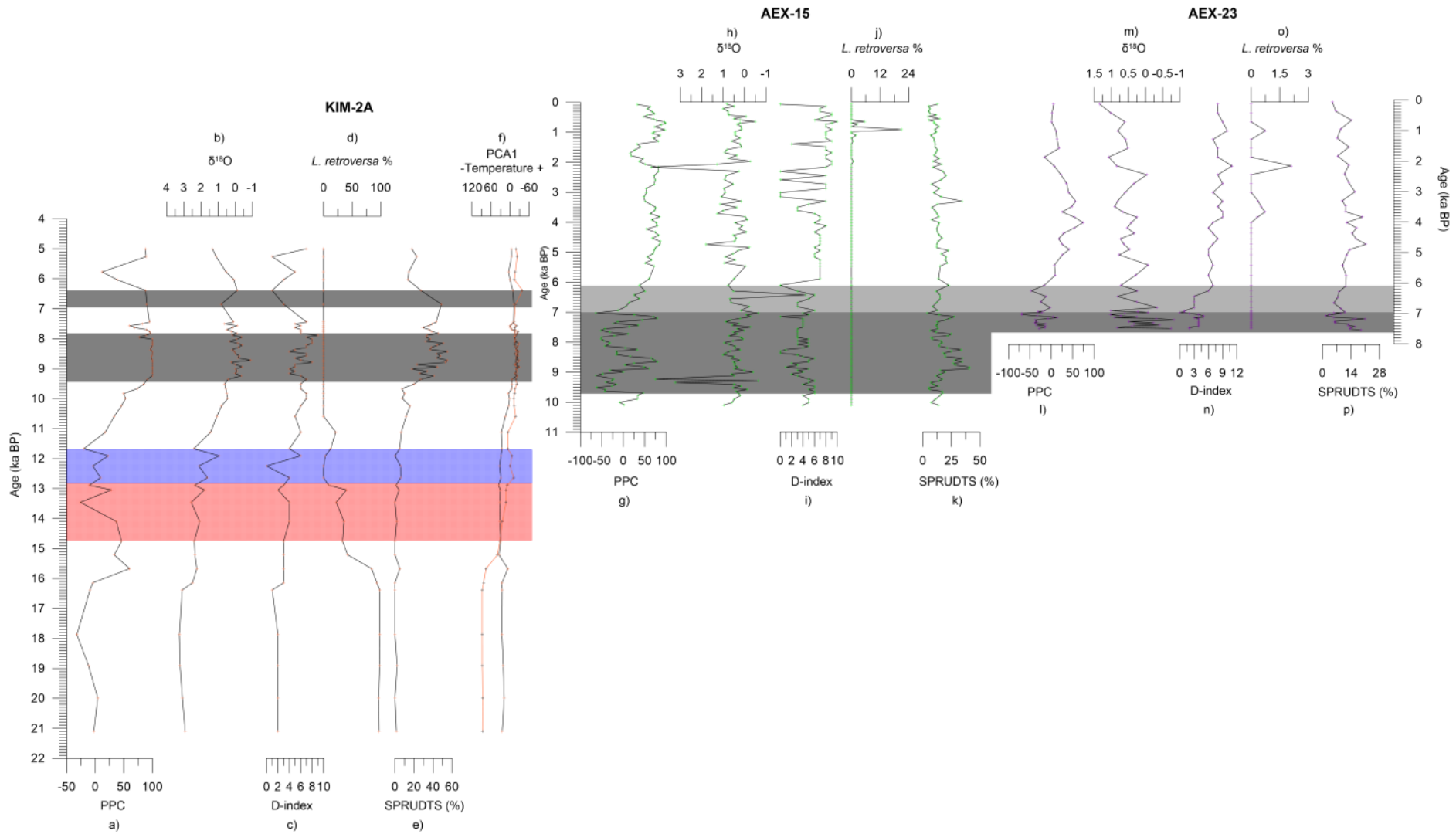
In this study, in order to reconstruct the palaeoclimatic evolution of Aegean Sea, the indices that were used were separated into three groups. The first group is related to Temperature indicators, and proxies that were used are the Planktonic Palaeoclimatic Curve (PPC), SPRUDTS group, Pteropoda species richness (D-index: Diversity index), *Limacina retroversa* relative abundance and $\delta^{18}\text{O}_{G.ruber}$ (Figure 33). The second group is associated with Sea Surface Productivity (SSP) with the following indicators; Eutrophication index (E-index), Upwelling index (U-index: *G. bulloides* %), *Limacina trochiformis* relative abundance as an upwelling indicator, and the $\delta^{13}\text{C}_{G.ruber}$ as a productivity proxy (Figure 34). The third group refers to the stratification of the water column and the main indicators used are the Stratification index (S-index) based on planktonic foraminifera and the Epipelagic/Mesopelagic pteropod ratio (E/M) (Figure 35). The E/M ratio is used for the first time in this study and is estimated using the sum of Epipelagic species (*L. retroversa*, *Limacina trochiformis*, *C. acicula*, *C. virgula* and *Cavolinia* spp.) versus the sum of Epipelagic plus Mesopelagic species (*L. bulimoides*, *C. pyramidata*, *C. cuspidata*, *D. trispinosa*). In the sum of mesopelagic species, it is considered crucial to exclude *H. inflatus*. This is due to its adaptation in a variable depth habitat during its growth stages, and also its

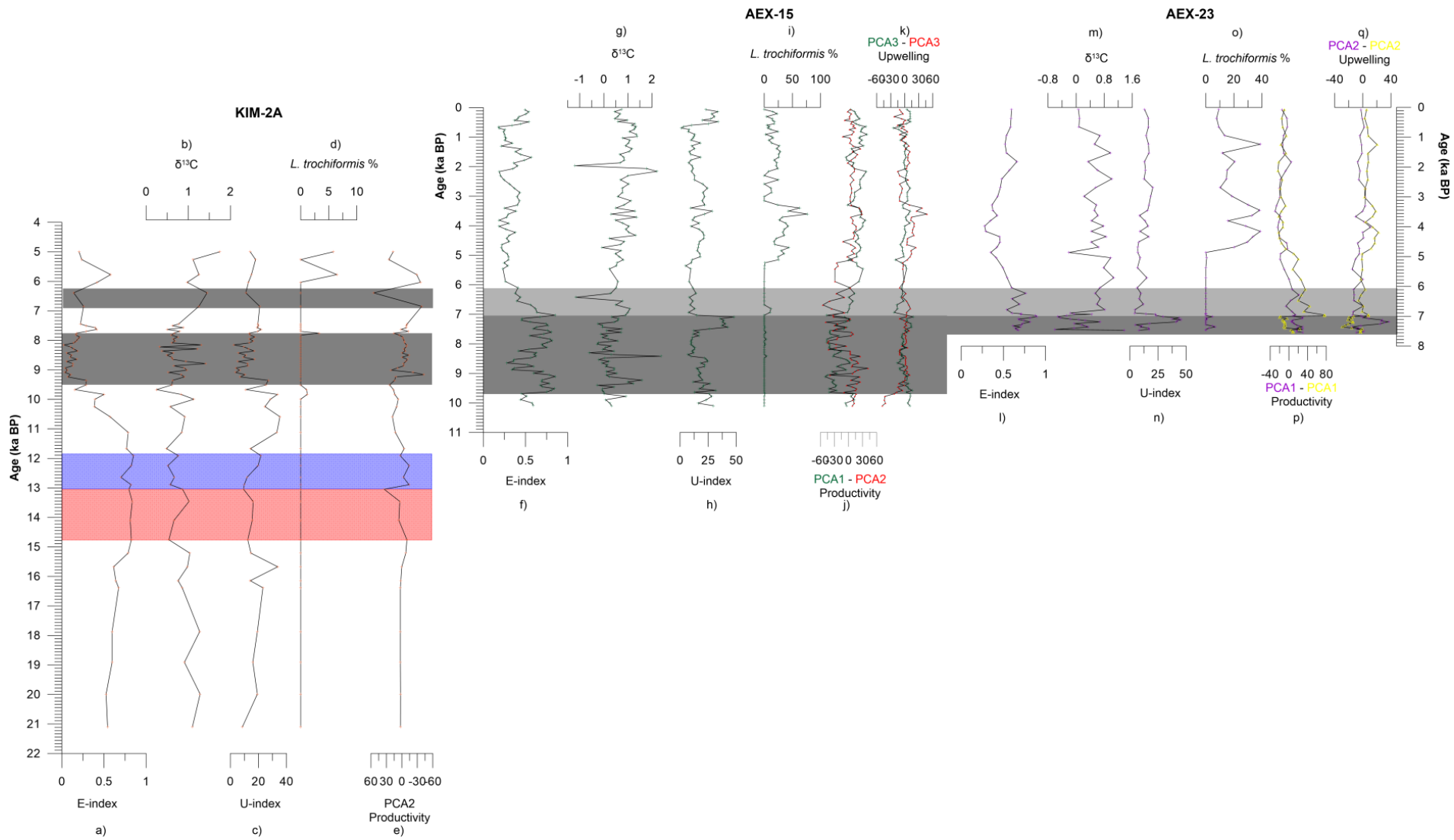
potential to stand very low oxygen concentrations (Almogi-Labin et al., 1998; Singh et al., 2005; Weikert, 1982; Weikert and Cederbaum, 1987). The values of E/M ratio vary between 0 and 1. When values are close to 1 epipelagic species prevail, suggesting a more stratified water column. On the contrary when E/M ratio is close to 0, mesopelagic species surpass the epipelagic, suggesting a well aerated water column. In all the above mentioned groups the resulted factors of PCA were included.

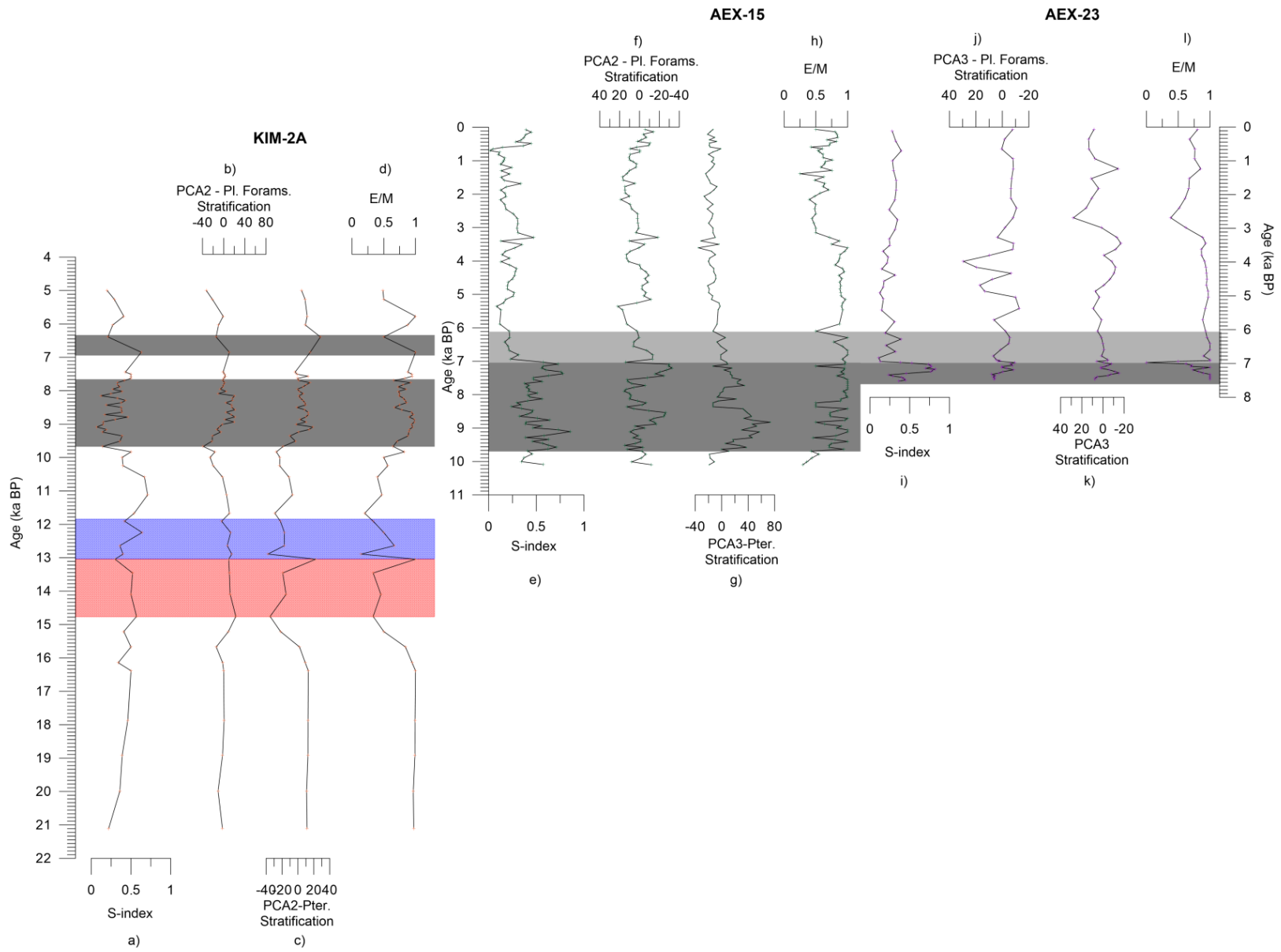
Fig. 33. Temperature indicators for the studied cores; For KIM-2A: a) PPC, b) $\delta^{18}\text{O}$, c) D-index, d) *L. retroversa* relative abundance, e) SPRUDTS group, f) PCA1 temperature indicator (black line represents planktonic foraminifera analysis whereas orange line pteropod analysis); for AEX-15: g) PPC, h) $\delta^{18}\text{O}$, i) D-index, j) *L. retroversa* relative abundance, k) SPRUDTS group; for AEX-23: l) PPC, m) $\delta^{18}\text{O}$, n) D-index, o) *L. retroversa* relative abundance, p) SPRUDTS group. Gray bands represent the sapropel S1 layers, light gray band represent the oxidized part of S1, red and blue band represent the Bølling–Allerød and Younger Dryas respectively.

Fig. 34. Productivity indicators for the studied cores; For KIM-2A: a) E-index, b) $\delta^{13}\text{C}$, c) U-index, d) *L. trochiformis* relative abundance, e) PCA2 productivity indicator derive from pteropod analysis; for AEX-15: f) E-index, g) $\delta^{13}\text{C}$, h) U-index, i) *L. trochiformis* relative abundance, j) PCA1 and PCA2 productivity indicator k) PCA3 upwelling indicator (for PCA green color represents planktonic foraminifera analysis whereas red color pteropod analysis); for AEX-23: l) E-index, m) $\delta^{13}\text{C}$, n) U-index, o) *L. trochiformis* relative abundance, p) PCA1 and PCA1 productivity indicator, q) PCA2 upwelling indicator (for PCA purple color represents planktonic foraminifera analysis whereas yellow color pteropod analysis). Gray bands represent the sapropel S1 layers, light gray band represent the oxidized part of S1, red and blue band represent the Bølling–Allerød and Younger Dryas respectively.

Fig. 35. Stratification indicators for the studied cores; For KIM-2A: a) S-index, b) PCA2; stratification indicator (from planktonic foraminifera analysis), c) PCA2; stratification indicator (from pteropoda analysis), d) E/M ratio; for AEX-15: e) S-index, f) PCA2; stratification indicator (from planktonic foraminifera analysis), g) PCA3; stratification indicator (from pteropoda analysis), h) E/M ratio; for AEX-23: i) S-index, j) PCA3; stratification indicator (from planktonic foraminifera analysis), k) PCA3; stratification indicator (from pteropoda analysis), and l) E/M ratio. Gray bands represent the sapropel S1 layers, light gray band represent the oxidized part of S1, red and blue band represent the Bølling–Allerød and Younger Dryas respectively.







7.2. Palaeoenvironmental Reconstruction

The geochemical records ($\delta^{18}\text{O}$, $\delta^{13}\text{C}$), in combination with the foraminiferal and pteropod abundance records, the palaeoceanographic indices and the results of the multivariate statistical analyses, are best interpreted as a series of successive changing, climatically driven dynamic regimes. The evidence of these changes is interpreted and discussed in terms of the events that mainly accompanied the transition out of the late glacial period (Late glacial, deglaciation), the deposition of sapropel S1 during the HCO, and the post-sapropel interval. These are described subsequently as a series of transitory states together with a detailed documentation of the main isotopic and faunal changes recognized in our north and south Aegean records (Figures 33–35). The timing of each state is in agreement with relevant paleoceanographic reconstructions (Grant et al., 2016; Siani et al., 2013) and may be considered typical of the particular climatic/circulation regime of the study area.

Late Glacial

During the late glacial period (21.1–15.7 ka BP), the heaviest $\delta^{18}\text{O}$ values (2.49–3.26‰), accompanied with relatively low PPC and D-index values (-32% to +4% and ≤ 2 respectively) suggest a cold upper water column (Figure 33a,b,c). The data of PCA (high values in both fauna taxa; Figure 33f) also support similar climatic conditions. Particularly, this interval is characterized by high percentages of the cold-water foraminifera species *T. quinqueloba* (~30%), accompanied by *G. glutinata* (9%), and *G. scitula* (8%) and significant percentages of the warm-water *G. ruber* f. *alba* (~34%) (Ib assemblage of q-mode analysis; Figure 27), that are suggestive of milder climate after the Last Glacial Maximum (LGM), which is in accordance with other records in the Mediterranean (Di Donato et al., 2008; Sprovieri et al., 2003). Pteropod fauna (Figure 22) is composed mainly by the cold-water species *L. retroversa* (98%) and the cold-tolerant mesopelagic *C. pyramidata* in very low percentages (3%) which is consistent with relevant late glacial Mediterranean records (Biekart, 1989; Wall-Palmer et al., 2014). Eutrophic species are also abundant in this interval (*N. pachyderma*, *N. dutertrei*, *T. quinqueloba* and *G. bulloides*; Figure 21) and are associated to the high values of E-index and PCA2 (Figure 34e). Notably, the high abundance of *N. pachyderma* (26%) indicates shallowing of the pycnocline and the formation of a DCM layer. In addition, $\delta^{13}\text{C}$ values, around +1‰, and the trend to higher S-index values (Figures 34b; 35a), also support the development of eutrophicated waters. The

moderate abundance of *G. bulloides* (U-index: 5%-17%; Figure 34c) suggests little to no upwelling and/or runoff contribution in primary productivity. Therefore, the injection of nutrients into the euphotic zone can be attributed to the intensification and southward shift of westerly winds, as indicated by atmospheric circulation models for this time interval (Kutzbach and Guetter, 1986).

Deglaciation

At 15.7 ka BP an abrupt shift of PPC to positive values accompanied by lighter $\delta^{18}\text{O}$ values (+2.2‰) (Figure 33a,b), are indicative of the climatic amelioration that occurred during the last deglaciation. These warmer conditions are also supported by the higher D-index value (Figure 33c), which is the outcome of the occurrence of the warm water species *H. inflatus* and *D. trispinosa* (up to 60% and 50% respectively), and the decrease in *L. retroversa* percentages (between 33% and 85%), reflected also in PCA1 (pteropod; Figure 33f). This warming trend is in agreement with relevant paleoclimatic records from the eastern Mediterranean and is attributed to the Bølling–Allerød (B-A) interstadial (Dormoy et al., 2009; Kontakiotis, 2016; Kotthoff et al., 2008a, 2011; Kuhnt et al., 2007). The increased SST and humidity are also recorded by the higher abundance of the terrestrial biomarkers in the south Aegean (Triantaphyllou et al., 2009b), and by a change in the benthic faunas from oxic to dysoxic indicator species (Kuhnt et al., 2007). In the beginning of this interval, Neogloboquadrinids are temporary replaced by *G. bulloides* (26%) suggesting local upwelling. Though, later on the eutrophic *N. pachyderma* and *N. dutertrei* present their highest abundance (42% and 14% respectively) (Figure 21). Additional components of this interval are *G. ruber* (both variants), *G. bulloides*, *T. quinqueloba* and *G. inflata* (Ia assemblage of q-mode analysis) suggesting temperate and meso- to eutrophic waters, with strong seasonal mixing and local upwelling.

This state persisted until the onset of the Younger Dryas (YD) at about 12.9 ka BP, which is depicted in the abrupt decrease in PPC (from +28% to -10%) and D-index (between 0 and 4) and in heavier values of $\delta^{18}\text{O}$ (1.0-2.5‰) (Figure 33a,b,c). The planktonic foraminiferal fauna shows an increase in cold water species (*N. pachyderma*, *T. quinqueloba*, *G. inflata* and *G. glutinata*). Pteropod fauna is composed mainly of the cold-water species epipelagic *L. retroversa*, and the mesopelagic temperate to warm-water species *C. pyramidata*, *D. trispinosa* while the warm-water *H. inflatus* presents a decreasing trend (Figure 22). This climate response of south Aegean

depression to the YD event (12.9-11.7 ka BP) seems to be in accordance with relevant signals from other Aegean sub-basins (Geraga et al., 2010; Kontakiotis, 2016). Towards the end of YD (12.6 – 12.2 ka BP) the species *G. rubescens*, *C. acicula* and *B. chierchiaie* are added to the fauna suggesting that mild climatic conditions prevailed for a brief time interval of about 400 years within the YD event. This brief climatic amelioration in the mid YD which has been attributed to the displacement of the polar front by a few degrees north (Cacho et al., 2001), has been also observed in north-central Aegean marine records (Dormoy et al., 2009; Kontakiotis, 2016) and coincides with the pattern of GRIP and NGRIP ice-core records (Björck et al., 1998; Rasmussen et al., 2007), pollen-based reconstructions from the Jura (Peyron et al., 2005) and the Balkans (Bordon et al., 2009), as well as chironomid-based reconstructions from North Italy (Larocque (Larocque and Finsinger, 2008). The increase of S-index, E-index and PCA2 (productivity foraminifera) at around 12.2 ka BP (Figures 34a,e and 35a) coincides with this amelioration, reflected by the improved ventilation and eutrophication of the water column.

Holocene

Pre-sapropel interval

With the ending of the YD, a general climatic amelioration is seen in the records of KIM-2A (increase in PPC, lighter values in $\delta^{18}\text{O}$, decline of temperature factors PCA1; Figure 33a,b,f) marking the beginning of the Holocene. Planktonic foraminifera fauna consists mainly by *G. ruber* f. *alba*, that increases in abundance towards the onset of sapropel deposition, along with *G. bulloides* and *N. pachyderma* (IIa assemblage of q-mode analysis; Figure 27). The two latter species present an opposite trend, decreasing towards the onset of sapropel deposition (Figure 21). This trend suggests the gradual development of stratified and oligotrophic surface waters. Pteropod fauna follows similar pattern with the decreasing abundances of the species *D. trispinosa* and *C. pyramidata*, which are indicative of a well-ventilated water column (Sijinkumar et al., 2010), and the increase in the epipelagic *B. chierchiaie* and *C. acicula* (Figure 22). Similar trend is observed in North Aegean core AEX-15 with high values (up to 50%) of PPC and light values in $\delta^{18}\text{O}$ (Figure 33g,h). The gradual depletion of $\delta^{18}\text{O}$ in both cores can be attributed to the global signal of meltwater pulse 1B. The slight shift to lighter $\delta^{18}\text{O}$ values signifies a gradual freshening of the upper water column. The close similarity in timing of the $\delta^{18}\text{O}$ changes in both *G. ruber* foraminiferal calcite (core AEX-15) and seawater (core LC-21;

Marino et al., 2009) provides evidence that this $\delta^{18}\text{O}_{G. ruber}$ depletion prior to S1 deposition is dominated by the inflow of isotopically light fresher surface waters into the Aegean Sea (Casford et al., 2002, 2003), and the consequent sea surface freshening propagates through the entire eastern Mediterranean away of the sites of freshwater discharge due to the efficient large-scale counter-clockwise circulation of the surface waters (Pinardi and Masetti, 2000).

In addition, in AEX-15 this interval is marked by high relative abundances of warm mixed layer species (including the pteropod *D. trispinosa*) and the high abundance of *G. glutinata* (Figures 23a and 24a). The latter species replaces *G. inflata* in KIM-2A (Figure 21). The shift toward the dominance of the shallower living species *G. glutinata*, in both cores, could be explained in terms of increased seasonality (Kontakiotis, 2016), suggested also by the Seasonality factor in KIM-2A (PCA3 of planktonic foraminifera; Figure 30c). The opportunistic response of *G. glutinata* to any increase in nutrient variability is also in agreement with (Casford et al., 2002), who presented a case for an initial period of 100–1500 yr of nutrient accumulation prior to the onset of S1 deposition. This is evident in all the productivity-related records (Figure 34), evidenced by the enrichment in $\delta^{13}\text{C}$ ($\sim 1\text{‰}$ in AEX-15 and $\sim 1.1\text{‰}$ in KIM-2A; equivalent to the second primary event of Casford et al. (2007), the increased numbers of E-index and U-index around ~ 9.8 ka BP (Figure 34a,c) and the presence of the epipelagic pteropods (mainly *C. acicula*) that proliferate in low salinity waters (Rottman, 1980). The evidence of seasonality is further reinforced by the presence of *G. bulloides* and *G. ruber* f. *alba*, which are the main exponents of the seasonal contrasts governing planktonic foraminiferal assemblages in the Mediterranean Sea during the Holocene (Goudeau, 2015; Wilke et al., 2009; Wit et al., 2010).

Sapropel Layers

By 9.6 ka BP in AEX-15 and 9.4 ka BP in KIM-2A, S1 deposition commences, as witnessed by high organic carbon content and Ba/Al ratio (Figures 15a and 16), and it coincides with the abrupt increase of primary productivity (E-index and U-index; Figure 34a,c,f,h), the start of the overall $\delta^{13}\text{C}$ depletion (Figure 34b,g), and the faunal shift to a dominance of species related to stratified water column (assemblage *G. ruber* f. *alba* IIB for south Aegean and assemblage I *T. quinqueloba* for north Aegean; Figures 27 and 28). Minor age discrepancies concerning the initiation of S1 and/or the differentiation of the sapropel subunits S1a and S1b in the analyzed cores reflect the local conditions of marine circulation, depositional depth and the amount of the

organic material that reached the sea floor (e.g., Casford et al., 2003; Kontakiotis, 2016; Kuhnt et al., 2007; Mercone et al., 2000). In all of the studies cores, during the sapropel S1 deposition, changes of the planktonic foraminifera fauna are characterized by an increase in SPRUDTS (Figure 33e,k,p). Steadily low (stabilized around zero) $\delta^{18}\text{O}$ values, together with high PPC values reflect a climatic invasion towards high temperatures (Figure 33b,h). However, the comparison of the north and south Aegean records shows significant changes among the north and south Aegean basins in the temperature, productivity and the stratification of the upper water column during this time period. Particularly, the high temperatures pattern in North Aegean records seems to be interrupted. Three events of lower PPC and heavier $\delta^{18}\text{O}$ values reflect lower SSTs are observed at around 9.5 – 9.1, 8.2 – 7.9 and 7.1 – 7.0 ka BP (Figure 33g,h). These short-term cooling events are also reflected in significant faunal changes in the north Aegean Sea, such as the increase in abundance of *G. bulloides* and *T. quinqueloba* replacing the SPRUDTS group (Figure 23). Immediately after these events, faunal abundance and isotopic profiles return rapidly to their previous enhanced levels, and a gradual increase can be observed for PPC values (Figure 33g). In contrast with the North Aegean records, South Aegean sediments core indicate only one cooling event at 7.9 – 6.8 ka BP which is related to the S1 interruption (detected here at 7.7 to 6.8 ka BP). This interval is marked by the decrease in PPC (from 90% to 60%) and the heavier values of $\delta^{18}\text{O}$ (+0.5‰) and $\delta^{13}\text{C}$ (+0.8‰) as shown in Figures 33a,b and 34b. The subsequent cooling is also reflected in significant faunal changes, such as the increase in abundance of *G. inflata*, *T. quinqueloba*, *G. bulloides* and *N. pachyderma* (Figure 21). These species are associated with relatively cold temperatures and increased food supply, suggesting high primary production and stronger mixing of the water column (Casford et al., 2002; Pujol and Vergnaud-Grazzini, 1995). In addition, the pteropod *L. trochiformis*, which is related to the mixed layer of the water column and thrives in upwelling conditions (Almogi-Labin et al., 1988; Bé and Gilmer, 1977; Sakthivel, 1969; Wormuth, 1981), presents a peak at the beginning of S1i (Figure 34d).

During sapropel S1 deposition increase in temperature and humidity has also been documented in all marine and terrestrial pollen records in the eastern Mediterranean region (Geraga et al., 2010; Giamali et al., 2019; Kontakiotis, 2016; Kotthoff et al., 2008b; Rossignol-Strick, 1995; Triantaphyllou et al., 2009a). This paleoclimate change coincides with the Holocene summer precession-related insolation maximum in the Northern Hemisphere (Laskar et al., 2004), and the monsoon intensification that resulted in a widespread increase in humidity over the

Mediterranean region and concomitant increase of freshwater input to the Mediterranean Sea (Rohling, 1994; Rossignol-Strick, 1983). In accordance with previous observations from the Aegean Sea (Geraga et al., 2010; Kontakiotis, 2016), the elevated percentages of the species *G. bulloides* and *T. quinqueloba* within S1 are more pronounced in the north than in south Aegean, and are related to low salinity and high fertility of the surficial waters (Rohling et al., 1997; Zachariasse et al., 1997), possibly due to the larger river inflows draining the north Aegean land. The elevated percentages of *T. quinqueloba* and *G. bulloides*, in AEX-15 and AEX-23 (Figures 23 and 25), especially between 8.2 and 7.0 cal ka BP, show that the freshening of sea surface waters driven by enhanced riverine discharges and land runoff due to intensified rainfall was greater towards the end of the sapropel. This is further supported by the contribution of Black Sea outflow after 8 ka (Sperling et al., 2003). This freshening of sea surface resulted in low salinity and eutrophic waters (Figure 34f,i). In contrast, U-index and $\delta^{13}\text{C}$ (Figure 34b,c) in south Aegean reveal that the rainfall was more intense during the lower part of S1a sapropel layer. This is also testified by the presence of the pteropod *L. bulimoides* in the upper part of S1a with peaks at 8.4 ka, 8.1 ka and 7.9 ka (~6%) (Figure 22). This species is indicative of arid conditions (Almogi-Labin et al., 1998, 2008; Edelman-Furstenberg et al., 2009) and thus suggests that during the end of S1a (8.6–7.7 ka) the conditions were more arid than during the onset of S1a (9.4 – 8.6 ka) and the interval of S1b (6.9–6.4 ka).

Another difference between the two basins seems to be the degree of stratification during the S1 deposition. Precisely, the S-index of cores AEX-15 and AEX-23 along with the stratification factor of planktonic foraminifera (PCA2 in AEX-15 and PCA3 in AEX-23) reflect weak stratification of the water column (Figure 35e,f,g,i,j,k). In contrast, the same indices (S-index, PCA2 for both taxa; Figure 35a,b,c) of core KIM-2A are indicative of a strong stratified water column. This indicate a persistence of local deep – water formation in northern Aegean Sea during S1 formation, and it has been also documented by other records in eastern Mediterranean (Kontakiotis, 2016; Kuhnt et al., 2007, 2008). Thus, the stratification in north Aegean Sea is mainly restricted to the surface and enhanced productivity (high E-index and productivity factor PCA; Figure 34f,j) plays the most important role on the formation of S1. This is also enhanced by the planktonic foraminifera fauna. SPRUDTS group relative abundances are higher in south Aegean (in both S1a and S1b) comparing to that of north (Figure 33e,k,p), indicating that stratification in the south Aegean is not limited to the surface, but it is continuous throughout the

euphotic layer. Overall, this can be explained by the cold spells from eastern European and Siberian sources that may have resulted in a repeated cooling of northern Aegean surface waters also during generally warm conditions of the early Holocene (Kuhnt et al., 2007; Rohling et al., 2002b). This could have led to the supplying of at least some oxygen to northern Aegean deep-sea basins while southern Aegean deep-sea basins received less oxygen. As far as the pteropod records for stratification (E/M ratio; %; PCA2 in KIM-2A, PCA3 in AEX-15; Figure 35c,d,g,h,k,l) are concerned, they seem to respond equally in changes the stratification of the water column in both studied areas. This can be explained by the pteropod composition which is not differentiated in these sub-basins. Particularly, in the humid and warmer conditions that persisted during the formation of S1, the subsequent stratification of the water column favored a strong and well developed OMZ that probably led to the reduction of mesopelagic species and thus to the high E/M ratio (Figure 35d,h,l). The presence of the mesopelagic *H. inflatus* into the sapropel sublayers can be explained by its habitat. More explicitly this species adopts a variable depth habitat during its growth stages, and it is more susceptible to the low oxygen concentration in the OMZ (Almogi-Labin et al., 1998; Weikert, 1982; Weikert and Cederbaum, 1987).

From the faunal content of the oxidized part of S1 in north Aegean Sea, it seems that the bottom-water oxygenation has resumed earlier than the final ending of sapropelic conditions indicated by Ba concentration (Figure 16). Specifically, the occurrence of the deep mixing species *G. inflata* and *N. pachyderma* (II *G. inflata* assemblage; Figure 28 and 29) reflects the prevalence of homogenization/overturn conditions in the water column (Casford et al., 2002; Rohling et al., 1997). This is also supported by the pteropod *L. trochiformis* which indicates upwelling conditions (Almogi-Labin et al., 1988; Bé and Gilmer, 1977; Sakthivel, 1969; Wormuth, 1981) (Figure 34i,o). The subsequent regime is also characterized by the slightly colder and less eutrophic conditions, as evidenced by the PPC drop and the relatively lower E-index values (Figures 33g,l and 34f,l). During this interval (7.0–6.1 ka BP), the presence of the bathypelagic *Clio pyramidata* and *C. cuspidata* suggest the recovery of the thermohaline circulation (Figures 24 and 26). Toward the Meghalayan, warm oligotrophic species (*G. ruber* f. *alba*, *G. sacculifer*, *G. rubescens*, and *G. siphonifera* gr.; Figures 23 and 25) prevail in the planktonic fauna, implying a significant reduction in primary productivity and the establishment of modern oligotrophic to mesotrophic conditions.

Post sapropel

From the termination of S1 deposition up to 5.0 ka BP in south Aegean Sea, a trend to heavier $\delta^{18}\text{O}$ values (from 0‰ to +1.3‰) and the drop of PPC (~60%) are recorded (Figure 33a,b). In planktonic foraminifera fauna increase in *G. inflata*, *G. truncatulinoides* and *N. pachyderma* (IIa assemblage; Figure 27) along with the reduction of *G. ruber* f. *rosea*, *G. siphonifera* gr. *O. universa* (Figure 21) indicate lower SST, and stronger seafloor oxygenation due to vertical mixing. This latter is also suggested by the increase in the mesopelagic pteropod *D. trispinosa*. The peak of *L. trochiformis* at 5.7 ka (Figure 34d) is suggestive of upwelling conditions. At this point and up to 5.0 ka increased percentages of *G. bulloides* and *G. sacculifer* are indicative of increased productivity. This is also indicated by the high values of E-index, the heavy $\delta^{13}\text{C}$ (up to +1.7‰) and the PCA2 factor of pteropods (Figure 34a,b,e).

In the north Aegean Sea the main change in the post-sapropel interval, is characterized by a decrease in *G. sacculifer* and *O. universa* (Figures 23 and 25; III *G. ruber* f. *alba* assemblage Figures 28 and 29) that reveals a river-runoff reduction and further coincides with the $\delta^{13}\text{C}$ enrichment trend (Figure 34g,m) observed in both cores. This is further associated with clay mineral data known from the literature (Ehrmann et al., 2007; Roussakis et al., 2004) across this interval, which indicate a change in weathering conditions on land that points to particularly dry conditions in the north Aegean catchment. Moreover, the reduction in the surface water Black Sea outflow at around 4.5 ka BP (Kuhnt et al., 2007; Sperling et al., 2003) has probably caused an increase in sea-surface salinity, which is also testified by the slightly heavier (up to 0.8‰ enrichment) planktic $\delta^{18}\text{O}$ record (Figure 33h,m), the reduction in the relative abundance of *L. trochiformis*, and the appearance of the stenohaline species *S. subula* at 3.3 ka BP (Figures 24 and 26) (Buccheri et al., 2002). These observations support the idea of a general trend to climatic aridification during the Meghalayan stage, which is in accordance with the salinity increase and oligotrophic nature of the water column of the modern north Aegean Sea.

7.3. Holocene climate variability and its relationship to large-scale climatic changes

The qualitative SST reconstructions for the Aegean Sea reveal a distinct pattern of climate oscillations that generally agrees with the previously reported series of millennial-scale fluctuations in the region (Kontakiotis, 2016; Kotthoff et al., 2008a, 2008b; Le Houedec et al., 2020; Rohling et al., 2002a), but which enriches that picture with centennial-scale details. The Holocene climatic instability of the study area is further supported by episodes of brief cooling, with the suggested mechanism that caused the development of these cooling spells to involve local features, such as intensified orographically channeled, northerly air outbreaks and/or land-sea contrasts (Brayshaw et al., 2011; Rohling et al., 2002a). Six distinct sea-surface cooling events in the north Aegean (referred to as “NAEGC”; Giamali et al., 2019) and two in the south Aegean Sea (referred to as “SAEGC”) have been identified in the present study (Figure 36 and Table 21), corresponding to similar short and abrupt cold/dry events that have been described in different basins in the Mediterranean (Cacho et al., 2001; Combourieu-Nebout et al., 2009, 2013; Desprat et al., 2013; Frigola et al., 2007; Geraga et al., 2008; Sbaffi et al., 2004; Schmiedl et al., 2010; Table 22). Furthermore, similarities to the GISP2 ice core, and their coincidence with times of weakening monsoonal activity (Incarbona and Sprovieri, 2020), lowering of lake levels in eastern Africa (Gasse, 2000), and glacier advances in Europe (Denton and Karlén, 1973), suggest correlations with the paleoclimatic changes occurring at high latitudes of the northern Atlantic and worldwide (Bond et al., 2001; Bond et al., 1997; Mayewski et al., 2004; Wanner et al., 2015; Wanner et al., 2011). These correlations reinforce earlier observations of teleconnections between Holocene climate variability of the (sub)tropics and the high latitudes at multi-centennial to millennial timescales (Marino et al., 2009; Rohling et al., 2002a). Each cooling event results in an approximate drop in temperature of 2–4° C, independently confirming what previous studies, using different methods, have shown (Cacho et al., 2001; Rohling et al., 2002a).

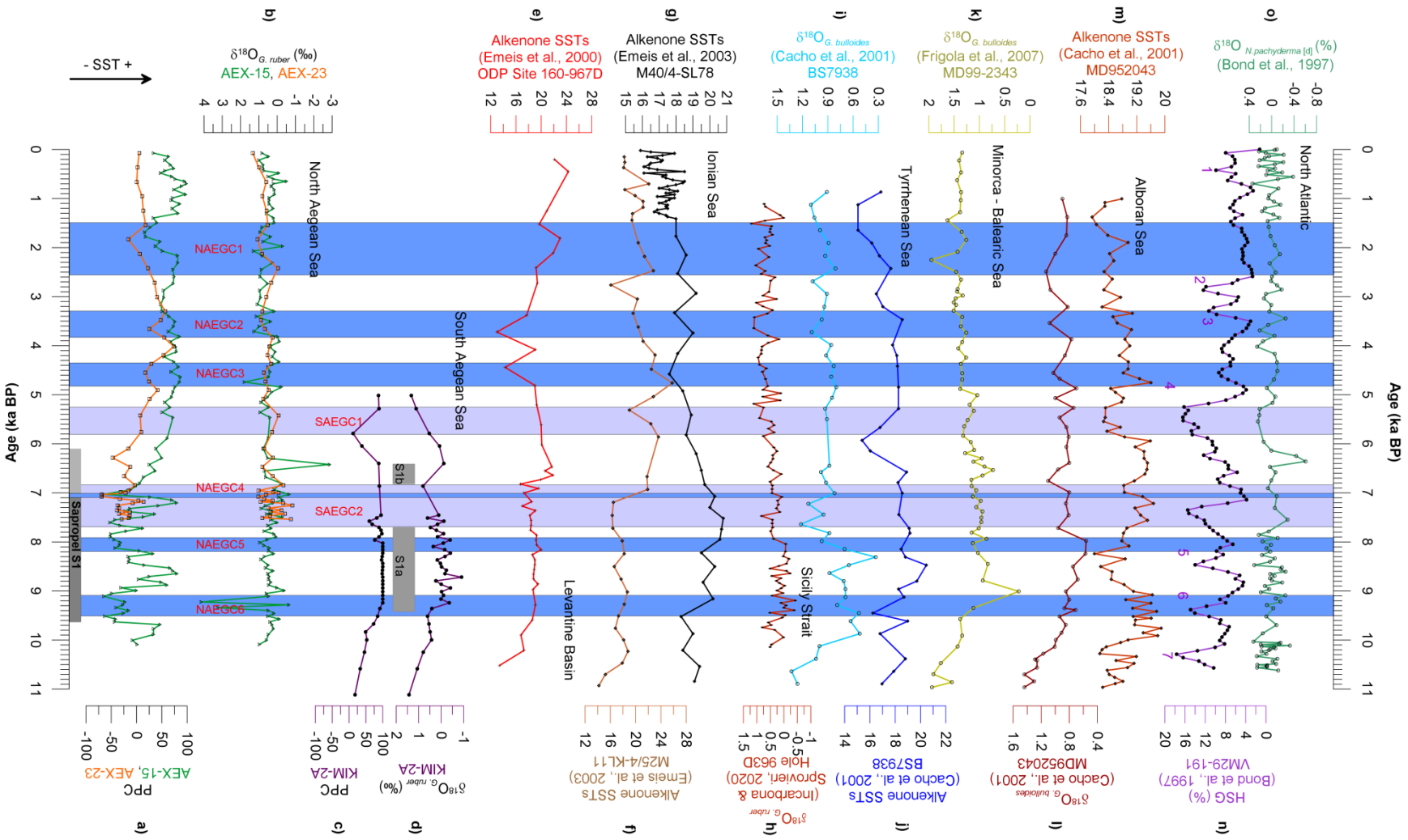


Fig. 36. Comparison of north and south Aegean results with relevant climate reconstructions of the eastern, central, and western Mediterranean and North Atlantic, including the following: a) Planktonic paleoclimatic curve (PPC) of north Aegean cores (green line for AEX-15 and orange line for AEX-23). b) Oxygen isotope record ($\delta^{18}\text{O}_{G. ruber}$) of north Aegean cores (green line for AEX-15 and orange line for AEX-23). c) Planktonic paleoclimatic curve (PPC) of core KIM-2A. d) Oxygen isotope record ($\delta^{18}\text{O}_{G. ruber}$) of core KIM-2A. e) Alkenone sea surface temperatures (SSTs) of ODP site 160-967D in the Levantine Basin (Emeis et al., 2000). f and g) Alkenone SSTs from cores M25/4-KL11 and M40/4-SL78, respectively, from the Ionian Sea (Emeis et al., 2003). h) Oxygen isotope record ($\delta^{18}\text{O}_{G. ruber}$) of core 963D from Sicily Strait (Incarbona and Sprovieri, 2020). i) $\delta^{18}\text{O}_{G. bulloides}$ of core BS7938 (Cacho et al., 2001). j) Alkenone SSTs of core BS7938 from the Tyrrhenean Sea (Cacho et al., 2001). k) $\delta^{18}\text{O}_{G. bulloides}$ from core MD99-2343 in the Balearic Sea (Frigola et al., 2007). l) $\delta^{18}\text{O}_{G. bulloides}$ of core MD952043 (Cacho et al., 2001). m) Alkenone SSTs of core MD952043 in the Alboran Sea (Cacho et al., 2001). n) Hematite stained grains (HSG)–based cold events for VM29-191 (Bond et al., 1997). o) $\delta^{18}\text{O}_{N. pachyderma}$ for VM29-191 (Bond et al., 1997). Blue bands correspond to North Aegean cooling events and light blue bands to the South Aegean cooling events, whereas gray and light gray bands to the sapropel S1 interval (or sapropel sublayers; S1a and S1b) and its oxidized part.

Table 21. Timing of the Holocene abrupt climate events in North and South Aegean.

North Aegean Sea	Age (ka BP)	Central Age (ka BP)	Duration (ka)	Time Since Previous Event (ka)
NAEGC1	2.6-1.5	2.05	1.1	1.5
NAEGC2	3.8-3.3	3.55	0.5	1.0
NAEGC3	4.8-4.3	4.55	0.5	2.5
NAEGC4	7.1-7.0	7.05	0.1	1.0
NAEGC5	8.2-7.9	8.05	0.3	1.25
NAEGC6	9.5-9.1	9.3	0.4	-
South Aegean Sea	Age (ka BP)	Central Age (ka BP)	Duration (ka)	Time Since Previous Event (ka)
SAEGC1	5.7-5.0	5.35	0.7	2.0
SAEGC2	7.9-6.8	7.35	1.1	-

7.3.1. Abrupt Holocene cooling events and their impact on eastern Mediterranean hydrologic regime

The Holocene abrupt events detected in the Aegean Sea have an average duration of 600 years and an observed periodicity of 1200 years (Table 21). The differences in time or the absence of some of the cooling events among the three cores is most likely due to the different sampling resolution, the different age model between north and south Aegean cores and the different hydrographic condition prevailing in the two basins.

The most pronounced Holocene abrupt cooling events (NAEGC6–NAEGC4 & SAEGC2–SAEGC1) occurred at 9.5–9.1, 8.2–7.9, and 7.1–7.0 ka BP in north Aegean and at 7.9–6.8 and 5.7–5.2 ka BP in south Aegean Sea. They punctuate the wettest phase as deduced by our planktonic foraminifera records during the Greenlandian–Northgrippian stages, and they seem to exert important control on sapropel deposition within the Mediterranean Sea. All these events parallel the widely documented abrupt cooling events punctuating the early–middle Holocene: the “Boreal Oscillation” at ~10.0 ka BP (Björck et al., 2001); the “9.3 ka event” (Rasmussen et al., 2007); the “8.2-event” (Alley et al., 1997); and a final event at ~7.4 ka BP (Bond et al., 2001), which likely corresponds to the drier episode detected at ~7.0 ka BP (Figure 36). They also coincide with the weakening activity in the West Africa and Indian monsoons (Fleitmann et al., 2003; Incarbona and Sprovieri, 2020). These events were related to a series of recurrent (dry) atmospheric climatic anomalies, which can be furthermore associated with meltwater pulse perturbation of the north Atlantic climate.

In particular, in North Aegean records, there are two sharp negative peaks in the PPC at 9.5 and 9.1 ka BP, coupled with two intervening $\delta^{18}\text{O}$ positive excursions (at ~9.3 and 9.2 ka BP), which are superimposed on a broader period of climatic deterioration in the Aegean Sea during this time interval (Figure 36a,b). Cooling event NAEGC6 is coeval with relevant cooling events in Tyrrhenian basin centered at 9.5 ka BP (Rohling et al., 1997; Sbaifi et al., 2004) and further coincides with aridification events based on pollen assemblage changes in the Alboran Sea (Combourieu Nebout et al., 2009) (Table 22). The forest decline (Giamali et al., 2019) at this time is associated with a prominent SST cooling event in the eastern Norwegian Sea (Berner et al., 2010) and coincides with cooling in the NGRIP (North Greenland Ice Core Project) record toward 9.95 ka BP, although this anomaly is not consistent across different Greenland records

(Rasmussen et al., 2007). NAEGC6 is possibly linked to an Atlantic meridional overturning circulation (AMOC) reduction because of a meltwater pulse at St. Lawrence Bay (Fleitmann et al., 2008) or alternatively to contemporaneous outburst floods from proglacial lakes such as Lake Agassiz (Teller and Leverington, 2004), Lake Labrador- Ungava (Jansson and Kleman, 2004), Lake Superior (Yu et al., 2010), or Baltic ice Lake in SW Sweden (Nesje et al., 2004), and with solar activity minima (Bond et al., 2001; Magny and Bégeot, 2004).

The following NAEGC5 event, constrained here by progressive $\delta^{18}\text{O}$ enrichment to maximum values (+0.95‰) centered on 8.1 ka BP, corresponds to the regional expression of the 8.2 ka BP cold/arid north Atlantic event (Bond et al., 1997, 2001). Surprisingly, that $\delta^{18}\text{O}$ enrichment appears coeval in time but not in amplitude to the negative 2‰ $\delta^{18}\text{O}_{\text{ice}}$ event in the Greenland ice cores (Rasmussen et al., 2007), which is thought to represent an $\sim 6^\circ\text{C}$ cooling of the air temperature over Greenland Summit (Alley et al., 1997). The significant decline in the PPC (from +32% to -42%; Figure 36a) provides evidence for an abrupt winter SST minimum on the northern Aegean borderlands in response to the 8.2 ka BP AMOC reduction (LeGrande et al., 2006; Wiersma and Renssen, 2006).

The SAEGC2 event detected in KIM-2A core seems to correspond as well to the 8.2 ka BP cold event. The cooling identified by PPC (drop from 100% to 60%) and $\delta^{18}\text{O}$ (from -0.3 to +0.8‰) records at 7.9–6.8 ka BP (Figure 36c,d), led to the S1 interruption (as evidenced also by the Corg; Figure 15). This event has also been identified in neighboring cores (C69-ST2 in Myrtoan Basin at 8.0–6.5 cal ka BP; (Geraga et al., 2005), in the central (Combourieu-Nebout et al., 2013; Sbaffi et al., 2001) and in the western Mediterranean Sea (Frigola et al., 2007) (Table 22). The weakening monsoonal activity and the intensification of the atmospheric circulation (Incarbona and Sprovieri, 2020; Marino et al., 2009) during SAEGC2 led to good ventilation conditions in the Aegean basin interrupting the S1 deposition, synchronously with the termination of the formation of the enriched in organic matter layer (organic rich layer; Cacho et al., 2002) in the Alboran Sea (western Mediterranean).

The sharp drop in PPC around 7.0 ka BP corresponds to the NAEGC4 cooling event (Figure 36a). This event is attributed to the strengthening and increases in frequency of winter cooling, driven by changes in intensity of high-latitude continental air masses (Rohling et al., 2002b). The intensification of the atmospheric circulation during this time interval led to improved ventilation

conditions in the eastern Mediterranean basin. This cooling event may have induced the resumption of deep-water formation in the north Aegean Sea. Indeed, density of the surficial waters was sufficiently high during that time interval to enable the ventilation of the deep north Aegean basin, because of the counterbalance between salinity depletion and SST decrease. This notion is also confirmed by the higher benthic $\delta^{13}\text{C}$ ($\sim 1.1\text{--}1.4\text{‰}$) values, the significant increase of the benthic foraminifera *Cibicidoides* (Abu-Zied et al., 2008; Kuhnt et al., 2007; Schmiedl et al., 2010) and the planktonic *G. inflata* recorded in the studied and other cores between 7.0 and 6.0 ka BP (Casford et al., 2002; Geraga et al., 2010; Kontakiotis, 2016), attesting the return to oxic conditions and the resumption of the north Aegean deep-water formation just after the end of S1. Similar short cooling events were detected using foraminiferal and pollen assemblages in the Minorca Basin (M7 event; (Frigola et al., 2007); Figure 36k) and the Siculo-Tunisian Strait (at 7.3–6.7 ka BP; (Desprat et al., 2013) (Table 22). In the Adriatic and Aegean basins (AdC5 and C69-ST2 events, respectively; Combourieu-Nebout et al., 2013; Geraga et al., 2005; Jimenez-Espejo et al., 2008), these events are supposed to be responsible for sapropel termination. Following the interpretation of Rohling et al., (2002a) and Casford et al., (2003), the absence of these events in $\delta^{18}\text{O}_{G. ruber}$ was suggested to reflect a seasonal offset between climate forcing and the proxy carrier, as cooling is a winter phenomenon and therefore is not recorded by *G. ruber*, which thrives in the summer mixed layer.

At 6.3 ka BP, negative values in the PPC (-46%) of core AEX-23 are observed that are not followed by any enrichment in $\delta^{18}\text{O}_{G. ruber}$ in the studied cores or negative PPC values of AEX-15 and KIM-2A (Figure 36a,b,c,d). No cooling event is identified in this time interval, and the observed negative PPC peak is suggested that is attributed to increased *T. quinqueloba* percentages (59%; Figures 23 and 25). A similar decrease in arboreal vegetation has also been observed during that time in north Aegean cores and possibly highlights the onset of the transition toward drier mid- to late Holocene (Giamali et al., 2019).

The trend to heavier values of $\delta^{18}\text{O}_{G. ruber}$ along with the negative peak of PPC (12%; Figure 36c,d) in the south Aegean core (KIM-2A), marks the SAEGC1 event (5.7–5.0 ka BP). This cooling has also been identified in Myrtoan Basin (C69-ST1; Geraga et al., 2005), in the Ionian Sea (Z1-CE3; Geraga et al., 2008), in central (SCE4; Sbaffi et al., 2004, TC3; Cacho et al., 2001, 5.6-5.0; Desprat et al., 2013, AdC3; Combourieu-Nebout et al., 2013) and in western

Mediterranean Sea (AC2; Cacho et al., 2001, ACP4; Combourieu Nebout et al., 2009) as shown in Table 22. The possible suggested causes of this event are the decline in solar output (Bond et al., 2001; Denton and Karlén, 1973; Mayewski et al., 2004). In the eastern Mediterranean, this event is correlated to the end of the sapropel S1 deposition (De Rijk et al., 1999; Geraga et al., 2005; Rohling et al., 1997).

The nature and intensity of the NAEGC3 event at 4.8–4.3 ka BP in the isotope record, resembling the previous events, also points to a climate origin and hence is thought to be the result of a cold and dry episode. The PPC drop of ~20% in both cores of north Aegean Sea is in phase and is associated with the 4.2 ka BP north Atlantic Holocene cold event (Bond et al., 2001; Bond et al., 1997) (Figure 36a,n,o), as well as with $U^{k'}_{37}$ -SST minima along the Mediterranean Sea (Cacho et al., 2001; Emeis et al., 2000, 2003). NAEGC3 could also correspond to the ACP4 of the Adriatic Sea (Combourieu Nebout et al., 2009), M5 in Minorca Basin (Frigola et al., 2007), the 4.5 ka BP event of the Siculo-Tunisian Strait (Desprat et al., 2013), the Ionian and Levantine Seas (Emeis et al., 2003; Emeis et al., 2000; Geraga et al., 2008), AdC3 in Adriatic Sea (Combourieu-Nebout et al., 2013), and the 4–4.4 ka BP of the north Aegean Sea (Kotthoff et al., 2008a; Schmiedl et al., 2010) (Table 22). This event is further evident on the northern side of the Mediterranean Basin (Magny et al., 2009; Peyron et al., 2011), in the Medjerda Valley (Faust et al., 2004; Zielhofer et al., 2004), and in the speleothems of Gueldaman Cave (Ruan et al., 2016). This cold episode, largely expressed in climate records as expanding from polar to tropical regions, has been attributed to a weakening of the Northern Hemisphere summer insolation (Bond et al., 2001; Mayewski et al., 2004). This cold and arid spell, although weakened in the north Aegean Sea (Kontakiotis, 2016), caused the temporary enhanced deep-water ventilation and consequently the restoration of oxic conditions in the north Aegean. This is further supported by the low accumulation rates of marine and terrestrial biomarkers and elevated $\delta^{15}N$ values from nearby north Aegean cores (Gogou et al., 2007), which indicate that the deep north Aegean was fully oxygenated during that period.

The interval between 3.8 and 3.3 ka BP comprises heavier $\delta^{18}O$ values, a drop in the PPC of ~25% in both cores (Figure 36a,b), and the first appearance of *L. retroversa* in the Holocene for core AEX-23 (Figure 33o). The latter species, previously was supposed to be accidentally present in the sediments of the upper Holocene, due to sampling processes (Janssen 2012).

However, this study shows that this cold-water species was able to enter the pteropod fauna of the eastern Mediterranean during the cold events. This can also be testified by the length of the cores (especially of AEX-23; retrieved from 142.5 cm). This episode (NAEGC2) coincides with equivalent events in the Mediterranean Sea based on planktonic foraminifera and pollen assemblages (Combourieu Nebout et al., 2009; Frigola et al., 2007; Sbaffi et al., 2004) (Table 22). In the Tyrrhenian Sea, this event appears to be intense with an approximate decrease in SST of 2.5–3.5°C based on alkenone and the modern analogue technic SSTs reconstructions (Sbaffi et al., 2004). At 2.6–1.5 ka BP, heavier isotope values, significant drop in PPC, appearance of the cold water pteropod *L. retoversa*, have been documented in both cores corresponding to NAEGC1 event (Figures 36a,b and 33i,o). This is correlated with the dry episode recorded from marine cores in the eastern Mediterranean between 3.0 and 1.7 ka BP (Jalut et al., 2009; Magny et al., 2003). It is also evident in the western and central part of the Mediterranean between 3.2 and 1.4 ka BP (Cacho et al., 2001; Combourieu Nebout et al., 2009; Frigola et al., 2007; Sbaffi et al., 2004) and is correlated to the NAC2 event (Bond et al., 1997) (Table 22).

Table 22. List of short Holocene cooling events recorded in the North and South Aegean Sea and their correspondence to the relevant dry/cooling events in different basins (Alboran Sea, Balearic Sea, Tyrrhenian Sea, Siculo-Tunisian Strait, Adriatic Sea, Ionian Sea, and Aegean Sea) of the Mediterranean Sea, in the North Atlantic, and globally. Names of each event were provided followed by ages in brackets (in ka BP). In cases where the events are not named, only ages are given.

MEDITERRANEAN SEA														North Atlantic	Globally
This study	Aegean Sea		Ionian Sea	Adriatic Sea	Siculo-Tunisian Strait	Tyrrhenian Sea		Minorca	Alboran Sea						
Age (ka BP)	Schmiel et al., 2010 & Kotthoff et al., 2008a	Geraga et al., 2005	Geraga et al., 2008	Comboureu - Nebout et al., 2013	Desprat et al., 2013	Cacho et al., 2001	Sbaffi et al., 2004	Frigola et al., 2007	Cacho et al., 2001	Comboureu - Nebout et al., 2009	Bond et al., 1997	Mayewski et al., 2004			
North Aegean Sea	NAEGC1	2.6-1.5	2.7-2.4				TC1 (1.9-1.0) & TC2 (3.45-2.5)	SCE1 (1,7-0,9) & SCE2 (3.2-2.4)	SCE2 (3.2-2.5)	M1(1.8-1.4) & M2 (2.6-2.3)	AC1 (1.90-1.01)	APC2 (2.6-2.3)	NAC2 (2.8)	RCC4 (3.5-2.5)	
	NAEGC2	3.8-3.3						SCE3 (3.9-3.5)	M3 (3.4-3.1)		APC3 (3.77-3.14)				
	NAEGC3	4.8-4.3	4.4-4.0	Z1-CE2 (4.0)	AdC 2 (4.2)	4.5				M5 (5.3-4.7)	AC2 (5.94-4.75)	ACP4 (6.0-4.5)	NAC3 (4.3)		
	NAEGC4	7.1-7.0	C69-ST2 (8-6.5)	Z1-CE4 (7.0)	AdC 5 (7.0)	7.3-6.7			SCE5 (7.6-6.9)	M7 (7.4-6.9)					
	NAEGC5	8.2-7.9	8.3-8	Z1-CE5 (8.2)	AdC 6 (8.2)	8.5-7.9		SCE5(8.2-7.5)		M8 (9.0-7.8)	AC3 (9.08-7.56)	APC5 (8.5-7.9)	NAC5 (8.2)	RCC1 (9.0-8.0)	
	NAEGC6	9.5-9.1				9.5-9.1	TC4 (9.62-9.13)		SCE6 (9.9-9.0)			APC6 (9.6-8.9)	NAC6 (9.5)		
South Aegean Sea	SAEGC1	5.7-5.0	C69 - ST1 (5.5)	Z1-CE3 (5.0)	AdC 3 (5.0)	5.6 -5.0	TC3 (6.58-5.28)	SCE4 (5.0-6.0)			AC2 (5.94-4.75)	ACP4 (6.0-4.5)	NAC4 (5.9)	RCC2 (6.0-5.0)	
	SAEGC2	7.9-6.8	6.7-6.3	C69 - ST2 (8.0 -6.5)	Z1-CE4 (7.0)	AdC 5 (7.0)	7.3-6.7	SCE5 (8.2-7.6)	SCE5 (7.6-6.9)	M7 (7.4-6.9)	AC3 (9.08-7.56)				

8. Conclusions

This main objective of this thesis was to contribute in the understanding of the palaeoclimate during the last ~21 ka, as depicted from the planktonic foraminifera and pteropod fauna retrieved from three gravity cores located at north and south Aegean. The interpretations were based on the abundances of planktonic foraminiferal and pteropod assemblages and the down-core variations of the stable isotope ($\delta^{18}\text{O}$, $\delta^{13}\text{C}$) values, combined with the results of multivariate statistical analysis, in association with temperature- productivity- and stratification related paleoceanographic data.

The main conclusions of this research are summarized below:

- Two cores from the North Aegean Trough and one from a submarine depression between Kimolos and Sifnos islands were examined. Based on their lithological characteristics the faunal content and the AMS radiocarbon (^{14}C) datings, the age model performed indicated that sediment levels used in this thesis span the last 10.1 ka in core AEX-15, 7.5 ka in AEX-23 and 21.1 ka in KIM-2A. The sedimentation rates that calculated confirm the already known data with higher sedimentation rates in the north Aegean Sea (17.3 and 42.8 cm/ka for AEX-15 and AEX-23 respectively) in comparison with the south Aegean (11.86 cm/ka).
- Apart from the already well known records on late Quaternary planktonic foraminifera assemblages in the Aegean Sea, this research provided for the first time information on late Quaternary pteropod fauna for this region. Specifically, the pteropod fauna of the Aegean Sea consists of 13 Euthecosomata species, with some of them encountered only in one of the two regions due to their habitat preferences and/or hydrologic conditions of the studied areas.
- The Q-mode analysis performed in the planktonic foraminiferal fauna revealed two and three distinct assemblages in south and north Aegean respectively, each one representative of different hydrological and climatic conditions. These assemblages were further divided were needed into sub-assemblages that correspond to sapropel, pre- or post- sapropel, and late glacial and deglaciation conditions.

- The Principal Component Analysis performed in both fauna groups, suggested that the sea surface temperature, productivity, stratification of the water column, upwelling and seasonality are the main controllers of the planktonic foraminifera distributions, whilst for the pteropod fauna the sea surface temperature, productivity, stratification of the water column, and upwelling control their distribution.
- The comparison of the data retrieved by the faunal distributions and the statistical analysis indicated differences between the two studied areas. Specifically, in the south Aegean Sea temperature seems to be the main controller, which is partly attributed to the time that sediments of core KIM-2A span. On the other hand, in the north Aegean Sea productivity is the main factor followed by stratification, factor that contributes in both studied areas and also affects both groups. Each described factor does not affect equally the different faunal groups.
- In order to proceed in the palaeoclimatic and palaeoenvironmental reconstruction, selected indices from the available bibliography were used. In those, a new index based on pteropods is suggested for the first time, so as to express the stratification of the water column, namely the E/M ratio.
- Combining all data available in this thesis a succession of Late glacial to Holocene paleoclimatic and paleoceanographic changes is revealed. During the Late Glacial, all the records in south Aegean Sea indicate the occurrence of cold and eutrophicated waters. The time interval of 15.9–11.7 ka, corresponding to the deglaciation phase, was characterized by gradual climatic amelioration. During this interval, the warm interstadial Bølling–Allerød was identified, while low SST records at 12.9 ka revealed the onset of the YD. During this event, mild climate conditions were observed for around 400 years, and are attributed to the displacement of the polar front by a few degrees north. With the onset of the Holocene, a general climatic amelioration was observed, with the gradual development of stratified oligotrophic surface waters. These conditions were intensified during the sapropel S1 deposition, which started at 9.6 ka and ended in 6.1 ka in north Aegean Sea, and appears in two layers in the south Aegean (S1a: 9.4–7.7 ka and S1b: 6.9–6.4 ka). The faunal and isotopic data suggest that conditions were more arid in the south Aegean, and especially towards the end of S1a. The interruption of sapropel

deposition (S1i) in core KIM-2A and the post-sapropel interval of all the cores are characterized by lower SST and stronger seafloor oxygenation due to vertical mixing.

- Overall, the high sedimentation rates encountered in the analyzed cores and the high-resolution sampling have contributed to the detection of six cold/arid events in the north Aegean Sea and two in the south Aegean, throughout the Holocene. Although absolute age control provides only modest constraint, these events also appear to correlate with equivalent events documented within and beyond the Mediterranean Sea in north latitude areas, northeastern Africa, and the Middle East, pointing to large, hemispheric-scale teleconnections.

9. References

1. Abu-Zied, R. H., Rohling, E. J., Jorissen, F. J., Fontanier, C., Casford, J. S. L., and Cooke, S., 2008, Benthic foraminiferal response to changes in bottom-water oxygenation and organic carbon flux in the eastern Mediterranean during LGM to Recent times: *Marine Micropaleontology*, v. 67, no. 1-2, p. 46-68.
2. Acker, J. G., and Byrne, R. H., 1989, The influence of surface state and saturation state on the dissolution kinetics of biogenic aragonite in seawater: *American Journal of Science*, v. 289, no. 9, p. 1098-1116.
3. Aksu, A. E., Yaşar, D., and Mudie, P. J., 1995, Paleoclimatic and paleoceanographic conditions leading to development of sapropel layer S1 in the Aegean Sea: *Palaeogeography, Palaeoclimatology, Palaeoecology*, v. 116, no. 1, p. 71-101.
4. Alley, R. B., Mayewski, P. A., Sowers, T., Stuiver, M., Taylor, K. C., and Clark, P. U., 1997, Holocene climatic instability: A prominent, widespread event 8200 yr ago: *Geology*, v. 25, no. 6, p. 483-486.
5. Almogi-Labin, A., 1982, Stratigraphic and paleoceanographic significance of Late Quaternary pteropods from deep-sea cores in the Gulf of Aqaba (Elat) and northernmost Red Sea: *Marine Micropaleontology*, v. 7, no. 1, p. 53-72.
6. Almogi-Labin, A., Bar-Matthews, M., Shriki, D., Kolosovsky, E., Paterne, M., Schilman, B., Ayalon, A., Aizenshtat, Z., and Matthews, A., 2009, Climatic variability during the last ~90ka of the southern and northern Levantine Basin as evident from marine records and speleothems: *Quaternary Science Reviews*, v. 28, no. 25, p. 2882-2896.
7. Almogi-Labin, A., Edelman-Furstenberg, Y., and Hemleben, C., 2008, Variations in the biodiversity of thecosomatous pteropods during the Late Quaternary as a response to environmental changes in the Gulf of Aden - Red Sea - Gulf of Aqaba ecosystem, *in* In Por, D. e. A.-E., ed., *The improbable Gulf. Environment, biodiversity and preservation.* , The Hebrew University Magnes Press, p. 31-48.
8. Almogi-Labin, A., Hemleben, C., and Deuser, W. G., 1988, Seasonal variation in the flux of euthecosomatous pteropods collected in a deep sediment trap in the Sargasso Sea: *Deep Sea Research Part A. Oceanographic Research Papers*, v. 35, no. 3, p. 441-464.

9. Almogi-Labin, A., Hemleben, C., and Meischner, D., 1998, Carbonate preservation and climatic changes in the central Red Sea during the last 380 kyr as recorded by pteropods: *Marine Micropaleontology*, v. 33, no. 1, p. 87-107.
10. Almogi-Labin, A., Hemleben, C., Meischner, D., and Erlenkeuser, H., 1991, Paleoenvironmental events during the last 13,000 years in the central Red Sea as recorded by pteropoda: *Paleoceanography*, v. 6, no. 1, p. 83-98.
11. Almogi-Labin, A., Luz, B., and Duplessy, J.-C., 1986, Quaternary paleo-oceanography, pteropod preservation and stable-isotope record of the Red Sea: *Palaeogeography, Palaeoclimatology, Palaeoecology*, v. 57, no. 2-4, p. 195-211.
12. Almogi-Labin, A., and Reiss, Z., 1977, Quaternary pteropods from Israel: *Revista Española de Micropaleontología*, v. 9, no. 1, p. 5-48.
13. Almogi-Labin, A., Schmiedl, G., Hemleben, C., Siman-Tov, R., Segl, M., and Meischner, D., 2000, The influence of the NE winter monsoon on productivity changes in the Gulf of Aden, NW Arabian Sea, during the last 530 ka as recorded by foraminifera: *Marine Micropaleontology*, v. 40, no. 3, p. 295-319.
14. Anastasakis, G. C., and Stanley, D. J., 1984, Sapropels and organic-rich variants in the Mediterranean: sequence development and classification: Geological Society, London, Special Publications, v. 15, no. 1, p. 497.
15. Angelova, V., Akova, V., Ivanov, K., and Licheva, P. A., 2014, Comparative study of titrimetric methods for determination of organic carbon in soils, compost and sludge: *J. of International Scientific Publications: Ecology and Safety*, v. 8, p. 430-440.
16. Antonarakou, A., Kontakiotis, G., Karageorgis, A. P., Besiou, E., Zarkogiannis, S., Drinia, H., Mortyn, G. P., and Tripsanas, E., 2019, Eco-biostratigraphic advances on late Quaternary geochronology and palaeoclimate: the marginal Gulf of Mexico analogue: *Geological Quarterly*, v. 63, no. 1.
17. Antonarakou, A., Kontakiotis, G., Mortyn P., G., Drinia, H., Sprovieri, M., Besiou, E., and Tripsanas, E., 2015, Biotic and geochemical ($\delta^{18}\text{O}$, $\delta^{13}\text{C}$, Mg/Ca, Ba/Ca) responses of *Globigerinoides ruber* morphotypes to upper water column variations during the last deglaciation, Gulf of Mexico: *Geochimica Cosmochimica Acta*, v. 170, p. 69-93.
18. Antonarakou, A., Kontakiotis, G., Zarkogiannis, S., Mortyn, P. G., Drinia, H., Koskeridou, E., and Anastasakis, G., 2018, Planktonic foraminiferal abnormalities in

coastal and open marine eastern Mediterranean environments: A natural stress monitoring approach in recent and early Holocene marine systems: *Journal of Marine Systems*, v. 181, p. 63-78.

19. Aurahs, R., Grimm, G., Hemleben, V., Hemleben, C., and Kucera, M., 2009, Aurahs R, Grimm GW, Hemleben V, Hemleben C, Kucera M.. Geographical distribution of cryptic genetic types in the planktonic foraminifer *Globigerinoides ruber*. *Mol Ecol* 18: 1692-1706: *Molecular ecology*, v. 18, p. 1692-1706.
20. Aurahs, R., Treis, Y., Darling, K., and Kucera, M., 2011, A revised taxonomic and phylogenetic concept for the planktonic foraminifer species *Globigerinoides ruber* based on molecular and morphometric evidence: *Marine Micropaleontology*, v. 79, p. 1-14.
21. Bazzicalupo, P., Maiorano, P., Girone, A., Marino, M., Combourieu-Nebout, N., Pelosi, N., Salgueiro, E., and Incarbona, A., 2020, Holocene climate variability of the Western Mediterranean: Surface water dynamics inferred from calcareous plankton assemblages: *The Holocene*, v. 30, no. 5, p. 691-708.
22. Bé, A. W. H., and Gilmer, R. W., 1977, A zoogeographic and taxonomic review of euthecosomatous Pteropoda: *Oceanic Micropaleontology*, v. 1, p. 733-808.
23. Bednaršek, N., Možina, J., Vogt, M., O'Brien, C., and Tarling, G. A., 2012a, The global distribution of pteropods and their contribution to carbonate and carbon biomass in the modern ocean: *Earth System Science Data*, v. 4, no. 1, p. 167-186.
24. Bednaršek, N., Tarling, G. A., Bakker, D. C. E., Fielding, S., Cohen, A., Kuzirian, A., McCorkle, D., Lézé, B., and Montagna, R., 2012b, Description and quantification of pteropod shell dissolution: a sensitive bioindicator of ocean acidification: *Global Change Biology*, v. 18, no. 7, p. 2378-2388.
25. Berger, W. H., Bonneau, M. C., and Parker, F. L., 1982, Foraminifera on the deep-sea floor-lysocline and dissolution rate: *Oceanologica Acta*, v. 5, no. 2, p. 249-258.
26. Berner, K. S., Koç, N., and Godtliabsen, F., 2010, High frequency climate variability of the Norwegian Atlantic Current during the early Holocene period and a possible connection to the Gleissberg cycle: *The Holocene*, v. 20, no. 2, p. 245-255.
27. Berner, R. A., and Honjo, S., 1981, Pelagic sedimentation of aragonite: its geochemical significance: *Science*, v. 211, no. 4485, p. 940-942.

28. Bhattacharjee, D., 1997, "Pteropod preservation spike" and its significance in the Andaman Sea: *Journal of The Paleontological Society of India*, v. 42, p. 11.
29. Biekart, W. J., 1989, Euthecosomatous pteropods as paleohydrological and paleoecological indicators in a Tyrrhenian deep-sea core: *Palaeogeography, Palaeoclimatology, Palaeoecology*, v. 71, no. 3, p. 205-224.
30. Bijma, J., Erez, J., and Hemleben, C., 1990a, Lunar and semi-lunar reproductive cycles in some spinose planktonic foraminifers: *The Journal of Foraminiferal Research*, v. 20, no. 2, p. 117-127.
31. Bijma, J., Faber, W. W., and Hemleben, C., 1990b, Temperature and salinity limits for growth and survival of some planktonic foraminifers in laboratory cultures: *The Journal of Foraminiferal Research*, v. 20, no. 2, p. 95-116.
32. Björck, S., Muscheler, R., Kromer, B., Andresen, C. S., Heinemeier, J., Johnsen, S. J., Conley, D., Koç, N., Spurk, M., and Veski, S., 2001, High-resolution analyses of an early Holocene climate event may imply decreased solar forcing as an important climate trigger: *Geology*, v. 29, no. 12, p. 1107-1110.
33. Björck, S., Walker, M., Cwynar, L., Johnsen, S., Knudsen, K., Lowe, J., and Wohlfarth, B., 1998, An event stratigraphy for the Last Termination in the North Atlantic region based on the Greenland ice-core record: a proposal by the INTIMATE group: *Journal of Quaternary Science*, v. 13, p. 283-292.
34. Blanc-Vernet, L., Chamley, H., and Froget, C., 1969, Paleoclimatological analysis of a core from the northwestern Mediterranean. Comparison of the results of three studies: Foraminifera, Pteropoda and sedimentology: *Palaeogeography, Palaeoclimatology, Palaeoecology*, v. 6, p. 215-235.
35. Bond, G., Broecker, W., Johnsen, S., McManus, J., Labeyrie, L., Jouzel, J., and Bonani, G., 1993, Correlations between climate records from North Atlantic sediments and Greenland ice: *Nature*, v. 365, no. 6442, p. 143-147.
36. Bond, G., Kromer, B., Beer, J., Muscheler, R., Evans, M. N., Showers, W., Hoffmann, S., Lotti-Bond, R., Hajdas, I., and Bonani, G., 2001, Persistent solar influence on North Atlantic climate during the Holocene: *Science*, v. 294, no. 5549, p. 2130-2136.

37. Bond, G., Showers, W., Cheseby, M., Lotti, R., Almasi, P., DeMenocal, P., Priore, P., Cullen, H., Hajdas, I., and Bonani, G., 1997, A pervasive millennial-scale cycle in North Atlantic Holocene and glacial climates: *science*, v. 278, no. 5341, p. 1257-1266.
38. Bonfardeci, A., Caruso, A., Bartolini, A., Bassinot, F., and Blanc-Valleron, M. M., 2018, Distribution and ecology of the *Globigerinoides ruber* — *Globigerinoides elongatus* morphotypes in the Azores region during the late Pleistocene-Holocene: *Palaeogeography, Palaeoclimatology, Palaeoecology*, v. 491, p. 92-111.
39. Bontes, B., and van der Spoel, S., 1998, Variation in the *Diacria trispinosa* group, new interpretation of colour patterns and description of *D. rubecula* n. sp.(Pteropoda): *Bulletin Zoologisch Museum*, v. 16, no. 11, p. 77-84.
40. Bordon, A., Peyron, O., Lezine, A.-M., Brewer, S., and Fouache, E., 2009, Pollen-inferred Late-Glacial and Holocene climate in southern Balkans (Lake Maliq): *Quaternary International*, v. 200, p. 19-30.
41. Brayshaw, D. J., Rambeau, C. M. C., and Smith, S. J., 2011, Changes in Mediterranean climate during the Holocene: Insights from global and regional climate modelling: *The Holocene*, v. 21, no. 1, p. 15-31.
42. Buccheri, G., 1984, Pteropods as climatic indicators in Quaternary sequences: a Lower-Middle Pleistocene sequence outcropping in Cava Puleo (Ficarazzi, Palermo, Sicilia): *Palaeogeogr. Palaeoclim. Palaeoecol.*, v. 45, p. 75-86
43. Buccheri, G., Capretto, G., Di Donato, V., Esposito, P., Ferruzza, G., Pescatore, T., Russo Ermolli, E., Senatore, M. R., Sprovieri, M., Bertoldo, M., Carella, D., and Madonia, G., 2002, A high resolution record of the last deglaciation in the southern Tyrrhenian Sea: environmental and climatic evolution: *Marine Geology*, v. 186, no. 3, p. 447-470.
44. Buccheri, G., Ferretti, O., Agate, M., Bertoldo, M., Immordino, F., and Lucido, M., 1998, Valutazioni stratigrafiche, sedimentologiche e paleoclimatiche sui sedimenti tardopleistocenici-Olocenici del Golfo di Castellamare (Sicilia Nordoccidentale): indagini sulle carote PaCa₂ e PaCa₃. : *Boll. Soc. Geol. It.* , v. 117, p. 219-248.
45. Buccheri, G., and Torelli, L., 1981, Stratigraphy and Paleoclimatic evaluations of the cores BS77-15 and BS77-33 (Sardinia Basin, Western Tyrrhenian Sea) by means of Pteropods assemblages, *Ateneo Parmense.* : *Acta Nat.*, v. 17, p. 73-94.

46. Buckley, H. A., Johnson, L. R., Shackleton, N. J., and Blow, R. A., 1982, Late glacial to recent cores from the eastern Mediterranean: Deep Sea Research Part A. Oceanographic Research Papers, v. 29, no. 6, p. 739-766.
47. Cacho, I., Grimalt, J. O., and Canals, M., 2002, Response of the Western Mediterranean Sea to rapid climatic variability during the last 50,000 years: a molecular biomarker approach: *Journal of Marine Systems*, v. 33-34, p. 253-272.
48. Cacho, I., Grimalt, J. O., Canals, M., Sbaffi, L., Shackleton, N. J., Schönfeld, J., and Zahn, R., 2001, Variability of the western Mediterranean Sea surface temperature during the last 25,000 years and its connection with the Northern Hemisphere climatic changes: *Paleoceanography*, v. 16, no. 1, p. 40-52.
49. Capotondi, L., Borsetti, A., and Morigi, C., 1999, Foraminiferal ecozones, a high resolution proxy for the Late Quaternary biochronology in the central Mediterranean Sea: *Marine Geology*, v. 153, p. 253-274.
50. Carboni, M. G., and Esu, D., 1987, Paleoclimatology of a late Peistocene – Holocene core from the Tyrrhenian Sea (Western Mediterranean): *Foraminifera and Pteropoda*: *Geologica Roma*, v. 26, p. 167–185.
51. Casford, J., Rohling, E. J., Abu-Zied, R., Cooke, S., Boessenkool, K. P., Brinkhuis, H., Vries, C., Wefer, G., Geraga, M., Papatheodorou, G., Croudace, I., Thomson, J., Wells, N., and Lykousis, V., 2001, Mediterranean climate variability during the Holocene: *Mediterranean Marine Science*, v. 2/1, p. 45-55.
52. Casford, J. S. L., Abu-Zied, R., Rohling, E. J., Cooke, S., Fontanier, C., Leng, M., Millard, A., and Thomson, J., 2007, A stratigraphically controlled multiproxy chronostratigraphy for the eastern Mediterranean: *Paleoceanography*, v. 22, no. 4.
53. Casford, J. S. L., Rohling, E. J., Abu-Zied, R., Cooke, S., Fontanier, C., Leng, M., and Lykousis, V., 2002, Circulation changes and nutrient concentrations in the late Quaternary Aegean Sea: A nonsteady state concept for sapropel formation: *Paleoceanography*, v. 17, no. 2, p. 14-11-14-11.
54. Casford, J. S. L., Rohling, E. J., Abu-Zied, R. H., Fontanier, C., Jorissen, F. J., Leng, M. J., Schmiedl, G., and Thomson, J., 2003, A dynamic concept for eastern Mediterranean circulation and oxygenation during sapropel formation: *Palaeogeography, Palaeoclimatology, Palaeoecology*, v. 190, p. 103-119.

55. Checa, H., Margaritelli, G., Pena, L. D., Frigola, J., Cacho, I., Rettori, R., and Lirer, F., 2020, High resolution paleo-environmental changes during the Sapropel 1 in the North Ionian Sea, central Mediterranean: The Holocene, p. 0959683620941095.
56. Combourieu-Nebout, N., Peyron, O., Bout-Roumazeilles, V., Goring, S., Dormoy, I., Joannin, S., Sadori, L., Siani, G., and Magny, M., 2013, Holocene vegetation and climate changes in the central Mediterranean inferred from a high-resolution marine pollen record (Adriatic Sea): *Climate of the Past*, v. 9, no. 5, p. 2023-2042.
57. Combourieu Nebout, N., Peyron, O., Dormoy, I., Desprat, S., Beaudouin, C., Kotthoff, U., and Marret, F., 2009, Rapid climatic variability in the west Mediterranean during the last 25 000 years from high resolution pollen data: *Climate of the Past*, v. 5, no. 3, p. 503-521.
58. Comeau, S., Jeffree, R., Teyssié, J.-L., and Gattuso, J.-P., 2010, Response of the Arctic Pteropod *Limacina helicina* to Projected Future Environmental Conditions: *PLOS ONE*, v. 5, no. 6, p. e11362.
59. Corselli, C., and Grecchi, G., 1990, Considerazioni sui Thecosomata attuali del Bacino Mediterraneo, *Lavori S.I.M. Atti del Congresso di Parma, Volume 24: Parma, Italia*, p. 91-105.
60. Cutter, G. A., and Radford-Knoery, J., 1991, Determination of Carbon, Nitrogen, Sulfur, and Inorganic Sulfur Species in Marine Particles: *Marine Particles: Analysis and Characterization*, p. 57-63.
61. Davis, J., 1988, *Statistics and Data Analysis in Geology: Biometrics*, v. 44.
62. De Lange, G. J., Thomson, J., Reitz, A., Slomp, C. P., Speranza Principato, M., Erba, E., and Corselli, C., 2008, Synchronous basin-wide formation and redox-controlled preservation of a Mediterranean sapropel: *Nature Geoscience*, v. 1, no. 9, p. 606-610.
63. De Rijk, S., Hayes, A., and Rohling, E. J., 1999, Eastern Mediterranean sapropel S1 interruption: an expression of the onset of climatic deterioration around 7 ka BP: *Marine Geology*, v. 153, no. 1-4, p. 337-343.
64. Denton, G. H., and Karlén, W., 1973, Holocene climatic variations—their pattern and possible cause: *Quaternary Research*, v. 3, no. 2, p. 155-205.
65. Desprat, S., Combourieu-Nebout, N., Essallami, L., Sicre, M.-A., Dormoy, I., Peyron, O., Siani, G., Bout Roumazeilles, V., and Turon, J.-L., 2013, Deglacial and Holocene

- vegetation and climatic changes in the southern Central Mediterranean from a direct land–sea correlation: *Climate of the Past*, v. 9, no. 2, p. 767-787.
66. Deuser, W. G., Ross, E. H., and Waterman, L. S., 1976, Glacial and pluvial periods: Their relationship revealed by Pleistocene sediments of the Red Sea and Gulf of Aden: *Science*, v. 191, no. 4232, p. 1168-1170.
67. Di Donato, V., Esposito, P., Garilli, V., Naimo, D., Buccheri, G., Caffau, M., Ciampo, G., Greco, A., and Stanzione, D., 2009, Surface–bottom relationships in the Gulf of Salerno (Tyrrhenian Sea) over the last 34 kyr: Compositional data analysis of palaeontological proxies and geochemical evidence: *Geobios*, v. 42, no. 5, p. 561-579.
68. Di Donato, V., Esposito, P., Russo-Ermolli, E., Scarano, A., and Cheddadi, R., 2008, Coupled atmospheric and marine palaeoclimatic reconstruction for the last 35ka in the Sele Plain–Gulf of Salerno area (southern Italy): *Quaternary International*, v. 190, no. 1, p. 146-157.
69. Di Geronimo, I., 1970, Heteropoda e Pteropoda Thecosomata in sedimenti abissali recenti dello Jonio. : *Thalassia Salentina*, v. 4, p. 41–115.
70. Dormoy, I., Peyron, O., Combourieu Nebout, N., Goring, S., Kotthoff, U., Magny, M., and Pross, J., 2009, Terrestrial climate variability and seasonality changes in the Mediterranean region between 15 000 and 4000 years BP deduced from marine pollen records: *Clim. Past*, v. 5, no. 4, p. 615-632.
71. Dowsett, H. J., 2007, *Paleoceanography, Biological Proxies| Planktic Foraminifera*.
72. Drinia, H., Antonarakou, A., Tsourou, T., Kontakiotis, G., Psychogiou, M., and Anastasakis, G., 2016, Foraminifera eco-biostratigraphy of the southern Evoikos outer shelf, central Aegean Sea, during MIS 5 to present: *Continental Shelf Research*, v. 126.
73. Edelman-Furstenberg, Y., Almogi-Labin, A., and Hemleben, C., 2009, Palaeoceanographic evolution of the central Red Sea during the late Holocene: *The Holocene*, v. 19, no. 1, p. 117-127.
74. Ehrmann, W., Schmiedl, G., Hamann, Y., Kuhnt, T., Hemleben, C., and Siebel, W., 2007, Clay minerals in late glacial and Holocene sediments of the northern and southern Aegean Sea: *Palaeogeography, Palaeoclimatology, Palaeoecology*, v. 249, no. 1-2, p. 36-57.

75. Emeis, K.-C., Schulz, H.-M., Struck, U., Sakamoto, T., Dose, H., Erlenkeuser, H., Howell, M., Kroon, D., and Paterne, M., 1998, 26. Stable isotope and alkenone temperature records of sapropels from Sites 964 and 967: Constraining the physical environment of sapropel formation in the eastern Mediterranean Sea v. 160.
76. Emeis, K. C., Struck, U., Blanz, T., Kohly, A., and Woß, M., 2003, Salinity changes in the central Baltic Sea (NW Europe) over the last 10 000 years. : Holocene v. 13, p. 411-421.
77. Emeis, K. C., Struck, U., Schulz, H. M., Rosenberg, M., Bernasconi, S. M., Erlenkeuser, H., Sakamoto, T., and Martinez-Ruiz, F. C., 2000, Temperature and salinity of Mediterranean Sea surface waters over the last 16 000 years: constraints on the physical environment of S1 sapropel formation based on stable oxygen isotopes and alkenone unsaturation ratios. : Palaeogeography, Palaeoclimatology, Palaeoecology, v. 158, p. 259–280.
78. Eurostat: <https://ec.europa.eu/eurostat/web/gisco/geodata/reference-data/administrative-units-statistical-units/countries>.
79. Facorellis, Y., and Maniatis, Y., 1998, Apparent ¹⁴C ages of marine mollusk shells from a Greek Island: Calculation of the marine reservoir effect in the Aegean Sea: Radiocarbon, v. 40.
80. Fairbanks, R., and Wiebe, P., 1980, Foraminifera and Chlorophyll Maximum: Vertical Distribution, Seasonal Succession, and Paleooceanographic Significance: Science (New York, N.Y.), v. 209, p. 1524-1526.
81. Faust, D., Zielhofer, C., Escudero, R. B., and del Olmo, F. D., 2004, High-resolution fluvial record of late Holocene geomorphic change in northern Tunisia: climatic or human impact?: Quaternary Science Reviews, v. 23, no. 16-17, p. 1757-1775.
82. Fhlaithearta, N., S., Reichart, G. J., Jorissen, F. J., Fontanier, C., Rohling, E. J., Thomson, J., and De Lange, G. J., 2010, Reconstructing the seafloor environment during sapropel formation using benthic foraminiferal trace metals, stable isotopes, and sediment composition: Paleooceanography, v. 25, no. 4.
83. Filippidi, A., Triantaphyllou, M., and de Lange, G., 2016, Eastern-Mediterranean ventilation variability during sapropel S1 formation, evaluated at two sites influenced by

- deep-water formation from Adriatic and Aegean Seas: *Quaternary Science Reviews*, v. 144, p. 95-106.
84. Fleitmann, D., Burns, S. J., Mudelsee, M., Neff, U., Kramers, J., Mangini, A., and Matter, A., 2003, Holocene forcing of the Indian monsoon recorded in a stalagmite from southern Oman: *science*, v. 300, no. 5626, p. 1737-1739.
 85. Fleitmann, D., Mudelsee, M., Burns, S. J., Bradley, R. S., Kramers, J., and Matter, A., 2008, Evidence for a widespread climatic anomaly at around 9.2 ka before present: *Paleoceanography*, v. 23, no. 1.
 86. Fraile, I., Schulz, M., Mulitza, S., Merkel, U., Prange, M., and Paul, A., 2009, Modeling the seasonal distribution of planktonic foraminifera during the Last Glacial Maximum: *Paleoceanography*, v. 24, no. 2.
 87. Frigola, J., Moreno, A., Cacho, I., Canals, M., Sierro, F. J., Flores, J. A., Grimalt, J. O., Hodell, D. A., and Curtis, J. H., 2007, Holocene climate variability in the western Mediterranean region from a deepwater sediment record: *Paleoceanography*, v. 22, no. 2.
 88. Froget, C., 1967, Les ptéropodes dans les sédiments sousmarins du Quaternaire: caractérisation du régime 'Nord-Atlantique' au cours des périodes glaciaires en Méditerranéen par le ptéropode *Spiratella retroversa* Fleming.: *Comptes rendus hebdomadaires des Séances de l'Académie des Sciences*, v. D264, no. 26, p. 2968-2969.
 89. Frontier, S., 1973, Zooplankton De La Région De No § Y-Bé Vii) Ptéropodes, Hétéropodes-Deuxième Partie: *Espèces Néritiques-Externes Et Océaniques Tolérantes*.
 90. Gaby, M. L., and Sengupta, B. K., 1985, Late Quaternary foraminifera of the Venezuela Basin.: *Marine Geology*, v. 24, p. 125-144.
 91. Garzoli, S., and Maillard, C., 1979, Winter circulation in the Sicily and Sardinia straits region: *Deep Sea Research Part A. Oceanographic Research Papers*, v. 26, no. 8, p. 933-954.
 92. Gasse, F., 2000, Hydrological changes in the African tropics since the Last Glacial Maximum: *Quaternary Science Reviews*, v. 19, no. 1-5, p. 189-211.
 93. Geraga, M., Ioakim, C., Lykousis, V., Tsaila-Monopolis, S., and Mylona, G., 2010, The high-resolution palaeoclimatic and palaeoceanographic history of the last 24,000 years in the central Aegean Sea, Greece: *Palaeogeography, Palaeoclimatology, Palaeoecology*, v. 287, no. 1, p. 101-115.

94. Geraga, M., Mylona, G., Tsaila-Monopoli, S., Papatheodorou, G., and Ferentinos, G., 2008, Northeastern Ionian Sea: Palaeoceanographic variability over the last 22 ka: *Journal of Marine Systems*, v. 74, no. 1, p. 623-638.
95. Geraga, M., Tsaila-Monopolis, S., Ioakim, C., Papatheodorou, G., and Ferentinos, G., 2000, Evaluation of palaeoenvironmental changes during the last 18,000 years in the Myrtoon Basin, SW Aegean Sea: *Palaeogeography, Palaeoclimatology, Palaeoecology*, v. 156, p. 1-17.
96. Geraga, M., Tsaila-Monopolis, S., Ioakim, C., Papatheodorou, G., and Ferentinos, G., 2005, Short-term climate changes in the southern Aegean Sea over the last 48,000 years: *Palaeogeography, Palaeoclimatology, Palaeoecology*, v. 220, no. 3, p. 311-332.
97. Gerhardt, S., Groth, H., Rühlemann, C., and Henrich, R., 2000, Aragonite preservation in late Quaternary sediment cores on the Brazilian Continental Slope: implications for intermediate water circulation: *International Journal of Earth Sciences*, v. 88, no. 4, p. 607-618.
98. Gerhardt, S., and Henrich, R., 2001, Shell preservation of *Limacina inflata* (Pteropoda) in surface sediments from the Central and South Atlantic Ocean: a new proxy to determine the aragonite saturation state of water masses: *Deep Sea Research Part I: Oceanographic Research Papers*, v. 48, no. 9, p. 2051-2071.
99. Giamali, C., Kontakiotis, G., Koskeridou, E., Ioakim, C., and Antonarakou, A., 2020, Key Environmental Factors Controlling Planktonic Foraminiferal and Pteropod Community's Response to Late Quaternary Hydroclimate Changes in the South Aegean Sea (Eastern Mediterranean): *Journal of Marine Science and Engineering*, v. 8, no. 9.
100. Giamali, C., Koskeridou, E., Antonarakou, A., Ioakim, C., Kontakiotis, G., Karageorgis, A. P., Roussakis, G., and Karakitsios, V., 2019, Multiproxy ecosystem response of abrupt Holocene climatic changes in the northeastern Mediterranean sedimentary archive and hydrologic regime: *Quaternary Research*, v. 92, no. 3, p. 665-685.
101. Giorgi, F., and Lionello, P., 2008, Climate change projections for the Mediterranean region: *Global and Planetary Change*, v. 63, no. 2, p. 90-104.
102. Gogou, A., Bouloubassi, I., Lykousis, V., Arnaboldi, M., Gaitani, P., and Meyers, P. A., 2007, Organic geochemical evidence of Late Glacial–Holocene climate instability in the

- North Aegean Sea: Palaeogeography, Palaeoclimatology, Palaeoecology, v. 256, no. 1-2, p. 1-20.
103. Goudeau, M. L. S., 2015, Seasonality variations in the Central Mediterranean during climate change events in the Late Holocene: Palaeogeography, palaeoclimatology, palaeoecology, v. 418, p. 304-318
104. Grant, K. M., Grimm, R., Mikolajewicz, U., Marino, G., Ziegler, M., and Rohling, E. J., 2016, The timing of Mediterranean sapropel deposition relative to insolation, sea-level and African monsoon changes: Quaternary Science Reviews, v. 140, p. 125-141.
105. Gregg, W. W., and Casey, N. W., 2007, Sampling biases in MODIS and SeaWiFS ocean chlorophyll data: Remote Sensing of Environment, v. 111, no. 1, p. 25-35.
106. Hammer, Ø., Harper, D. A. T., and D, R. P., 2001, PAST: Paleontological Statistics software package for education and data analysis: Palaeontologia Electronica, v. 4, no. 1, p. 9.
107. Hayes, A., Rohling, E. J., De Rijk, S., Kroon, D., and Zachariasse, W. J., 1999, Mediterranean planktonic foraminiferal faunas during the last glacial cycle: Marine Geology, v. 153, no. 1, p. 239-252.
108. Hemleben, C., Spindler, M., and Anderson, O., 1989, Modern Planktic Foraminifera.
109. Herman, Y., 1968, Evidence of climatic changes in Red Sea cores. , *in* Morrison, R. B., and Wright, H. E., eds., VII Congress International Association for Quaternary Research: University of Utah Press, Salt Lake City, p. 325-348.
110. Herman, Y., 1971, Vertical and horizontal distribution of pteropods in Quaternary sequences, *in* Funnell, B. M., and Reidel, W. R., eds., The Micropalaeontology of Oceans: Cambridge, Cambridge University Press, p. 463–486.
111. Herman, Y., 1981, Paleoclimatic and paleohydrologic record of Mediterranean deep-sea cores based on pteropods, planktonic and benthonic foraminifera. : Riv. Esp. Micropaleontol., v. XIII, , p. 171-200.
112. Herman, Y., 1989, Late Quaternary paleoceanography of the eastern Mediterranean: the deep-sea record: Marine geology, v. 87, no. 1, p. 1-4.
113. Herman, Y., and Rosenberg, P. E., 1969, Pteropods as bathymetric indicators: Marine Geology, v. 7, no. 2, p. 169-173.

114. Herrle, J. O., Bollmann, J., Gebühr, C., Schulz, H., Sheward, R. M., and Giesenberg, A., 2018, Black Sea outflow response to Holocene meltwater events: Scientific reports, v. 8, no. 1, p. 1-6.
115. Hilgersom, P. C. J., and Van der Spoel, S., 1987, East-west variation in *Diacria* off Northwestern Africa.: Malacological Review, v. 20, p. 8.
116. Horton, T., Kroh, A., Ahyong, S., Bailly, N., Boyko, C. B., Brandão, S. N., Gofas, S., Hooper, J. N. A., Hernandez, F., Holovachov, O., Mees, J., Molodtsova, T. N., Paulay, G., Decock, W., Dekeyzer, S., Poffyn, G., Vandepitte, L., Vanhoorne, B., Adlard, R., Agatha, S., Ahn, K. J., Akkari, N., Alvarez, B., Anderberg, A., Anderson, G., Angel, M. V., Antic, D., Arango, C., Artois, T., Atkinson, S., Auffenberg, K., Baldwin, B. G., Bank, R., Barber, A., Barbosa, J. P., Bartsch, I., Bellan-Santini, D., Bergh, N., Bernot, J., Berta, A., Bezerra, T. N., Bieler, R., Blanco, S., Blasco-Costa, I., Blazewicz, M., Bock, P., Bonifacino de León, M., Böttger-Schnack, R., Bouchet, P., Boury-Esnault, N., Boxshall, G., Bray, R., Bruce, N. L., Cairns, S., Calvo Casas, J., Carballo, J. L., Cárdenas, P., Carstens, E., Chan, B. K., Chan, T. Y., Cheng, L., Christenhusz, M., Churchill, M., Coleman, C. O., Collins, A. G., Collins, G. E., Corbari, L., Cordeiro, R., Cornils, A., Coste, M., Costello, M. J., Crandall, K. A., Cremonte, F., Cribb, T., Cutmore, S., Dahdouh-Guebas, F., Daly, M., Daneliya, M., Dauvin, J. C., Davie, P., De Broyer, C., De Grave, S., de Mazancourt, V., de Voogd, N. J., Decker, P., Defaye, D., d'Hondt, J. L., Dippenaar, S., Dohrmann, M., Dolan, J., Domning, D., Downey, R., Ector, L., Eisendle-Flöckner, U., Eitel, M., Encarnação, S. C. d., Enghoff, H., Epler, J., Ewers-Saucedo, C., Faber, M., et al., 2021, World Register of Marine Species (WoRMS), WoRMS Editorial Board.
117. Howes, E. L., Eagle, R. A., Gattuso, J.-P., and Bijma, J., 2017, Comparison of Mediterranean Pteropod Shell Biometrics and Ultrastructure from Historical (1910 and 1921) and Present Day (2012) Samples Provides Baseline for Monitoring Effects of Global Change: PLOS ONE, v. 12, no. 1, p. e0167891.
118. Howes, E. L., Stemmann, L., Assailly, C., Irisson, J. O., Dima, M., Bijma, J., and Gattuso, J. P., 2015, Pteropod time series from the North Western Mediterranean (1967-2003): impacts of pH and climate variability: Marine Ecology Progress Series, v. 531, p. 193-206.

119. Hunt, B., Pakhomov, E., Hosie, G. W., Siegel, V., Ward, P., and Bernard, K., 2008, Pteropods in Southern Ocean ecosystems: Progress In Oceanography, v. 78, p. 193-221.
120. Incarbona, A., and Sprovieri, M., 2020, The Postglacial Isotopic Record of Intermediate Water Connects Mediterranean Sapropels and Organic-Rich Layers: Paleoceanography and Paleoclimatology, v. 35, no. 10, p. e2020PA004009.
121. Ioc, I., BODC, 2003, Centenary Edition of the GEBCO Digital Atlas, published on CD-ROM on behalf of the Intergovernmental Oceanographic Commission and the International Hydrographic Organization as part of the General Bathymetric Chart of the Oceans: British Oceanographic Data Centre, Liverpool, UK.
122. İşler, E., Hiscott, R., and Isler, E., 2016, Late Quaternary chronostratigraphy of the Aegean Sea sediments: Special reference to the ages of sapropels S1–S5: Turkish Journal of Earth Sciences, v. 25, p. 1-18.
123. Ivanova, E. V., 1985, Late Quaternary biostratigraphy and paleotemperatures of the Red Sea and the Gulf of Aden based on planktonic foraminifera and pteropods: Marine Micropaleontology, v. 9, no. 4, p. 335-364.
124. Jalali, B., Sicre, M. A., Bassetti, M. A., and Kallel, N., 2016, Holocene climate variability in the North-Western Mediterranean Sea (Gulf of Lions): Clim. Past, v. 12, no. 1, p. 91-101.
125. Jalut, G., Dedoubat, J. J., Fontugne, M., and Otto, T., 2009, Holocene circum-Mediterranean vegetation changes: climate forcing and human impact: Quaternary international, v. 200, no. 1-2, p. 4-18.
126. Janssen, A., 2012, Late Quaternary to Recent holoplanktonic Mollusca (Gastropoda) from bottom samples of the eastern Mediterranean Sea: systematics, morphology: Bollettino Malacologico, p. 1-105.
127. Janssen, A., Bush, S., and Bednaršek, N., 2019, The shelled pteropods of the northeast Pacific Ocean (Mollusca: Heterobranchia, Pteropoda): Zoosymposia, v. 13, p. 305.
128. Janssen, A. W., 2018, Notes on the systematics, morphology and biostratigraphy of holoplanktic Mollusca, 25. Once more: the correct name for the type species of the genus *Creseis* Rang, 1828 (Pteropoda, Euthecosomata, Creseidae). . 82(4-6): 110-112.: Basteria, v. 82, no. 4-6, p. 110-112.

129. Janssen, A. W., and Peijnenburg, K. T. C. A., 2014, Holoplanktonic Mollusca: development in the Mediterranean basin during the last 30 million years and their future, *The Mediterranean Sea*, Springer, p. 341-362.
130. Jansson, K. N., and Kleman, J., 2004, Early Holocene glacial lake meltwater injections into the Labrador Sea and Ungava Bay: *Paleoceanography*, v. 19, no. 1.
131. Jimenez-Espejo, F. J., Martinez-Ruiz, F., Rogerson, M., González-Donoso, J. M., Romero, O. E., Linares, D., Sakamoto, T., Gallego-Torres, D., Rueda Ruiz, J. L., and Ortega-Huertas, M., 2008, Detrital input, productivity fluctuations, and water mass circulation in the westernmost Mediterranean Sea since the Last Glacial Maximum: *Geochemistry, Geophysics, Geosystems*, v. 9, no. 11.
132. Johnson, R., Manno, C., and Ziveri, P., 2020, Spring distribution of shelled pteropods across the Mediterranean Sea: *Biogeosciences Discuss.*, v. 2020, p. 1-23.
133. Jorissen, F. J., Asioli, A., Borsetti, A. M., Capotondi, L., de Visser, J. P., Hilgen, F. J., Rohling, E. J., van der Borg, K., Vergnaud Grazzini, C., and Zachariasse, W. J., 1993, Late Quaternary central Mediterranean biochronology: *Marine Micropaleontology*, v. 21, no. 1, p. 169-189.
134. Jung, P., 1973, Pleistocene pteropods, Leg. 15, Site 147., Washington D.C., USGP Office, Initial Rept. DSDP Drilling Project 15.
135. Karageorgis, A., Ioakim, C., Rousakis, G., Sakellariou, D., Vougioukalakis, G., I.P., P., E, Z., Koutsopoulou, E., Kanellopoulos, T., Papatrechas, C., Georgiou, P., N, X., Stavrakaki, I., Vakalas, I., I, M., Koutsovitis, P., Drakopoulou, P., Ch, K., and I, M., 2016, Geomorphology, sedimentology and geochemistry in the marine area between Sifnos and Kimolos Islands, Greece: *Bulletin of the Geological Society of Greece*, v. 50, no. 1, p. 334-344.
136. Karageorgis, A. P., Anagnostou, C. L., and Kaberi, H., 2005, Geochemistry and mineralogy of the NW Aegean Sea surface sediments: implications for river runoff and anthropogenic impact: *Applied Geochemistry*, v. 20, no. 1, p. 69-88.
137. Karageorgis, A. P., Gardner, W. D., Georgopoulos, D., Mishonov, A. V., Krasakopoulou, E., and Anagnostou, C., 2008, Particle dynamics in the Eastern Mediterranean Sea: A synthesis based on light transmission, PMC, and POC archives (1991–2001): *Deep Sea Research Part I: Oceanographic Research Papers*, v. 55, no. 2, p. 177-202.

138. Karageorgis, A. P., Katsanevakis, S., and Kaberi, H., 2009, Use of Enrichment Factors for the Assessment of Heavy Metal Contamination in the Sediments of Koumoundourou Lake, Greece: *Water, Air, and Soil Pollution*, v. 204, no. 1, p. 243.
139. Karakitsios, V., Roveri, M., Lugli, S., Manzi, V., Gennari, R., Antonarakou, A., Triantaphyllou, M., Agiadi, K., Kontakiotis, G., Kafousia, N., and de Rafelis, M., 2017, A record of the Messinian salinity crisis in the eastern Ionian tectonically active domain (Greece, eastern Mediterranean): *Basin Research*, v. 29, no. 2, p. 203-233.
140. Kontakiotis, G., 2012, Palaeoceanographic and Palaeoclimatic Study of Eastern Mediterranean During Late Quaternary, Based on Planktonic Foraminiferal Assemblages (PhD Thesis). (in Greek, with English extended abstract): National and Kapodistrian University of Athens, Greece, 247 p.
141. Kontakiotis, G., 2016, Late Quaternary paleoenvironmental reconstruction and paleoclimatic implications of the Aegean Sea (eastern Mediterranean) based on paleoceanographic indexes and stable isotopes: *Quaternary International*, v. 401, p. 28-42.
142. Kontakiotis, G., Antonarakou, A., Mortyn, P. G., Drinia, H., Anastasakis, G., Zarkogiannis, S., and Möbius, J., 2017, Morphological recognition of *Globigerinoides ruber* morphotypes and their susceptibility to diagenetic alteration in the eastern Mediterranean Sea: *Journal of Marine Systems*, v. 174, p. 12-24.
143. Kontakiotis, G., Antonarakou, A., and Zachariasse, W. J., 2013, Late Quaternary palaeoenvironmental changes in the Aegean Sea: interrelations and interactions between north and south Aegean Sea: *Bulletin of the Geological Society of Greece*, v. 47, no. 1, p. 167-177.
144. Kontakiotis, G., Besiou, E., Antonarakou, A., Zarkogiannis, S. D., Kostis, A., Mortyn, P. G., Moissette, P., Cornée, J. J., Schulbert, C., Drinia, H., Anastasakis, G., and Karakitsios, V., 2019, Decoding sea surface and paleoclimate conditions in the eastern Mediterranean over the Tortonian-Messinian Transition: *Palaeogeography, Palaeoclimatology, Palaeoecology*, v. 534, p. 109312.
145. Kontakiotis, G., Efstathiou, E., Zarkogiannis, S.D., Besiou, E., Antonarakou, A., 2021, Latitudinal Differentiation among Modern Planktonic Foraminiferal Populations of Central Mediterranean: Species-Specific Distribution Patterns and Size Variability.

Journal of Marine Science And Engineering, 9, no. 5, p. 551.
<https://doi.org/10.3390/jmse9050551>

146. Kontakiotis, G., Mortyn, G. P., Antonarakou, A., and Drinia, H., 2016, Assessing the reliability of foraminiferal Mg/Ca thermometry by comparing field-samples and culture experiments: a review: *Geological Quarterly*, v. 60, no. 3, p. 547-560.
147. Kontakiotis, G., Mortyn, P. G., Antonarakou, A., Martínez-Botí, M. A., and Triantaphyllou, M. V., 2011, Field-based validation of a diagenetic effect on *G. ruber* Mg/Ca paleothermometry: Core top results from the Aegean Sea (eastern Mediterranean): *Geochemistry, Geophysics, Geosystems*, v. 12, no. 9.
148. Koskeridou, E., Giamali, C., Antonarakou, A., Kontakiotis, G., and Karakitsios, V., 2017, Early Pliocene gastropod assemblages from the eastern Mediterranean (SW Peloponnese, Greece) and their palaeobiogeographic implications: *Geobios*, v. 50, no. 4, p. 267-277.
149. Kotthoff, U., Koutsodendris, A., Pross, J., Schmiedl, G., Bornemann, A., Kaul, C., Marino, G., Peyron, O., and Schiebel, R., 2011, Impact of Lateglacial cold events on the northern Aegean region reconstructed from marine and terrestrial proxy data: *Journal of Quaternary Science*, v. 26.
150. Kotthoff, U., Müller, U. C., Pross, J., Schmiedl, G., Lawson, I. T., van de Schootbrugge, B., and Schulz, H., 2008a, Lateglacial and Holocene vegetation dynamics in the Aegean region: an integrated view based on pollen data from marine and terrestrial archives: *The Holocene*, v. 18, no. 7, p. 1019-1032.
151. Kotthoff, U., Pross, J., Müller, U. C., Peyron, O., Schmiedl, G., Schulz, H., and Bordon, A., 2008b, Climate dynamics in the borderlands of the Aegean Sea during formation of sapropel S1 deduced from a marine pollen record: *Quaternary Science Reviews*, v. 27, no. 7, p. 832-845.
152. Koukouvelas, I., and Aydin, A., 2002, Fault structure and related basins of the North Aegean Sea and its surroundings: *Tectonics*, v. 21.
153. Kouli, K., Gogou, A., Bouloubassi, I., Triantaphyllou, M. V., Ioakim, C., Katsouras, G., Roussakis, G., and Lykousis, V., 2012, Late postglacial paleoenvironmental change in the northeastern Mediterranean region: Combined palynological and molecular biomarker evidence: *Quaternary International*, v. 261, p. 118-127.

154. Koutrouli, A., Anastasakis, G., Kontakiotis, G., Ballengee, S., Kuehn, S., Pe-Piper, G., and Piper, D. J. W., 2018, The early to mid-Holocene marine tephrostratigraphic record in the Nisyros-Yali-Kos volcanic center, SE Aegean Sea: *Journal of Volcanology and Geothermal Research*, v. 366, p. 96-111.
155. Kucera, M., Weinelt, M., Kiefer, T., Pflaumann, U., Hayes, A., Weinelt, M., Chen, M.-T., Mix, A. C., Barrows, T. T., Cortijo, E., Duprat, J., Juggins, S., and Waelbroeck, C., 2005, Reconstruction of sea-surface temperatures from assemblages of planktonic foraminifera: multi-technique approach based on geographically constrained calibration data sets and its application to glacial Atlantic and Pacific Oceans: *Quaternary Science Reviews*, v. 24, no. 7, p. 951-998.
156. Kuhnt, T., Schmiedl, G., Ehrmann, W., Hamann, Y., and Andersen, N., 2008, Stable isotopic composition of Holocene benthic foraminifers from the Eastern Mediterranean Sea: past changes in productivity and deep water oxygenation: *Palaeogeography, Palaeoclimatology, Palaeoecology*, v. 268, no. 1-2, p. 106-115.
157. Kuhnt, T., Schmiedl, G., Ehrmann, W., Hamann, Y., and Hemleben, C., 2007, Deep-sea ecosystem variability of the Aegean Sea during the past 22 kyr as revealed by Benthic Foraminifera: *Marine Micropaleontology*, v. 64, no. 3, p. 141-162.
158. Kutzbach, J. E., and Guetter, P. J., 1986, The Influence of Changing Orbital Parameters and Surface Boundary Conditions on Climate Simulations for the Past 18 000 Years: *Journal of the Atmospheric Sciences*, v. 43, no. 16, p. 1726-1759.
159. Lalli, C. M., and Gilmer, R. W., 1989, *Pelagic Snails: The Biology of Holoplanktonic Gastropod Mollusks*, Stanford University Press.
160. Larocque, I., and Finsinger, W., 2008, Late-glacial chironomid-based temperature reconstructions for Lago Piccolo di Avigliana in the southwestern Alps (Italy): *Palaeogeography, Palaeoclimatology, Palaeoecology*, v. 257, no. 1, p. 207-223.
161. Laskar, J., Robutel, P., Joutel, F., Gastineau, M., Correia, A. C. M., and Levrard, B., 2004, A long-term numerical solution for the insolation quantities of the Earth: *A&A*, v. 428, no. 1, p. 261-285.
162. Le Houedec, S., Mojtahid, M., Bicchi, E., de Lange, G. J., and Hennekam, R., 2020, Suborbital Hydrological Variability Inferred From Coupled Benthic and Planktic

- Foraminiferal-Based Proxies in the Southeastern Mediterranean During the Last 19 ka: *Paleoceanography and Paleoclimatology*, v. 35, no. 2, p. e2019PA003827.
163. LeGrande, A. N., Schmidt, G. A., Shindell, D. T., Field, C. V., Miller, R. L., Koch, D. M., Faluvegi, G., and Hoffmann, G., 2006, Consistent simulations of multiple proxy responses to an abrupt climate change event: *Proceedings of the National Academy of Sciences*, v. 103, no. 4, p. 837-842.
164. Lirer, F., Sprovieri, M., Vallefucio, M., Ferraro, L., Pelosi, N., Giordano, L., and Capotondi, L., 2014, Planktonic foraminifera as bio-indicators for monitoring the climatic changes that have occurred over the past 2000 years in the southeastern Tyrrhenian Sea: *Integrative Zoology*, v. 9, no. 4, p. 542-554.
165. Lochte, K., and Pfannkuche, O., 2003, Processes driven by the small sized organisms at the water-sediment interface, *in* Wefer, G. B. D. H. D. J. B. B. S. M., and Weering, T. C., eds., *Ocean Margin Systems*: Heidelberg, Germany, Springer.
166. Lourens, L., Hilgen, F., Gudjonsson, L., and Zachariasse, W. J., 1992, Late Pliocene to early Pleistocene astronomically forced sea surface productivity and temperature variations in the Mediterranean: *Marine Micropaleontology*, v. 19, p. 49-78.
167. Louvari, M. A., Drinia, H., Kontakiotis, G., Di Bella, L., Antonarakou, A., and Anastasakis, G., 2019, Impact of latest-glacial to Holocene sea-level oscillations on central Aegean shelf ecosystems: A benthic foraminiferal palaeoenvironmental assessment of South Evoikos Gulf, Greece: *Journal of Marine Systems*, v. 199, p. 103181.
168. Lykousis, V., Chronis, G., Tselepides, A., Price, N. B., Theocharis, A., Siokou-Frangou, I., Van Wambeke, F., Danovaro, R., Stavrakakis, S., Duineveld, G., Georgopoulos, D., Ignatiades, L., Souvermezoglou, A., and Voutsinou-Taliadouri, F., 2002, Major outputs of the recent multidisciplinary biogeochemical researches undertaken in the Aegean Sea: *Journal of Marine Systems*, v. 33-34, p. 313-334.
169. Magny, M., and Bégeot, C., 2004, Hydrological changes in the European midlatitudes associated with freshwater outbursts from Lake Agassiz during the Younger Dryas event and the early Holocene: *Quaternary Research*, v. 61, no. 2, p. 181-192.

170. Magny, M., Bégeot, C., Guiot, J., and Peyron, O., 2003, Contrasting patterns of hydrological changes in Europe in response to Holocene climate cooling phases: *quaternary science reviews*, v. 22, no. 15-17, p. 1589-1596.
171. Magny, M., Vanni re, B., Zanchetta, G., Fouache, E., Touchais, G., Petrika, L., Coussot, C., Walter-Simonnet, A.-V., and Arnaud, F., 2009, Possible complexity of the climatic event around 4300—3800 cal. BP in the central and western Mediterranean: *The Holocene*, v. 19, no. 6, p. 823-833.
172. Malanotte-Rizzoli, P., and Robinson, A. R., 1988, POEM: Physical Oceanography of the Eastern Mediterranean: *Eos, Transactions American Geophysical Union*, v. 69, no. 14, p. 194-203.
173. Mallo, M., Ziveri, P., Mortyn, P. G., Schiebel, R., and Grelaud, M., 2017, Low planktic foraminiferal diversity and abundance observed in a spring 2013 west–east Mediterranean Sea plankton tow transect: *Biogeosciences*, v. 14, no. 9, p. 2245-2266.
174. Manno, C., Bednar sek, N., Tarling, G. A., Peck, V. L., Comeau, S., Adhikari, D., Bakker, D. C. E., Bauerfeind, E., Bergan, A. J., Berning, M. I., Buitenhuis, E., Burridge, A. K., Chierici, M., Fl oter, S., Fransson, A., Gardner, J., Howes, E. L., Keul, N., Kimoto, K., Kohnert, P., Lawson, G. L., Lischka, S., Maas, A., Mekkes, L., Oakes, R. L., Pebody, C., Peijnenburg, K. T. C. A., Seifert, M., Skinner, J., Thibodeau, P. S., Wall-Palmer, D., and Ziveri, P., 2017, Shelled pteropods in peril: Assessing vulnerability in a high CO₂ ocean: *Earth-Science Reviews*, v. 169, p. 132-145.
175. Margaritelli, G., Cacho, I., Catal a, A., Barra, M., Bellucci, L. G., Lubritto, C., Rettori, R., and Lirer, F., 2020, Persistent warm Mediterranean surface waters during the Roman period: *Scientific Reports*, v. 10, no. 1, p. 10431.
176. Margaritelli, G., Cisneros, M., Cacho, I., Capotondi, L., Vallefucio, M., Rettori, R., and Lirer, F., 2018, Climatic variability over the last 3000 years in the central - western Mediterranean Sea (Menorca Basin) detected by planktonic foraminifera and stable isotope records: *Global and Planetary Change*, v. 169, p. 179-187.
177. Marino, G., Rohling, E., Sangiorgi, F., Hayes, A., Casford, J., Lotter, A. F., Kucera, M., and Brinkhuis, H., 2009, Early and middle Holocene in the Aegean Sea: interplay between high and low latitude climate variability.: *Quaternary Science Reviews*, v. 28, p. 3246-3262.

178. Martínez-Ruiz, F., Kastner, M., González-Donoso, J. M., Linares, D., Bernasconi, S., and Jiménez-Espejo, F., 2003, A comparative study of the geochemical and mineralogical characteristics of the S1 sapropel in the western and eastern Mediterranean: *Palaeogeography, Palaeoclimatology, Palaeoecology*, v. 190, p. 23-37.
179. Mascle, J., and Martin, L., 1990, Shallow structure and recent evolution of the Aegean Sea: A synthesis based on continuous reflection profiles: *Marine Geology*, v. 94, no. 4, p. 271-299.
180. Mayewski, P. A., Rohling, E. E., Stager, J. C., Karlén, W., Maasch, K. A., Meeker, L. D., Meyerson, E. A., Gasse, F., van Kreveld, S., and Holmgren, K., 2004, Holocene climate variability: *Quaternary research*, v. 62, no. 3, p. 243-255.
181. McGowan, J. A., 1989, *Pelagic ecology and Pacific climate*, Washington, D.C., Geophysical Monograph.
182. Mélières, M. A., Rossignol-Strick, M., and Malaizé, B., 1997, Relation between low latitude insolation and $\delta^{18}\text{O}$ change of atmospheric oxygen for the last 200 kyrs, as revealed by Mediterranean sapropels: *Geophysical Research Letters*, v. 24, no. 10, p. 1235-1238.
183. Mercone, D., Thomson, J., Croudace, I. W., Siani, G., Paterne, M., and Troelstra, S., 2000, Duration of S1, the most recent sapropel in the eastern Mediterranean Sea, as indicated by accelerator mass spectrometry radiocarbon and geochemical evidence: *Paleoceanography*, v. 15, no. 3, p. 336-347.
184. Millot, C., Candela, J., Fuda, J.-L., and Tber, Y., 2006, Millot C, Candela J, Fuda J-L, Tber Y.. Large warming and salinification of the Mediterranean outflow due to changes in its composition. *Deep-Sea Res pt 1* 53: 656-666: *Deep Sea Research Part I: Oceanographic Research Papers*, v. 53, p. 656-666.
185. Nesje, A., Dahl, S. O., and Bakke, J., 2004, Were abrupt Lateglacial and early-Holocene climatic changes in northwest Europe linked to freshwater outbursts to the North Atlantic and Arctic Oceans?: *The Holocene*, v. 14, no. 2, p. 299-310.
186. Nieuwenhuize, J., Maas, Y. E. M., and Middelburg, J. J., 1994, Rapid analysis of organic carbon and nitrogen in particulate materials: *Marine Chemistry*, v. 45, no. 3, p. 217-224.
187. Numberger-Thuy, L., Hemleben, C., Ch, Hoffmann, M., Mackensen, Schulz, H., Wunderlich, J. M., and Kucera, M., 2009, Habitats, abundance patterns and isotopic

- signals of morphotypes of the planktonic foraminifer *Globigerinoides ruber* (d'Orbigny) in the eastern Mediterranean Sea since the Marine Isotopic Stage 12: *Marine Micropaleontology*, v. 73, 1-2: 90-104.
188. Oyama, M., and Takehara, M., 1970, Revised standard soil color charts.
189. Panchang, R., Nigam, R., Riedel, F., Janssen, A., Ko, U., and Hla, Y., 2007, A review of the studies on pteropods from the northern Indian Ocean region with a report on the pteropods of Irrawaddy continental shelf off Myanmar (Burma): *Indian Journal of Marine Sciences*, v. 36, p. 384-398.
190. Perez-Folgado, M., Sierro, F., Flores, J. A., Cacho, I., Grimalt, J., Zahn, R., and Shackleton, N., 2003, Western Mediterranean planktonic foraminifera events and millennial climatic variability during the last 70 kyr: *Marine Micropaleontology*, v. 48, p. 49-70.
191. Peyron, O., Bégeot, C., Brewer, S., Heiri, O., Magny, M., Millet, L., Ruffaldi, P., Campo, E., and Yu, G., 2005, Lateglacial climate in the Jura mountains (France) based on different quantitative reconstruction approaches from pollen, lake-levels, and chironomids: *Quaternary Research*, v. 64, p. 197-211.
192. Peyron, O., Goring, S., Dormoy, I., Kotthoff, U., Pross, J., De Beaulieu, J.-L., Drescher-Schneider, R., Vanni re, B., and Magny, M., 2011, Holocene seasonality changes in the central Mediterranean region reconstructed from the pollen sequences of Lake Accesa (Italy) and Tenaghi Philippon (Greece): *The Holocene*, v. 21, no. 1, p. 131-146.
193. Pierrot-Bults, A., and Peijnenburg, K., 2015, Pteropods: *Encyclopedia of marine geosciences*, p. 1-10.
194. Pinardi, N., and Masetti, E., 2000, Variability of the large scale general circulation of the Mediterranean Sea from observations and modelling: a review: *Palaeogeography, Palaeoclimatology, Palaeoecology*, v. 158, no. 3-4, p. 153-173.
195. Piper, D., and Perissoratis, C., 2003, Quaternary neotectonics of the South Aegean arc: *Marine Geology*, v. 198, p. 259-288.
196. Poulos, S. E., 2009, Origin and distribution of the terrigenous component of the unconsolidated surface sediment of the Aegean floor: A synthesis: *Continental Shelf Research*, v. 29, no. 16, p. 2045-2060.

197. Poulos, S. E., 2020, The Mediterranean and Black Sea Marine System: An overview of its physico-geographic and oceanographic characteristics: *Earth-Science Reviews*, v. 200, p. 103004.
198. Poulos, S. E., Drakopoulos, P. G., and Collins, M. B., 1997, Seasonal variability in sea surface oceanographic conditions in the Aegean Sea (Eastern Mediterranean): an overview: *Journal of Marine Systems*, v. 13, no. 1, p. 225-244.
199. Principato, M., Giunta, S., Corselli, C., and Negri, A., 2003, Late Pleistocene-Holocene planktonic assemblages in three box-cores from the Mediterranean Ridge area (west-southwest of Crete): Palaeoecological and palaeoceanographic reconstruction of sapropel S1 interval: *Palaeogeography, Palaeoclimatology, Palaeoecology*, v. 190, p. 61-77.
200. Pujol, C., and Vergnaud-Grazzini, C., 1995, Distribution patterns of live planktic foraminifers as related to regional hydrology and productive systems of the Mediterranean Sea: *Marine Micropaleontology*, v. 25, p. 187-217.
201. Rampal, J., 2002, Biodiversité et biogéographie chez les Cavoliniidae (Mollusca, Gastropoda, Opisthobranchia, Euthecosomata). Régions faunistiques marines: *Zoosystema*, v. 24, no. 2, p. 209-258.
202. Rampal, J., 2011, Clés de détermination des Thecosomata (Pteropoda) (Mollusca Opisthobranchia Holoplanctoniques) de Méditerranée et de l'Atlantique Eurafriquein. : *Revue des Travaux de l'Institut des Pêches maritimes* v. 37, no. 3, p. 369-389.
203. Rampal, J., 2017, Euthecosomata (Mollusca, Gastropoda, Thecosomata). Taxonomic review: *bioRxiv*, p. 098475.
204. Rasmussen, S. O., Vinther, B. M., Clausen, H. B., and Andersen, K. K., 2007, Early Holocene climate oscillations recorded in three Greenland ice cores: *Quaternary Science Reviews*, v. 26, no. 15, p. 1907-1914.
205. Reimer, P., Bard, E., Bayliss, A., Beck, J., Blackwell, P., Ramsey, C., Buck, C., Cheng, H., Edwards, R., Friedrich, M., Grootes, P., Guilderson, T., Haflidason, H., Hajdas, I., Christine, H., Heaton, T., Hogg, A., Hughen, K., Kaiser, K., and Staff, R., 2013, IntCal13 and MARINE13 radiocarbon age calibration curves 0-50,000 years cal BP: *Radiocarbon*, v. 55, p. 1869–1887.
206. Reiss, Z., Halicz, E., and Luz, B., 1999, Late-holocene foraminifera from the SE Levantine Basin: *Israel Journal of Earth Sciences*, v. 48, p. 1-27.

207. Reiss, Z., Luz, B., Almogi-Labin, A., Halicz, E., Winter, A., Wolf, M., and Ross, D. A., 1980, Late Quaternary paleoceanography of the Gulf of Aqaba (Elat), Red Sea: *Quaternary research*, v. 14, no. 3, p. 294-308.
208. Rohling, E., Jorissen, F., and Stigter, H., 1997, 200 Year interruption of Holocene sapropel formation in the Adriatic Sea: *Journal of Micropalaeontology - J MICROPALAEONTOL*, v. 16, p. 97-108.
209. Rohling, E., Mayewski, P., Abu-Zied, R., Casford, J., and Hayes, A., 2002a, Holocene atmosphere-ocean interactions: records from Greenland and the Aegean Sea: *Climate Dynamics*, v. 18, no. 7, p. 587-593.
210. Rohling, E. J., 1991, Shoaling of the Eastern Mediterranean pycnocline due to reduction of excess evaporation: implications for sapropel formation: *Paleoceanography*, v. 6, no. 6, p. 747-753.
211. Rohling, E. J., 1994, Glacial conditions in the Red Sea: *Paleoceanography*, v. 9, no. 5, p. 653-660.
212. Rohling, E. J., Cane, T. R., Cooke, S., Sprovieri, M., Bouloubassi, I., Emeis, K. C., Schiebel, R., Kroon, D., Jorissen, F. J., and Lorre, A., 2002b, African monsoon variability during the previous interglacial maximum: *Earth and Planetary Science Letters*, v. 202, no. 1, p. 61-75.
213. Rohling, E. J., De Stigter, H. C., Vergnaud-Grazzini, C., and Zaalberg, R., 1993a, Temporary repopulation by low-oxygen tolerant benthic foraminifera within an upper Pliocene sapropel: evidence for the role of oxygen depletion in the formation of sapropels: *Marine Micropaleontology*, v. 22, no. 3, p. 207-219.
214. Rohling, E. J., Dulk, M., Pujol, C., and Vergnaud-Grazzini, C., 1995, Abrupt hydrographic change in the Alboran Sea (western Mediterranean) around 8000 yrs BP: *Deep Sea Research Part I: Oceanographic Research Papers*, v. 42, p. 1609-1619.
215. Rohling, E. J., Grant, K., Bolshaw, M., Roberts, A., Siddall, M., Hemleben, C., and Kucera, M., 2009, Antarctic temperature and global sea level closely coupled over the past five glacial cycles: *Nature Geoscience*.
216. Rohling, E. J., Jorissen, F., Grazzini, C. V., and Zachariasse, W. J., 1993b, Northern Levantine and Adriatic Quaternary planktic foraminifera; Reconstruction of paleoenvironmental gradients: *Marine Micropaleontology*, v. 21, p. 191-218.

217. Rohling, E. J., Marino, G., and Grant, K. M., 2015, Mediterranean climate and oceanography, and the periodic development of anoxic events (sapropels): *Earth-Science Reviews*, v. 143, p. 62-97.
218. Rohling, E. J., and Pälike, H., 2005, Centennial-scale climate cooling with a sudden cold event around 8,200 years ago: *nature*, v. 434, no. 7036, p. 975-979.
219. Rohling, E. J., Sprovieri, M., Cane, T., Casford, J. S. L., Cooke, S., Bouloubassi, I., Emeis, K. C., Schiebel, R., Rogerson, M., and Hayes, A., 2004, Reconstructing past planktic foraminiferal habitats using stable isotope data: a case history for Mediterranean sapropel S5: *Marine Micropaleontology*, v. 50, no. 1-2, p. 89-123.
220. Rossignol-Strick, M., 1983, African monsoons, an immediate climate response to orbital insolation: *Nature*, v. 304, no. 5921, p. 46-49.
221. Rossignol-Strick, M., 1985, Mediterranean Quaternary sapropels, an immediate response of the African monsoon to variation of insolation: *Palaeogeography, Palaeoclimatology, Palaeoecology*, v. 49, no. 3, p. 237-263.
222. Rossignol-Strick, M., 1995, Sea-land correlation of pollen records in the Eastern Mediterranean for the glacial-interglacial transition: *Biostratigraphy versus radiometric time-scale: Quaternary Science Reviews*, v. 14, p. 893.
223. Rottman, M. L., 1980, Net tow and surface sediment distributions of pteropods in the South China Sea region: Comparison and oceanographic implications: *Marine Micropaleontology*, v. 5, p. 71-110.
224. Roussakis, G., Karageorgis, A. P., Conispoliatis, N., and Lykousis, V., 2004, Last glacial–Holocene sediment sequences in N. Aegean basins: structure, accumulation rates and clay mineral distribution: *Geo-Marine Letters*, v. 24, no. 2, p. 97-111.
225. Ruan, J., Kherbouche, F., Genty, D., Blamart, D., Cheng, H., Dewilde, F., Hachi, S., Edwards, R. L., Régnier, E., and Michelot, J. L., 2016, Evidence of a prolonged drought ca. 4200 yr BP correlated with prehistoric settlement abandonment from the Gueldaman GLD1 Cave, Northern Algeria: *Climate of the Past*, v. 12, no. 1, p. 1-14.
226. Sakthivel, M., 1969, A preliminary report on the distribution and relative abundance of Euthecosomata with a note on the seasonal variation of *Limacina* species in the Indian Ocean: *Bull Nat Inst Sci India*, v. 38, p. 700-717.

227. Sbaffi, L., Wezel, F., Kallel, N., Paterne, M., Cacho, I., Ziveri, P., and Shackleton, N., 2001, Response of the pelagic environment to palaeoclimatic changes in the central Mediterranean Sea during the Late Quaternary: *Marine Geology*, p. 39-62.
228. Sbaffi, L., Wezel, F. C., Curzi, G., and Zoppi, U., 2004, Millennial- to centennial-scale palaeoclimatic variations during Termination I and the Holocene in the central Mediterranean Sea: *Global and Planetary Change*, v. 40, p. 201.
229. Schiebel, R., and Hemleben, C., 2005, Modern Planktic Foraminifera: *Paläontologische Zeitschrift*, v. 79, p. 135-148.
230. Schiebel, R., Waniek, J., Bork, M., and Hemleben, C., 2001, Planktic foraminiferal production stimulated by chlorophyll redistribution and entrainment of nutrients: *Deep Sea Research Part I: Oceanographic Research Papers*, v. 48, p. 721–740.
231. Schiebel, R., Zeltner, A., Treppke, U. F., Waniek, J. J., Bollmann, J., Rixen, T., and Hemleben, C., 2004, Distribution of diatoms, coccolithophores and planktic foraminifers along a trophic gradient during SW monsoon in the Arabian Sea: *Marine Micropaleontology*, v. 51, no. 3-4, p. 345-371.
232. Schmiedl, G., Kuhnt, T., Ehrmann, W., Emeis, K.-C., Hamann, Y., Kotthoff, U., Dulski, P., and Pross, J., 2010, Climatic forcing of eastern Mediterranean deep-water formation and benthic ecosystems during the past 22 000 years: *Quaternary Science Reviews*, v. 29, no. 23-24, p. 3006-3020.
233. Schneider, A., Wallace, W. R. D., and Kortzinger, A., 2007, Alkalinity of the Mediterranean Sea: *Geophysical Research Letters*, v. 34.
234. Schroeder, K., Lafuente, J., Josey, S., Artale, V., Buongiorno Nardelli, B., Carrillo, A., Gacic, M., Gasparini, G., Herrmann, M., Lionello, P., Ludwig, W., Millot, C., Özsoy, E., Pisacane, G., Sánchez-Garrido, J., Sannino, G., Santoleri, R., Somot, S., Struglia, M., and Zodiatis, G., 2012, *Circulation Of The Mediterranean Sea And Its Variability*, p. 187-256.
235. Siani, G., Magny, M., Paterne, M., Debret, M., and Fontugne, M., 2013, Paleohydrology reconstruction and Holocene climate variability in the South Adriatic Sea: *Clim. Past*, v. 9, no. 1, p. 499-515.

- 236.Siani, G., Paterne, M., and Colin, C., 2010, Late glacial to Holocene planktic foraminifera bioevents and climatic record in the South Adriatic Sea: *Journal of Quaternary Science*, v. 25, no. 5, p. 808-821.
- 237.Sijinkumar, A. V., Bejugam, N., and Guptha, M. V. s., 2010, Late Quaternary record of pteropod preservation from the Andaman Sea: *Marine Geology*, v. 275.
- 238.Singh, A., N.R, N., Joydas, T., and Joydas, V., 2005, Distribution patterns of Recent pteropods in surface sediments of the western continental shelf of India: *Journal of Micropalaeontology*, v. 24, p. 39.
- 239.Singh, A., Ramachandran, K., Samsuddin, M., Nisha, N., and Haneeshkumar, V., 2001, Significance of pteropods in deciphering the late Quaternary sea-level history along the southwestern Indian shelf: *Geo-Marine Letters*, v. 20, no. 4, p. 243-252.
- 240.Singh, A. D., Rajarama, K. N., Ramachandran, K. K., Suchindan, G. K., and Samsuddin, M., 1998, Pteropods as bathometers: a case study from the continental shelf off Kerala coast, India: *Current Science*, p. 620-623.
- 241.Skliris, N., Mantziafou, A., Sofianos, S., Gkanasos, A., 2010, Satellite-derived variability of the Aegean Sea ecohydrodynamics. *Continental Shelf Research*, v. 30, no. 5, p. 403–418.
- 242.Sperling, M., Schmiedl, G., Hemleben, C., Emeis, K. C., Erlenkeuser, H., and Grootes, P. M., 2003, Black Sea impact on the formation of eastern Mediterranean sapropel S1? Evidence from the Marmara Sea: *Palaeogeography, Palaeoclimatology, Palaeoecology*, v. 190, p. 9-21.
- 243.Spero, H. J., Mielke, K. M., Kalve, E. M., Lea, D. W., and Pak, D. K., 2003, Multispecies approach to reconstructing eastern equatorial Pacific thermocline hydrography during the past 360 kyr: *Paleoceanography*, v. 18, no. 1.
- 244.Sprovieri, R., Stefano, E., Incarbona, A., and Gargano, M., 2003, A high-resolution record of the last deglaciation in the Sicily Channel based on foraminifera and calcareous nannofossil quantitative distribution: *Palaeogeography, Palaeoclimatology, Palaeoecology*, v. 202, p. 119-142.
- 245.Stuiver, M., and Reimer, P. J., 1993, Extended (super 14) C data base and revised CALIB 3.0 (super 14) C age calibration program: *Radiocarbon*, v. 35, no. 1.

246. Teller, J. T., and Leverington, D. W., 2004, Glacial Lake Agassiz: A 5000 yr history of change and its relationship to the $\delta^{18}\text{O}$ record of Greenland: Geological Society of America Bulletin, v. 116, no. 5-6, p. 729-742.
247. Theocharis, A., Balopoulos, E., Kioroglou, S., Kontoyiannis, H., and Iona, A., 1999a, A synthesis of the circulation and hydrography of the South Aegean Sea and the Straits of the Cretan Arc (March 1994–January 1995): Progress In Oceanography, v. 44, p. 469-509.
248. Theocharis, A., and Georgopoulos, D., 1993, Dense water formation over the Samothraki and Limnos Plateaux in the north Aegean Sea (Eastern Mediterranean Sea): Continental Shelf Research, v. 13, p. 919-939.
249. Theocharis, A., Georgopoulos, D., Lascaratos, A., and Nittis, K., 1993, Water masses and circulation in the central region of the Eastern Mediterranean: Eastern Ionian, South Aegean and Northwest Levantine, 1986–1987: Deep Sea Research Part II: Topical Studies in Oceanography, v. 40, p. 1121-1142.
250. Theocharis, A., Nittis, K., Kontoyiannis, H., Papageorgiou, E., and Balopoulos, E., 1999b, Climatic changes in the Aegean Sea influence the Eastern Mediterranean thermohaline circulation (1986-1997): Geophysical Research Letters, v. 20, p. 1617-1620.
251. Thunell, R., 1978, Distribution of recent planktonic foraminifera in surface sediments of the Mediterranean Sea: Marine Micropaleontology - MAR MICROPALAEONTOLOGY, v. 3, p. 147-173.
252. Torelli, L., and Buccheri, G., 1983, Le associazioni a pteropodi del Pleistocene mediterraneo, 1. Analisi paleoclimatica della carota n. 1 del pozzo DSDP 125 (leg 13): Geologica Romana, v. 22, p. 157-175.
253. Trégouboff, G., and Rose, M., 1957, Manuel de planctonologie méditerranéenne et exto.
254. Tréguer, P., Legendre, L., Rivkin, R. T., Ragueneau, O., and Dittert, N., 2003, Water column biogeochemistry below the euphotic zone, Ocean Biogeochemistry, Springer, p. 145-156.
255. Triantaphyllou, M. V., Antonarakou, A., Kouli, K., Dimiza, M., Kontakiotis, G., Papanikolaou, M. D., Ziveri, P., Mortyn, P. G., Lianou, V., Lykousis, V., and Dermitzakis, M. D., 2009a, Late Glacial–Holocene ecostratigraphy of the south-eastern

- Aegean Sea, based on plankton and pollen assemblages: *Geo-Marine Letters*, v. 29, no. 4, p. 249-267.
256. Triantaphyllou, M. V., Ziveri, P., Gogou, A., Marino, G., Lykousis, V., Bouloubassi, I., Emeis, K. C., Kouli, K., Dimiza, M., Rosell-Melé, A., Papanikolaou, M., Katsouras, G., and Nunez, N., 2009b, Late Glacial–Holocene climate variability at the south-eastern margin of the Aegean Sea: *Marine Geology*, v. 266, no. 1, p. 182-197.
257. Tsiolakis, E., Tsaila-Monopoli, S., Kontakiotis, G., Antonarakou, A., Sprovieri, M., Geraga, M., Ferentinos, G., and Zissimos, A., 2019, Integrated paleohydrology reconstruction and Pliocene climate variability in Cyprus Island (eastern Mediterranean): *IOP Conference Series: Earth and Environmental Science*, v. 362, p. 012103.
258. Van der Spoel, S., 1976, *Pseudothecosomata, Gymnosomata and Heteropoda (Gastropoda)*, Utrecht, the Netherlands, Bohn, Scheltema, and Holkema.
259. Vasiliev, I., Karakitsios, V., Bouloubassi, I., Agiadi, K., Kontakiotis, G., Antonarakou, A., Triantaphyllou, M., Gogou, A., Kafousia, N., de Rafélis, M., Zarkogiannis, S., Kaczmar, F., Parinos, C., and Pasadakis, N., 2019, Large Sea Surface Temperature, Salinity, and Productivity-Preservation Changes Preceding the Onset of the Messinian Salinity Crisis in the Eastern Mediterranean Sea: *Paleoceanography and Paleoclimatology*, v. 34, no. 2, p. 182-202.
260. Velaoras, D., and Lascaratos, A., 2005, Deep water mass characteristics and interannual variability in the North and Central Aegean Sea: *Journal of Marine Systems*, v. 53, p. 59-85.
261. Verardo, D. J., Froelich, P. N., and McIntyre, A., 1990, Determination of organic carbon and nitrogen in marine sediments using the Carlo Erba NA-1500 analyzer: *Deep Sea Research Part A. Oceanographic Research Papers*, v. 37, no. 1, p. 157-165.
262. Vergnaud-Grazzini, C., Ryan, W., and Cita, M., 1977, Stable isotope fractionation, climate change and episodic stagnation in the Eastern Mediterranean during the Late Quaternary: *Marine Micropaleontology*, v. 2, p. 353-370.
263. Vinogradov, M., 1961, Food sources for the deep water fauna. Speed of decomposition of dead Pteropoda: *Dokl Akad Nauk SSSR*, v. 138, p. 1439-1442.

264. Walkley, A., and Black, I. A., 1934, An examination of the Degtjareff Method for determining soil organic matter, and a proposed modification of the chromic acid titration method: *Soil Science*, v. 37, no. 1.
265. Wall-Palmer, D., Hart, M. B., Smart, C. W., Sparks, R. S. J., Le Friant, A., Boudon, G., Deplus, C., and Komorowski, J. C., 2012, Pteropods from the Caribbean Sea: variations in calcification as an indicator of past ocean carbonate saturation: *Biogeosciences*, v. 9, no. 1, p. 309-315.
266. Wall-Palmer, D., Smart, C. W., and Hart, M. B., 2013, In-life pteropod shell dissolution as an indicator of past ocean carbonate saturation: *Quaternary Science Reviews*, v. 81, p. 29-34.
267. Wall-Palmer, D., Smart, C. W., Hart, M. B., Leng, M. J., Borghini, M., Manini, E., Aliani, S., and Conversi, A., 2014, Late Pleistocene pteropods, heteropods and planktonic foraminifera from the Caribbean Sea, Mediterranean Sea and Indian Ocean: *Micropaleontology*, v. 60, no. 6, p. 557-578.
268. Wang, B., Wu, R., and Fu, X., 2000, Pacific–East Asian Teleconnection: How Does ENSO Affect East Asian Climate?: *Journal of Climate*, v. 13, no. 9, p. 1517-1536.
269. Wanner, H., Mercolli, L., Grosjean, M., and Ritz, S. P., 2015, Holocene climate variability and change; a data-based review: *Journal of the Geological Society*, v. 172, no. 2, p. 254-263.
270. Wanner, H., Solomina, O., Grosjean, M., Ritz, S. P., and Jetel, M., 2011, Structure and origin of Holocene cold events: *Quaternary Science Reviews*, v. 30, no. 21-22, p. 3109-3123.
271. Weikert, H., 1982, The vertical distribution of zooplankton in relation to habitat zones in the area of the Atlantis II Deep, central Red Sea: *Marine Ecology Progress Series*, v. 8, no. 2, p. 129-143.
272. Weikert, H. G., and Cederbaum, L. S., 1987, Particle-number-dependent theory of few- and many-body systems: *Few-Body Systems*, v. 2, no. 1, p. 33-51.
273. Wiersma, A. P., and Renssen, H., 2006, Model–data comparison for the 8.2 ka BP event: confirmation of a forcing mechanism by catastrophic drainage of Laurentide Lakes: *Quaternary Science Reviews*, v. 25, no. 1-2, p. 63-88.

274. Wilke, I., Meggers, H., and Bickert, T., 2009, Depth habitats and seasonal distributions of recent planktic foraminifers in the Canary Islands region (29°N) based on oxygen isotopes: *Deep Sea Research Part I: Oceanographic Research*, v. 56, p. 89.
275. Winter, A., Almogi-Labin, A., Erez, Y., Halicz, E., Luz, B., and Reiss, Z., 1983, Salinity tolerance of marine organisms deduced from Red Sea Quaternary record: *Marine Geology*, v. 53, no. 1, p. M17-M22.
276. Wit, J. C., Reichert, G. J., A Jung, S. J., and Kroon, D., 2010, Approaches to unravel seasonality in sea surface temperatures using paired single-specimen foraminiferal $\delta^{18}\text{O}$ and Mg/Ca analyses: *Paleoceanography*, v. 25, no. 4.
277. Wormelle, R. L., 1962, A survey of the standing crop of plankton of the Florida Current. VI. A study of the distribution of the pteropods of the Florida Current: *Bulletin of Marine Science*, v. 12, no. 1, p. 95-136.
278. Wormuth, J., 1981, Vertical distributions and diel migrations of Euthecosomata in the northwest Sargasso Sea: *Deep Sea Research Part A. Oceanographic Research Papers*, v. 28, p. 1493-1515.
279. Yu, S.-Y., Colman, S. M., Lowell, T. V., Milne, G. A., Fisher, T. G., Breckenridge, A., Boyd, M., and Teller, J. T., 2010, Freshwater outburst from Lake Superior as a trigger for the cold event 9300 years ago: *Science*, v. 328, no. 5983, p. 1262-1266.
280. Zachariasse, W., Jorissen, F., Perissoratis, C., Rohling, E., and Tsapralis, V., Late Quaternary foraminiferal changes and the nature of sapropel S1 in Skopelos Basin, *in Proceedings 5th Hellenic Symposium of Oceanography and Fisheries, Kavala, Greece, 07/27 1997, Volume 1*, p. 391–394.
281. Zarkogiannis, S., Kontakiotis, G., and Antonarakou, A., 2020, Recent planktonic foraminifera population and size response to Eastern Mediterranean hydrography: *Revue de micropaleontologie*, v. 69, p. 100450.
282. Zarkogiannis, S., Kontakiotis, G., Antonarakou, A., Mortyn, P., and Drinia, H., 2019a, Latitudinal Variation of Planktonic Foraminifera Shell Masses During Termination I: *IOP Conference Series: Earth and Environmental Science*, v. 221, p. 012052.
283. Zarkogiannis, S. D., Antonarakou, A., Tripathi, A., Kontakiotis, G., Mortyn, P. G., Drinia, H., and Greaves, M., 2019b, Influence of surface ocean density on planktonic foraminifera calcification: *Scientific Reports*, v. 9, no. 1, p. 533.

284. Zarkogiannis, S.D.; Kontakiotis, G.; Gkaniatsa, G.; Kuppili, V.S.C.; Marathe, S.; Wanelik, K.; Lianou, V.; Besiou, E.; Makri, P.; Antonarakou, A., 2020, An Improved Cleaning Protocol for Foraminiferal Calcite from Unconsolidated Core Sediments: HyPerCal—A New Practice for Micropaleontological and Paleoclimatic Proxies. *Journal of Marine Science and Engineering*, v. 8, no. 12, 998. <https://doi.org/10.3390/jmse8120998>
285. Zervakis, G. I., Theocharis, A., and Georgopoulos, D., 2005a, Circulation and hydrography of the open Seas., Athens, HCMR Publication, State of the Hellenic Marine Environment.
286. Zervakis, V., Georgopoulos, D., and Drakopoulos, P. G., 2000, The role of the North Aegean in triggering the recent Eastern Mediterranean climatic changes: *Journal of Geophysical Research: Oceans*, v. 105, no. C11, p. 26103-26116.
287. Zervakis, V., Georgopoulos, D., Karageorgis, A. P., and Theocharis, A., 2004, On the response of the Aegean Sea to climatic variability: a review: *International Journal of Climatology: A Journal of the Royal Meteorological Society*, v. 24, no. 14, p. 1845-1858.
288. Zervakis, V., Karageorgis, A. P., Kontoyiannis, H., Papadopoulos, V., and Lykousis, V., 2005b, Hydrology, circulation and distribution of particulate matter in Thermaikos Gulf (NW Aegean Sea), during September 2001–October 2001 and February 2002: *Continental Shelf Research*, v. 25, no. 19, p. 2332-2349.
289. Zielhofer, C., Faust, D., Escudero, R. B., del Olmo, F. D., Kadereit, A., Moldenhauer, K.-M., and Porras, A., 2004, Centennial-scale late-Pleistocene to mid-Holocene synthetic profile of the Medjerda Valley, northern Tunisia: *The Holocene*, v. 14, no. 6, p. 851-861.

10. Appendix

AEX 15: Planktonic foraminifera and pteropod abundances (%)											
Species/Samples	1,5	3	4,5	6,25	8	9	10	11,25	12,5	13,5	14,5
<i>O. universa</i>	0,00	0,61	1,15	1,75	1,45	3,30	0,00	1,38	1,55	5,34	4,88
<i>G. ruber alba</i>	27,52	30,67	37,93	40,35	45,89	41,98	30,63	32,57	41,45	54,85	40,49
<i>G. ruber rosea</i>	8,05	11,04	6,32	12,28	8,21	8,02	11,26	11,93	19,69	17,48	31,22
<i>G. sacculifer</i>	0,00	0,00	0,00	0,00	0,00	0,47	0,00	2,29	2,07	3,40	3,90
<i>G. inflata</i>	0,00	0,00	0,00	0,00	0,00	0,00	0,00	0,00	0,00	0,97	0,49
<i>G. bulloides</i>	22,82	33,74	28,16	30,70	27,54	19,81	33,78	25,23	10,36	3,40	0,98
<i>G. rubescens</i>	12,75	3,07	2,30	2,63	1,45	8,02	3,15	5,05	0,00	0,49	0,00
<i>G. aequilateralis</i>	0,00	1,23	2,87	0,88	3,38	0,00	1,35	3,21	1,55	0,49	0,98
<i>G. calida</i>	0,00	0,00	0,00	0,00	0,00	0,00	0,00	2,75	0,00	0,00	0,00
<i>N. pachyderma s</i>	0,00	0,00	0,00	0,00	0,00	0,00	0,00	0,00	0,00	0,00	0,00
<i>N. pachyderma d</i>	4,70	6,75	6,90	0,00	2,90	0,94	3,15	8,26	14,51	12,62	17,07
<i>N. dutertrei d</i>	0,00	1,84	0,00	0,00	0,00	0,00	0,00	0,00	0,00	0,00	0,00
<i>N. dutertrei s</i>	0,00	0,61	0,00	0,00	0,00	0,00	0,00	0,00	0,00	0,00	0,00
<i>T. quinueloba</i>	19,46	9,82	13,79	10,53	8,70	15,09	16,22	9,17	8,29	0,97	0,00
<i>G. glutinata</i>	4,70	0,61	0,57	0,88	0,48	2,36	0,45	0,46	0,00	0,00	0,00
<i>G. scitula</i>	0,00	0,00	0,00	0,00	0,00	0,00	0,00	0,46	0,52	0,00	0,00
<i>B. digitata</i>	0,00	0,00	0,00	0,00	0,00	0,00	0,00	0,00	0,00	0,00	0,00
<i>H. inflatus</i>	0,00	4,88	4,23	10,39	5,83	10,97	6,61	6,33	6,67	16,20	14,77
<i>L. retroversa</i>	0,00	0,00	0,00	0,00	0,00	0,00	0,00	0,00	0,00	4,23	0,00
<i>L. trochiformis</i>	0,00	14,63	22,54	3,90	14,17	14,19	18,18	16,46	0,00	7,04	4,55
<i>C. virgula</i>	0,00	18,29	11,27	12,99	14,17	25,81	7,44	11,39	3,33	6,34	0,00
<i>C. acicula</i>	0,00	26,83	26,76	41,56	20,00	13,55	16,53	17,72	13,33	3,52	6,82
<i>H. striata</i>	0,00	1,22	0,00	0,00	0,83	1,94	0,00	0,00	0,00	0,70	1,14
<i>S. subula</i>	0,00	1,22	2,82	1,30	2,50	3,23	5,79	2,53	13,33	6,34	5,11
<i>C. cuspidata</i>	0,00	0,00	0,00	0,00	0,83	1,94	0,83	0,00	0,00	0,70	1,14
<i>C. pyramidata</i>	0,00	14,63	9,86	10,39	24,17	8,39	12,40	20,25	23,33	11,97	17,05
<i>D. trispinosa</i>	0,00	0,00	0,00	0,00	0,00	0,00	0,00	0,00	0,00	0,00	0,00
<i>Cavolinia spp.</i>	0,00	4,88	2,82	5,19	8,33	9,03	9,09	10,13	6,67	7,04	14,20

Species/Samples	15,5	17	19	20,5	21,5	23	25	27	29	31	33
<i>O. universa</i>	2,16	0,97	4,40	0,88	1,01	2,42	0,86	0,91	1,56	1,19	0,45
<i>G. ruber alba</i>	41,62	48,31	60,44	50,66	45,73	46,38	45,26	54,09	39,45	45,24	39,19
<i>G. ruber rosea</i>	21,08	15,46	4,40	13,66	18,59	21,74	11,64	15,00	6,25	9,92	9,01
<i>G. sacculifer</i>	5,95	2,42	3,85	4,85	2,51	0,00	3,02	5,00	2,34	1,19	1,80
<i>G. inflata</i>	1,62	0,00	0,00	0,00	0,00	0,00	0,00	0,00	0,00	0,00	0,00
<i>G. bulloides</i>	8,11	7,25	13,19	12,33	11,56	9,66	18,10	10,45	12,89	8,33	9,46
<i>G. rubescens</i>	1,62	5,80	0,00	1,76	2,01	0,97	3,02	1,36	3,52	1,59	1,35
<i>G.aequilateralis</i>	1,62	2,90	2,20	2,64	3,02	3,38	2,59	2,73	3,52	3,57	4,95
<i>G. calida</i>	0,00	1,93	0,00	1,76	2,01	0,00	0,00	0,00	0,00	3,17	4,05
<i>N. pachyderma s</i>	0,00	0,00	0,00	0,00	0,00	0,00	0,00	0,00	0,00	0,00	0,00
<i>N. pachyderma d</i>	12,43	5,31	9,89	0,88	2,01	7,25	3,88	2,73	1,95	2,38	0,90
<i>N. dutertrei d</i>	1,08	0,00	0,55	0,00	0,00	1,45	0,00	0,00	0,00	0,00	0,00
<i>N. dutertrei s</i>	0,00	0,00	0,00	0,00	0,00	0,97	0,00	0,00	0,00	0,00	0,00
<i>T. quinueloba</i>	2,16	10,63	1,10	11,89	12,56	4,83	11,64	7,27	28,13	25,79	31,53
<i>G. glutinata</i>	0,00	0,97	0,00	0,44	1,01	0,97	0,00	0,45	0,39	0,79	1,35
<i>G. scitula</i>	0,54	0,00	0,00	0,00	0,00	0,00	0,00	0,00	0,00	0,00	0,00
<i>B. digitata</i>	0,00	0,00	0,00	0,00	0,00	0,00	0,00	0,00	0,00	0,00	0,00
<i>H. inflatus</i>	7,55	7,53	7,63	5,06	8,33	10,92	8,70	8,88	7,69	5,56	10,59
<i>L. retroversa</i>	1,89	0,00	17,80	0,00	0,00	1,68	0,00	0,59	0,00	0,00	0,00
<i>L. trochiformis</i>	9,43	21,51	1,69	12,66	15,63	7,56	13,04	26,04	0,00	20,00	16,47
<i>C. virgula</i>	11,32	5,38	3,39	27,22	14,58	8,40	13,04	7,10	0,00	8,89	0,00
<i>C. acicula</i>	4,72	6,45	5,08	8,86	13,54	11,76	2,90	7,10	0,00	3,33	1,18
<i>H. striata</i>	0,00	0,00	0,00	0,00	1,04	0,00	1,45	0,00	0,00	0,00	0,00
<i>S. subula</i>	15,09	10,75	3,39	4,43	8,33	8,40	8,70	5,33	0,00	11,11	7,06
<i>C. cuspidata</i>	0,00	1,08	0,85	1,27	0,00	0,00	0,00	0,59	0,00	1,11	4,71
<i>C. pyramidata</i>	14,15	16,13	20,34	13,92	19,79	15,13	21,74	13,02	46,15	15,56	22,35
<i>D. trispinosa</i>	0,00	0,00	0,00	0,00	0,00	0,00	0,00	0,00	0,00	0,00	0,00
<i>Cavolinia spp.</i>	9,43	10,75	11,02	13,29	7,29	11,76	11,59	16,57	0,00	8,89	5,88

Species/Samples	35	37	39	41	43	45	47	49	51	53	55
<i>O. universa</i>	1,91	0,44	0,42	0,85	1,99	2,11	0,42	2,11	0,00	0,39	1,67
<i>G. ruber alba</i>	26,32	33,19	42,37	41,28	41,83	65,82	54,39	48,95	46,31	49,41	37,92
<i>G. ruber rosea</i>	9,09	9,29	10,17	10,21	9,96	6,75	9,21	8,02	11,07	6,67	8,33
<i>G. sacculifer</i>	2,87	4,87	5,93	2,98	3,98	2,95	6,69	2,53	1,23	0,78	1,25
<i>G. inflata</i>	0,00	0,44	0,00	0,00	0,00	0,00	0,00	0,00	0,00	0,39	0,00
<i>G. bulloides</i>	18,18	9,73	7,63	10,64	11,55	10,13	12,97	12,66	20,08	24,31	20,42
<i>G. rubescens</i>	0,48	1,77	2,54	2,55	5,18	1,69	3,35	9,28	6,56	3,92	4,58
<i>G.aequilateralis</i>	3,83	2,65	3,39	2,55	2,79	2,11	5,02	4,22	4,51	2,35	4,17
<i>G. calida</i>	2,39	0,00	2,12	0,00	2,39	0,00	2,09	2,11	3,69	0,00	2,92
<i>N. pachyderma s</i>	0,00	0,00	0,00	0,00	0,00	0,00	0,00	0,00	0,00	0,00	0,00
<i>N. pachyderma d</i>	5,26	1,77	3,81	1,28	1,59	0,00	0,00	0,00	0,00	1,57	4,17
<i>N. dutertrei d</i>	0,00	0,00	0,00	0,00	0,00	0,00	0,00	0,00	0,00	0,39	0,00
<i>N. dutertrei s</i>	0,00	0,00	0,00	0,00	0,00	0,00	0,00	0,00	0,00	0,00	0,00
<i>T. quinueloba</i>	32,06	35,40	23,73	27,66	21,12	8,44	6,69	10,97	9,84	9,02	17,50
<i>G. glutinata</i>	0,00	0,00	0,00	0,00	0,00	0,00	1,26	1,27	0,41	0,78	0,00
<i>G. scitula</i>	0,00	0,44	0,00	0,00	0,00	0,00	0,00	0,00	0,00	0,00	0,00
<i>B. digitata</i>	0,00	0,00	0,00	0,00	0,00	0,00	0,00	0,00	0,00	0,00	0,00
<i>H. inflatus</i>	12,22	16,20	10,84	8,39	3,13	4,10	0,00	6,25	0,00	8,89	4,81
<i>L. retroversa</i>	0,00	0,00	0,00	0,70	0,00	0,00	0,00	0,00	0,00	0,00	0,00
<i>L. trochiformis</i>	24,44	17,32	22,09	20,28	23,96	7,38	0,00	23,44	0,00	12,06	12,83
<i>C. virgula</i>	5,56	13,41	20,88	11,19	3,13	2,46	0,00	7,81	0,00	10,48	9,09
<i>C. acicula</i>	7,78	1,68	4,02	5,59	6,25	18,85	0,00	3,13	0,00	12,38	15,51
<i>H. striata</i>	0,00	0,00	0,00	0,00	0,00	0,00	0,00	0,00	0,00	0,00	0,00
<i>S. subula</i>	6,67	10,61	14,86	15,38	26,04	25,41	0,00	15,63	0,00	35,87	28,34
<i>C. cuspidata</i>	1,11	1,12	0,40	1,40	1,04	0,82	0,00	4,69	0,00	0,95	2,14
<i>C. pyramidata</i>	18,89	14,53	8,43	18,18	18,75	24,59	0,00	21,88	0,00	10,79	14,97
<i>D. trispinosa</i>	1,11	0,00	0,00	0,00	1,04	0,00	0,00	0,00	0,00	0,00	0,00
<i>Cavalinia spp.</i>	12,22	8,94	9,24	9,09	10,42	4,92	0,00	4,69	0,00	2,22	2,67

Species/Samples	57	59	61	63	65	67	69	71	73	75	77
<i>O. universa</i>	1,88	0,00	0,00	0,43	0,00	0,48	1,03	2,46	0,85	2,31	1,70
<i>G. ruber alba</i>	39,47	37,59	13,37	47,86	44,24	48,56	50,00	59,84	57,87	54,17	44,26
<i>G. ruber rosea</i>	12,03	6,57	11,05	16,24	8,76	8,65	10,31	7,38	2,55	10,65	14,89
<i>G. sacculifer</i>	0,38	2,19	0,00	0,85	0,92	1,92	0,52	2,87	1,70	2,78	1,70
<i>G. inflata</i>	0,00	0,00	0,00	0,00	0,00	0,00	0,00	0,00	0,00	0,00	0,00
<i>G. bulloides</i>	21,80	19,71	22,09	9,40	28,57	21,63	12,89	11,07	17,02	9,72	17,02
<i>G. rubescens</i>	5,26	7,30	31,40	4,27	5,07	5,77	4,64	2,05	2,55	3,70	5,11
<i>G.aequilateralis</i>	1,13	4,38	2,91	4,70	1,84	2,40	3,61	6,56	2,13	5,56	3,83
<i>G. calida</i>	0,75	2,19	0,00	2,56	0,00	0,00	2,58	0,00	0,00	0,00	0,00
<i>N. pachyderma s</i>	0,00	0,00	0,00	0,00	0,00	0,00	0,00	0,00	0,00	0,00	0,00
<i>N. pachyderma d</i>	0,00	1,82	0,00	0,00	2,30	0,00	1,03	1,23	1,28	0,93	2,13
<i>N. dutertrei d</i>	0,00	0,00	0,00	0,00	0,00	0,00	0,00	0,00	0,00	0,00	0,00
<i>N. dutertrei s</i>	0,00	0,00	0,00	0,00	0,00	0,00	0,00	0,00	0,00	0,00	0,00
<i>T. quinueloba</i>	17,67	20,44	15,70	14,53	6,45	5,77	11,86	5,74	11,06	8,33	7,23
<i>G. glutinata</i>	0,38	0,00	3,49	1,28	1,84	4,81	3,61	0,82	2,55	1,85	1,28
<i>G. scitula</i>	0,00	0,00	0,00	0,43	0,00	0,00	0,52	0,00	0,00	0,00	0,00
<i>B. digitata</i>	0,00	0,00	0,00	0,00	0,00	0,00	0,00	0,00	0,43	0,00	0,85
<i>H. inflatus</i>	0,00	0,00	14,29	6,90	22,22	7,69	10,40	16,22	9,52	12,12	12,86
<i>L. retroversa</i>	0,00	0,00	0,00	0,00	0,00	0,00	0,00	0,00	0,00	0,00	0,00
<i>L. trochiformis</i>	0,00	0,00	23,81	58,62	33,33	76,92	32,00	26,58	38,10	42,42	35,71
<i>C. virgula</i>	0,00	0,00	14,29	3,45	0,00	0,00	12,00	9,01	13,33	7,58	4,29
<i>C. acicula</i>	0,00	0,00	4,76	0,00	0,00	0,00	9,60	2,25	2,86	7,58	2,86
<i>H. striata</i>	0,00	0,00	0,00	0,00	0,00	0,00	0,00	0,00	0,00	0,00	0,00
<i>S. subula</i>	0,00	0,00	9,52	0,00	0,00	0,00	0,00	0,00	0,00	0,00	0,00
<i>C. cuspidata</i>	0,00	0,00	2,38	0,00	11,11	0,00	0,00	0,90	0,95	0,00	1,43
<i>C. pyramidata</i>	0,00	0,00	7,14	10,34	0,00	0,00	3,20	5,86	7,62	10,61	11,43
<i>D. trispinosa</i>	0,00	0,00	0,00	0,00	0,00	0,00	0,00	0,00	0,00	0,00	0,00
<i>Cavalinia spp.</i>	0,00	0,00	4,76	6,90	0,00	7,69	12,00	12,61	5,71	4,55	10,00

Species/Samples	79	81	83	85	87	89	91	93	95	97	99
<i>O. universa</i>	0,46	0,44	0,00	1,80	0,79	0,45	0,00	0,86	0,00	0,43	1,16
<i>G. ruber alba</i>	35,78	36,89	35,98	33,53	36,36	43,05	41,47	33,48	36,86	17,09	38,61
<i>G. ruber rosea</i>	12,84	18,22	20,83	18,56	27,67	22,42	20,74	14,59	15,29	31,62	15,83
<i>G. sacculifer</i>	1,83	4,89	3,03	0,00	2,37	1,35	0,46	3,86	0,78	0,00	1,54
<i>G. inflata</i>	0,00	0,44	0,00	0,00	0,00	0,00	0,00	0,00	0,39	0,00	0,00
<i>G. bulloides</i>	20,18	21,33	21,21	17,37	16,60	16,14	15,21	17,60	18,04	10,68	10,04
<i>G. rubescens</i>	5,50	4,44	5,68	12,57	7,91	5,38	7,83	15,02	11,76	17,95	12,74
<i>G.aequilateralis</i>	4,13	2,67	4,92	2,40	1,58	4,93	3,69	2,58	3,53	2,14	3,47
<i>G. calida</i>	0,00	0,00	0,00	0,00	0,00	0,00	0,00	0,00	0,00	0,00	0,00
<i>N. pachyderma s</i>	0,00	0,00	0,00	0,00	0,00	0,00	0,00	0,00	0,00	0,00	0,00
<i>N. pachyderma d</i>	1,38	0,44	0,76	0,00	0,40	0,00	0,46	0,43	1,18	0,43	0,77
<i>N. dutertrei d</i>	0,00	0,00	0,00	0,60	0,00	0,00	0,00	0,00	0,00	0,00	0,00
<i>N. dutertrei s</i>	0,00	0,00	0,00	0,00	0,00	0,00	0,00	0,00	0,00	0,00	0,00
<i>T. quinueloba</i>	15,60	7,56	4,92	12,57	4,74	4,93	6,45	9,44	9,41	18,38	13,13
<i>G. glutinata</i>	2,29	2,22	1,52	0,60	0,79	1,35	3,23	2,15	2,75	1,28	1,54
<i>G. scitula</i>	0,00	0,00	0,00	0,00	0,00	0,00	0,46	0,00	0,00	0,00	0,39
<i>B. digitata</i>	0,00	0,44	0,76	0,00	0,79	0,00	0,00	0,00	0,00	0,00	0,77
<i>H. inflatus</i>	15,00	16,09	15,95	8,60	11,23	9,45	7,02	9,66	7,77	10,22	5,63
<i>L. retroversa</i>	0,00	0,00	0,00	0,00	0,00	0,00	0,00	0,00	0,00	0,00	0,00
<i>L. trochiformis</i>	32,50	34,10	20,86	17,20	18,72	41,73	29,82	35,17	24,27	25,27	0,70
<i>C. virgula</i>	10,50	8,43	6,75	29,03	9,63	6,30	10,53	6,90	20,39	7,53	36,27
<i>C. acicula</i>	5,50	2,30	9,20	11,83	8,02	2,36	4,39	8,97	4,85	15,05	11,97
<i>H. striata</i>	0,00	0,00	0,00	0,00	0,00	0,00	0,00	0,00	0,00	0,00	0,00
<i>S. subula</i>	0,00	0,00	0,00	0,00	0,00	0,00	0,00	0,00	0,00	0,00	0,00
<i>C. cuspidata</i>	0,50	0,00	0,61	1,08	1,07	2,36	0,00	0,69	0,00	0,00	0,70
<i>C. pyramidata</i>	4,50	3,07	7,36	5,38	5,88	4,72	7,89	6,90	6,80	2,15	4,58
<i>D. trispinosa</i>	0,00	0,00	0,00	0,00	0,00	0,00	0,00	0,00	0,00	0,00	0,00
<i>Cavalinia spp.</i>	8,50	9,20	14,11	7,53	12,83	8,66	12,28	12,41	8,74	12,90	14,08

Species/Samples	101	103	105	107	109	111	113	115	117	119	120,5
<i>O. universa</i>	2,13	2,67	1,05	1,12	2,76	2,18	3,79	4,07	4,10	3,01	1,78
<i>G. ruber alba</i>	52,48	59,16	49,12	27,72	35,43	28,00	36,36	17,78	13,93	9,40	5,33
<i>G. ruber rosea</i>	2,48	5,34	11,93	13,11	14,57	13,09	7,95	14,44	14,75	15,79	5,78
<i>G. sacculifer</i>	3,19	1,15	3,51	2,62	1,97	3,64	2,27	1,85	0,00	1,88	0,00
<i>G. inflata</i>	0,00	0,38	0,70	3,00	3,54	3,27	6,06	18,52	18,44	32,33	0,44
<i>G. bulloides</i>	4,96	9,54	8,07	11,24	14,17	8,36	11,36	8,89	13,11	7,52	15,11
<i>G. rubescens</i>	5,67	3,05	5,26	7,87	5,51	5,45	5,68	2,96	1,64	3,76	0,89
<i>G.aequilateralis</i>	5,67	5,73	2,11	7,49	1,57	2,18	3,41	2,96	2,46	3,01	0,89
<i>G. calida</i>	4,61	2,67	1,75	3,37	0,00	1,09	0,00	0,00	0,00	1,13	0,00
<i>N. pachyderma s</i>	0,00	0,00	0,00	0,00	0,00	0,00	0,00	0,00	0,41	0,00	0,00
<i>N. pachyderma d</i>	0,00	0,76	0,70	1,50	3,15	3,27	1,89	13,33	15,98	7,89	0,00
<i>N. dutertrei d</i>	0,00	0,00	0,35	0,37	0,39	0,73	0,00	0,37	0,00	1,13	0,00
<i>N. dutertrei s</i>	0,00	0,00	0,00	0,00	0,00	0,00	0,00	0,00	0,00	0,00	0,00
<i>T. quinueloba</i>	22,34	11,83	15,44	23,22	15,35	26,18	20,08	14,81	11,89	13,53	68,44
<i>G. glutinata</i>	0,35	0,38	1,75	0,75	1,18	1,09	0,38	0,00	1,23	0,75	0,89
<i>G. scitula</i>	0,71	0,00	0,00	0,00	0,39	1,45	0,00	0,00	0,00	0,00	0,00
<i>B. digitata</i>	0,00	0,00	0,00	0,00	0,00	0,36	0,00	0,00	0,41	0,00	0,44
<i>H. inflatus</i>	9,29	4,56	2,47	0,00	13,33	5,17	2,99	6,25	5,88	13,64	13,95
<i>L. retroversa</i>	0,00	0,00	0,00	0,00	0,00	0,00	0,00	0,00	0,00	0,00	0,00
<i>L. trochiformis</i>	0,37	0,28	0,00	0,00	0,00	0,00	0,00	0,00	0,00	0,00	0,00
<i>C. virgula</i>	33,09	39,03	37,04	0,00	37,78	15,52	49,25	62,50	52,94	22,73	46,51
<i>C. acicula</i>	9,67	13,39	4,94	0,00	0,00	0,00	0,00	0,00	0,00	4,55	0,00
<i>H. striata</i>	0,00	0,00	0,00	0,00	0,00	0,00	0,00	0,00	0,00	0,00	0,00
<i>S. subula</i>	0,00	0,00	0,00	0,00	0,00	0,00	0,00	0,00	0,00	0,00	0,00
<i>C. cuspidata</i>	0,74	1,71	2,47	0,00	0,00	5,17	2,99	0,00	0,00	0,00	0,00
<i>C. pyramidata</i>	6,32	4,56	7,41	0,00	0,00	3,45	2,99	0,00	0,00	4,55	0,00
<i>D. trispinosa</i>	0,00	0,00	0,00	0,00	0,00	0,00	0,00	0,00	0,00	0,00	2,33
<i>Cavalinia spp.</i>	23,79	23,65	24,69	0,00	17,78	15,52	17,91	6,25	5,88	13,64	20,93

Species/Samples	121,5	122,5	123,5	124,5	125,5	126,5	127,5	128,5	129,5	130,5	131,5
<i>O. universa</i>	8,58	17,91	13,33	7,09	4,71	6,02	4,55	2,80	3,04	1,13	4,76
<i>G. ruber alba</i>	8,58	11,57	12,59	8,58	4,31	4,14	14,46	16,78	7,60	7,89	5,13
<i>G. ruber rosea</i>	9,33	14,93	18,52	16,42	8,63	6,39	10,74	12,94	6,08	5,26	14,29
<i>G. sacculifer</i>	2,24	2,61	4,07	1,49	0,78	0,00	1,65	1,75	1,90	0,75	0,73
<i>G. inflata</i>	0,37	0,00	0,37	0,00	0,00	0,00	0,00	0,35	0,00	0,00	0,00
<i>G. bulloides</i>	48,13	35,82	38,89	37,69	40,39	37,22	42,56	26,22	12,17	16,92	11,72
<i>G. rubescens</i>	0,37	0,00	2,22	7,09	5,10	2,63	2,48	3,15	3,04	2,26	1,47
<i>G.aequilateralis</i>	3,36	7,09	3,70	3,73	1,96	3,76	2,89	3,50	3,04	1,88	2,93
<i>G. calida</i>	0,00	0,00	0,00	0,00	0,00	0,00	0,00	1,05	1,90	0,00	1,47
<i>N. pachyderma s</i>	0,00	0,00	0,00	0,00	0,00	0,00	0,00	0,00	0,00	0,00	0,00
<i>N. pachyderma d</i>	0,37	0,00	0,37	0,00	0,78	0,00	2,07	1,05	0,38	0,38	0,00
<i>N. dutertrei d</i>	0,00	0,37	0,00	0,00	0,00	0,00	1,24	0,00	0,00	0,00	0,37
<i>N. dutertrei s</i>	0,00	0,00	0,00	0,00	0,00	0,00	0,00	0,00	0,00	0,00	0,37
<i>T. quinueloba</i>	18,66	9,70	5,56	17,54	32,55	37,97	16,94	30,07	60,46	62,41	57,88
<i>G. glutinata</i>	0,00	0,00	0,37	0,00	0,78	0,75	0,41	1,05	1,52	0,75	0,00
<i>G. scitula</i>	0,00	0,00	0,00	0,00	0,00	0,00	0,00	0,00	0,38	0,00	0,00
<i>B. digitata</i>	0,00	0,00	0,00	0,00	0,00	1,13	0,00	0,35	0,38	0,38	0,37
<i>H. inflatus</i>	14,58	0,00	26,83	4,35	19,39	18,28	28,06	22,58	30,30	39,39	38,46
<i>L. retroversa</i>	0,00	0,00	0,00	0,00	0,00	0,00	0,00	0,00	0,00	0,00	0,00
<i>L. trochiformis</i>	0,00	0,00	0,00	0,00	0,00	0,00	0,00	0,00	0,00	0,00	0,00
<i>C. virgula</i>	42,71	0,00	17,07	58,70	38,78	44,09	23,02	41,94	51,52	15,15	9,89
<i>C. acicula</i>	1,04	0,00	0,00	0,00	0,00	0,00	0,00	0,00	0,00	0,00	0,00
<i>H. striata</i>	0,00	0,00	0,00	0,00	0,00	0,00	0,00	0,00	0,00	0,00	0,00
<i>S. subula</i>	0,00	0,00	0,00	0,00	0,00	0,00	0,00	0,00	0,00	0,00	0,00
<i>C. cuspidata</i>	0,00	0,00	0,00	0,00	0,00	0,00	0,00	0,00	0,00	0,00	0,00
<i>C. pyramidata</i>	0,00	0,00	1,22	0,00	0,00	0,00	0,00	0,00	0,00	0,00	0,00
<i>D. trispinosa</i>	3,13	0,00	0,00	4,35	5,10	3,23	6,47	3,23	0,00	0,00	0,00
<i>Cavalinia spp.</i>	16,67	0,00	7,32	8,70	4,08	11,83	8,63	9,68	3,03	3,03	2,20

Species/Samples	132,5	133,5	134,5	135,5	136,5	137,5	138,5	139,5	140,5	141,5	142,5
<i>O. universa</i>	8,90	7,50	2,78	2,92	3,65	7,38	6,92	6,99	12,21	22,18	13,31
<i>G. ruber alba</i>	8,19	3,57	3,97	4,58	1,09	3,32	5,00	5,51	7,25	11,28	10,08
<i>G. ruber rosea</i>	14,59	12,86	10,32	8,75	8,76	10,33	9,62	4,78	10,69	13,62	13,71
<i>G. sacculifer</i>	5,34	6,07	1,59	0,83	0,73	1,11	0,38	0,00	0,76	0,39	0,00
<i>G. inflata</i>	0,00	0,00	0,00	0,42	0,00	0,37	0,00	0,37	0,38	0,00	0,00
<i>G. bulloides</i>	16,73	10,71	10,71	9,58	10,22	9,59	11,15	13,24	12,60	10,51	12,10
<i>G. rubescens</i>	1,78	0,71	2,38	0,42	3,65	1,85	3,85	5,15	5,34	5,84	7,66
<i>G.aequilateralis</i>	7,12	4,29	0,79	3,75	6,20	6,27	3,46	2,21	3,05	5,06	3,63
<i>G. calida</i>	1,78	2,86	0,00	0,00	0,73	0,00	0,00	0,00	0,00	0,00	0,00
<i>N. pachyderma s</i>	0,00	0,00	0,00	0,00	0,00	0,00	0,00	0,00	0,00	0,00	0,00
<i>N. pachyderma d</i>	0,00	0,00	0,00	0,42	0,36	0,74	0,38	0,37	0,00	0,00	0,00
<i>N. dutertrei d</i>	1,07	0,00	0,40	0,00	0,36	0,00	0,00	0,00	0,38	0,78	0,81
<i>N. dutertrei s</i>	0,36	0,00	0,00	0,00	0,00	0,00	0,00	0,37	0,00	0,78	0,00
<i>T. quinueloba</i>	35,59	53,93	66,67	67,08	63,87	58,30	59,23	61,03	47,33	29,57	37,50
<i>G. glutinata</i>	0,36	0,00	0,40	0,83	0,36	0,37	0,00	0,00	0,00	0,00	0,81
<i>G. scitula</i>	0,00	0,00	0,00	0,00	0,00	0,00	0,00	0,00	0,00	0,00	0,00
<i>B. digitata</i>	0,00	0,36	0,00	0,42	0,73	0,37	0,00	0,00	0,00	0,00	0,40
<i>H. inflatus</i>	43,62	10,84	8,11	4,11	0,00	4,76	4,76	27,94	0,00	0,00	0,00
<i>L. retroversa</i>	0,00	0,00	0,00	0,00	0,00	0,00	0,00	0,00	0,00	0,00	0,00
<i>L. trochiformis</i>	0,00	0,00	0,00	0,00	0,00	0,00	0,00	0,00	0,00	0,00	0,00
<i>C. virgula</i>	18,09	31,33	32,43	50,68	50,94	31,75	9,52	47,06	35,71	0,00	0,00
<i>C. acicula</i>	0,00	0,00	0,00	0,00	0,00	1,59	0,00	0,00	14,29	0,00	0,00
<i>H. striata</i>	0,00	0,00	0,00	0,00	0,00	0,00	0,00	0,00	0,00	0,00	0,00
<i>S. subula</i>	0,00	0,00	0,00	0,00	0,00	0,00	0,00	0,00	0,00	0,00	0,00
<i>C. cuspidata</i>	0,00	0,00	0,00	0,00	0,00	0,00	0,00	0,00	0,00	0,00	0,00
<i>C. pyramidata</i>	0,00	0,00	0,00	2,74	0,00	0,00	0,00	5,88	0,00	0,00	0,00
<i>D. trispinosa</i>	0,00	0,00	0,00	1,37	1,89	1,59	0,00	0,00	7,14	0,00	0,00
<i>Cavalinia spp.</i>	4,26	12,05	2,70	5,48	15,09	19,05	9,52	4,41	7,14	0,00	0,00

Species/Samples	143,5	144,5	145,5	146,5	147,5	148,5	149,5	150,5	151,5	152,5	153,5
<i>O. universa</i>	9,42	4,83	5,88	19,91	13,70	6,23	3,68	9,58	25,97	27,45	7,66
<i>G. ruber alba</i>	13,41	7,43	11,03	8,33	11,85	12,46	7,72	4,98	9,52	13,33	6,93
<i>G. ruber rosea</i>	8,33	10,78	14,34	20,37	24,81	25,61	13,24	7,28	12,99	12,94	6,57
<i>G. sacculifer</i>	0,00	0,00	0,00	0,00	0,00	0,00	0,00	0,00	0,00	0,00	0,00
<i>G. inflata</i>	0,36	0,00	0,37	0,00	0,00	0,00	0,00	0,00	0,00	0,00	0,00
<i>G. bulloides</i>	6,88	9,67	22,06	23,61	24,81	18,34	22,06	21,84	14,72	16,47	16,79
<i>G. rubescens</i>	2,54	13,75	7,35	10,65	8,52	22,84	20,59	15,71	9,09	7,45	7,66
<i>G.aequilateralis</i>	6,16	0,74	3,68	3,70	5,19	3,46	2,21	3,07	5,19	4,31	0,00
<i>G. calida</i>	0,00	0,00	0,00	0,00	0,00	0,00	0,00	0,00	0,00	0,00	0,00
<i>N. pachyderma s</i>	0,00	0,00	0,00	0,00	0,00	0,00	0,00	0,00	0,00	0,00	0,00
<i>N. pachyderma d</i>	0,00	0,74	0,00	0,00	0,00	0,00	0,37	0,00	0,00	0,00	0,00
<i>N. dutertrei d</i>	0,36	0,00	0,00	0,00	0,00	1,38	1,10	0,00	0,00	0,39	0,00
<i>N. dutertrei s</i>	0,00	0,00	0,00	0,00	0,00	0,00	0,00	0,00	0,00	0,00	0,00
<i>T. quinueloba</i>	52,54	52,04	32,35	12,50	10,74	7,61	28,31	37,55	22,08	16,47	54,38
<i>G. glutinata</i>	0,00	0,00	0,37	0,46	0,00	0,35	0,37	0,00	0,00	0,00	0,00
<i>G. scitula</i>	0,00	0,00	0,00	0	0,00	0,00	0,00	0,00	0,00	0,00	0,00
<i>B. digitata</i>	0,00	0,00	2,57	0,46	0,37	1,73	0,37	0,00	0,43	1,18	0,00
<i>H. inflatus</i>	0,00	50,00	47,73	52,43	61,31	63,38	42,86	63,86	100,00	61,43	71,43
<i>L. retroversa</i>	0,00	0,00	0,00	0,00	0,00	0,00	0,00	0,00	0,00	0,00	0,00
<i>L. trochiformis</i>	0,00	0,00	0,00	0,00	0,00	0,00	0,00	0,00	0,00	0,00	0,00
<i>C. virgula</i>	0,00	0,00	22,73	21,62	11,68	9,15	14,29	25,30	0,00	10,00	21,43
<i>C. acicula</i>	0,00	0,00	0,00	1,08	0,00	0,00	0,00	0,00	0,00	0,00	0,00
<i>H. striata</i>	0,00	0,00	0,00	0,00	0,00	0,00	0,00	0,00	0,00	0,00	0,00
<i>S. subula</i>	0,00	0,00	0,00	0,00	0,00	0,00	0,00	0,00	0,00	0,00	0,00
<i>C. cuspidata</i>	0,00	0,00	0,00	0,00	0,00	0,00	0,00	0,00	0,00	0,00	0,00
<i>C. pyramidata</i>	0,00	0,00	4,55	5,95	5,84	4,23	0,00	1,20	0,00	2,14	2,38
<i>D. trispinosa</i>	0,00	0,00	0,00	2,70	0,73	0,70	0,00	0,00	0,00	4,29	0,00
<i>Cavalinia spp.</i>	0,00	3,85	2,27	0,54	5,11	4,23	0,00	0,00	0,00	1,43	0,00

Species/Samples	154,5	155,5	156,5	158,5	159,5	160,5	161,5	162,5	163,5	164,5	165,5
<i>O. universa</i>	12,63	13,43	9,85	11,84	7,87	1,37	3,00	2,48	2,18	0,37	10,86
<i>G. ruber alba</i>	8,07	1,41	1,09	9,21	6,37	7,17	9,74	11,16	9,61	11,48	7,24
<i>G. ruber rosea</i>	13,33	4,59	1,82	5,26	11,99	8,53	14,98	4,55	0,44	1,48	0,45
<i>G. sacculifer</i>	0,00	0,00	0,00	0,00	0,00	0,00	0,00	0,00	0,00	0,00	1,81
<i>G. inflata</i>	0,00	0,00	0,00	0,00	0,00	0,00	0,00	0,00	0,00	0,00	0,00
<i>G. bulloides</i>	18,60	16,25	17,52	20,18	11,61	26,62	20,97	20,25	17,03	31,85	12,67
<i>G. rubescens</i>	4,91	1,06	0,36	0,00	2,25	2,05	0,75	1,65	0,00	3,70	0,45
<i>G.aequilateralis</i>	1,40	1,06	1,46	4,39	3,00	2,73	4,49	9,50	3,06	1,85	3,62
<i>G. calida</i>	0,00	0,00	0,00	0,88	1,12	0,68	1,12	0,00	0,00	0,00	0,00
<i>N. pachyderma s</i>	0,00	0,00	0,00	0,00	0,00	0,00	0,00	0,00	0,00	0,00	0,00
<i>N. pachyderma d</i>	0,00	0,00	0,00	0,44	0,00	0,00	0,00	0,00	0,00	0,00	0,00
<i>N. dutertrei d</i>	0,00	0,00	0,00	0,00	1,87	0,00	0,37	0,00	0,44	3,33	0,90
<i>N. dutertrei s</i>	0,00	0,00	0,00	0,00	0,00	0,00	0,00	0,00	0,44	0,00	0,00
<i>T. quinueloba</i>	40,35	61,48	67,15	48,25	53,93	50,17	44,57	48,76	65,07	44,07	61,09
<i>G. glutinata</i>	0,35	0,71	0,73	0,44	1,12	1,37	1,12	1,65	1,75	1,85	0,90
<i>G. scitula</i>	0,00	0,00	0,00	0,00	0,00	0,00	0,00	0,00	0,00	0,00	0,00
<i>B. digitata</i>	0,35	0,00	0,00	0,00	0,00	0,00	0,00	0,00	0,00	0,00	0,00
<i>H. inflatus</i>	55,56	33,33	79,17	57,41	66,92	31,25	30,43	20,83	46,81	57,14	15,07
<i>L. retroversa</i>	0,00	0,00	0,00	0,00	0,00	0,00	0,00	0,00	0,00	0,00	0,00
<i>L. trochiformis</i>	0,00	0,00	0,00	0,00	0,00	0,00	0,00	0,00	0,00	0,00	0,00
<i>C. virgula</i>	20,47	66,67	12,50	25,00	6,77	0,00	21,74	4,17	7,09	14,29	24,66
<i>C. acicula</i>	0,00	0,00	8,33	4,63	3,01	12,50	4,35	12,50	15,60	9,52	32,88
<i>H. striata</i>	0,00	0,00	0,00	0,00	0,00	0,00	0,00	0,00	0,00	0,00	0,00
<i>S. subula</i>	0,00	0,00	0,00	0,00	0,00	0,00	0,00	0,00	0,00	0,00	0,00
<i>C. cuspidata</i>	0,00	0,00	0,00	0,00	0,00	0,00	0,00	0,00	0,00	0,00	0,00
<i>C. pyramidata</i>	4,68	0,00	0,00	1,85	3,76	0,00	0,00	0,00	3,55	4,76	2,74
<i>D. trispinosa</i>	0,00	0,00	0,00	4,63	10,53	6,25	0,00	8,33	6,38	4,76	1,37
<i>Cavalinia spp.</i>	1,75	0,00	0,00	0,00	2,26	12,50	8,70	8,33	1,42	0,00	5,48

Species/Samples	166,5	168	170	172	173,5
<i>O. universa</i>	11,19	10,15	4,96	2,01	0,00
<i>G. ruber alba</i>	35,82	30,08	35,88	27,71	18,88
<i>G. ruber rosea</i>	1,49	3,38	3,44	2,81	3,21
<i>G. sacculifer</i>	1,12	0,75	1,53	0,40	0,00
<i>G. inflata</i>	0,00	0,00	0,38	0,00	0,00
<i>G. bulloides</i>	25,75	28,20	23,28	16,06	29,72
<i>G. rubescens</i>	1,87	0,38	3,82	4,42	13,65
<i>G.aequilateralis</i>	2,99	2,26	0,76	0,40	0,00
<i>G. calida</i>	0,00	1,50	0,00	0,00	0,00
<i>N. pachyderma s</i>	0,00	0,00	0,00	0,00	0,00
<i>N. pachyderma d</i>	0,00	0,00	0,00	0,00	0,00
<i>N. dutertrei d</i>	0,00	1,13	0,38	0,40	0,00
<i>N. dutertrei s</i>	0,00	0,38	0,76	1,20	0,00
<i>T. quinueloba</i>	17,16	18,42	14,89	34,14	22,09
<i>G. glutinata</i>	2,61	4,89	9,92	10,44	12,45
<i>G. scitula</i>	0,00	0,00	0,00	0,00	0,00
<i>B. digitata</i>	0,00	0,00	0,00	0,00	0,00
<i>H. inflatus</i>	31,58	5,92	4,00	9,46	0,00
<i>L. retroversa</i>	0,00	0,00	0,00	0,00	0,00
<i>L. trochiformis</i>	0,88	0,00	0,00	0,00	0,00
<i>C. virgula</i>	5,26	0,00	3,00	1,35	0,86
<i>C. acicula</i>	19,30	48,68	38,00	28,38	26,72
<i>H. striata</i>	0,00	0,00	0,00	0,00	0,00
<i>S. subula</i>	0,00	0,00	0,00	0,00	0,00
<i>C. cuspidata</i>	0,00	0,00	0,00	0,00	0,00
<i>C. pyramidata</i>	12,28	19,08	15,00	12,16	7,76
<i>D. trispinosa</i>	21,93	21,05	38,00	40,54	58,62
<i>Cavalinia spp.</i>	0,00	0,00	0,00	0,00	0,00

AEX 23: Planktonic foraminifera and pteropod abundances (%)											
Species/Samples	2,5	12,5	22,5	32,5	42,5	52,5	62,5	72,5	82,5	92,5	102,5
<i>O. universa</i>	0,00	0,00	0,44	0,00	0,80	0,00	0,47	0,00	0,90	0,39	0,86
<i>G. ruber alba</i>	29,95	23,47	16,89	31,22	32,93	29,00	20,93	25,89	36,94	33,73	30,47
<i>G. ruber rosea</i>	3,38	10,80	8,44	5,06	6,02	5,19	5,58	4,46	2,70	4,71	9,44
<i>G. sacculifer</i>	0,00	0,00	1,33	0,84	0,80	0,87	0,00	0,00	1,80	0,39	0,86
<i>B. digitata</i>	0,00	0,00	0,00	0,00	0,00	0,00	0,47	0,00	0,00	0,00	0,00
<i>G. inflata</i>	0,48	0,47	0,00	0,00	0,00	0,00	0,00	0,00	0,00	0,00	0,00
<i>G. bulloides</i>	13,04	16,43	16,44	14,35	16,47	16,88	13,02	13,84	12,61	20,39	18,45
<i>G. rubescens</i>	3,86	4,23	11,11	7,17	4,02	9,52	6,51	9,82	7,21	10,20	12,02
<i>G. aequilateralis</i>	0,97	2,35	1,33	0,84	1,61	2,60	0,00	2,23	0,90	1,96	2,15
<i>G. calida</i>	0,00	0,00	0,00	0,00	0,00	0,00	0,00	0,89		0,00	0,00
<i>N. pachyderma s</i>	0,97	0,47	0,89	0,42	0,00	0,87	0,93	0,45	0,90	0,00	0,00
<i>N. pachyderma d</i>	10,14	2,82	1,78	3,80	1,61	2,16	5,12	2,68	4,05	0,39	1,72
<i>N. dutertrei d</i>	2,90	0,00	0,89	0,00	0,00	0,00	0,00	3,57	0,00	0,78	0,00
<i>N. dutertrei s</i>	0,48	0,00	1,33	0,00	0,00	0,00	0,00	0,00	0,00	0,00	0,00
<i>T. quinueloba</i>	27,05	35,21	32,44	32,49	30,12	31,60	46,05	34,82	28,38	22,75	22,32
<i>G. glutinata</i>	6,28	3,29	6,22	3,80	5,22	0,87	0,93	1,34	2,70	1,57	1,29
<i>G. scitula</i>	0,48	0,47	0,44	0,00	0,00	0,43	0,00	0,89	0,90	0,00	0,00
<i>H. inflata</i>	6,61	8,70	5,09	5,95	9,26	4,26	11,18	7,58	8,03	6,62	17,97
<i>L. retroversa</i>	0,00	0,00	0,00	0,74	0,00	0,00	0,00	2,11	0,00	0,00	0,00
<i>L. trochiformis</i>	9,25	7,73	9,26	13,38	38,89	11,70	20,59	15,16	14,72	10,26	18,75
<i>C. virgula</i>	16,30	10,63	12,50	21,19	14,81	20,21	7,06	3,58	14,05	9,60	12,50
<i>C. acicula</i>	24,67	15,94	18,52	10,04	5,56	5,32	7,65	10,32	6,69	7,28	3,91
<i>H. striata</i>	0,88	1,45	1,39	1,12	0,00	0,00	0,59	0,21	0,00	0,00	0,00
<i>S. subula</i>	3,52	10,14	6,48	8,55	1,85	10,64	11,76	12,84	26,76	45,36	16,41
<i>C. cuspidata</i>	0,00	0,00	0,46	0,37	0,00	1,06	0,00	0,42	0,67	0,66	0,00
<i>C. pyramidata</i>	11,01	14,49	12,50	10,78	9,26	14,89	12,94	14,95	14,38	6,62	10,16
<i>D. trispinosa</i>	0,00	0,00	0,00	0,00	0,00	0,00	0,00	0,42	0,00	0,33	0,00
<i>Cavolinia spp.</i>	9,25	16,43	20,83	15,24	5,56	18,09	13,53	13,47	9,03	5,63	7,81

Species/Samples	112,5	122,5	132,5	142,5	152,5	162,5	172,5	182,5	192,5	202,5	212,5
<i>O. universa</i>	0,40	0,49	0,00	0,00	0,00	0,45	0,86	0,00	0,82	0,39	1,57
<i>G. ruber alba</i>	35,48	41,87	37,84	26,67	20,43	24,32	31,76	20,16	12,65	26,85	40,16
<i>G. ruber rosea</i>	17,34	5,42	5,41	18,10	38,72	27,48	4,29	16,05	22,04	22,96	4,33
<i>G. sacculifer</i>	0,00	0,49	1,80	0,48	2,13	0,45	0,00	1,23	0,00	0,39	1,18
<i>B. digitata</i>	0,00	0,00	0,00	0,95	0,00	0,00	0,00	0,00	0,00	0,00	0,00
<i>G. inflata</i>	0,40	0,00	0,00	0,00	0,43	1,35	0,00	0,00	0,00	0,39	0,00
<i>G. bulloides</i>	16,94	15,76	8,56	13,33	16,17	9,01	16,74	7,82	6,94	7,00	9,06
<i>G. rubescens</i>	8,06	7,88	8,56	14,29	7,23	13,96	11,59	12,76	18,37	9,73	7,09
<i>G. aequilateralis</i>	1,21	2,46	0,90	3,81	2,55	1,80	2,15	2,47	2,04	2,72	1,97
<i>G. calida</i>	0,00	0,00	0,00	0,00	0,00	0,00	0,00	0,00	0,00	0,00	0,00
<i>N. pachyderma s</i>	0,40	0,00	0,00	0,48	0,00	0,00	0,43	0,00	0,41	0,00	0,00
<i>N. pachyderma d</i>	2,02	1,97	1,35	0,95	2,13	0,90	1,72	1,65	1,22	3,50	0,39
<i>N. dutertrei d</i>	0,00	0,00	0,45	0,95	0,00	0,00	0,00	0,00	0,00	0,39	0,00
<i>N. dutertrei s</i>	0,00	0,00	0,00	0,00	0,00	0,00	0,00	0,00	0,00	0,00	0,00
<i>T. quinueloba</i>	16,13	17,24	30,18	17,62	8,51	16,67	23,18	35,39	32,65	22,57	30,31
<i>G. glutinata</i>	0,81	2,96	1,35	1,43	1,28	2,70	4,72	1,65	1,22	2,72	2,76
<i>G. scitula</i>	0,00	0,49	0,90	0,00	0,43	0,00	0,00	0,00	0,00	0,39	0,00
<i>H. inflata</i>	12,92	11,34	13,72	13,07	8,06	6,38	8,81	5,95	4,59	7,24	7,45
<i>L. retroversa</i>	0,37	0,52	0,72	0,33	0,00	0,00	0,00	0,00	0,00	0,00	0,00
<i>L. trochiformis</i>	30,26	38,40	32,85	15,69	28,44	38,84	33,57	29,76	20,14	0,00	0,62
<i>C. virgula</i>	23,25	15,98	9,03	14,38	16,59	9,86	9,76	13,69	19,79	33,79	43,48
<i>C. acicula</i>	4,06	4,38	6,50	8,17	7,58	13,33	10,48	15,77	10,60	21,03	9,94
<i>H. striata</i>	0,00	0,00	0,00	0,00	0,00	0,00	0,00	0,00	0,00	0,00	0,00
<i>S. subula</i>	0,37	0,00	0,00	0,00	0,00	0,00	0,00	0,00	0,00	0,00	0,00
<i>C. cuspidata</i>	0,37	0,00	0,36	0,65	1,42	0,00	0,48	0,60	0,35	0,34	0,00
<i>C. pyramidata</i>	7,75	4,64	9,03	8,17	4,74	4,93	3,33	2,68	3,89	1,72	1,86
<i>D. trispinosa</i>	0,00	0,26	0,36	0,33	0,00	0,00	0,00	0,30	0,00	0,00	0,00
<i>Cavolinia spp.</i>	8,86	8,76	13,00	21,90	14,22	10,14	13,10	13,10	19,79	13,10	13,04

Species/Samples	222,5	232,5	242,5	252,5	262,5	272,5	282,5	288,25	289,75	291	293
<i>O. universa</i>	1,18	3,38	1,21	1,16	1,49	1,49	2,28	3,35	1,42	1,21	0,42
<i>G. ruber alba</i>	37,40	16,92	19,43	10,85	24,54	17,91	18,63	13,88	12,06	7,27	5,04
<i>G. ruber rosea</i>	1,57	16,54	7,69	4,26	7,81	7,46	17,87	14,35	10,64	12,73	3,36
<i>G. sacculifer</i>	1,18	0,75	0,40	0,39	0,37	0,00	0,00	0,96	0,00	0,00	0,00
<i>B. digitata</i>	0,00	0,38	0,00	0,00	0,00	0,37	0,00	0,00	0,00	0,00	0,00
<i>G. inflata</i>	0,79	0,00	1,62	3,49	4,09	23,51	0,76	0,48	8,51	0,61	0,00
<i>G. bulloides</i>	6,69	15,04	6,48	9,69	8,18	11,94	4,56	4,31	14,18	22,42	23,53
<i>G. rubescens</i>	5,12	6,02	6,48	4,65	4,09	1,87	2,28	2,39	3,55	6,67	2,94
<i>G. aequilateralis</i>	2,36	1,13	3,24	1,94	1,49	1,87	4,56	4,31	0,71	1,21	0,00
<i>G. calida</i>	0,00	0,00	0,00	0,00	0,00	0,00	0,00	0,00	0,00	0,00	0,00
<i>N. pachyderma s</i>	0,00	0,00	0,00	0,78	0,00	0,37	0,00	0,00	0,00	0,00	0,00
<i>N. pachyderma d</i>	0,39	2,26	0,81	1,55	0,37	5,22	1,52	1,91	3,55	3,03	0,00
<i>N. dutertrei d</i>	0,39	0,00	0,00	0,39	0,00	0,00	0,00	0,00	0,00	0,00	0,00
<i>N. dutertrei s</i>	0,00	0,00	0,00	0,00	0,00	0,00	0,00	0,00	0,00	0,00	0,00
<i>T. quinueloba</i>	39,37	36,09	48,18	59,30	47,21	27,24	46,77	52,63	43,26	42,42	63,87
<i>G. glutinata</i>	1,18	0,75	3,24	1,55	0,00	0,37	0,76	1,44	0,00	2,42	0,84
<i>G. scitula</i>	0,79	0,75	0,40	0,00	0,00	0,00	0,00	0,00	2,13	0,00	0,00
<i>H. inflata</i>	8,66	7,53	2,42	7,69	7,27	3,03	0,00	0,00	0,00	0,00	14,29
<i>L. retroversa</i>	0,00	0,00	0,00	0,00	0,00	0,00	0,00	0,00	0,00	0,00	0,00
<i>L. trochiformis</i>	0,00	0,00	0,00	0,00	0,00	0,00	0,00	0,00	0,00	0,00	0,00
<i>C. virgula</i>	31,77	48,12	58,18	49,77	41,82	66,67	53,33	100,00	100,00	0,00	0,00
<i>C. acicula</i>	13,36	0,42	1,21	0,00	0,00	0,00	6,67	0,00	0,00	0,00	0,00
<i>H. striata</i>	0,00	0,00	0,00	0,00	0,00	0,00	0,00	0,00	0,00	0,00	0,00
<i>S. subula</i>	0,00	0,00	0,00	0,00	0,00	0,00	0,00	0,00	0,00	0,00	0,00
<i>C. cuspidata</i>	0,72	0,84	1,21	0,45	0,00	0,00	0,00	0,00	0,00	0,00	0,00
<i>C. pyramidata</i>	4,69	6,69	3,64	1,81	0,00	0,00	0,00	0,00	0,00	0,00	0,00
<i>D. trispinosa</i>	0,36	0,00	1,21	0,90	0,00	0,00	6,67	0,00	0,00	0,00	4,76
<i>Cavolinia spp.</i>	27,44	9,21	22,42	16,29	7,27	6,06	0,00	0,00	0,00	0,00	0,00

Species/Samples	295	297,5	299,5	300,75	302,25	304,75	307,75	310	312	314	316	318,5	320
<i>O. universa</i>	0,41	2,30	7,46	11,03	9,16	3,85	1,04	7,72	6,31	4,38	7,77	5,34	10,76
<i>G. ruber alba</i>	2,45	7,66	6,44	1,78	4,38	7,69	9,34	4,88	8,64	0,73	6,36	6,41	0,87
<i>G. ruber rosea</i>	6,53	5,36	9,49	8,19	6,77	4,55	11,42	10,98	17,28	12,77	15,90	14,95	12,79
<i>G. sacculifer</i>	0,41	0,77	4,41	5,34	3,59	1,05	1,73	0,41	2,99	9,12	2,83	1,78	2,62
<i>B. digitata</i>	0,00	0,00	0,00	0,00	0,40	0,00	0,35	0,81	0,00	0,00	0,00	1,07	0,58
<i>G. inflata</i>	0,00	0,38	0,00	0,00	0,00	0,00	0,35	0,41	0,00	0,00	0,00	0,00	0,00
<i>G. bulloides</i>	29,39	44,06	37,29	45,55	42,63	41,26	17,30	4,88	10,63	9,12	16,61	17,08	7,85
<i>G. rubescens</i>	0,82	1,15	1,02	1,42	0,40	0,70	0,69	0,81	1,00	0,36	1,06	0,00	0,00
<i>G.aequilateralis</i>	0,00	1,15	3,39	3,20	1,59	0,35	2,42	3,25	2,33	2,19	2,12	5,34	4,94
<i>G. calida</i>	0,00	0,00	0,00	0,00	0,00	0,00	0,00	0,00	0,00	0,00	0,00	0,00	0,00
<i>N. pachyderma s</i>	0,00	0,00	0,00	0,00	0,00	0,00	0,00	0,00	0,00	0,00	0,00	0,00	0,00
<i>N. pachyderma d</i>	2,45	1,15	0,34	0,00	0,40	0,70	0,00	0,00	0,33	0,00	0,00	0,36	0,00
<i>N. dutertrei d</i>	0,00	0,00	0,34	0,00	0,00	0,00	0,00	0,00	0,00	0,00	0,00	0,00	0,00
<i>N. dutertrei s</i>	0,00	0,00	0,00	0,00	0,00	0,00	0,00	0,00	0,00	0,00	0,00	0,00	0,00
<i>T. quinueloba</i>	57,55	35,63	29,83	23,49	30,68	38,81	53,63	64,23	50,17	60,95	47,00	47,69	59,59
<i>G. glutinata</i>	0,00	0,00	0,00	0,00	0,00	1,05	1,38	0,81	0,33	0,36	0,35	0,00	0,00
<i>G. scitula</i>	0,00	0,38	0,00	0,00	0,00	0,00	0,00	0,00	0,00	0,00	0,00	0,00	0,00
<i>H. inflata</i>	19,05	24,59	14,71	10,20	11,63	24,21	37,17	46,51	26,98	6,72	2,33	0,00	0,00
<i>L. retroversa</i>	0,00	0,00	0,00	0,00	0,00	0,00	0,00	0,00	0,00	0,00	0,00	0,00	0,00
<i>L. trochiformis</i>	4,76	0,00	0,98	0,00	0,00	0,00	0,00	0,00	4,76	6,72	2,33	0,00	0,00
<i>C. virgula</i>	19,05	9,02	8,82	10,20	11,63	13,68	16,81	15,12	15,87	46,22	25,58	29,03	47,44
<i>C. acicula</i>	0,00	1,64	0,00	0,00	0,00	0,00	0,00	0,00	0,00	0,00	0,00	0,00	0,00
<i>H. striata</i>	0,00	0,00	0,00	0,00	0,00	0,00	0,00	0,00	0,00	0,00	0,00	0,00	0,00
<i>S. subula</i>	0,00	0,00	0,00	0,00	0,00	0,00	0,00	0,00	0,00	0,00	0,00	0,00	0,00
<i>C. cuspidata</i>	0,00	0,00	0,00	0,00	0,00	0,00	0,00	0,00	0,00	0,00	0,00	0,00	0,00
<i>C. pyramidata</i>	0,00	0,00	0,00	0,00	0,00	0,00	0,00	0,00	0,00	0,00	0,00	0,00	0,00
<i>D. trispinosa</i>	14,29	6,56	5,88	0,00	2,33	6,32	4,42	2,33	0,00	0,00	0,00	0,00	0,00
<i>Cavolinia spp.</i>	0,00	5,74	3,92	6,12	9,30	3,16	4,42	5,81	11,11	2,52	18,60	19,35	24,36

KIM-2A: Planktonic foraminifera and pteropod abundances (%)											
Species/Samples	6	14,5	28	34	41,5	50,25	61	61,5	62,5	63,5	64,5
<i>O. universa</i>	2,58	1,79	2,59	7,39	5,49	14,07	18,04	10,53	11,37	7,32	11,79
<i>G. ruber alba</i>	57,94	44,84	21,76	35,02	40,29	12,17	25,77	20,00	18,96	21,95	26,67
<i>G. ruber rosea</i>	3,00	8,97	7,25	6,23	14,65	14,45	9,28	10,53	4,74	9,76	9,74
<i>G. sacculifer</i>	10,30	8,07	0,00	0,00	14,65	9,51	7,73	6,32	7,11	4,39	4,62
<i>B. digitata</i>	0,00	0,00	0,00	1,56	0,00	1,14	0,00	1,05	0,47	2,44	0,00
<i>G. inflata</i>	4,72	4,48	31,09	17,51	1,83	0,38	2,06	3,16	5,69	8,78	1,54
<i>G. bulloides</i>	14,16	17,94	15,03	12,84	10,99	20,91	19,59	20,00	18,96	21,95	19,49
<i>G. rubescens</i>	0,00	4,48	1,55	0,00	0,00	1,52	7,73	8,42	4,74	3,90	6,15
<i>G. aequilateralis</i>	4,72	7,17	5,70	3,11	5,49	15,21	7,73	10,53	8,53	7,80	9,23
<i>G. calida</i>	0,00	1,35	4,66	1,56	1,47	7,22	2,06	2,63	3,32	3,41	4,10
<i>N. pachyderma</i> d	0,86	0,90	6,22	7,00	0,00	0,00	0,00	0,00	7,11	5,85	4,10
<i>N. dutertrei</i> d	0,00	0,00	0,52	0,00	0,00	0,00	0,00	2,63	0,00	0,00	0,00
<i>N. dutertrei</i> s	0,00	0,00	0,00	0,00	0,00	0,00	0,00	0,00	0,00	0,00	0,00
<i>T. quinueloba</i>	0,43	0,00	0,52	0,00	0,37	1,90	0,00	1,05	4,27	2,44	2,56
<i>G. truncatulinoides</i>	0,00	0,00	0,00	7,00	0,00	0,00	0,00	0,00	0,00	0,00	0,00
<i>G. glutinata</i>	0,00	0,00	2,59	0,00	2,93	1,52	0,00	2,63	4,74	0,00	0,00
<i>H. inflata</i>	46,38	57,14	19,35	16,67	100,00	14,81	21,00	24,59	36,99	32,98	23,19
<i>L. bulimoides</i>	0,00	0,00	0,00	0,00	0,00	0,00	1,83	1,64	0,00	2,13	10,14
<i>L. retroversa</i>	0,00	0,00	0,00	0,00	0,00	0,00	0,00	0,00	0,00	0,00	0,00
<i>L. trochiformis</i>	5,80	0,00	6,45	0,00	0,00	0,00	0,00	0,00	0,00	0,00	0,00
<i>C. virgula</i>	2,90	0,00	25,81	0,00	0,00	40,74	15,07	0,00	17,81	0,00	20,29
<i>C. acicula</i>	2,90	0,00	3,23	0,00	0,00	0,00	0,46	0,00	0,00	0,00	0,00
<i>Creseis</i> sp.	0,00	0,00	0,00	0,00	0,00	0,00	29,68	36,07	5,48	20,21	0,00
<i>H. striata</i>	1,45	0,00	0,00	0,00	0,00	0,00	0,00	0,00	1,37	0,00	0,00
<i>S. subula</i>	15,22	0,00	0,00	0,00	0,00	0,00	0,00	0,00	0,00	0,00	0,00
<i>C. pyramidata</i>	0,00	0,00	0,00	0,00	0,00	0,00	5,48	1,64	2,74	4,26	5,80
<i>D. trispinosa</i>	0,00	0,00	0,00	8,33	0,00	0,00	0,00	0,00	0,00	0,00	1,45
<i>Cavolinia</i> spp.	1,45	0,00	35,48	58,33	0,00	37,04	8,22	18,03	24,66	10,64	13,04

Species/Samples	65,5	66,5	67,5	68,5	69,5	70,5	71,5	72,5	73,5	74,5	75,5
<i>O. universa</i>	15,77	20,10	19,65	22,62	20,93	16,81	28,17	30,21	23,27	27,18	42,04
<i>G. ruber alba</i>	27,48	29,15	30,57	36,20	25,58	41,18	17,46	19,57	17,14	27,67	23,67
<i>G. ruber rosea</i>	18,02	9,05	11,35	6,33	18,60	12,18	28,97	26,38	30,61	16,99	15,51
<i>G. sacculifer</i>	4,50	4,02	0,00	0,00	2,79	2,10	1,19	0,00	0,82	0,49	0,00
<i>B. digitata</i>	0,00	0,00	0,44	0,00	0,00	1,26	1,59	1,70	2,04	1,46	2,04
<i>G. inflata</i>	2,25	0,50	1,75	2,26	0,00	0,00	0,00	0,00	0,00	0,49	0,00
<i>G. bulloides</i>	13,51	14,07	17,47	13,57	16,28	13,45	2,38	9,79	13,06	16,99	5,71
<i>G. rubescens</i>	0,00	4,02	0,00	0,00	1,86	0,00	0,00	0,00	1,22	0,00	0,00
<i>G. aequilateralis</i>	9,46	13,07	11,35	8,14	9,30	7,98	16,27	9,79	11,02	7,77	11,02
<i>G. calida</i>	9,01	4,52	2,18	1,81	2,33	4,20	3,97	2,55	0,00	0,00	0,00
<i>N. pachyderma d</i>	0,00	1,01	0,44	0,45	0,00	0,00	0,00	0,00	0,00	0,00	0,00
<i>N. dutertrei d</i>	0,00	0,00	0,00	0,00	0,00	0,00	0,00	0,00	0,00	0,00	0,00
<i>N. dutertrei s</i>	0,00	0,00	0,00	0,00	0,00	0,00	0,00	0,00	0,00	0,00	0,00
<i>T. quinueloba</i>	0,00	0,50	0,00	0,90	0,00	0,00	0,00	0,00	0,82	0,97	0,00
<i>G. truncatulinooides</i>	0,00	0,00	2,62	4,52	0,00	0,00	0,00	0,00	0,00	0,00	0,00
<i>G. glutinata</i>	0,00	0,00	0,00	2,26	0,00	0,00	0,00	0,00	0,00	0,00	0,00
<i>H. inflata</i>	57,14	45,61	35,86	30,19	30,04	32,86	25,68	27,14	33,54	34,20	40,00
<i>L. bulimoides</i>	0,00	1,75	6,57	1,89	3,04	6,71	2,70	2,01	1,54	1,73	6,67
<i>L. retroversa</i>	0,00	0,00	0,00	0,00	0,00	0,00	0,00	0,00	0,00	0,00	0,00
<i>L. trochiformis</i>	3,30	0,00	0,00	0,00	0,00	0,00	0,00	0,00	0,00	0,00	0,00
<i>C. virgula</i>	8,79	14,91	18,69	25,16	19,77	25,80	27,70	22,11	26,15	26,84	40,00
<i>C. acicula</i>	0,00	0,88	0,51	0,00	0,38	0,00	0,00	0,00	0,00	0,00	0,00
<i>Creseis sp.</i>	0,00	0,00	0,00	0,00	0,00	0,00	0,00	0,00	0,00	0,00	0,00
<i>H. striata</i>	1,10	0,00	1,52	0,00	1,14	1,06	0,34	0,00	1,23	0,00	0,00
<i>S. subula</i>	0,00	0,00	0,00	0,63	0,00	0,00	0,68	0,50	0,00	0,00	0,00
<i>C. pyramidata</i>	2,20	5,26	4,55	3,14	6,46	3,89	8,11	4,52	4,31	4,76	6,67
<i>D. trispinosa</i>	0,00	0,00	0,51	1,26	1,14	1,06	0,34	0,50	0,92	0,00	0,00
<i>Cavolinia spp.</i>	12,09	13,16	10,10	14,47	7,98	8,48	6,08	9,55	7,38	12,12	0,00

Species/Samples	76,5	77,5	78,5	79,5	80,5	81,5	82,5	83,5	84,5	85,5	86,5
<i>O. universa</i>	21,33	30,38	30,18	44,41	38,63	5,02	40,93	5,33	21,27	10,95	29,57
<i>G. ruber alba</i>	17,67	15,00	26,67	25,59	14,44	29,39	22,06	37,78	45,25	45,27	41,94
<i>G. ruber rosea</i>	27,33	27,69	11,93	14,12	19,86	34,77	29,54	37,78	17,19	18,41	10,22
<i>G. sacculifer</i>	0,00	0,38	0,00	0,00	0,00	0,00	0,00	0,00	0,00	0,00	1,61
<i>B. digitata</i>	1,67	2,69	0,70	0,88	2,17	0,00	0,00	0,00	0,00	0,00	0,00
<i>G. inflata</i>	0,00	0,38	0,00	0,00	0,00	0,00	0,00	0,00	0,00	0,00	0,00
<i>G. bulloides</i>	11,00	9,23	17,19	5,29	12,27	12,54	3,91	6,67	3,62	10,45	6,99
<i>G. rubescens</i>	2,33	0,77	2,81	0,59	2,89	0,00	0,36	0,00	0,00	0,00	0,00
<i>G. aequilateralis</i>	14,67	13,46	7,02	6,47	6,14	16,13	3,20	12,44	12,67	14,43	9,68
<i>G. calida</i>	3,67	0,00	2,81	2,65	3,61	1,79	0,00	0,00	0,00	0,50	0,00
<i>N. pachyderma</i> d	0,00	0,00	0,00	0,00	0,00	0,00	0,00	0,00	0,00	0,00	0,00
<i>N. dutertrei</i> d	0,00	0,00	0,00	0,00	0,00	0,00	0,00	0,00	0,00	0,00	0,00
<i>N. dutertrei</i> s	0,00	0,00	0,00	0,00	0,00	0,00	0,00	0,00	0,00	0,00	0,00
<i>T. quinueloba</i>	0,00	0,00	0,00	0,00	0,00	0,00	0,00	0,00	0,00	0,00	0,00
<i>G. truncatulinooides</i>	0,00	0,00	0,00	0,00	0,00	0,00	0,00	0,00	0,00	0,00	0,00
<i>G. glutinata</i>	0,00	0,00	0,70	0,00	0,00	0,00	0,00	0,00	0,00	0,00	0,00
<i>H. inflata</i>	23,96	40,47	34,80	37,38	37,97	27,98	45,20	46,64	32,78	15,79	44,55
<i>L. bulimoides</i>	3,13	1,95	0,00	0,00	0,25	0,00	0,00	0,00	0,00	0,00	0,00
<i>L. retroversa</i>	0,00	0,00	0,00	0,00	0,00	0,00	0,00	0,00	0,00	0,00	0,00
<i>L. trochiformis</i>	0,00	0,00	0,00	0,00	0,00	0,00	0,00	0,00	0,00	0,00	0,00
<i>C. virgula</i>	34,38	23,35	19,44	15,85	17,62	20,16	17,06	0,00	22,22	18,42	12,73
<i>C. acicula</i>	0,00	0,78	0,00	0,00	0,00	0,00	0,00	21,48	0,00	0,00	23,64
<i>Creseis</i> sp.	0,00	0,00	0,00	0,00	0,00	0,00	0,00	0,00	0,00	0,00	0,00
<i>H. striata</i>	1,04	0,00	2,82	0,20	0,25	0,00	0,00	0,00	0,00	0,00	0,00
<i>S. subula</i>	0,00	0,39	0,00	0,00	0,00	0,00	0,00	0,00	1,67	0,00	0,00
<i>C. pyramidata</i>	16,67	7,39	3,13	1,57	2,73	0,41	0,43	1,68	1,11	7,89	3,64
<i>D. trispinosa</i>	1,04	0,00	0,00	0,00	0,74	0,00	0,00	0,00	0,00	0,00	1,82
<i>Cavolinia</i> spp.	7,29	10,89	25,08	24,46	16,13	3,70	4,69	3,69	39,44	57,89	10,00

Species/Samples	88	90	92	94	96	99	103	109	115	117,5	121
<i>O. universa</i>	11,11	10,44	2,92	1,12	2,98	2,05	0,00	0,00	0,00	0,00	0,00
<i>G. ruber alba</i>	42,86	45,60	66,42	33,52	44,64	36,99	17,65	13,25	12,14	30,43	10,95
<i>G. ruber rosea</i>	0,00	3,30	2,19	2,79	1,79	0,68	5,88	0,00	1,43	0,00	0,00
<i>G. sacculifer</i>	7,41	2,75	0,00	2,79	1,19	6,85	0,00	0,00	0,00	0,00	0,00
<i>B. digitata</i>	0,00	0,00	0,00	0,00	0,00	0,00	0,00	0,00	0,00	0,00	0,00
<i>G. inflata</i>	1,59	1,65	2,19	3,91	2,98	4,11	0,00	3,97	2,14	0,00	10,95
<i>G. bulloides</i>	26,98	25,27	10,95	33,52	28,57	24,66	35,29	33,11	14,29	21,74	19,71
<i>G. rubescens</i>	0,00	1,10	1,46	0,00	2,98	6,85	11,76	6,62	0,00	0,00	5,84
<i>G. aequilateralis</i>	8,47	5,49	2,92	4,47	0,60	0,00	0,00	0,00	5,00	0,00	0,00
<i>G. calida</i>	0,00	0,55	0,00	1,68	0,00	0,00	0,00	0,00	0,00	0,00	0,00
<i>N. pachyderma d</i>	0,00	0,00	0,73	4,47	0,60	2,05	11,76	26,49	25,00	30,43	36,50
<i>N. dutertrei d</i>	0,00	0,00	0,00	0,00	0,00	0,00	0,00	6,62	14,29	10,87	8,76
<i>N. dutertrei s</i>	0,00	0,00	0,00	0,00	0,00	0,00	0,00	0,00	0,00	0,00	0,00
<i>T. quinueloba</i>	0,00	0,55	0,00	2,79	2,98	2,74	0,00	3,31	5,71	8,70	2,92
<i>G. truncatulinooides</i>	1,59	1,65	8,76	2,79	3,57	6,16	0,00	0,00	4,29	0,00	0,00
<i>G. glutinata</i>	0,00	1,65	0,73	5,59	7,14	6,85	17,65	6,62	15,71	10,43	4,38
<i>H. inflata</i>	36,40	50,38	35,42	25,88	24,44	29,23	45,45	33,33	12,50	25,00	0,00
<i>L. bulimoides</i>	2,19	1,50	0,00	0,00	2,22	0,00	0,00	3,03	0,00	0,00	0,00
<i>L. retroversa</i>	0,00	0,00	0,00	0,00	0,00	0,00	0,00	21,21	12,50	3,13	0,00
<i>L. trochiformis</i>	0,00	0,00	1,04	1,18	0,00	0,00	0,00	0,00	0,00	0,00	0,00
<i>C. virgula</i>	9,21	3,76	2,08	3,53	2,22	3,08	0,00	0,00	0,00	0,00	0,00
<i>C. acicula</i>	34,21	20,30	31,25	54,12	24,44	29,23	9,09	3,03	0,00	3,13	0,00
<i>Creseis sp.</i>	0,00	0,00	0,00	0,00	0,00	0,00	9,09	0,00	0,00	12,50	0,00
<i>H. striata</i>	0,00	0,00	0,00	0,00	0,00	0,00	0,00	0,00	0,00	0,00	0,00
<i>S. subula</i>	0,00	0,00	0,00	0,00	2,22	0,00	0,00	0,00	0,00	0,00	0,00
<i>C. pyramidata</i>	0,88	5,26	14,58	10,59	15,56	13,85	9,09	18,18	37,50	12,50	0,00
<i>D. trispinosa</i>	3,07	3,01	4,17	2,35	6,67	12,31	18,18	6,06	12,50	25,00	0,00
<i>Cavolinia spp.</i>	2,19	0,00	0,00	1,18	0,00	1,54	0,00	0,00	0,00	0,00	0,00

Species/Samples	125	127	129	133	139	145	149	153	157
<i>O. universa</i>	1,19	0,99	0,00	0,00	0,00	0,00	0,00	0,00	0,00
<i>G. ruber alba</i>	20,83	14,85	21,85	14,78	15,65	9,35	20,69	34,06	28,13
<i>G. ruber rosea</i>	1,19	0,99	2,65	0,00	0,00	15,89	0,00	0,00	0,00
<i>G. sacculifer</i>	0,00	0,00	0,00	0,00	1,83	0,00	0,00	1,69	0,00
<i>B. digitata</i>	0,00	0,00	0,00	0,00	0,00	0,00	0,00	0,00	0,00
<i>G. inflata</i>	11,90	9,90	7,91	4,76	8,26	2,06	0,00	5,62	3,15
<i>G. bulloides</i>	11,90	9,90	9,35	16,19	15,60	12,37	14,66	33,71	14,17
<i>G. rubescens</i>	4,76	0,00	0,00	0,00	0,00	0,00	0,00	0,00	0,00
<i>G. aequilateralis</i>	0,00	0,00	0,00	0,00	0,00	0,00	0,00	3,37	0,00
<i>G. calida</i>	0,00	0,00	4,32	0,00	0,00	0,00	0,00	0,00	0,00
<i>N. pachyderma d</i>	35,71	44,55	45,32	37,14	41,28	44,33	41,38	10,11	33,07
<i>N. dutertrei d</i>	0,00	7,92	5,76	12,38	13,76	15,46	12,93	2,25	4,72
<i>N. dutertrei s</i>	0,00	0,00	0,00	0,00	0,00	0,00	0,00	1,12	0,00
<i>T. quineloba</i>	5,95	4,95	1,32	10,43	0,00	7,48	6,90	3,49	21,25
<i>G. truncatulinoides</i>	0,00	1,98	1,44	0,95	0,92	0,00	0,00	0,00	0,00
<i>G. glutinata</i>	5,36	3,96	5,96	8,70	1,74	0,00	2,59	4,37	3,75
<i>H. inflata</i>	20,00	0,00	60,00	22,22	21,43	0,00	0,00	0,00	0,00
<i>L. bulimoides</i>	0,00	0,00	0,00	0,00	0,00	0,00	0,00	0,00	0,00
<i>L. retroversa</i>	0,00	9,09	40,00	22,22	35,71	33,33	42,31	84,21	93,33
<i>L. trochiformis</i>	0,00	0,00	0,00	0,00	0,00	0,00	0,00	0,00	0,00
<i>C. virgula</i>	20,00	0,00	0,00	0,00	0,00	0,00	0,00	0,00	0,00
<i>C. acicula</i>	20,00	0,00	0,00	0,00	0,00	0,00	0,00	0,00	0,00
<i>Creseis sp.</i>	0,00	0,00	0,00	0,00	0,00	0,00	0,00	0,00	0,00
<i>H. striata</i>	0,00	0,00	0,00	0,00	0,00	0,00	0,00	0,00	0,00
<i>S. subula</i>	0,00	0,00	0,00	0,00	0,00	0,00	0,00	0,00	0,00
<i>C. pyramidata</i>	0,00	45,45	0,00	22,22	35,71	16,67	7,69	1,75	2,67
<i>D. trispinosa</i>	20,00	9,09	0,00	22,22	7,14	50,00	34,62	14,04	2,67
<i>Cavolinia spp.</i>	0,00	0,00	0,00	0,00	0,00	0,00	0,00	0,00	0,00

Species/Samples	159	171	179	187	195
<i>O. universa</i>	0,00	0,00	0,00	0,00	0,00
<i>G. ruber alba</i>	23,40	22,58	25,32	34,53	29,84
<i>G. ruber rosea</i>	0,00	0,00	0,00	0,00	0,00
<i>G. sacculifer</i>	0,00	0,00	1,14	0,00	1,55
<i>B. digitata</i>	0,00	0,00	0,57	0,00	0,00
<i>G. inflata</i>	0,00	0,00	0,00	0,00	0,00
<i>G. bulloides</i>	23,19	19,23	16,00	19,23	8,53
<i>G. rubescens</i>	0,00	0,00	0,57	0,00	0,00
<i>G. aequilateralis</i>	0,00	0,00	0,00	0,00	0,00
<i>G. calida</i>	0,00	0,00	0,00	0,00	0,00
<i>N. pachyderma</i> d	31,88	40,38	25,71	24,04	37,98
<i>N. dutertrei</i> d	5,80	0,00	2,86	0,00	7,75
<i>N. dutertrei</i> s	5,07	0,00	4,57	0,00	0,00
<i>T. quinueloba</i>	14,89	30,11	20,68	20,14	22,51
<i>G. truncatulinooides</i>	0,00	0,00	0,00	0,00	0,00
<i>G. glutinata</i>	9,04	7,53	7,59	3,60	6,28
<i>H. inflata</i>	0,00	0,00	0,00	0,00	0,00
<i>L. bulimoides</i>	0,00	0,00	0,00	0,00	0,00
<i>L. retroversa</i>	98,46	98,45	98,31	96,51	97,22
<i>L. trochiformis</i>	0,00	0,00	0,00	0,00	0,00
<i>C. virgula</i>	0,00	0,00	0,00	0,00	0,00
<i>C. acicula</i>	0,00	0,00	0,00	0,00	0,00
<i>Creseis</i> sp.	0,00	0,00	0,00	0,00	0,00
<i>H. striata</i>	0,00	0,00	0,00	0,00	0,00
<i>S. subula</i>	0,00	0,00	0,00	0,00	0,00
<i>C. pyramidata</i>	0,00	0,78	0,85	3,49	2,78
<i>D. trispinosa</i>	0,00	0,00	0,00	0,00	0,00
<i>Cavolinia</i> spp.	0,00	0,00	0,00	0,00	0,00

Multiproxy ecosystem response of abrupt Holocene climatic changes in the northeastern Mediterranean sedimentary archive and hydrologic regime

Christina Giamali^{a*}, Efterpi Koskeridou^a, Assimina Antonarakou^a, Chryssanthi Ioakim^b, George Kontakiotis^a, Aristomenis P. Karageorgis^c, Grigoris Roussakis^c, Vassilis Karakitsios^a

^aFaculty of Geology and Geoenvironment, School of Earth Sciences, Department of Historical Geology-Palaeontology, National and Kapodistrian University of Athens, Panepistimiopolis, 15784 Zografou, Greece

^bInstitute of Geology and Mineral Exploration (IGME), Olympic Village, 13677 Acharnae, Greece

^cHellenic Centre for Marine Research, Institute of Oceanography, 46.7 km Athens-Sounio Avenue, 19013 Anavyssos, Greece

*Corresponding author e-mail address: gchristi@geol.uoa.gr (C. Giamali).

(RECEIVED July 23, 2018; ACCEPTED May 31, 2019)

Abstract

Aspects of paleoclimatic and paleoceanographic evolution of the north Aegean Sea through the Holocene are revealed by the study of quantitative variations in planktonic foraminiferal, pteropodal, and palynomorph assemblages; the isotopic composition of planktonic foraminifera; and hydrographic-related indices, extracted from two high-sedimentation rate cores from the North Aegean Trough. Focusing on the last ~10 cal ka BP, the current Holocene subdivision (Greenlandian, Northgrippian, and Meghalayan) confirms the traditional understanding of an evolution from wetter (Greenlandian) to gradually drier (Northgrippian and Meghalayan) climatic conditions and further highlights the role of changing seasonality during this time. The most warm and humid phase corresponds to the time of the sapropel S1 deposition (9.6–6.1 cal ka BP). The Holocene climatic instability of the study area is further supported by six episodes of brief cooling (North Aegean cooling; NAEGC6–NAEGC1) centered at 9.30, 8.05, 7.05, 4.55, 3.55, and 2.05 cal ka BP, reflected by significant faunal changes and oxygen isotope enrichments. These cold/arid events are coeval with equivalent cooling events that have been described in different basins of the Mediterranean Sea, while signal similarities with equivalent changes in the intensity of the Siberian high suggest a climatic link between the studied area and the high-latitude areas.

Keywords: Holocene cooling events; Planktonic foraminifera; Pteropods; Palynomorphs; Stable isotopes; Paleoceanographic evolution; Sapropel S1; Late Quaternary; North Aegean Sea

INTRODUCTION

Over the last decades, there has been considerable interest in the role of the subtropical oceans in climate change and, in particular, oceanic subbasins and marginal seas. These bodies are often more responsive to paleoceanographic and paleoclimatic changes than global oceans because of their smaller size and partial isolation. As an example, the relatively small volume of the Mediterranean Sea causes changes in its climatic forcing to be recorded virtually instantaneously in paleoceanographic proxy data, such as stable isotope and

other geochemical ratios, and in microfossil abundances. Specifically, the signals registered by changes in abundance and distribution of fossil microorganisms, such as planktonic foraminifera, provide a reliable and well-documented record at both global and local scales (Cacho et al., 2001; Siani et al., 2010, 2013; Lirer et al., 2014; Antonarakou et al., 2015, 2019; Bonfardeci et al., 2018). The basin's limited communication with the open ocean implies that any climatic signals will be recorded in an amplified fashion in Mediterranean properties, such as temperature, salinity, and specific elemental concentrations (Casford et al., 2002; Marino et al., 2009; Kontakiotis, 2016; Louvari et al., 2019).

The Aegean Sea is ideal for the analysis of climate change to the proposed forcing mechanism because of its intermediate position between the higher-latitude and lower-latitude climate systems (subtropical high pressure and subpolar

Cite this article: Giamali, C., Koskeridou, E., Antonarakou, A., Ioakim, C., Kontakiotis, G., Karageorgis, A. P., Roussakis, G., Karakitsios, V. 2019. Multiproxy ecosystem response of abrupt Holocene climatic changes in the northeastern Mediterranean sedimentary archive and hydrologic regime. *Quaternary Research* 1–21. <https://doi.org/10.1017/qua.2019.38>

depression; Zervakis et al., 2004; Giorgi and Lionello, 2008; Rohling et al., 2009). Its geographic and oceanographic setting contributes to the enhanced imprint and preservation of climatic perturbations associated with mid- and low-latitude climate conditions. The unusually high sedimentation rates characterizing this study area allow detailed records of changes to be preserved and facilitate the assessment of basin-integrated paleoceanographic responses.

Environmental changes of the water column have an impact on the abundance and distribution of fossil micro- and macro-organisms, such as planktonic foraminifera, pteropods, and palynomorphs. This makes them extremely valuable for both stratigraphic correlation and paleoenvironmental reconstructions (Casford et al., 2007; Comeau et al., 2010; Antonarakou et al., 2015, 2018; Drinia et al., 2016; Jaouadi et al., 2016; Kontakiotis et al., 2016; Wilson et al., 2018). These fossils have been used for the detection of long- and short-duration paleoclimatic and paleoceanographic changes in the study area (Casford et al., 2003; Geraga et al., 2005, 2010; Triantaphyllou et al., 2009; İşler et al., 2016; Kontakiotis, 2016; Howes et al., 2017; Antonarakou et al., 2018), especially during the last glacial cycle (including the last glacial maximum, Bølling-Allerød, Younger Dryas, and Holocene climatic optimum [HCO]). However, little attention has been paid toward the investigation of the Aegean Sea pteropod assemblages.

In the present study, high-resolution analysis on two sediment cores (AEX-15 and AEX-23) from the North Aegean Trough was conducted to advance the understanding of the

spatial and temporal variability of climatic and oceanographic changes recorded in the study area and to elucidate forcing mechanisms. Paleoceanographic reconstruction and climatic oscillations in the North Aegean Sea were based on the abundances of planktonic foraminifera, pteropods, and palynomorphs, as well as variations of oxygen and carbon isotopic signal. The short-term events detected in this study were further compared with previously published circum-Mediterranean climate records (e.g., Emeis et al., 2000, 2003; Cacho et al., 2001; Frigola et al., 2007).

REGIONAL OCEANOGRAPHIC SETTING

The Aegean Sea is separated into two major subbasins with different climatic conditions: the “north” and the “south” Aegean Sea. The north is more humid than the semiarid south (Lykousis et al., 2002). The north Aegean Sea is characterized by an alternation of deep trenches and troughs, shallow shelves, and sills. The dominant bathymetric feature in the northern sector of the Aegean Sea is the 800- to 1590-m-deep northeast–southwest (NE–SW) elongated depression, known as the North Aegean Trough (Fig. 1a). It includes several interconnected subbasin depressions (Saros, 1061 m deep; Limnos, 1590 m; Athos, 1149 m; and Sporades, 1470 m), widening toward the west, that are separated from each other by 100- to 350-m-deep intervening shoals and associated islands (Papanikolaou et al., 2002; Roussakis et al., 2004).

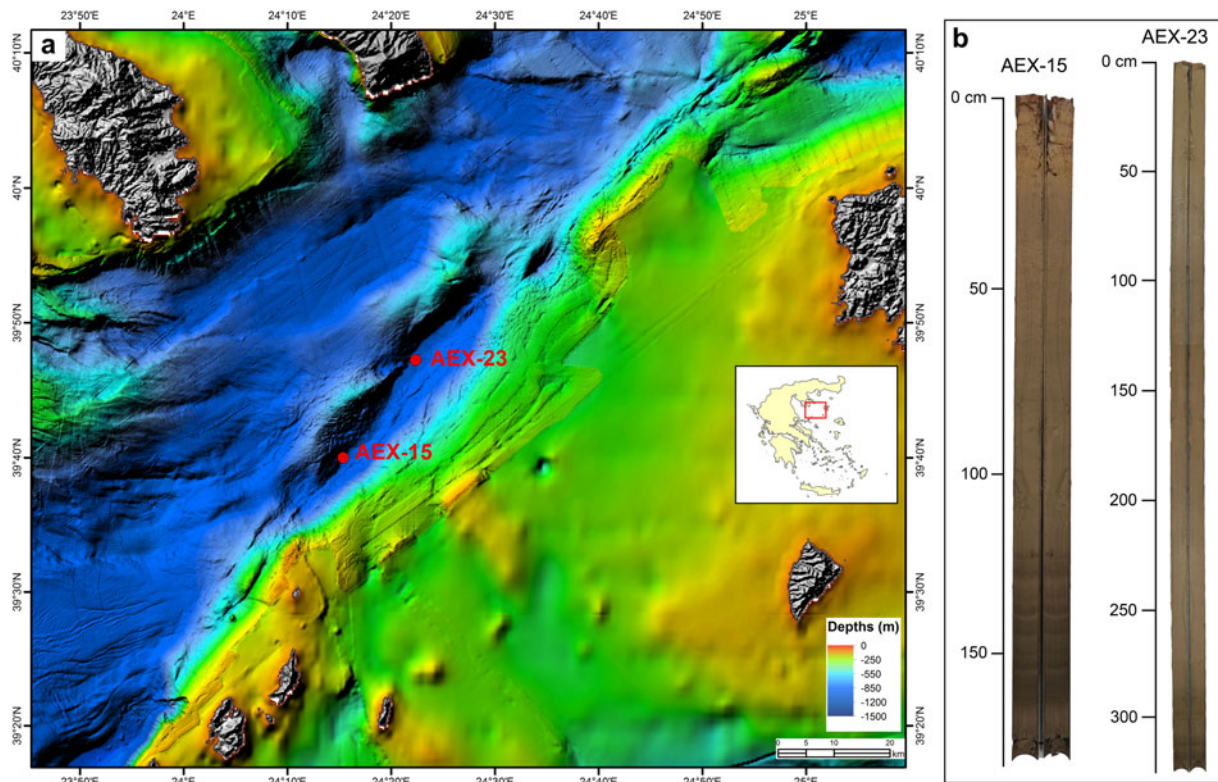


Figure 1. (color online) (a) Location of the gravity cores AEX-15 and AEX-23 in the North Aegean Trough. (b) Lithologic log of cores AEX-15 and AEX-23.

The physical oceanography of the north Aegean Sea is controlled by the regional climate, the freshwater discharge from major rivers (Axios, Strymon, Nestos, and Evros) draining southeastern Europe, and Black Sea surface-water outflow through the Dardanelles Straits. Previous studies revealed a general cyclonic water circulation in the Aegean Sea, on which a number of mesoscale cyclonic and anticyclonic eddies are superimposed (Casford et al., 2002). The water column structure comprises three major water masses: the superficial nutrient-rich and less saline Black Sea Water (9–22°C and 22–23 psu), the Levantine Intermediate Water (16–25°C and 39.2–39.5 psu) with higher salinity, and the North Aegean Deep Water (13–14°C and 39.1–39.2 psu; Velaoras and Lascaratos, 2005). The surface and intermediate waters follow the general counterclockwise circulation of the Aegean Sea and progressively mix as they flow southward along the east coast of Greece (Karageorgis et al., 2003).

MATERIAL AND METHODS

Location and description of cores

Two gravity cores (AEX-15 and AEX-23) from the North Aegean Trough (Fig. 1) were recovered with R/V *Aegaeo* in October 2013 and cover most of the Holocene epoch (the last ~10 ka and 8 ka, respectively). Both cores were collected from a relatively isolated elongated subbasin of the north Aegean Sea, oriented NE–SW, with dimensions of approximately 42 × 7 km and a maximum depth of 1290 m. Core AEX-15 (39°39.900'N, 24°15.369'E; 1242 m water depth, length 178 cm) was recovered from the southern sector of the basin; core AEX-23 (39°49.464'N, 24°22.354'E; 1226 m water depth, length 322 cm) was recovered near the depocenter of the basin.

The interval between 0 and 6.5 cm of AEX-15 consists of mud of yellowish-brown color (Munsell soil color 2.5Y 5/3), followed by an interval (6.5 to 14.5 cm) of yellow (2.5Y 6/4) mud with some shell debris. From 21 cm to 122 cm, olive (5Y 6/2) mud with dense darker laminae is observed. The interval between 122 cm to 165 cm is characterized by an olive gray color (5Y 6/2) mud. The last 13 cm consists of grayish olive (7.5Y 6/2) mud (Fig. 1b).

The interval between 0 cm and 246 cm of core AEX-23 consists of olive yellow (7.5Y 6/3) mud that becomes grayish olive (5Y 6/2) up to 286 cm. The rest of the core (286–322 cm) is composed of dark olive gray (2.5GY 4/1) mud. In the top 4 cm of this interval (286–290 cm) lens of mud rich in organic matter with dark olive gray color (2.5GY 4/1) is observed (Fig. 1b).

All samples taken (118 from AEX-15 and 43 from AEX-23) were used for paleontological (planktonic foraminifera, pollen, dinoflagellate cysts, and pteropods) and geochemical (oxygen, $\delta^{18}\text{O}$, and carbon, $\delta^{13}\text{C}$, isotopes) analyses. Samples were taken from all the intervals of the cores but with different sampling resolution. For the olive gray and dark olive gray intervals, the sampling resolution was 1 cm for AEX-15 and 2.5 cm for AEX-23; beyond

these intervals, the sampling was 2 cm for AEX-15 and 5 cm for AEX-23.

Chronostratigraphy

The chronostratigraphy of the cores is based on three accelerator mass spectroscopy radiocarbon (AMS ^{14}C) dates (two for AEX-15 and one for core AEX-23 on *Globigerinoides ruber* tests at Beta Analytics laboratories), supplemented by the detected additional control points, as defined by Ba, Al, and organic carbon measurements (this study) and well-dated correlation horizons from nearby north Aegean cores (Fig. 2). Conventional ^{14}C ages were calibrated by means of the Calib version 7.0.2 software (Stuiver and Reimer, 1993) and the Marine13 data set with a regional reservoir age correction (ΔR) of 58 ± 85 yr outside the sapropel S1 interval (Reimer et al., 2013). Hereafter, ages in this study are reported in calibrated thousands of years before present, notated cal ka BP.

Determination of organic carbon (C_{org}) and major elements (Al) and barium (Ba) were performed on selected sediment samples from both cores to detect the depth where the onset and termination of S1 deposition occurred (e.g., Martínez-Ruiz et al., 2003, and references therein) (Fig. 2). C_{org} was determined in a Fisons Instruments EA-1108 CHNS analyzer. The operating parameters were very similar to those reported by Cutter and Radford-Knoery (1991), Nieuwenhuize et al. (1994), and Verardo et al. (1990). The precision of the method is within 5%. A detailed description of the analytical procedure is given by Karageorgis et al. (2009).

Major element concentrations were determined on fused beads using an X-ray fluorescence spectrometer (Panalytical PW-2400) at the biogeochemical laboratory of the Hellenic Centre for Marine Research, which is accredited according to ELOT EN ISO/IEC 17025:2005. Aluminum and barium were determined as oxides following the procedure described in Karageorgis et al. (2005). In addition, barium excess (Ba_{ex}) that represents marine barite, and thus enhanced productivity (Martínez-Ruiz et al., 2003), was estimated according to Karageorgis et al. (2005). The analytical precision is 5–10% on the basis of duplicate runs of standards and unknowns, whereas accuracy was assessed using the international reference material PACS-2.

Micropaleontological analyses

All samples were prepared following standard micropaleontological procedures. For the faunal analyses, approximately 3 cm³ of dried sediment was washed and sieved through 63 μm and 125 μm sieves, and residues were dried in an oven at 50°C. Qualitative and quantitative analyses have been performed on both the planktonic foraminiferal and pteropod assemblages for the >125 μm fraction, split into aliquots, each one containing at least 300 specimens. All shells were handpicked, identified (additionally at morphospecies level where possible; *G. ruber*), and counted in each sample and then converted into percentages, based on the extrapolation of a counted split (Figs. 3 and 4). The palynomorphs

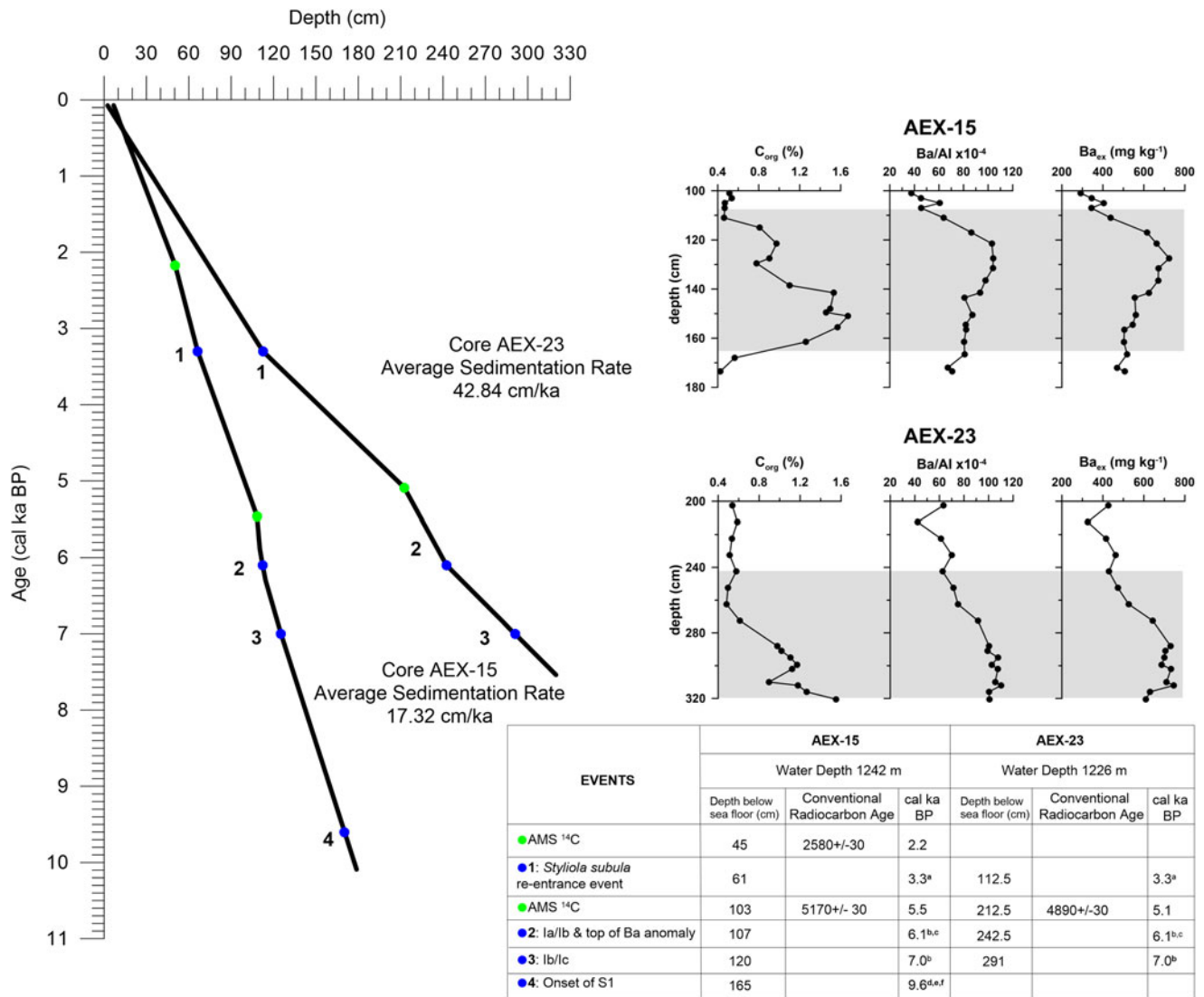


Figure 2. Time stratigraphic framework (age model and mean sedimentation rates) of the study cores along with C_{org} and Ba_{ex} concentrations and Ba/Al ratios. Blue dots represent control points and bioevents according to the following: ^a Buccheri et al. (2002), ^b Casford et al. (2002), ^c Casford et al. (2007), ^d Kotthoff et al. (2008a), ^e Geraga et al. (2010), and ^f Herrle et al. (2018). Green dots represent accelerator mass spectrometry (AMS) ¹⁴C datings. (For interpretation of the references to color in this figure legend, the reader is referred to the web version of this article.)

(when possible 400 specimens were counted and identified) were extracted using 10% HCl and 38% HF acids followed by several sievings (wet sieving through 125 μ m and ultrasonic 10 μ m sieves). The residues were mounted in glycerine gel on microscope slides for analysis under a binocular Nikon transmission microscope at 500 \times and 1000 \times (oil immersion) magnification. Pollen percentages for each taxon presented here are based on the main pollen sum excluding *Pinus* and Pteridophyte spores (Fig. 5). Planktonic foraminiferal taxonomy followed the work of Hemleben et al. (1989) with additional updates from Kontakiotis et al. (2017); for pteropods, we referred to Di Geronimo (1970), Van der Spoel (1976), and Janssen (2012); and for pollen and dinoflagellate cysts, we referred to Polunin (1988), Marret and Zonnefeld (2003), and Zonneveld et al. (2013). Finally, planktonic species with phylogenetic

affinities and similar ecological characteristics were counted together and grouped to better interpret distribution patterns (Fig. 3). All morphotypes of *G. ruber* (“Normal,” “Platys,” “Elongate,” and “Twin” types; Kontakiotis et al., 2017) were plotted together, distinguishing only the “alba” and “rosea” varieties because of different ecological characteristics. Similarly, pollen data were summarized into selected ecological groups: Mediterranean taxa, cool temperate summergreen, cool temperate evergreen, warm temperate summergreen, total nonarboreal pollen (NAP), and the total arboreal pollen (AP) (Fig. 6).

Stable isotope analyses

For stable oxygen and carbon isotope measurements ($\delta^{18}O$, $\delta^{13}C$), 30 specimens of the planktonic species

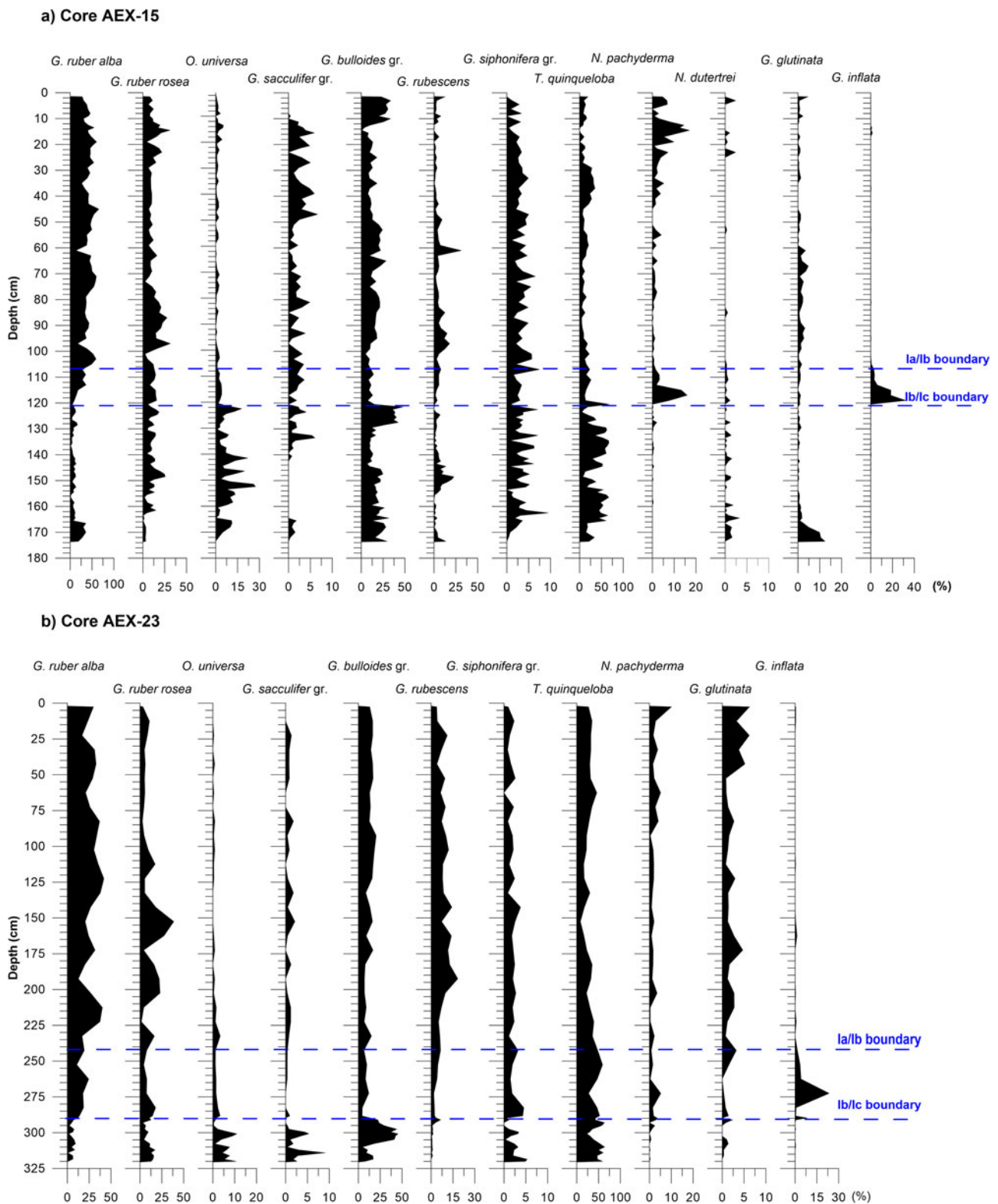


Figure 3. Frequency curves of the most indicative planktonic foraminiferal species in core AEX-15 (a) and AEX-23 (b). *Globigerina bulloides* group includes the species *Globigerina bulloides* and *Globigerina falconensis*, the *Globigerinoides sacculifer* group includes *Globigerinoides trilobus* and *Globigerinoides sacculifer*, and the *Globigerinella siphonifera* group includes the species *Globigerinella aequilateralis*, *Globigerina calida*, and *Globigerina digitata*. The species *Globigerinita glutinata* includes the morphotypes with and without bulla. Within the group of neogloboquadrinids, two types have been discerned: *Neogloboquadrina pachyderma* and *Neogloboquadrina dutertrei*. The dashed blue lines represent the Ia/Ib and Ib/Ic boundaries. (For interpretation of the references to color in this figure legend, the reader is referred to the web version of this article.)

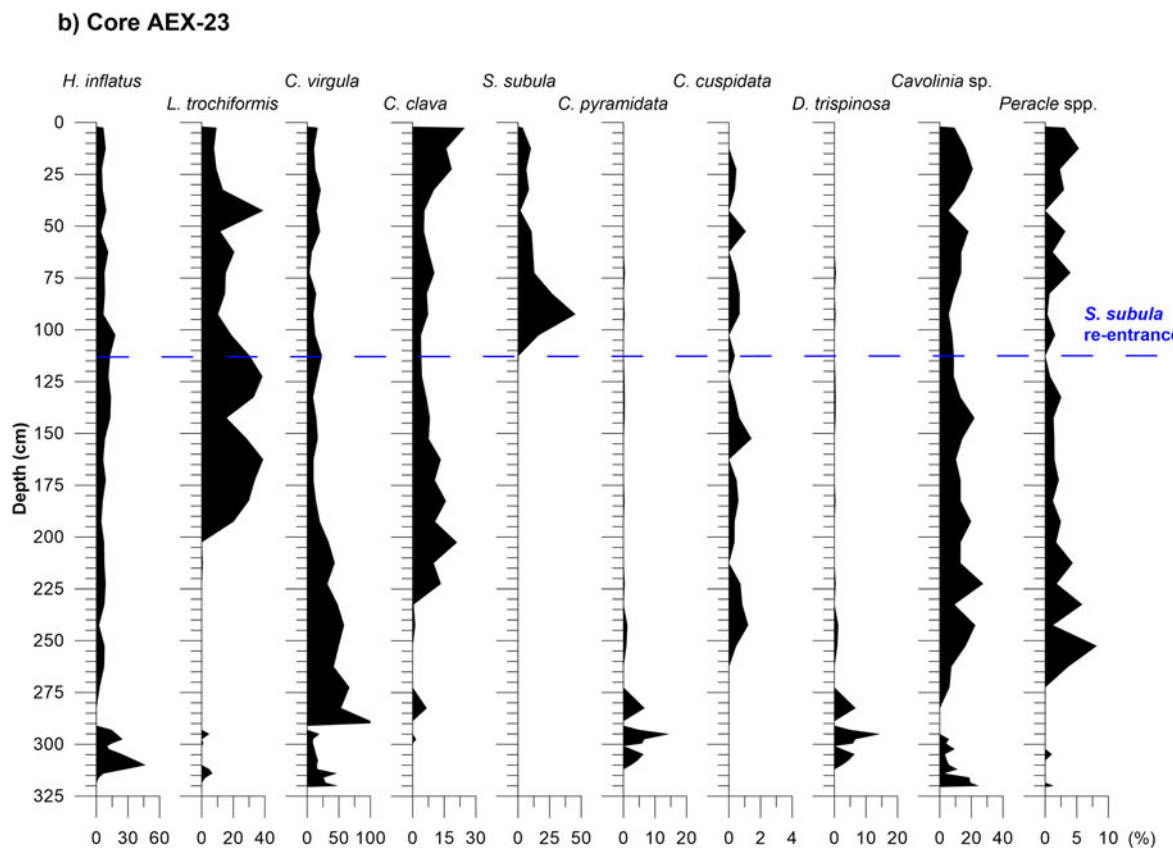
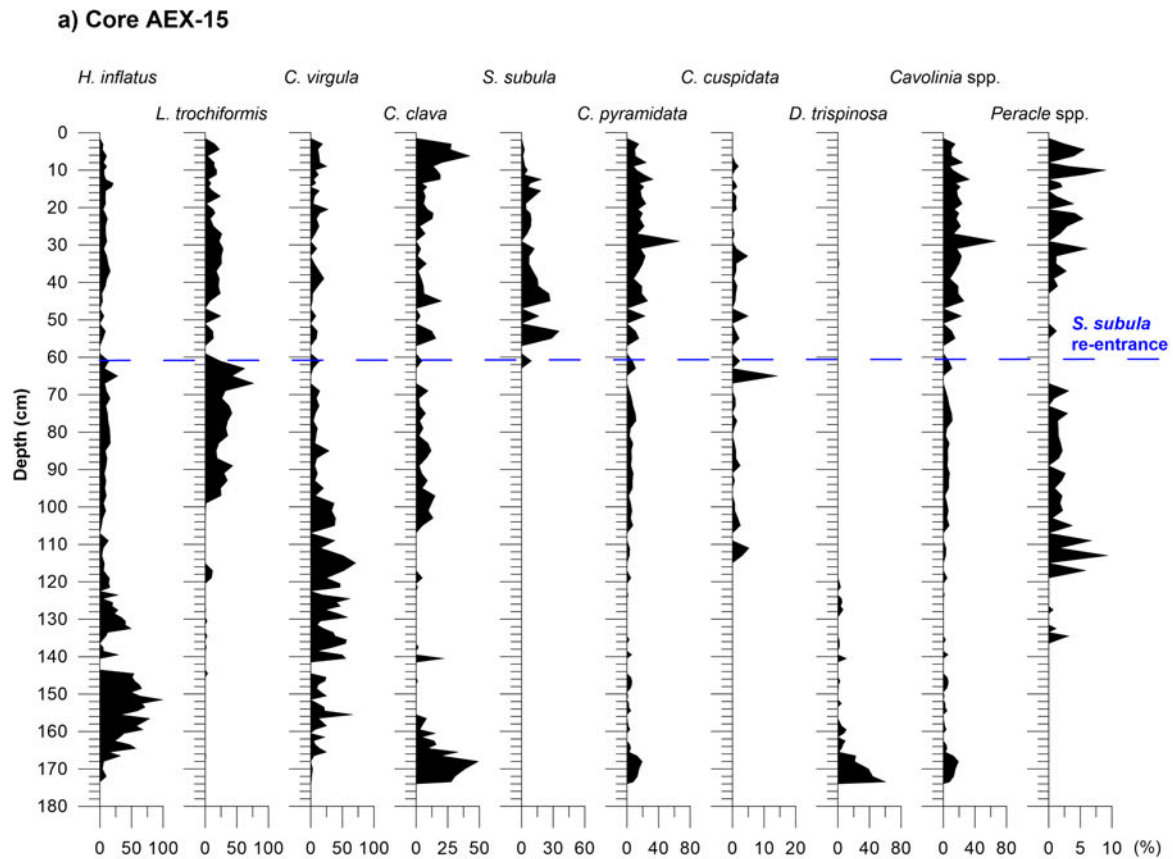


Figure 4. Frequency curves of the most indicative pteropoda in core AEX-15 (a) and AEX-23 (b). The dashed blue line represents the re-entrance of the pteropod *Styliola subula*. (For interpretation of the references to color in this figure legend, the reader is referred to the web version of this article.)

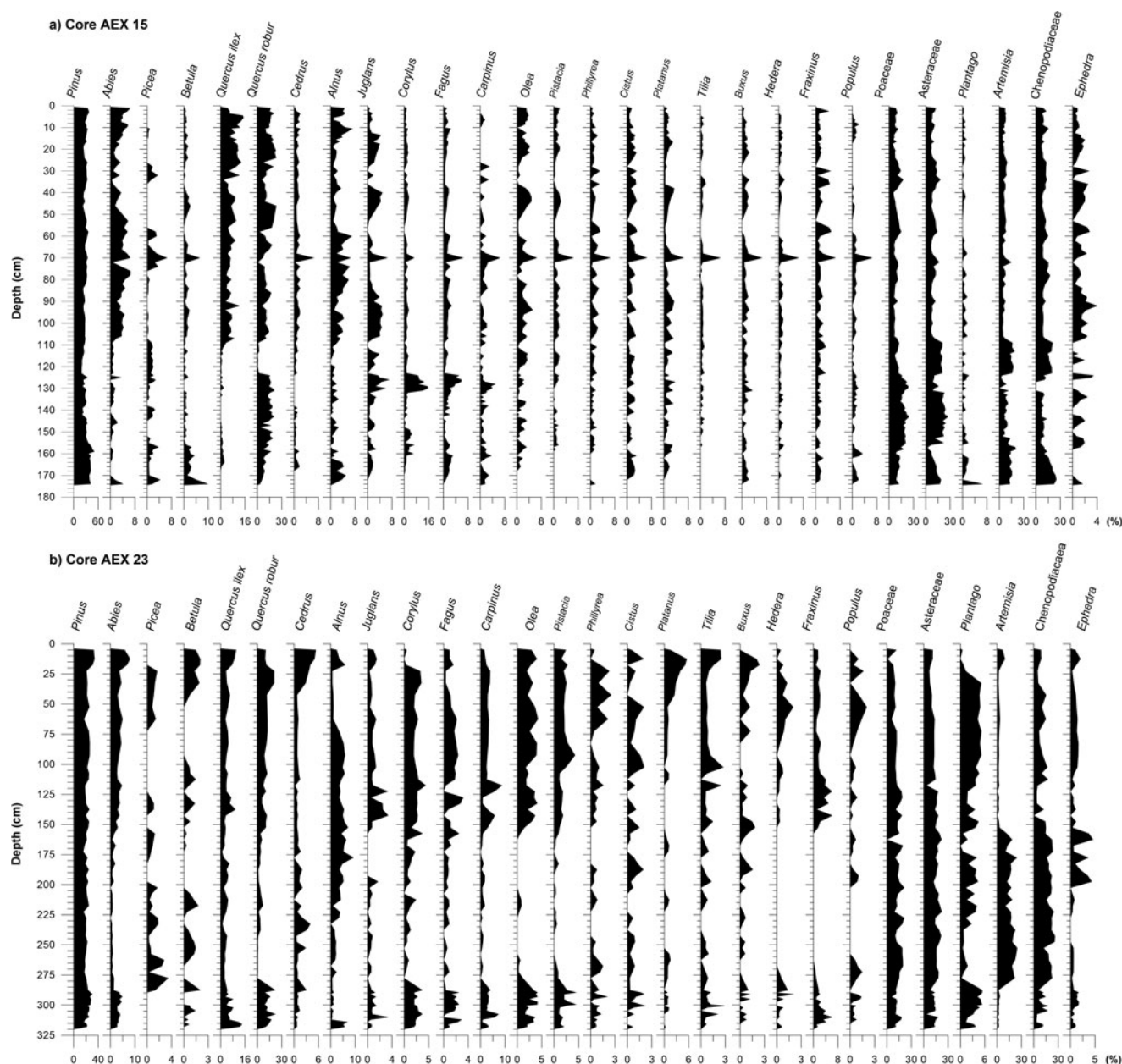


Figure 5. Frequency curves of pollen species for core AEX-15 (a) and core AEX-23 (b).

Globigerinoides ruber f. *alba* were picked from the 250–300 μm size fraction. In particular, we exclusively used the morphotype “Normal” (usually represented to *G. ruber* sensu stricto) of Kontakiotis et al. (2017) in order to minimize potential morphotype-specific differential responses in stable isotope compositions. This size fraction limitation was used to minimize ontogenetic and growth rate effects on shell geochemistry (Spero et al., 2003). The analyses were carried out at the Laboratory of Geology and Geophysics at Edinburgh University. Foraminiferal $\delta^{18}\text{O}$ and $\delta^{13}\text{C}$ data were calibrated to National Bureau of Standards 19 (NBS19), and the isotope values are reported in ‰ relative to Vienna Pee Dee belemnite scale. The external standard errors of the stable carbon and oxygen isotope analyses are $<0.06\text{‰}$ and 0.08‰ , respectively.

Paleoceanography proxy records

The planktonic foraminiferal relative distributions are used as a first-order estimate of sea-surface temperature (SST) variations. An index of the SST variations was constructed based on the down-core variation of planktonic foraminiferal abundances, referred to as planktonic paleoclimatic curve (PPC). The PPC was obtained by the formula $100 \times (w - c)/(w + c)$, where w represents the warm-water indicators (*G. ruber alba*, *G. ruber rosea*, *Orbulina universa*, *Globigerinoides sacculifer* gr., *Globoturborotalita rubescens*, and *Globigerinella siphonifera* gr.), and c the cold-water indicators (*Globorotalia inflata*, *Globorotalia truncatulinoides*, *Turborotalita quinqueloba*, *Globigerinita glutinata*, and *Globorotalia scitula*).

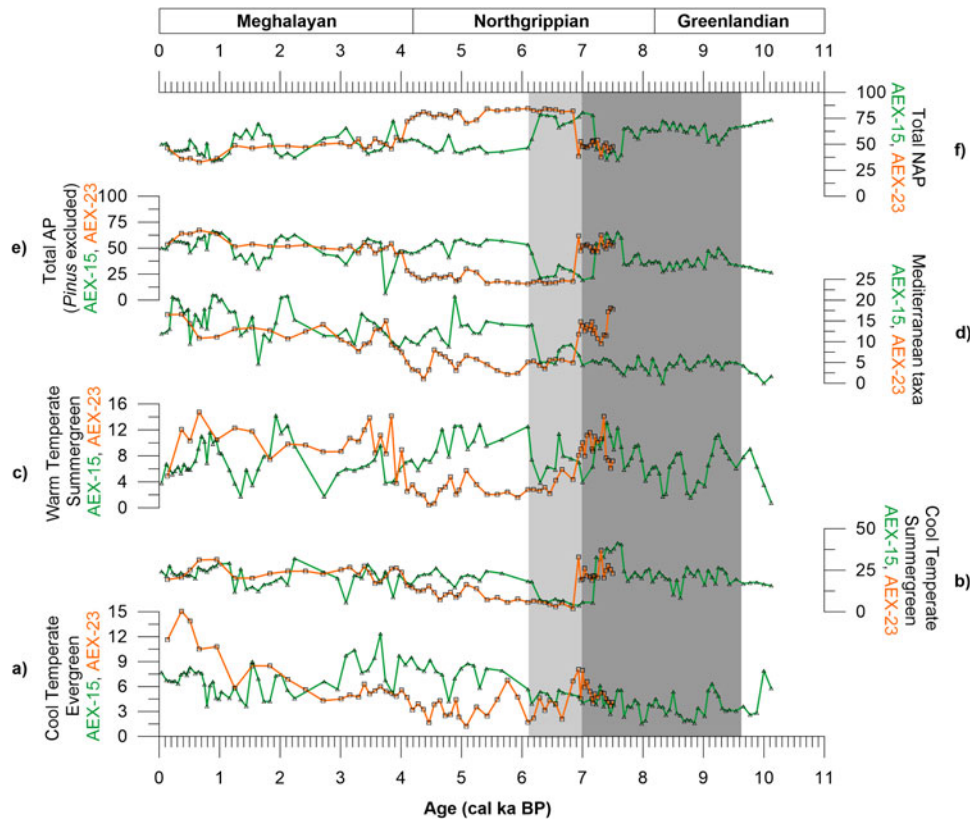


Figure 6. Down-core variations of cool temperate evergreen taxa (*Abies*, *Picea*, *Cedrus*, *Buxus*, and *Hedera*) (a), cool temperate summergreen taxa (*Betula*, *Quercus robur*, *Alnus*, *Corylus*, *Fagus*, *Carpinus*, and *Tilia*) (b), warm temperate summergreen taxa (c), Mediterranean taxa (*Cistus*, *Quercus ilex*, *Phillyrea*, *Olea*, and *Pistacia*) (d), arboreal pollen (AP) groups (excluding *Pinus*) (e), and nonarboreal pollen (NAP) (*Poaceae*, *Asteraceae*, *Chenopodiaceae*, *Artemisia*, *Plantago*, and *Ephedra*) (f); green line with triangle for AEX-15 and orange line with square for AEX-23. Gray and light gray bands correspond to the sapropel S1 and its oxidized part, respectively. (For interpretation of the references to color in this figure legend, the reader is referred to the web version of this article.)

(Rohling et al., 1993). The stable isotopes ($\delta^{18}\text{O}$, $\delta^{13}\text{C}$) were used to infer SST and productivity variations, respectively.

Following the recent findings of Kontakiotis (2016) from the eastern Mediterranean Sea, we also present the paleoceanographic indices of eutrophication and upwelling (E-index and U-index) as representative of the hydrographic evolution and ecosystem dynamics of the north Aegean Sea. The eutrophication index (E-index) was estimated using the sum of the eutrophic species (*Neogloboquadrina pachyderma*, *Neogloboquadrina dutertrei*, *Globigerina bulloides*, *T. quinqueloba*, and *G. inflata*) versus the sum of the eutrophic plus oligotrophic species (*G. ruber alba*, *G. ruber rosea*, *G. rubescens*, *G. sacculifer*, *O. universa*, and *G. siphonifera*). The percentage of *G. bulloides* was estimated as an upwelling index (U-index). The species *G. siphonifera* gr., *G. rubescens*, *O. universa*, and *G. sacculifer* gr. are referred as SPRUDTS group, following the ecological characteristics of Rohling et al. (1993).

RESULTS

Planktonic foraminifera distribution pattern

Planktonic foraminifera are abundant and well preserved in all the samples from both analyzed cores. The qualitative

analysis of the planktonic foraminifera allow the identification of 18 species lumped into 15 groups: *Globigerinoides ruber alba*, *Globigerinoides ruber rosea*, *Globigerina bulloides* group, *Orbulina universa*, *Globigerinoides sacculifer* group, *Globoturbotalita rubescens*, *Globigerinoides conglobatus*, *Globogenerinella siphonifera* group, *Globorotalia inflata*, *Turbotalita quinqueloba*, *Globorotalia truncatulinoides*, *Globigerinita glutinata*, *Globorotalia scitula*, *Neogloboquadrina dutertrei*, and *Neogloboquadrina pachyderma*. The down-core stratigraphic distributions of their relative abundance are shown in Figure 3.

From the bottom of core AEX-15 (173.5 cm) up to 165 cm, the assemblage is dominated by *G. ruber f. alba* with percentages up to 35%, along with *T. quinqueloba* (34%) and *G. bulloides* (29%). Present with low percentages in this interval are the species *G. glutinata* (12%), *G. rubescens* (13%), and *O. universa* (11%). Between 165 cm and 120 cm (AEX-15), the warm subtropical species (*G. ruber f. rosea* and *O. universa*) are abundant with percentages up to 25%, and the species *Turbotalita quinqueloba* and *G. bulloides* present their maximum percentages (~68% and 48%, respectively). At the same interval neogloboquadrinids occur sporadically and with very low percentages (<2%), and *G. inflata* is totally absent (Fig. 3a). The relative abundance curves of

G. sacculifer group, *G. siphonifera* group, and *O. universa* display highly variable down-core patterns, occasionally reaching significant percentages (10–30%). *G. ruber* f. *alba* and *G. rubescens* are continuously present but in small percentages. At 120 cm in AEX-15 and 291 cm in AEX-23, a sharp increase in the abundance of *G. inflata* (32% in AEX-15 and 23% in AEX-23) and *N. pachyderma* (16% in AEX-15 and 5% in AEX-23) is observed. Later on (119 cm to 1.5 cm in AEX-15 and 290 cm to 2.5 cm in AEX-23), the distribution pattern of these species is limited, with the exception of the upper part of the cores, which is marked by a sharp increase of *N. pachyderma*. During this interval, *G. ruber* f. *alba* reaches maximum abundances (up to 65% and 40% for AEX-15 and AEX-23, respectively). *G. ruber* f. *rosea* (~10–15%) and *T. quinqueloba* (~15–30%) are still present but less abundant, whereas *O. universa* decreases dramatically (Fig. 3). Increasing percentages of *G. rubescens* (~15–30%) and *G. glutinata* (~5%) are also recorded.

Pteropod distribution pattern

All samples examined for foraminifera include variable amounts of aragonitic pteropods. A total of 11 species of Euthecosomata (*Heliconoides inflatus*, *Limacina trochiformis*, *Limacina retroversa*, *Creseis virgula*, *Creseis clava*, *Hyalocyclis striata*, *Styliola subula*, *Clio pyramidata*, *Clio cuspidata*, *Diacria trispinosa*, and *Cavolinia* spp.) and 2 genera of Pseudothecosomata (*Gleba* sp. and *Peracle* spp.) were identified. Heteropoda of the family of Atlantidae were hand-picked and counted without further identification. Generally, the specimens are well preserved, and the majority of them are juveniles. Adult specimens where presented were fragmented (*Cavolinia*, *C. pyramidata*, and *C. cuspidata*). The identification of some species or genera was made by their protoconchs (*Creseis*, *Diacria*, and *Cavolinia*), which was the only left residue. The down-core variation of their abundance is presented in Figure 4.

The assemblage observed from 173.5 cm to 165 cm of AEX-15 consists of high percentages of the warm-water *D. trispinosa* (up to 60%) and *C. clava* (27–49%) accompanied by *C. pyramidata* (~20%) and *H. inflatus* (~10%). Between 165 cm and 120 cm (AEX-15) and 320 cm and 291 cm (AEX-23), the fauna is characterized by the high relative abundance of *H. inflatus* (79% in AEX-15 and 46.5% in AEX-23), *C. virgula* (58% in AEX-15 and 47.5% in AEX-23), and *Cavolinia* spp. (22% in AEX-15 and 24.3% in AEX-23) (Fig. 4). The species *C. pyramidata* and *D. trispinosa* decrease dramatically during this interval in AEX-15 (0–6% and 0–11%, respectively), whereas in AEX-23 *D. trispinosa* shows two significant influxes at 305 cm and at 295 cm (up to 6% and 14%, respectively). *Peracle* spp. appear in abundance from 117 cm in AEX-15 and 262.5 cm in AEX-23 (Fig. 4). The interval between 119 cm and 1.5 cm in AEX-15 and 290 cm and 2.5 cm in AEX-23 presents similarities in both cores with percentages of *H. inflatus* decreasing (less than 28% in AEX-15 and 18% in AEX-23) and the epipelagic *Creseis* spp. and *Cavolinia*

spp. being present throughout the whole interval. *Limacina trochiformis* appears for the first time in this interval at 103 cm in AEX-15 and at 192.5 cm in AEX-23, reaching percentages of 62% in AEX-15 and 39% in AEX-23. The stenohaline epipelagic warm-water species *S. subula* enters the fauna at 61 cm in AEX-15 and at 112.5 cm in AEX-23 (Fig. 4).

Pollen distribution pattern

Both cores provided abundant and well-preserved palynomorphs. The qualitative analyses allowed the identification of the most important species: 26 of AP (*Pinus*, *Abies*, *Picea*, *Betula*, *Quercus ilex*, *Quercus robur*, *Cedrus*, *Alnus*, *Juglans*, *Corylus*, *Ulmus*, *Fagus*, *Carpinus*, *Olea*-type, *Pistacia*-type, *Phillyrea*, *Cistus*, *Platanus*, *Tilia*, *Ostrya*, *Acer*, *Buxus*, *Hedera*, *Fraxinus*, *Hippophae*, and *Populus*) and 6 of NAP (Poaceae, Asteraceae, Chenopodiaceae, *Plantago*, *Artemisia*, and *Ephedra*). The down-core variation of their abundance is shown in Figure 5.

Between 173.5 cm and 165 cm of AEX-15, the flora is dominated by Chenopodiaceae (25%), Asteraceae (18%), *Artemisia* (15%), and Poaceae (13%). Apart from *Q. robur* (10%), the AP (*Betula*, *Alnus*, and *Carpinus*) is represented with low percentages (~4%). At 165 cm in the core AEX-15, an increase in the AP concentration and diversity is observed. Specifically, the Mediterranean taxa *Pistacia*, *Phillyrea*, and *Olea* present their first appearance, and deciduous *Quercus* remains a dominant element of the flora (20%) (Fig. 5a). From 107 cm, species such as *Q. ilex*, *Q. robur*, *Abies*, *Alnus*, *Juglans*, *Fraxinus*, and *Olea* become more abundant in AEX-15. The interval between 242.5 cm and 152.5 cm in AEX-23 presents a sharp decline in percentages of *Populus*, *Fraxinus*, *Hedera*, *Pistacia*, *Olea*, and *Phillyrea*. From 152.5 cm to the top of AEX-23, the abovementioned species increase in abundance (Fig. 5b).

Dinoflagellate distribution pattern

Nineteen species of dinoflagellate cysts were recognized from the sediments of both cores (*Brigantedinium simplex*, *Brigantedinium cariacense*, *Polysphaeridium zoharyi*, *Impagidinium aculeatum*, *Operculodinium israelianum*, *Impagidinium patulum*, *Impagidinium sphaericum*, *Lingulodinium machaerophorum*, *Nematosphaeropsis labyrinthus*, *Operculodinium centrocarpum*, *Tetactodinium psilatium*, *Spiniferites delicatus*, *Tuberculodinium vancampoae*, *Spiniferites mirabilis*, *Spiniferites bentorii*, *Spiniferites ramosus*, *Spiniferites bulloideus*, *Spiniferites hyperacanthus*, and *Bitectatodinium tepikiense*). Their down-core variation is shown in Figure 7.

Between 173.5 cm and 165 cm of AEX-15, dinocysts exhibit low relative abundances with the only exceptions being the *S. ramosus* (37%) and *L. machaerophorum* (17%). Dinoflagellate cyst percentages between 165 cm and 120 cm of AEX-15 present highly variable down-core patterns with the species *S. ramosus*, *L. machaerophorum*, and *O. centrocarpum* being dominant in the whole interval.

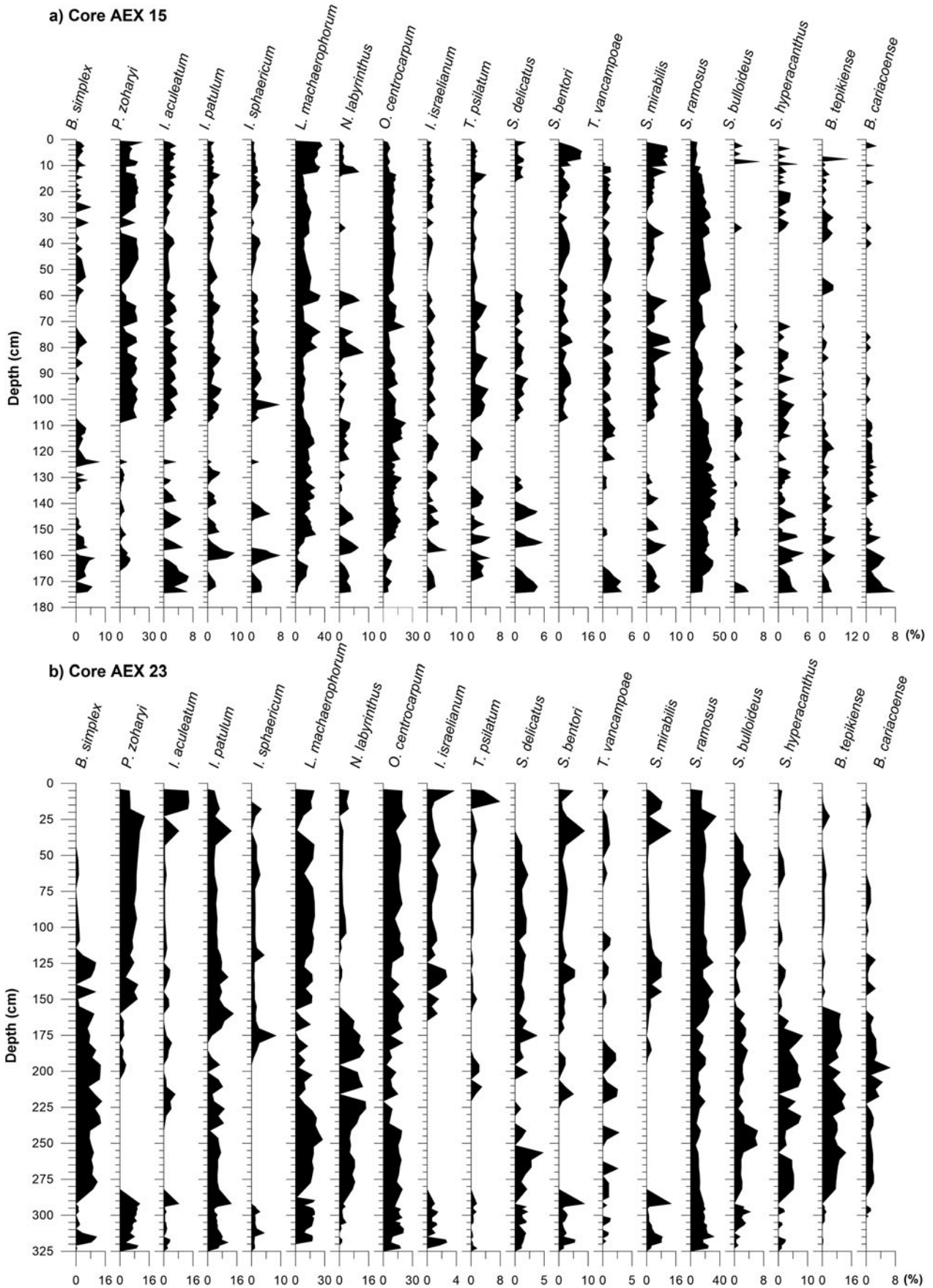


Figure 7. Frequency curves of dinoflagellate cysts for core AEX-15 (a) and core AEX-23 (b).

In AEX-23 toward 291 cm, the species *B. simplex*, *P. zoharyi*, *I. patulum*, and *S. mirabilis* are also present with higher percentages than in AEX-15. Between 120 cm and 107 cm in AEX-15 and 291 cm and 242.5 cm in AEX-23, species such as *P. zoharyi*, *I. aculeatum*, *I. sphaericum*, and *S. mirabilis* present an abrupt disappearance. From 93 cm in AEX-15 and 152.5 cm in AEX-23 to the top of both cores, the dinoflagellate cysts assemblage recovers with species such as *L. machaerophorum*, *S. bentorii*, *S. mirabilis*, and *Spiniferites* dfsp., reaching their maximum relative abundances (37%, 12%, and 7% respectively), whereas the species *S. hyperacanthus*, *B. tepikiense*, and *B. cariacoense* exhibit low relative abundance.

Stable isotopes

Oxygen and carbon isotopic values are presented in Figures 8 and 9. Oxygen isotopic values of *G. ruber* (Fig. 9b) display considerable scatter in the intervals between 173.5 cm and 120 cm of AEX-15 and 320 cm and 291 cm of core AEX-23. Less variable and rather light values are observed in the part toward the top of both cores. In detail, $\delta^{18}\text{O}$ values between 173.5 cm and 120 cm in core AEX-15 range from -2.86‰ to $+4.15\text{‰}$ (Fig. 9b); the most significant enrichments up to $\sim 4\text{‰}$ are evident at 160.5 cm (3.24‰) and at 158.5 cm (4.15‰). At about 146 cm, a shift to heavier $\delta^{18}\text{O}$ values is observed (from 0.2‰ to 0.8‰) and is followed by a recovery of light values. The same pattern is observed again at 141 cm with $\delta^{18}\text{O}$ values ranging from 0.1‰ to 0.9‰ . In core AEX-23 between 320 cm and 291 cm, slight enrichment (-0.1‰ to $+1\text{‰}$) in $\delta^{18}\text{O}$ values is observed. From this point on, $\delta^{18}\text{O}$ values are relatively stable in both

cores, stabilizing around zero, with the only exceptions of three peaks in AEX-15 (a negative -2.8‰ at 111 cm and two positives at 89 cm [$+1.8\text{‰}$] and at 43 cm [$+1.29\text{‰}$]) and two positive peaks in AEX-23 ($+1.07\text{‰}$ at 62.5 cm and $+1.34\text{‰}$ at 2.5 cm).

The carbon isotope analyses ($\delta^{13}\text{C}$) exhibit more scatter (Fig. 8a) than the $\delta^{18}\text{O}$ records, especially in the lower part of both cores. In AEX-15, $\delta^{13}\text{C}_{G. ruber}$ shows a gradual decrease up to 120 cm, culminating in a minimum at about 142.5 cm. The only exceptions in this interval are the following positive peaks: 160.5 cm ($+1.2\text{‰}$), 158.5 cm ($+1.6\text{‰}$), and 144.5 ($+2.4\text{‰}$). From 120 cm to the top of this core, the general trend shows values ranging from approximately $+0.3\text{‰}$ to $+1\text{‰}$ with two distinct negative excursions at 41 cm (-1.2‰) and at 111 cm (-1.1‰) along with a positive one at 45 cm ($+2.2\text{‰}$). In AEX-23, between 320 cm and 291 cm $\delta^{13}\text{C}$ values are depleted (from -0.6‰ to $+0.3\text{‰}$). The interval between 288 cm and 212.5 cm is characterized by heavier values (average $+0.6\text{‰}$). From 212.5 cm to the top, $\delta^{13}\text{C}_{G. ruber}$ exhibits slightly lighter values with a negative peak at 202.5 cm (-0.2‰).

DISCUSSION

Time stratigraphic framework and sedimentation rates

The age model of the analyzed cores was established by linear interpolation between all dating points. In addition to the AMS ^{14}C dates, the biostratigraphic control provides two well-dated correlation horizons, the biozone Ia/Ib and Ib/Ic boundaries of Casford et al. (2002). Correlations are also

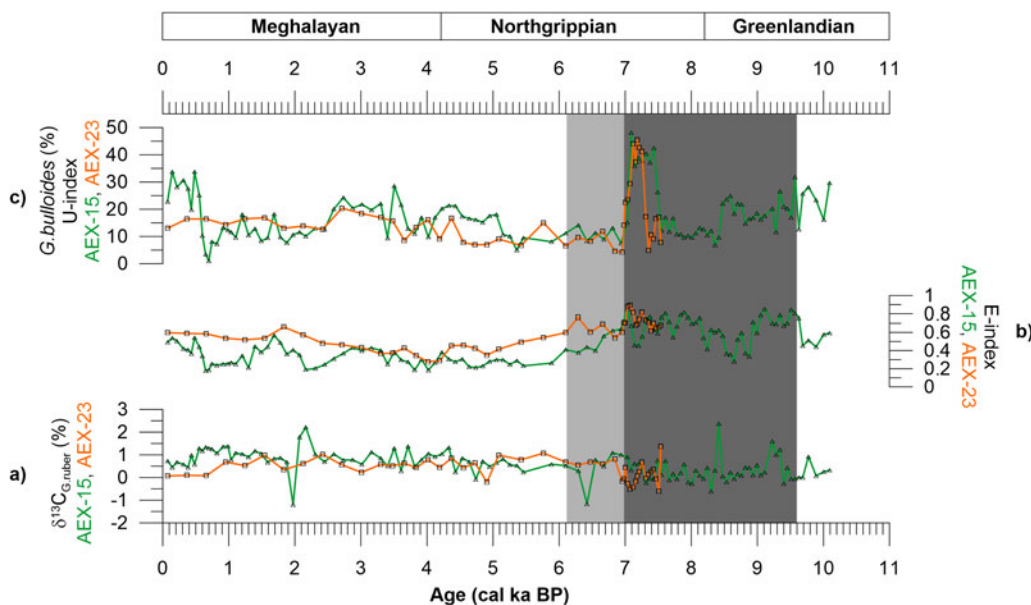


Figure 8. Productivity records (green line with triangle for AEX-15 and orange line with square for AEX-23). (a) Carbon isotope record ($\delta^{13}\text{C}_{G. ruber}$). (b) Eutrophication index (E-index). (c) *G. bulloides* % abundance (U-index). Gray and light gray bands correspond to the sapropel S1 and its oxidized part, respectively. (For interpretation of the references to color in this figure legend, the reader is referred to the web version of this article.)

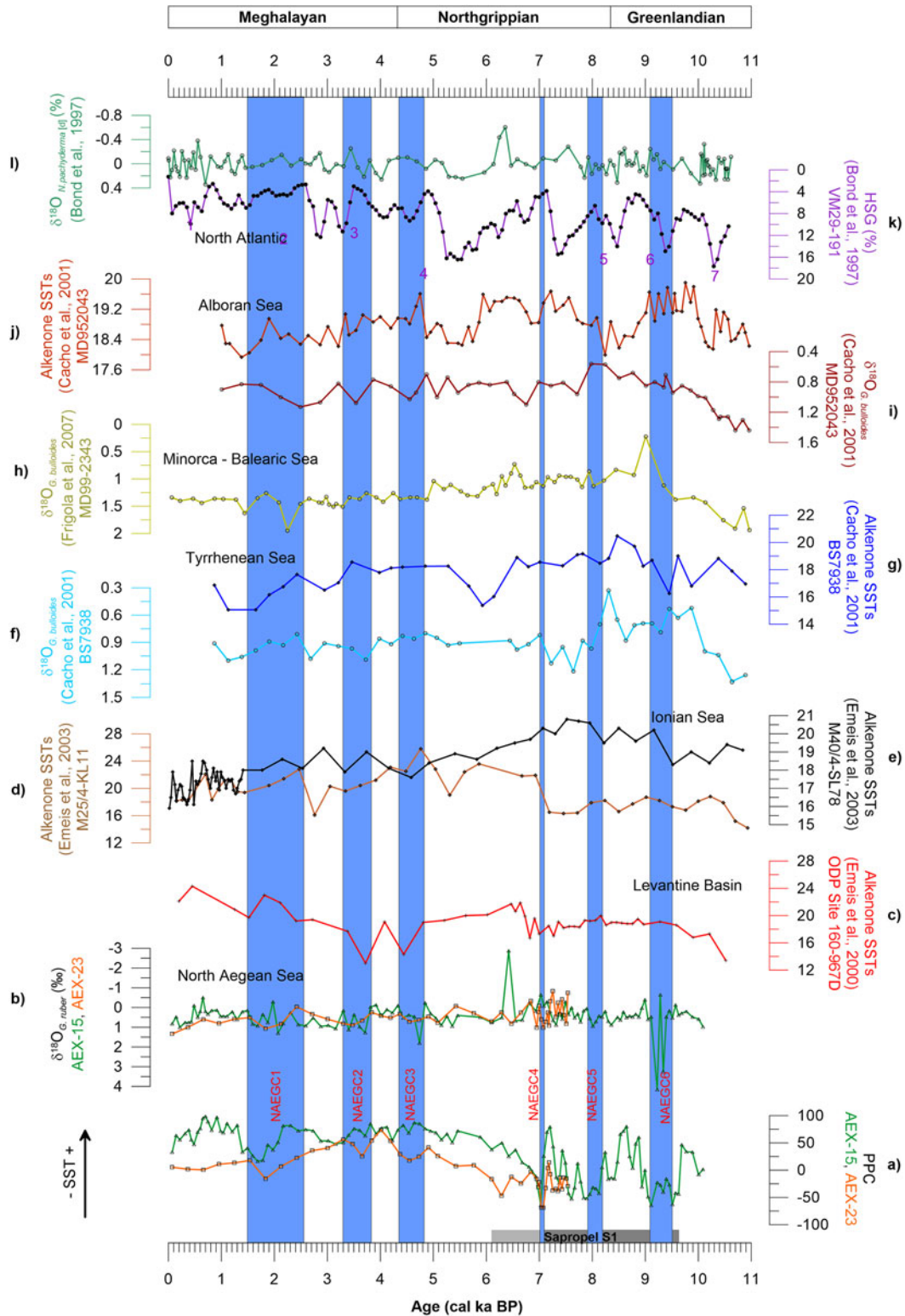


Figure 9. Comparison of North Aegean results (green line for AEX-15 and orange line for AEX-23) with relevant climate reconstructions of the eastern, central, and western Mediterranean and North Atlantic, including the following: (a) Planktonic paleoclimatic curve (PPC). (b) Oxygen isotope record ($\delta^{18}O_{G. ruber}$). (c) Alkenone sea surface temperatures (SSTs) of ODP site 160-967D in the Levantine Basin (Emeis et al., 2000). (d and e) Alkenone SSTs from cores M25/4-KL11 and M40/4-SL78, respectively, from the Ionian Sea (Emeis et al., 2003). (f) $\delta^{18}O_{G. bulloides}$. (g) Alkenone SSTs of core BS7938 from the Tyrrhenean Sea (Cacho et al., 2001). (h) $\delta^{18}O_{G. bulloides}$ from core MD99-2343 in the Balearic Sea (Frigola et al., 2007). (i) $\delta^{18}O_{G. bulloides}$. (j) Alkenone SSTs of core MD952043 in the Alboran Sea (Cacho et al., 2001). (k) Hematite stained grains (HSG)-based cold events. (l) $\delta^{18}O_{N. pachyderma}$ (d) for VM29-191 (Bond et al., 1997). Blue bands correspond to North Aegean cooling events, whereas gray and light gray bands to the sapropeal S1 interval and its oxidized part. (For interpretation of the references to color in this figure legend, the reader is referred to the web version of this article.)

suggested by variations in the Ba/Al and C_{org} concentrations. These are useful chronological standards for dating late Quaternary sequences in the central and eastern Mediterranean (including the Aegean Sea; Casford et al., 2002, 2007; Geraga et al., 2010; Kontakiotis et al., 2013; Drinia et al., 2016; Kontakiotis, 2016) because of their Mediterranean-wide applicability and synchronicity (Capotondi et al., 1999; Hayes et al., 1999; Casford et al., 2001).

Based on our age model, the planktonic foraminifera distribution pattern allows identification of the biozone Ia/Ib and Ib/Ic boundaries (Casford et al., 2002). Subzone Ic (173 cm–120 cm, AEX-15) was identified by the warm subtropical species (*G. ruber* f. *rosea*, and *O. universa*) as well as by *T. quinqueloba* and *G. bulloides* (Fig. 3a). The sharp increase in the abundance of *G. inflata* and *N. pachyderma* at 120 cm in AEX-15 and at 291 cm in AEX-23 is inferred to mark the onset of the Ib subzone, whereas the Ia/Ib boundary is marked by their decrease (107 cm in AEX-15 and 242.5 cm in AEX-23). This subzone is also characterized by the maximum abundances of *G. ruber* f. *alba* and the sharp increase of *N. pachyderma* at the upper part (Fig. 3).

Although the onset of sapropel S1 (~9.6 cal ka BP; Casford et al., 2002, 2007) is clearly depicted in organic carbon content (C_{org} ; sharp increase from background values, Fig. 2), its termination is obscured by oxidation processes. In this case, Ba is a more reliable proxy to record the original thickness of the sapropel layer (De Lange et al., 2008). Therefore, in core AEX-15, the vertical distribution of C_{org} with respect to Ba/Al and Ba_{ex} shows that sapropel S1 deposition commenced at 165 cm and terminated at 107 cm, with the sediments between 107 and 120 cm representing the oxidized sapropel. In core AEX-23, elemental profiles corroborate termination at 242.5 cm, while the oxidation zone extends up to 291 cm, and the onset of S1 deposition is not reached in the core (Fig. 2). As a result, the upper boundary of S1 is determined by the Ba/Al ratios, which have been dated at 6.1 ka in the Aegean Sea (Casford et al., 2007). This age is consistent with the Ia/Ib boundary, which is defined by the termination of the higher percentages of *G. inflata* (Casford et al., 2002) and correlates well with the AMS dating (5170 cal yr BP) at a 103 cm depth. Assemblage Ic, which is mainly characterized by the sapropel fauna, also occurs all over the Aegean Sea and ends on average at 7.0 cal ka BP (Casford et al., 2002).

Based on the adopted chronostratigraphic framework, sediment levels used in this study span the last 10.1 cal ka BP for core AEX-15 and 7.5 cal ka BP for AEX-23, with an average sedimentation rate of 17.3 and 42.8 cm/ka, respectively (Fig. 2). These rates assume that the sediment accumulation has been consistent throughout each interval, and they are in good agreement to those reported in the north Aegean Sea (>20 cm/ka; Zachariasse et al., 1997; Kuhnt et al., 2007; Kotthoff et al., 2008a, 2008b; Kontakiotis, 2016). The differing rates between the two cores expresses the heterogeneity of sedimentation rates previously documented in the north Aegean Sea (Roussakis et al., 2004), resulting from large seafloor topographic contrasts and variable

sedimentary processes in the study area. In particular, the higher sedimentation rate of core AEX-23 is explained by the adjacent slope that transports sedimentary inputs by deep bottom currents.

Paleoenvironmental reconstruction

The geochemical records ($\delta^{18}O$, $\delta^{13}C$), in combination with the foraminiferal, pteropod, pollen, and dinocyst abundance records, are best interpreted as a series of successive changing, climatically driven dynamic regimes. The evidence of these changes is interpreted and discussed in terms of the events that mainly accompanied the transition out of the late glacial period (Termination 1b; Casford et al., 2002), the deposition of sapropel S1 during the HCO, and the post-sapropel interval. These are described subsequently as a series of transitory states together with a detailed documentation of the main isotopic and faunal/floral changes recognized in our north Aegean records (Figs. 6, 8 and 9). The timing of each state is in agreement with relevant paleoceanographic reconstructions (Siani et al., 2013; Grant et al., 2016) and may be considered typical of the particular climatic/circulation regime of the study area.

Termination 1b

From ~10.1 cal ka BP to the onset of the sapropel S1 layer, a gradual depletion of $\delta^{18}O$ is recorded and can be attributed to the global signal of meltwater pulse 1B. The slight shift to lighter $\delta^{18}O$ values signifies a gradual freshening of the upper water column. The close similarity in timing of the $\delta^{18}O$ changes in both *G. ruber* foraminiferal calcite (core AEX-15) and seawater (core LC-21; Marino et al., 2009) provides evidence that this $\delta^{18}O_{G. ruber}$ depletion prior to S1 deposition is dominated by the inflow of isotopically light, fresher surface waters into the Aegean Sea, and the consequent sea-surface freshening propagates through the entire eastern Mediterranean away of the sites of freshwater discharge (including the north Aegean Sea) because of the efficient large-scale counterclockwise circulation of the surface waters.

However, the difference in magnitude with relevant $\delta^{18}O$ data from the south Aegean Sea during this time (e.g., Marino et al., 2009; Fhlaithearta et al., 2010) suggests that the advection of fresher surface waters from the north through river runoff becomes inhibited because of the intense thermohaline front to the north of the study core sites, which prevents southward extension of the influence of the north Aegean surface waters. Early Holocene pollen records indicate increased precipitation over the north Aegean borderland (Kotthoff et al., 2008a, 2008b), and so the position of this front was controlled by the local cyclonic circulation of the basin. Its intensity was the same or even stronger than today.

The accompanied high values (up to 50%) of PPC and the increasing trend of warm temperate summergreen, as well the subtropical-temperate dinocysts (*P. zoharyi*, *I. aculeatum*, *I. sphaericum*, *S. mirabilis*, and *Tetactodinium psilatium*)

(Figs. 6 and 7c), indicate the climate amelioration. This interval is marked by high relative abundances of warm mixed-layer species (including the pteropod *Diacria trispinosa*) and the high abundance of *G. glutinata* (Figs. 3 and 4). The former is interpreted as indicative of an increase of depth and extent of the thermocline, and therefore the strengthening of summer stratification in a generally well-oxygenated environment. The shift toward the dominance of the shallower-living species *G. glutinata* could be explained in terms of increased seasonality. The opportunistic response of this species to any increase in nutrient variability is also in agreement with Casford et al. (2002), who presented a case for an initial period of 100–1500 yr of nutrient accumulation prior to the onset of S1 deposition. This is evident in all the productivity-related records, evidenced by the enrichment in $\delta^{13}\text{C}$ ($\sim 1\%$; equivalent to the second primary event of Casford et al. [2007]) and the increased numbers of E-index and *G. bulloides* abundances around 9.8 cal ka BP (Fig. 8c). The evidence of seasonality is further reinforced by the presence of *G. bulloides* and *G. ruber* f. *alba*, which are the main exponents of the seasonal contrasts governing planktonic foraminiferal assemblages in the Mediterranean Sea during the Holocene (Wilke et al., 2009; Wit et al., 2010; Goudeau et al., 2015).

Sapropel S1 interval

Distinct fluctuations in the isotopic and faunal records of both cores indicate a remarkable climate and hydrographic variability during this interval. By 9.6 cal ka BP, S1 deposition commences, and it coincides with the abrupt increase of primary productivity ($0.7 < \text{E-index} < 0.8$, *G. bulloides* $\sim 30\%$), the start of the overall $\delta^{13}\text{C}$ depletion, the faunal shift to a dominance of mixed-layer species, and the dominance of AP over NAP (Figs. 6 and 8). Steadily low (stabilized around zero) $\delta^{18}\text{O}$ values, together with high PPC values, reflect a climatic invasion toward high temperatures, with the only exception of three events (obtained around 9.5–9.1, 8.2–7.9, and 7.1–7.0 cal ka BP), where lower PPC and heavier $\delta^{18}\text{O}$ values reflect lower SSTs during the early–middle Holocene (Greenlandian–Northgrippian stages) (Fig. 9a and b). These short-term cooling events are also reflected in significant faunal changes in the north Aegean Sea, such as the increase in abundance of *G. bulloides* and *T. quinqueloba* replacing the SPRUDTS group. Immediately after these events, faunal abundance and isotopic profiles return rapidly to their previous enhanced levels, and a gradual increase can be observed for PPC values (Fig. 9a and b).

The warm/humid conditions because of the monsoon intensification (Rossignol-Strick, 1985) enhanced riverine inputs and resulted in low salinity and eutrophic waters, as these are documented by the elevated percentages of *T. quinqueloba*, especially between 8.2 and 7.5 cal ka BP. This is further supported by the contribution of Black Sea outflow after 8.0 cal ka BP (Sperling et al., 2003; Ehrmann et al., 2007). Moreover, the $\delta^{13}\text{C}$ signatures reveal that the rainfall was more intense during that time, while the *G. bulloides*

abundance records (Fig. 8c) show that the freshening of sea-surface waters was greater toward 7.0 cal ka BP. The reduction in NAP and the simultaneous increase in arboreal trees at 7.7 to 6.9 cal ka BP suggest higher humidity, which is in accordance with the pollen-based climatic models (Kotthoff et al., 2008a), exhibiting 50% higher precipitation than in the previous time interval.

From the faunal content of the oxidized part of S1, it seems that the bottom-water oxygenation has resumed earlier than the final ending of sapropelic conditions indicated by Ba concentration. Specifically, the occurrence of the deep mixing species *G. inflata* and *N. pachyderma* reflects the prevalence of homogenization/overturn conditions in the water column (Rohling et al., 1997; Casford et al., 2002). The subsequent regime is also characterized by the slightly colder and less eutrophic conditions, as evidenced by the PPC drop and the relatively lower E-index values (Figs. 8b and 9a). During this interval (7.0–6.1 cal ka BP), the presence of the bathypelagic *Clio pyramidata*, *C. cuspidata*, and *Peracle* spp. suggest the recovery of the thermohaline circulation. In addition, a reduction in AP and an increase in NAP along with a slight retreat in cool temperate summergreen vegetation characterize the termination of the S1. The dinocyst species *P. zoharyi*, *I. aculeatum*, and *I. sphaericum* present an abrupt disappearance in this interval, whereas an increase in abundance of *L. machaerophorum*, *O. centrocarpum*, *Brigantedinium simplex*, and *Spiniferites* sp. is observed (Fig. 7). Toward the Meghalayan, warm oligotrophic species (*G. ruber alba*, *G. sacculifer*, *G. rubescens*, and *G. siphonifera* gr.) prevail in the planktonic fauna, implying a significant reduction in primary productivity and the establishment of modern oligotrophic to mesotrophic conditions.

Late Holocene (Meghalayan stage) interval

Climatic and oceanographic boundary conditions of the north Aegean Sea change in the late Holocene. The main change is characterized by a decrease in *G. sacculifer* and *O. universa* (Fig. 3) that reveals a river-runoff reduction and further coincides with the $\delta^{13}\text{C}$ enrichment trend (Fig. 8a) observed in both cores. This is further associated with clay mineral data known from the literature (Roussakis et al., 2004; Ehrmann et al., 2007) across this interval, which indicate a change in weathering conditions on land that points to particularly dry conditions in the north Aegean catchment. Moreover, the reduction in the surface water Black Sea outflow at around 4.5 cal ka BP (Sperling et al., 2003; Kuhnt et al., 2007) has probably caused an increase in sea-surface salinity, which is also testified by the slightly heavier (up to 0.8‰ enrichment) planktic $\delta^{18}\text{O}$ record (Fig. 9b), the reduction in the relative abundance of *L. trochiformis*, and the appearance of the stenohaline species *S. subula* at 3.3 cal ka BP (Fig. 4) (Buccheri et al., 2002). These observations support the idea of a general trend to climatic aridification during the Meghalayan stage, which is in accordance with the salinity increase and oligotrophic nature of the water column of the modern north Aegean Sea.

Holocene climate variability and its relationship to large-scale climatic changes

Our qualitative SST reconstructions for the north Aegean Sea reveal a distinct pattern of climate oscillations that generally agrees with the previously reported series of millennial-scale fluctuations in the region (Rohling et al., 2002; Kotthoff et al., 2008a, 2008b; Kontakiotis, 2016), but which enriches that picture with centennial-scale details. The Holocene climatic instability of the study area is further supported by episodes of brief cooling, with the suggested mechanism that caused the development of these cooling spells to involve local features, such as intensified orographically channeled, northerly air outbreaks and/or land-sea contrasts (Rohling et al., 2002; Brayshaw et al., 2011). Six distinct sea-surface cooling events in the north Aegean Sea (referred to as “NAEGC”) have been identified in the present study (Fig. 9), corresponding to similar short and abrupt cold/dry events that have been described in different basins in the Mediterranean (Cacho et al., 2001; Sbaifi et al., 2004; Geraga et al., 2008; Frigola et al., 2007; Combourieu-Nebout et al., 2009, 2013; Schmiedl et al., 2010; Desprat et al., 2013; Table 1). Furthermore, similarities to the GISP2 ice core, and their coincidence with times of reduced monsoonal rainfall, lowering of lake levels in eastern Africa (Gasse, 2000), and glacier advances in Europe (Denton and Karlen, 1973), suggest correlations with the paleoclimatic changes occurring at high latitudes of the northern Atlantic and worldwide (Bond et al., 1997, 2001; Mayewski et al., 2004; Wanner et al., 2011, 2014). These correlations reinforce earlier observations of teleconnections between Holocene climate variability of the (sub)tropics and the high latitudes at multicentennial to millennial timescales (Rohling et al., 2002; Marino et al., 2009). Each cooling event results in an approximate drop in temperature of 2–4° C, independently confirming what previous studies, using different methods, have shown (Rohling et al., 1997, 2002; Cacho et al., 2001).

Impact of abrupt centennial-scale Holocene cooling events on eastern Mediterranean hydrologic regime

The most pronounced Holocene abrupt cooling events (NAEGC6–NAEGC4) occurred at 9.5–9.1, 8.2–7.9, and 7.1–7.0 cal ka BP. They punctuate the wettest phase as deduced by our pollen records during the Greenlandian–Northgrippian stages, and they seem to exert important control on sapropel deposition within the Mediterranean Sea. All these events parallel the widely documented abrupt coolings punctuating the early–middle Holocene: the “Boreal Oscillation” at ~10.0 cal ka BP (Björck et al., 2001); the “9.3 ka event” (Rasmussen et al., 2007); the “8.2-event” (Alley et al., 1997); and a final event at ~7.4 cal ka BP (Bond et al., 2001), which likely corresponds to the drier episode detected at ~7.0 cal ka BP (Fig. 6). These events were related to a series of recurrent (dry) atmospheric climatic anomalies, which can be furthermore associated with meltwater pulse perturbation of the north Atlantic climate.

Table 1. List of short Holocene cooling events recorded in the North Aegean Sea and their correspondence to the relevant dry/cooling events in different basins (Alboran Sea, Balearic Sea, Tyrrhenian Sea, Siculo-Tunisian Strait, Adriatic Sea, Ionian Sea, and Aegean Sea) of the Mediterranean Sea, in the North Atlantic, and globally. Names of each event were provided followed by ages in brackets (in cal ka BP). In cases where the events are not named, only ages are given.

This study	MEDITERRANEAN SEA							North Atlantic	Globally			
	Aegean Sea	Ionian Sea	Adriatic Sea	Siculo-Tunisian Strait	Tyrrhenian Sea	Minorea	Alboran Sea					
North Aegean Sea	Schmiedl et al. (2010), Kotthoff et al. (2008a)	Geraga et al. (2005)	Geraga et al. (2008)	Combourieu-Nebout et al. (2013)	Desprat et al. (2013)	Cacho et al. (2001)	Shaffi et al. (2004)	Frigola et al. (2007)	Cacho et al. (2001)	Combourieu-Nebout et al. (2009)	Bond et al. (1997)	Mayewski et al. (2004)
NAEGC1	2.6–1.5	2.7–2.4				TC1 (1.9–1.0), TC2 (3.45–2.5)	SCE1 (1.7–0.9), SCE2 (3.2–2.5)	M1 (1.8–1.4), M2 (2.6–2.3)	AC1 (1.90–1.01)	APC2 (2.6–2.3)	NAC2 (2.8)	RCC4 (3.5–2.5)
NAEGC2	3.8–3.3						SCE2 (3.2–2.4), SCE3 (3.9–3.5)	M3 (3.4–3.1)		APC3 (3.77–3.14)		
NAEGC3	4.8–4.3	4.4–4.0			4.5			M5 (5.3–4.7), M7 (7.4–6.9)	AC2 (5.94–4.75)	APC4 (6.0–4.5)	NAC3 (4.3)	
NAEGC4	7.1–7.0				7.3–6.7		SCE5 (7.6–6.9)	M8 (9.0–7.8)	AC3 (9.08–7.56)	APC5 (8.5–7.9)	NAC5 (8.2)	RCC1 (9.0–8.0)
NAEGC5	8.2–7.9	8.3–8			8.5–7.9		SCE5 (8.2–7.5)			APC6 (9.6–8.9)	NAC6 (9.5)	
NAEGC6	9.5–9.1				9.5–9.1		TC4 (9.62–9.13), SCE6 (9.9–9.0)					

In particular, there are two sharp negative peaks in the PPC at 9.6 and 9.1 cal ka BP, coupled with two intervening $\delta^{18}\text{O}$ positive excursions (at ~ 9.3 and 9.2 cal ka BP), which are superimposed on a broader period of climatic deterioration in the Aegean Sea during this time interval. Cooling event NAEGC6 is coeval with relevant cooling events in Tyrrhenian basin centered at 9.5 cal ka BP (Rohling et al. 1997; Sbaifi et al., 2004) and further coincides with aridification events based on pollen assemblage changes in the Alboran Sea (Combourieu-Nebout et al., 2009) (Table 1). The forest decline (Fig. 6d) at this time is associated with a prominent SST cooling event in the eastern Norwegian Sea (Berner et al., 2010) and coincides with cooling in the NGRIP (North Greenland Ice Core Project) record toward 9.95 cal ka BP, although this anomaly is not consistent across different Greenland records (Rasmussen et al., 2007). NAEGC6 is possibly linked to an Atlantic meridional overturning circulation (AMOC) reduction because of a meltwater pulse at St. Lawrence Bay (Fleitmann et al., 2008) or alternatively to contemporaneous outburst floods from proglacial lakes such as Lake Agassiz (Teller et al., 2002), Lake Labrador-Ungava (Jansson and Kleman, 2004), Lake Superior (Yu et al., 2010), or Baltic ice Lake in SW Sweden (Nesje et al., 2004), and with solar activity minima (Bond et al., 2001; Magny and Bégeot, 2004).

The following NAEGC5 event, constrained here by progressive $\delta^{18}\text{O}$ enrichment to maximum values ($+0.95\%$) centered on 8.1 cal ka BP, corresponds to the regional expression of the 8.2 cal ka BP cold/arid north Atlantic event (Bond et al., 1997, 2001). Surprisingly, that $\delta^{18}\text{O}$ enrichment appears coeval in time but not in amplitude to the negative 2% $\delta^{18}\text{O}_{\text{ice}}$ event in the Greenland ice cores (Rasmussen et al., 2007), which is thought to represent an $\sim 6^\circ\text{C}$ cooling of the air temperature over Greenland Summit (Alley et al., 1997). The significant decline in the PPC (from $+32\%$ to -42% ; Fig. 9a) also coincides well with pollen-based data (drop in deciduous trees; Fig. 6b and c) and provides evidence for an abrupt winter SST minimum on the northern Aegean borderlands in response to the 8.2 cal ka BP AMOC reduction (LeGrande et al., 2006; Wiersma and Renssen, 2006). The intensification of the atmospheric circulation (Marino et al., 2009) during NAEGC5 led to good ventilation conditions in the Aegean basin interrupting the S1 deposition, synchronously with the termination of the formation of the enriched in organic matter layer (organic rich layer; Cacho et al., 2002) in the Alboran Sea (western Mediterranean).

The sharp drop in PPC around 7.0 cal ka BP corresponds to the NAEGC4 cooling event (Fig. 9). This event is attributed to the strengthening and increases in frequency of winter cooling, driven by changes in intensity of high-latitude continental air masses (Rohling et al., 2002). The intensification of the atmospheric circulation during this time interval led to improved ventilation conditions in the eastern Mediterranean basin. We argue that this cooling event may have induced the resumption of deep-water formation in the north Aegean Sea. Indeed, density of the surficial waters was sufficiently high during that time interval to enable the ventilation of the

deep north Aegean basin, because of the counterbalance between salinity depletion and SST decrease. This notion is also confirmed by the higher benthic $\delta^{13}\text{C}$ ($\sim 1.1\text{--}1.4\%$) values, the significant increase of the benthic foraminifera *Cibicides* (Kuhnt et al., 2007; Abu-Zhied et al., 2008; Schmiedl et al., 2010) and the planktonic *G. inflata* recorded in the studied and other cores between 7.0 and 6.0 cal ka BP (Casford et al., 2002; Geraga et al., 2010; Kontakiotis, 2016), attesting the return to oxic conditions and the resumption of the north Aegean deep-water formation just after the end of S1. Similar short cooling events were detected using foraminiferal and pollen assemblages in the Minorca Basin (M7 event; Frigola et al., 2007) and the Siculo-Tunisian Strait (at 7.3–6.7 cal ka BP; Desprat et al., 2013) (Table 1). In the Adriatic and Aegean basins (AdC5 and C69-ST2 events, respectively) (Geraga et al., 2005; Jimenez-Espejo et al., 2008; Combourieu-Nebout et al., 2013), these events are supposed to be responsible for sapropel termination. Following the interpretation of Rohling et al. (2002) and Casford et al. (2003), the absence of these events in $\delta^{18}\text{O}_{G. ruber}$ was suggested to reflect a seasonal offset between climate forcing and the proxy carrier, as cooling is a winter phenomenon and therefore is not recorded by *G. ruber*, which thrives in the summer mixed layer.

At 6.3 cal ka BP, negative values in the PPC (-46%) of core AEX-23 are observed that are not followed by any enrichment in $\delta^{18}\text{O}_{G. ruber}$ in both cores or negative PPC values of AEX-15 (Fig. 9a and b). We suggest that the observed negative PPC peak is marked by increased *T. quinqueloba* percentages (59%; Fig. 3). A similar decrease in arboreal vegetation has also been observed during that time and possibly highlights the onset of the transition toward drier mid- to late Holocene.

The nature and intensity of the NAEGC3 event at 4.8–4.3 cal ka BP in our isotope record, resembling the previous events, also points to a climate origin and hence is thought to be the result of a cold and dry episode. The PPC drop of $\sim 20\%$ in both cores is in phase with concurrent expansion of NAP (Fig. 6f) and is associated with the 4.2 cal ka BP north Atlantic Holocene cold event (Bond et al., 1997, 2001), as well as with U_{37}^k -SST minima along the Mediterranean Sea (Emeis et al., 2000, 2003; Cacho et al., 2001) (Fig. 9). NAEGC3 could also correspond to the ACP4 of the Adriatic Sea (Combourieu-Nebout et al., 2009), M5 in Minorca Basin (Frigola et al., 2007), the 4.5 cal ka BP event of the Siculo-Tunisian Strait (Desprat et al., 2013), the Ionian and Levantine Seas (Emeis et al., 2000, 2003; Geraga et al., 2008), AdC3 in Adriatic Sea (Combourieu-Nebout et al., 2013), and the 4–4.4 cal ka BP of the north Aegean Sea (Kotthoff et al., 2008a; Schmiedl et al., 2010) (Table 1). This event is further evident on the northern side of the Mediterranean Basin (Magny et al., 2009; Peyron et al., 2011), in the Medjerda Valley (Faust et al., 2004; Zielhofer et al., 2004), and in the speleothems of Gueldaman Cave (Ruan et al., 2016). This cold episode, largely expressed in climate records as expanding from polar to tropical regions, has been attributed to a weakening of the Northern Hemisphere summer

insolation (Bond et al., 2001; Mayewski et al., 2004). This cold and arid spell, although weakened in the north Aegean Sea (Kontakiotis, 2016), caused the temporary enhanced deep-water ventilation and consequently the restoration of oxic conditions in the north Aegean. This is further supported by the low accumulation rates of marine and terrestrial biomarkers and elevated $\delta^{15}\text{N}$ values from nearby north Aegean cores (Gogou et al., 2007), which indicate that the deep north Aegean was fully oxygenated during that period.

The interval between 3.8 and 3.3 cal ka BP comprises heavier $\delta^{18}\text{O}$ values and a drop in the PPC of $\sim 25\%$ in both cores (Fig. 9a and b). This episode (NAEGC2) coincides with equivalent events in the Mediterranean Sea based on planktonic foraminifera and pollen assemblages (Sbaffi et al., 2004; Frigola et al., 2007; Combourieu-Nebout et al., 2009) (Table 1). In the Tyrrhenian Sea, this event appears to be intense with an approximate decrease in SST of 2.5–3.5°C based on alkenone and the modern analogue technic SSTs reconstructions (Sbaffi et al., 2004). At 2.6–1.5 cal ka BP, heavier isotope values, significant drop in PPC, and abrupt deciduous forest reduction have been documented in our cores corresponding to NAEGC1 event (Fig. 9). This is correlated with the dry episode recorded from marine cores in the eastern Mediterranean between 3.0 and 1.7 cal ka BP (Magny et al., 2003; Jalut et al., 2009). It is also evident in the western and central part of the Mediterranean between 3.2 and 1.4 cal ka BP (Cacho et al., 2001; Sbaffi et al., 2004; Frigola et al., 2007; Combourieu-Nebout et al., 2009) and is correlated to the NAC2 event (Bond et al., 1997) (Table 1).

CONCLUSIONS

A multidisciplinary study of the sediments of cores AEX-15 and AEX-23 from the North Aegean Trough enables the understanding of long- and short-term oceanographic and climatic variations of the last ~ 10 cal ka BP in the north Aegean Sea. The interpretations are based on the down-core variations of the stable isotope ($\delta^{18}\text{O}$, $\delta^{13}\text{C}$) values and the abundances of planktonic foraminiferal, pteropod, and palynomorph assemblages, in association with temperature- and productivity-related paleoceanographic data. Overall, the high sedimentation rates encountered in the analyzed cores and the high-resolution sampling have contributed to the detection of six cold/arid events throughout the Holocene, as well as the preservation of their processes and mechanisms. Although absolute age control provides only modest constraint, these events also appear to correlate with equivalent events documented within and beyond the Mediterranean Sea in north latitude areas, northeastern Africa, and the Middle East, pointing to large, hemispheric-scale teleconnections.

ACKNOWLEDGMENTS

This work was supported by the National Strategic Development Program EE (NSRF 2007–2013) and was carried out in the frame of the “YPOTHER” project realized at the Institute of Geology and Mineral Exploration in collaboration with the Institute of

Oceanography of the Hellenic Centre for Marine Research (HCMR). We wish to thank the captain and crew of R/V *Aegaeo* (HCMR) for their technical assistance during the YPOTHER cruises, and Mrs. A. Androni (HCMR) for the organic carbon analysis. Constructive comments by two anonymous reviewers have been essential in improving this manuscript and Dr. Louisa Bradtmiller (associate editor) is thanked for her editorial handling.

REFERENCES

- Abu-Zied, R.H., Rohling, E.J., Jorissen, F.J., Fontanier, C., Casford, J.S.L., Cooke, S., 2008. Benthic foraminiferal response to changes in bottom water oxygenation and organic carbon flux in the eastern Mediterranean during LGM to Recent times. *Marine Micropaleontology* 67, 46–68.
- Alley, R.B., Mayewski, P., Sowers, T., Stuiver, M., Taylor, K.C., Clark, P.U., 1997. Holocene climatic instability: a prominent, widespread event 8200 yr ago. *Geology* 25, 483–486.
- Antonarakou, A., Kontakiotis, G., Mortyn, P.G., Drinia, H., Sprovieri, M., Besiou, E., Tripsanas, E., 2015. Biotic and geochemical ($\delta^{18}\text{O}$, $\delta^{13}\text{C}$, Mg/Ca, Ba/Ca) responses of *Globigerinoides ruber* morphotypes to upper water column variations during the last deglaciation, Gulf of Mexico. *Geochimica et Cosmochimica Acta* 170, 69–93.
- Antonarakou, A., Kontakiotis, G., Zarkogiannis, S., Mortyn, P.G., Drinia, H., Koskeridou, E., Anastasakis, G., 2018. Planktonic foraminiferal abnormalities in coastal and open marine eastern Mediterranean environments: a natural stress monitoring approach in recent and early Holocene marine systems. *Journal of Marine Systems* 181, 63–78.
- Antonarakou, A., Kontakiotis, G., Karageorgis, A.P., Besiou, E., Zarkogiannis, S., Drinia, H., Mortyn, P.G., Tripsanas, E., 2019. Eco-biostratigraphic advances on late Quaternary geochronology and paleoclimate: The marginal Gulf of Mexico analogue. *Geological Quarterly* 63 (1), 178–191.
- Berner, K.S., Koç, N., Godtliebsen, F., 2010. High frequency climate variability of the Norwegian Atlantic Current during the early Holocene period and a possible connection to the Gleissberg cycle. *Holocene* 20, 245–255.
- Björck, S., Muscheler, R., Kromer, B., Andresen, C.S., Heinemeier, J., Johnsen, S.J., Conley, D., Koç, N., Spurk, M., Veski, S., 2001. High-resolution analyses of an early Holocene climate event may imply decreased solar forcing as an important climate trigger. *Geology* 29, 1107–1110.
- Bond, G., Kromer, B., Beer, J., Muscheler, R., Evans, M.N., Showers, W., Hoffmann, S., Lotti-Bond, R., Hajdas, I., Bonani, G., 2001. Persistent solar influence on North Atlantic climate during the Holocene. *Science* 294, 2130–2136.
- Bond, G., Showers, W., Cheseby, M., Lotti, R., Almasi, P., DeMenocal, P., Priore, P., Cullen, H., Hajdas, I., Bonani, G., 1997. A pervasive millennial-scale cycle in North Atlantic Holocene and glacial climates. *Science* 278, 1257–1266.
- Bonfardedi, A., Caruso, A., Bartolini, A., Bassinot, F., Blanc-Valleron, M.M., 2018. Distribution and ecology of the *Globigerinoides ruber*–*Globigerinoides elongatus* morphotypes in the Azores region during the late Pleistocene–Holocene. *Palaeogeography, Palaeoclimatology, Palaeoecology* 491, 92–111.
- Brayshaw, D.J., Rambeau, C.M.C., Smith, S.J., 2011. Changes in Mediterranean climate during the Holocene: insights from global and regional climate modelling. *Holocene* 21, 15–31.

- Buccheri, G., Carpetto, G., Di Donato, V., Esposito, P., Feruzza, G., Pescatore, T., Russo Ermolli, E., et al., 2002. A high resolution record of the last deglaciation in the southern Tyrrhenian Sea: environmental and climatic evolution. *Marine Geology* 186, 447–470.
- Cacho, I., Grimalt, J.O., Canals, M., 2002. Response of the western Mediterranean Sea to rapid climatic variability during the last 50,000 years: a molecular biomarker approach. *Journal of Marine Systems* 33–34, 253–272.
- Cacho, I., Grimalt, J.O., Canals, M., Sbaiffi, L., Shackleton, N.J., Schönfeld, J., Zahn, R., 2001. Variability of the western Mediterranean Sea surface temperatures during the last 25,000 years and its connection with the Northern Hemisphere climatic changes. *Paleoceanography* 16, 40–52.
- Capotondi, L., Borsetti, A.M., Morigi, C., 1999. Foraminiferal ecozones, a high resolution proxy for the Late Quaternary biochronology in the central Mediterranean Sea. *Marine Geology* 153, 253–274.
- Casford, J.S.L., Abu-Zied, R., Rohling, E.J., Cooke, S., Boessenkool, K.P., Brinkhuis, H., De Vries, C., et al., 2001. Mediterranean climate variability during the Holocene. *Mediterranean Marine Science* 2, 45–55.
- Casford, J.S.L., Abu-Zied, R.H., Rohling, E.J., Cooke, S., Fontanier, C., Leng, M., Millard, A., Thomson, J., 2007. A stratigraphically controlled multiproxy chronostratigraphy for the eastern Mediterranean. *Paleoceanography* 22, PA4215.
- Casford, J.S.L., Rohling, E.J., Abu-Zied, R., Cooke, S., Fontanier, C., Leng, M., Lykousis, V., 2002. Circulation changes and nutrient concentrations in the late Quaternary Aegean Sea: a nonsteady state concept for sapropel formation. *Paleoceanography* 17, 1024–1034.
- Casford, J.S.L., Rohling, E.J., Abu-Zied, R.H., Fontanier, C., Jorissen, F.J., Leng, M.J., Schmiedl, G., Thomson, J., 2003. A dynamic concept for eastern Mediterranean circulation and oxygenation during sapropel formation. *Palaeogeography, Palaeoclimatology, Palaeoecology* 190, 103–119.
- Combourieu-Nebout, N., Peyron, O., Bout-Roumazielles, V., Goring, S., Dormoy, I., Joannin, S., Sadori, L., Siani, G., Magny, M., 2013. Holocene vegetation and climate changes in the central Mediterranean inferred from a high-resolution marine pollen record (Adriatic Sea). *Climate of the Past* 9, 2023–2042.
- Combourieu-Nebout, N., Peyron, O., Dormoy, I., Desprat, S., Beaudouin, C., Kotthoff, U., Marret, F., 2009. Rapid climatic variability in the west Mediterranean during the last 25 000 years from high resolution pollen data. *Climate of the Past* 5, 503–521.
- Comeau, S., Jeffree, R., Teyssié, J.L., Gattuso, J.P., 2010. Response of the Arctic pteropods *Limacina helicina* to projected future environmental conditions. *PLoS ONE* 5, e11362.
- Cutter, G.A., Radford-Knoery, J., 1991. Determination of carbon, nitrogen, sulfur and inorganic sulfur species in marine particles. In: Hurd, D.C., Spencer, D.W. (Eds.), *Marine Particles: Analysis and Characterization. Geophysical Monograph* 63. American Geophysical Union, Washington, D.C., pp 57–63.
- De Lange, G.J., Thomson, J., Reitz, A., Slomp, C.P., Principato, M.S., Erba, E., Corselli, C., 2008. Synchronous basin-wide formation and redox-controlled preservation of a Mediterranean sapropel. *Nature* 455, 606–610.
- Denton, G.H., Karlen, W., 1973. Holocene climatic variations their pattern and possible cause. *Quaternary Research* 3, 155–205.
- Desprat, S., Combourieu-Nebout, N., Essallami, L., Sicre, M.-A., Dormoy, I., Peyron, O., Siani, G., Bout Roumazielles, V., Turon, J.L., 2013. Deglacial and Holocene vegetation and climatic changes in the southern central Mediterranean from a direct land–sea correlation. *Climate of the Past* 9, 767–787.
- Di Geronimo, I., 1970. Heteropoda e Pteropoda Thecosomata in sedimenti abissali recenti dello Jonio. *Thalassia Salentina* 4, 41–115.
- Drinia, H., Antonarakou, A., Tsourou, T., Kontakiotis, G., Psychogiou, M., Anastakis, G., 2016. Foraminifera ecostratigraphy of the southern Evoikos outer shelf, central Aegean Sea, during MIS 5 to present. *Continental Shelf Research* 126, 36–49.
- Ehrmann, W., Schmiedl, G., Hamann, Y., Kuhnt, T., Hemleben, C., Siebel, W., 2007. Clay minerals in late glacial and Holocene sediments of the northern and southern Aegean Sea. *Palaeogeography, Palaeoclimatology, Palaeoecology* 249, 36–57.
- Emeis, K.C., Struck, U., Blanz, T., Kohly, A., Woß, M., 2003. Salinity changes in the central Baltic Sea (NW Europe) over the last 10 000 years. *Holocene* 13, 411–421.
- Emeis, K.C., Struck, U., Schulz, H.M., Rosenberg, M., Bernasconi, S.M., Erlenkeuser, H., Sakamoto, T., Martinez-Ruiz, F.C., 2000. Temperature and salinity of Mediterranean Sea surface waters over the last 16 000 years: constraints on the physical environment of S1 sapropel formation based on stable oxygen isotopes and alkenone unsaturation ratios. *Palaeogeography, Palaeoclimatology, Palaeoecology* 158, 259–280.
- Faust, D., Zielhofer, C., Baena-Escudero, R., Diaz del Olmo, F., 2004. High-resolution fluvial record of late Holocene geomorphic change in northern Tunisia: climatic or human impact? *Quaternary Science Reviews* 23, 1757–1775.
- Fhlaithearta, S.N., Reichert, G.J., Jorissen, F.J., Fontanier, C., Rohling, E.J., Thomson, J., De Lange, G.J., 2010. Reconstructing the seafloor environment during sapropel formation using benthic foraminiferal trace metals, stable isotopes, and sediment composition. *Paleoceanography* 25, PA4225.
- Fleitmann, D., Mudelsee, M., Burns, S.J., Bradley, S.R., Kramers, J., Matter, A., 2008. Evidence for a widespread climatic anomaly at around 9.2 ka before present. *Paleoceanography* 23, PA1102.
- Frigola, J., Moreno, A., Cacho, I., Sierro, F.J., Flores, J.A., Grimalt, J.O., Hodell, D.A., Curtis, J.H., 2007. Holocene climate variability in the western Mediterranean region from a deepwater sediment record. *Paleoceanography* 22, PA2209.
- Gasse, F., 2000. Hydrological changes in the African tropics since the Last Glacial Maximum. *Quaternary Science Reviews* 19, 189–211.
- Geraga, M., Ioakim, C., Lykousis, V., Tsaila Monopolis, S., Mylona, G., 2010. The high-resolution palaeoclimatic and palaeoceanographic history of the last 24,000 years in the central Aegean Sea, Greece. *Palaeogeography, Palaeoclimatology, Palaeoecology* 287, 101–115.
- Geraga, M., Mylona, G., Tsaila-Monopoli, S., Papatheodorou, G., Ferentinos, G., 2008. Northeastern Ionian Sea: palaeoceanographic variability over the last 22 ka. *Journal of Marine Systems* 74, 623–638.
- Geraga, M., Tsaila-Monopolis, S., Ioakim, C., Papatheodorou, G., Ferentinos, G., 2005. Short-term climate changes in the southern Aegean Sea over the last 48000 years. *Palaeogeography, Palaeoclimatology, Palaeoecology* 220, 311–332.
- Giorgi, F., Lionello, P., 2008. Climate change projections for the Mediterranean region. *Global and Planetary Change* 63, 90–104.
- Gogou, A., Bouloubassi, I., Lykousis, V., Arnaboldi, M., Gaitani, P., Meyers, P.A., 2007. Organic geochemical evidence of abrupt late



- glacial-Holocene climate changes in the North Aegean Sea. *Palaeogeography, Palaeoclimatology, Palaeoecology* 256, 1–20.
- Goudeau, M.L.S., Reichart, G.-J., Wit, J.C., de Nooijer, L.J., Grauel, A.-L., Bernasconi, S.M., de Lange, G.J., 2015. Seasonality variations in the central Mediterranean during climate change events in the Late Holocene. *Palaeogeography, Palaeoclimatology, Palaeoecology* 418, 304–318.
- Grant, K.M., Grimm, R., Mikolajewicz, U., Marino, G., Ziegler, M., Rohling, E.J., 2016. The timing of Mediterranean sapropel deposition relative to insolation, sea-level and African monsoon changes. *Quaternary Science Reviews* 140, 125–141.
- Hayes, A., Rohling, E.J., De Rijk, S., Kroon, D., Zachariasse, W.J., 1999. Mediterranean planktic foraminiferal faunas during the last glacial cycle. *Marine Geology* 153, 239–252.
- Hemleben, C., Spindler, M., Anderson, O.R., 1989. *Modern Planktic Foraminifera*. Springer, New York.
- Herrle, J.O., Bollmann, J., Gebühr, C., Schulz, H., Sheward, R.M., Giesenberg, A., 2018. Black Sea outflow response to Holocene meltwater events. *Scientific Reports* 8, 4081.
- Howes, E.L., Eagle, R.A., Gattuso, J.P., Bijm, J., 2017. Comparison of Mediterranean pteropod shell biometrics and ultrastructure from historical (1910 and 1921) and present day (2012) samples provides baseline for monitoring effects of global change. *PLoS ONE* 12, e0167891.
- İşler, E.B., Aksu, A.E., Hiscott, R.N., 2016. Late Quaternary paleoceanographic evolution of the Aegean Sea: planktonic foraminifera and stable isotopes. *Turkish Journal of Earth Science* 25, 19–45.
- Jalut, G., Dedoubat, J.J., Fontugne, M., Otto, T., 2009. Holocene circum-Mediterranean vegetation changes: climate forcing and human impact. *Quaternary International* 200, 4–18.
- Janssen, A.W., 2012. Late Quaternary to Recent holoplanktonic Mollusca (Gastropoda) from bottom samples of the eastern Mediterranean Sea: systematics, morphology. *Bolletino Malacologico* 48, 1–105.
- Jansson, K.N., Kleman, J., 2004. Early Holocene glacial lake meltwater injections into the Labrador Sea and Ungava Bay. *Paleoceanography* 19, PA1001.
- Jaouadi, S., Lebreton, V., Bout-Roumzeilles, V., Siani, G., Lakhdar, R., Boussoffara, R., Dezileau, L., Kallel, N., Mannai-Tayech, B., Combourieu-Nebout, N., 2016. Environmental changes, climate and anthropogenic impact in south-east Tunisia during the last 8 kyr. *Climate of the Past* 12, 1339–1359.
- Jimenez-Espejo, F.J., Martinez-Ruiz, F., Rogerson, M., González-Donoso, J.M., Romero, O.E., Linares, D., Sakamoto, T., et al., 2008. Detrital input, productivity fluctuations, and water mass circulation in the westernmost Mediterranean Sea since the Last Glacial Maximum. *Geochemistry, Geophysics, Geosystems* 9, 1–19.
- Karageorgis, A.P., Anagnostou, C.L., Kaberi, H., 2005. Geochemistry and mineralogy of the NW Aegean Sea surface sediments: implications for river runoff and anthropogenic impact. *Applied Geochemistry* 20, 69–88.
- Karageorgis, A.P., Kaberi, H.G., Tengberg, A., Zervakis, V., Anagnostou, C.L., Hall, P., 2003. Comparison of particulate matter distribution, in relation to hydrography, in the mesotrophic Skagerrak and the oligotrophic northeastern Aegean Sea. *Continental Shelf Research* 23, 1787–1809.
- Karageorgis, A.P., Katsanevakis, S., Kaberi, H., 2009. Use of enrichment factors for the assessment of heavy metal contamination in the sediments of Koumoundourou Lake, Greece. *Water, Air, and Soil Pollution* 204, 243–258.
- Kontakiotis, G., 2016. Late Quaternary paleoenvironmental reconstruction and paleoclimatic implications of the Aegean Sea (eastern Mediterranean) based on paleoceanographic indexes and stable isotopes. *Quaternary International* 401, 28–42.
- Kontakiotis, G., Antonarakou, A., Mortyn, P.G., Drinia, H., Anastasakis, G., Zarkogiannis, S., Möbius, J., 2017. Morphological recognition of *Globigerinoides ruber* morphotypes and their susceptibility to diagenetic alteration in the eastern Mediterranean Sea. *Journal of Marine Systems* 174, 12–24.
- Kontakiotis, G., Antonarakou, A., Zachariasse, W.J., 2013. Late Quaternary palaeoenvironmental changes in the Aegean Sea: interrelations and interactions between north and south Aegean Sea. *Bulletin of the Geological Society of Greece* 47, 167–177.
- Kontakiotis, G., Karakitsios, V., Mortyn, P.G., Antonarakou, A., Drinia, H., Anastasakis, G., Agiadi, K., Kafousia, N., De Rafelis, M., 2016. New insights into the early Pliocene hydrographic dynamics and their relationship to the climatic evolution of the Mediterranean Sea. *Palaeogeography, Palaeoclimatology, Palaeoecology* 459, 348–364.
- Kotthoff, U., Müller, U.C., Pross, J., Schmiidl, G., Lawson, I.T., van de Schootbrugge, B., Schulz, H., 2008a. Late Glacial and Holocene vegetation dynamics in the Aegean region: an integrated view based on pollen data from marine and terrestrial archives. *Holocene* 18, 1019–1032.
- Kotthoff, U., Pross, J., Müller, U.C., Peyron, O., Schmiidl, G., Schulz, H., Bordon, A., 2008b. Climate dynamics in the borderlands of the Aegean Sea during formation of sapropel 1 deduced from a marine pollen record. *Quaternary Science Reviews* 27, 832–845.
- Kuhnt, T., Schmiidl, G., Ehrmann, W., Hamann, Y., Hemleben, C., 2007. Deep-sea ecosystem variability of the Aegean Sea during the past 22 kyr as revealed by benthic foraminifera. *Marine Micro-paleontology* 64, 147–162.
- LeGrande, A.H., Schmidt, G.A., Shindell, D.T., Field, V., Miller, R.L., Kocj, D.M., Faluvegi, G., Hoffmann, G., 2006. Consistent simulations of multiple proxy responses to an abrupt climate change event. *Proceedings of the National Academy of Sciences of the United States of America* 103, 837–842.
- Lirer, F., Sprovieri, M., Vallefucio, M., Ferraro, L., Pelosi, N., Giordano, L., Capotondi, L., 2014. Planktonic foraminifera as bio-indicators for monitoring the climatic changes occurred during the last 2000 years in the SE Tyrrhenian Sea. *Integrative Zoology* 9, 542–554.
- Louvari, M.A., Drinia, H., Kontakiotis, G., Di Bella, L., Antonarakou, A., Anastasakis, G., 2019. Impact of latest-glacial to Holocene sea-level oscillations on central Aegean shelf ecosystems: a benthic foraminiferal palaeoenvironmental assessment of South Evoikos Gulf, Greece. *Journal of Marine Systems* (in press). <https://doi.org/10.1016/j.jmarsys.2019.05.007>.
- Lykousis, V., Chronis, G., Tselepidis, A., 2002. Major outputs of the recent multidisciplinary biogeochemical researches undertaken in the Aegean Sea. *Journal of Marine Systems* 33–34, 313–334.
- Magny, M., Bégeot, C., 2004. Hydrological changes in the European midlatitudes associated with freshwater outbursts from Lake Agassiz during the Younger Dryas event and the early Holocene. *Quaternary Research* 61, 181–192.
- Magny, M., Bégeot, C., Guiot, J., Peyron, O., 2003. Contrasting patterns of hydrological changes in Europe in response to Holocene climate cooling phases. *Quaternary Science Reviews* 22, 1589–1596.

- Magny, M., Vannière, B., Zanchetta, G., Fouache, E., Touchais, G., Petrika, L., Coussot, C., Walter-Simonnet, A.V., Arnaud, F., 2009. Possible complexity of the climatic event around 4300–3800 cal. BP in the central and western Mediterranean. *Holocene* 19, 823–833.
- Marino, G., Rohling, E.J., Sangiorgi, F., Hayes, A., Casford, J.L., Lotter, A.F., Kucera, M., Brinkhuis, H., 2009. Early and middle Holocene in the Aegean Sea: interplay between high and low latitude climate variability. *Quaternary Science Reviews* 28, 3246–3262.
- Marret, F., Zonnefeld, K., 2003. Atlas of organic walled dinoflagellate cysts. *Review of Palaeobotany and Palynology* 125, 1–200.
- Martínez-Ruiz, F., Paytan, A., Kastner, M., González-Donoso, J.M., Linares, D., Bernasconi, S.M., Jimenez-Espejo, F.J., 2003. A comparative study of the geochemical and mineralogical characteristics of the S1 sapropel in the western and eastern Mediterranean. *Palaeogeography, Palaeoclimatology, Palaeoecology* 190, 23–37.
- Mayewski, P.A., Rohling, E.E., Stager, J.C., Karlen, W., Maasch, K.A., Meeker, L.D., Meyerson, E.A., et al., 2004. Holocene climate variability. *Quaternary Research* 62, 243–255.
- Nesje, A., Dahl, S.O., Bakke, J., 2004. Were abrupt Lateglacial and early-Holocene climatic changes in northwest Europe linked to freshwater outbursts to the North Atlantic and Arctic Oceans? *Holocene* 14, 299–310.
- Nieuwenhuize, J., Maas, Y.E.M., Middelburg, J.J., 1994. Rapid analysis of organic carbon and nitrogen in particulate materials. *Marine Chemistry* 45, 217–224.
- Papanikolaou, D., Alexandri, M., Nomikou, P., Ballas, D., 2002. Morphotectonic structure of the western part of the North Aegean Basin based on swath bathymetry. *Marine Geology* 190, 465–492.
- Peyron, O., Goring, S., Dormoy, I., Kotthoff, U., Pross, J., de Beaulieu, J.L., Drescher-Schneider, R., Vannière, B., Magny, M., 2011. Holocene seasonality changes in the central Mediterranean region reconstructed from the pollen sequences of Lake Accesa (Italy) and Tenaghi Philippon (Greece). *Holocene* 21, 131–146.
- Polunin, O., 1988. *Flowers of Greece and the Balkans: A Field Guide*. Oxford University Press, Oxford.
- Rasmussen, S.O., Vinther, B.M., Clausen, H.B., Andersen, K.K., 2007. Early Holocene climate oscillations recorded in three Greenland ice cores. *Quaternary Science Reviews* 26, 1907–1914.
- Reimer, P.J., Bard, E., Bayliss, A., Beck, J.W., Blackwell, P.G., Ramsey, C.B., Buck, C.E., et al., 2013. IntCal13 and Marine13 radiocarbon age calibration curves 0–50,000 years cal BP. *Radiocarbon* 55, 1869–1887.
- Rohling, E.J., Abu-Zied, R., Casford, J.S.L., Hayes, A., Hoogakker, B.A.A., 2009. The marine environment: present and past. In: Woodward, J. (Ed.), *The Physical Geography of the Mediterranean*. Oxford University Press, New York, pp. 33–67.
- Rohling, E.J., Jorissen, F.J., De Stigter, H.C., 1997. 200 Year interruption of Holocene sapropel formation in the Adriatic Sea. *Journal of Micropalaeontology* 16, 97–108.
- Rohling, E.J., Jorissen, F.J., Vergnaud-Grazzini, C., Zachariasse, W.J., 1993. Northern Levantine and Adriatic Quaternary planktic foraminifera: reconstruction of paleoenvironmental gradients. *Marine Micropaleontology* 21, 191–218.
- Rohling, E.J., Mayewski, P.A., Abu-Zied, R.H., Casford, J.S.L., Hayes, A., 2002. Holocene atmosphere ocean interactions: records from Greenland and the Aegean Sea. *Climate Dynamics* 18, 587–593.
- Rosignol-Strick, M., 1985. Mediterranean Quaternary sapropels, an immediate response of the African monsoon to variation of insolation. *Palaeogeography, Palaeoclimatology, Palaeoecology* 49, 237–263.
- Roussakis, G., Karageorgis, A.P., Conispoliatis, N., Lykousis, V., 2004. Last glacial–Holocene sediment sequences in North Aegean basins: structure, accumulation rates and clay mineral distribution. *Geo-Marine Letters* 24, 97–111.
- Ruan, J., Kherbouche, F., Genty, D., Blamart, D., Cheng, H., Dewilde, F., Hachi, S., Edwards, R.L., Régner, E., Michelot, J.L., 2016. Evidence of a prolonged drought ca. 4200 yr BP correlated with prehistoric settlement abandonment from the Gueldaman GLD1 Cave, northern Algeria. *Climate of the Past* 12, 1–14.
- Sbaffi, L., Wezel, F.C., Curzi, G., Zoppi, U., 2004. Millennial to centennial-scale palaeoclimatic variations during Termination I and the Holocene in the central Mediterranean Sea. *Global and Planetary Change* 40, 201–217.
- Schmiedl, G., Kuhnt, T., Ehrmann, W., Emeis, K.C., Hamann, Y., Kotthoff, U., Dulski, P., Pross, J., 2010. Climatic forcing of eastern Mediterranean deep-water formation and benthic ecosystems during the past 22 000 years. *Quaternary Science Reviews* 29, 3006–3020.
- Siani, G., Magny, M., Paterne, M., 2013. Paleohydrology reconstruction and Holocene climate variability in the South Adriatic Sea. *Climate of the Past* 9, 499–515.
- Siani, G., Paterne, M., Colin, C., 2010. Late Glacial to Holocene planktonic foraminifera bioevents and climatic record in the South Adriatic Sea. *Journal of Quaternary Science* 25, 808–821.
- Sperling, M., Schmiedl, G., Hemleben, C., Emeis, K.C., Erlenkeuser, H., Grootes, P.M., 2003. Black Sea impact on the formation of eastern Mediterranean sapropel S1? Evidence from the Marmara Sea. *Palaeogeography, Palaeoclimatology, Palaeoecology* 190, 9–21.
- Spero, H.J., Mielke, K.M., Kalve, E.M., Lea, D.W., Pak, D.K., 2003. Multispecies approach to reconstructing eastern equatorial Pacific thermocline hydrography during the past 360 kyr. *Paleoceanography* 18, 1022.
- Stuiver, M., Reimer, P.J., 1993. Extended C-14 data-base and revised Calib 3.0 C-14 age calibration program. *Radiocarbon* 35, 215–230.
- Teller, J.T., Leverington, D.W., Mann, J.D., 2002. Freshwater outbursts to the oceans from glacial Lake Agassiz and their role in climate change during the last deglaciation. *Quaternary Science Reviews* 21, 879–887.
- Triantaphyllou, M.V., Antonarakou, A., Kouli, K., Dimiza, M., Kontakiotis, G., Papanikolaou, M.D., Ziveri, P., et al., 2009. Late Glacial–Holocene ecostratigraphy of the south-eastern Aegean Sea, based on plankton and pollen assemblages. *Geo-Marine Letters* 29, 249–267.
- Van der Spoel, S., 1976. *Pseudothecosomata, Gymnosomata and Heteropoda (Gastropoda)*. Bohn, Scheltema, and Holkema, Utrecht, the Netherlands.
- Velaoras, D., Lascaratos, A., 2005. Deep water mass characteristics and interannual variability in the North and Central Aegean Sea. *Journal of Marine Systems* 53, 59–85.
- Verardo, D.J., Froelich, P.N., McIntyre, A., 1990. Determinations of organic carbon and nitrogen in marine sediments using the Carlo Erba NA-1500 Analyzer. *Deep-Sea Research* 37, 157–165.
- Wanner, H., Mercolli, L., Grosjean, M., Ritz, S.P., 2014. Holocene climate variability and change: a data-based review. *Journal of the Geological Society* 172, 254–263.
- Wanner, H., Solomina, O., Grosjean, M., Ritz, S.P., Jetel, M., 2011. Structure and origin of Holocene cold events. *Quaternary Science Reviews* 30, 3109–3123.

- Wiersma, A.P., Renssen, H., 2006. Model data comparison for the 8.2 ka B.P. event: confirmation of a forcing mechanism by catastrophic drainage of Laurentide Lakes. *Quaternary Science Reviews* 25, 63–88.
- Wilke, I., Meggers, H., Bickert, T., 2009. Depth habitats and seasonal distributions of recent planktic foraminifers in the Canary Islands region (29N) based on oxygen isotopes. *Deep Sea Research* 56, 89–106.
- Wilson, J.D., Monteiro, F.M., Schmidt, D.N., Ward, B.A., Ridgwell, A., 2018. Linking marine plankton ecosystems and climate: a new modeling approach to the warm early Eocene climate. *Paleoceanography and Paleoclimatology* 33, 1439–1452.
- Wit, J.C., Reichert, G.-J., Jung, S.J.A., Kroon, D., 2010. Approaches to unravel seasonality in sea surface temperatures using paired single-specimen foraminiferal $\delta^{18}\text{O}$ and Mg/Ca analyses. *Paleoceanography* 25, PA4220.
- Yu, S.Y., Colman, S.M., Lowell, T.V., Milne, G.A., Fisher, T.G., Breckenridge, A., Boyd, M., Teller, J.T., 2010. Freshwater outburst from Lake Superior as a trigger for the cold event 9300 years ago. *Science* 328, 1262–1266.
- Zachariasse, W.J., Jorissen, F.J., Perissoratis, C., Rohling, E.J., Tsapralis, V., 1997. Late Quaternary foraminiferal changes and the nature of sapropel S1 in Skopelos Basin. In: Proceedings of the Fifth Hellenic Symposium of Oceanography and Fisheries, Kavala, Greece, 1, pp. 391–394.
- Zervakis, V., Georgopoulos, D., Karageorgis, A.P., Theocharis, A., 2004. On the response of the Aegean Sea to climatic variability. *International Journal of Climatology* 24, 1845–1858.
- Zielhofer, C., Faust, D., Escudero, R.B., Diaz del Olmo, F., Kadereit, A., Moldenhauer, K.-M., Porras, A., 2004. Centennial-scale late-Pleistocene to mid-Holocene synthetic profile of the Medjerda Valley, northern Tunisia. *Holocene* 14, 851–861.
- Zonneveld, K.A.F., Marret, F., Versteegh, G., Bogus, K., Bonnet, S., Bouimetarhan, I., Crouch, E., *et al.*, 2013. Atlas of modern dinoflagellate cyst distribution based on 2405 data points. *Review of Palaeobotany and Palynology* 191, 1–197.

Article

Key Environmental Factors Controlling Planktonic Foraminiferal and Pteropod Community's Response to Late Quaternary Hydroclimate Changes in the South Aegean Sea (Eastern Mediterranean)

Christina Giamali ^{1,2,*}, George Kontakiotis ^{1,*} , Efterpi Koskeridou ¹ , Chryssanthi Ioakim ³ and Assimina Antonarakou ¹

¹ Department of Historical Geology and Paleontology, Faculty of Geology and Geoenvironment, National and Kapodistrian University of Athens, Panepistimiopolis, 15784 Athens, Greece; ekosker@geol.uoa.gr (E.K.); aantonar@geol.uoa.gr (A.A.)

² The Goulandris Natural History Museum, Levidou 13, 14562 Kifissia, Greece

³ Institute of Geology and Mineral Exploration (I.G.M.E.), Olympic Village, 13677 Acharnae, Greece; cioakim@otenet.gr

* Correspondence: gchristi@geol.uoa.gr (C.G.); gkontak@geol.uoa.gr (G.K.); Tel.: +30-210-8015-870 (ext. 510) (C.G.); +30-210-7274-804 (G.K.)

Received: 27 August 2020; Accepted: 10 September 2020; Published: 14 September 2020



Abstract: A multidisciplinary study was conducted in order to investigate the environmental factors affecting the planktonic foraminiferal and pteropod communities of the south Aegean Sea. Aspects of the Late Quaternary paleoceanographic evolution were revealed by means of quantitative analyses of planktonic foraminiferal and pteropod assemblages (including multivariate statistical approach; principal component analysis (PCA)), the oxygen ($\delta^{18}\text{O}$) and carbon ($\delta^{13}\text{C}$) isotopic composition of planktonic foraminifera and related paleoceanographic (planktonic paleoclimatic curve (PPC), productivity (E-index), stratification (S-index), seasonality) indices, extracted by the gravity core KIM-2A derived from the submarine area between Kimolos and Sifnos islands. Focusing on the last ~21 calibrated thousands of years before present (ka BP), cold and eutrophicated conditions were identified during the Late Glacial period (21.1–15.7 ka BP) and were followed by warmer and wetter conditions during the deglaciation phase. The beginning of the Holocene was marked by a climatic amelioration and increased seasonality. The more pronounced environmental changes were identified during the deposition of the sapropel sublayers S1a (9.4–7.7 ka BP) and S1b (6.9–6.4 ka BP), with extremely warm and stratified conditions. Pteropod fauna during the sapropel deposition were recorded for the first time in the south Aegean Sea, suggesting arid conditions towards the end of S1a. Besides sea surface temperature (SST), which shows the highest explanatory power for the distribution of the analyzed fauna, water column stratification, primary productivity, and seasonality also control their communities during the Late Quaternary.

Keywords: paleoceanographic evolution; planktonic foraminifera; pteropods; stable isotopes; sea surface temperature (SST); stratification; productivity; sapropel S1; Aegean Sea; Late Quaternary

1. Introduction

The Aegean Sea is an ideal archive to investigate climatic evolution at both global and local scale because of its intermediate position between the higher- and lower-latitude climate systems [1–3], high sedimentation rate marine records compared to the open Mediterranean Sea [4–7], and its paleo-latitudinal and land-locked configuration [8,9]. Such marginal seas are often more responsive to

paleoceanographic and paleoclimatic changes than global oceans, with climatic signals to be recorded in an amplified fashion in Mediterranean properties such as temperature, salinity and specific elemental concentrations, because of their smaller size and partial isolation [10], and therefore can be considered miniature oceans. In addition to interactions with the Black Sea, northern Aegean, and Levantine basins with remote and local atmospheric forcing [1,11], the south Aegean Sea is characterized by intense biogeochemical contrasts in its hydrology in response to a climatic gradient from mid-latitude to subtropical regimes that appears to be very sensitive to climate changes. However, most of the current paleoclimatic and paleoceanographic studies are still limited to deep marine records [6,12–15], and consequently little is known about the continental shelf and/or coastal areas within this marginal Sea [16–21].

Environmental changes related to the different water column and/or sediment characteristics can be recorded virtually instantaneously in paleoceanographic proxy data, such as stable isotope and other geochemical ratios [22–31], and micro-fossil abundances, such as planktonic foraminifera and pteropods [15,17,28,32–36]. This makes them extremely valuable for both stratigraphic correlations and paleoenvironmental/paleoclimate reconstructions [15,23,28,29,32,35,37–45]. Their significance in the study of modern and past marine ecosystems in the eastern Mediterranean Sea is well underlined [20,31,46–51]. Particularly, they are used as indicators of temperature, salinity, density, and nutrient content of the water column, making it possible to identify past circulation through the sedimentary record [7,15,29,47,52,53] and detect long- and short-term paleoclimatic and paleoceanographic changes in the study area [6,10,12,15,16,53–55] during the last glacial cycle.

Pteropods are widespread and abundant in the global ocean and entirely adapted to a pelagic life cycle [56,57]. Owing to the aragonite nature of their shells which increases their weight as settling particles and hence their sinking speed [58], their deposition is expected to be close to their habitat [59]. Particularly in the Mediterranean Sea, preservation of pteropods shells is excellent as a result of the relatively shallow water, high bottom water temperatures, and probably the limited number of mud feeders [60]. A considerable number of studies (e.g., [33,34,61–66]) have shown that Late Quaternary pteropod assemblages and their distribution pattern in the world oceans have changed with temperature and the overall climatic conditions that also affect the aragonite compensation depth (ACD). Recent studies [67] have shown that modern eastern Mediterranean pteropod communities are found to be more abundant than in those at western Mediterranean Sea. Their abundances are positively correlated with the aragonite saturation state (Ω_{ar}), O_2 concentration, pH, salinity and temperature, and negatively correlated with nutrient concentrations [67,68]. However, pteropod assemblages and their distribution in the Aegean Sea during the Late Quaternary are poorly documented.

The present study focuses on identifying and describing key environmental factors that control Late Quaternary planktonic foraminiferal and pteropod distribution in the south Aegean Sea, based on marine sediments retrieved by a 2-m long gravity (KIM-2A) core. In addition, paleoclimatic data were revealed from their distribution patterns coupled with variations of oxygen and carbon isotopic signals. The combination of the above data enables speculation on the factors' response to the climatic changes.

2. Regional and Climatic Setting

The Aegean Sea is in the northern sector of the eastern Mediterranean (Figure 1a), between the Turkish coastline to the east, the Greek mainland to the north and west, and bounded on the south by the island of Crete and Cretan Arc. It is connected to the Black Sea through the Straits of Bosphorus and Dardanelles, and to the Levantine Sea through several larger and deeper straits between Peloponnesus, the islands of Crete and Rhodes, and south-western Turkey (Figure 1b). It is characterized, in general, by a cyclonic water circulation, although the most active dynamic features are the mesoscale cyclonic and anticyclonic eddies, either permanent and/or recurrent [8]. It is separated into two major sub-basins with different climatic conditions: the “north” and the “south” Aegean Sea. The north is more humid than the semiarid south [8].

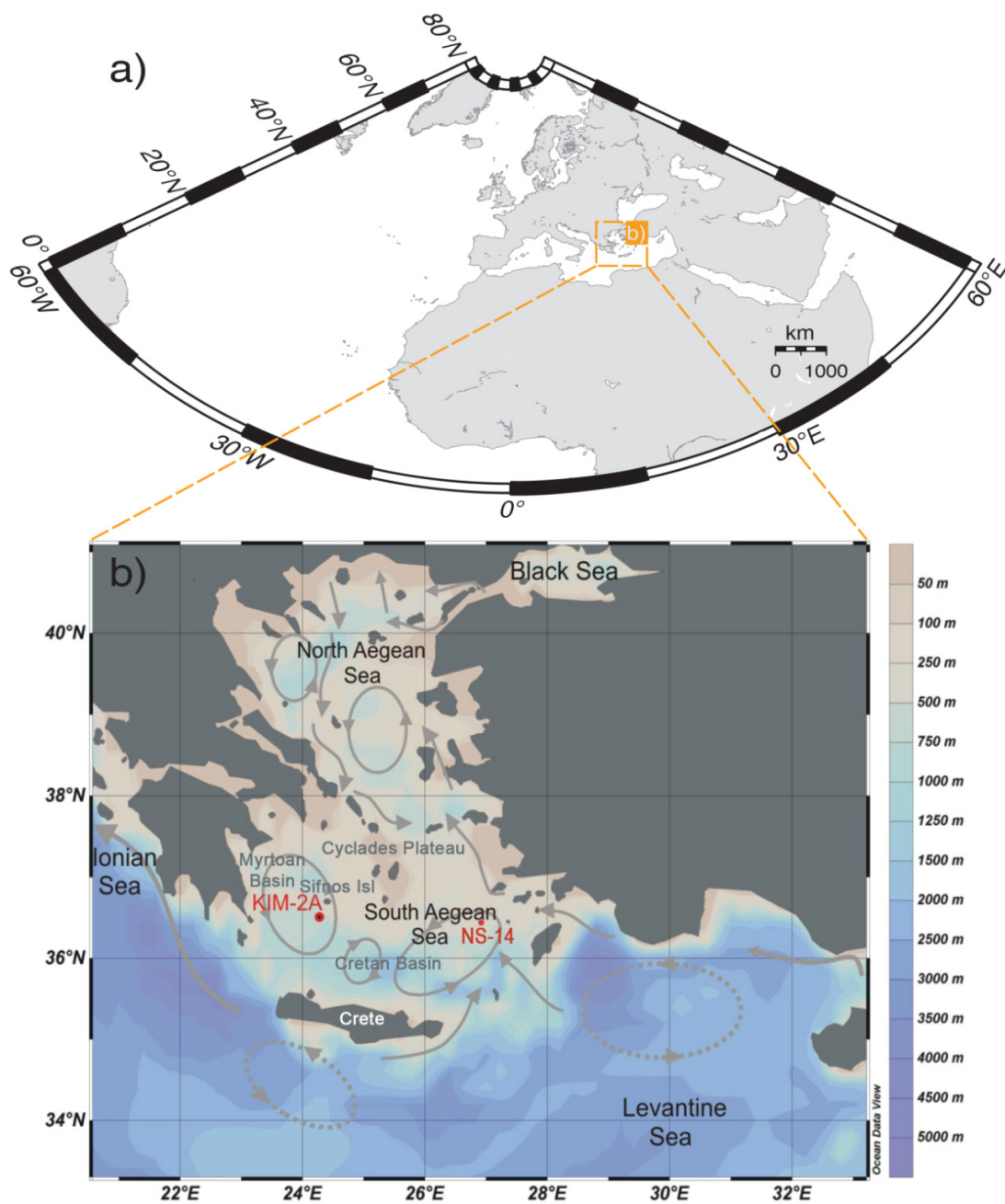


Figure 1. (a) Map of the Mediterranean Sea (including the Aegean Sea); (b) inset shows location of the south Aegean sediment core KIM-2A (36°95.464'N, 24°06.354'E, 640 m depth; in red), and the main patterns of sea surface-water circulation (grey arrows), cyclonic (solid grey circles) and anticyclonic gyres (dashed grey circles) in the Levantine and Aegean Seas. Location of the core NS-14 [7,16], that was used for the age model construction. Map contours show paleobathymetry (water depth in meters) of the study area.

The south Aegean (extend in between 35°N and 37°N) is one of the most oligotrophic areas in the Mediterranean Sea [8], with its surface water circulation mostly affected by arid climatic conditions, while it is also modulated by the effect of the Cretan gyre [69]. It mainly consists of the Cretan basin and the shallow shelf of the Cyclades Plateau, along with the Myrtoan Sea at the NW part of the region (Figure 1b). Milos and Kimolos islands lie in the westernmost sector of the Cyclades plateau. Both islands are part of the south Aegean Volcanic Arc; the most important geological structure of the Aegean Sea. The submarine area between Kimolos and Sifnos Islands is characterized by a rather

complex relief [70] as it is related to the volcanic arc. The sedimentary and Quaternary tectonic evolution of the aforementioned submarine area have been studied previously [71], and it is separated into three parts (the southern, the eastern, and the northern; [70]). The core studied derives from a submarine depression located at the northern part.

3. Materials and Methods

3.1. Location and Sampling Strategy of Core KIM-2A

A gravity core (KIM-2A; 200 cm length) was recovered with R/V Aegaeo in May 2015 from the south Aegean Sea and covers the Late Quaternary (the last ~21 ka BP). Core KIM-2A was collected from the Cyclades plateau, from a submarine depression (640 m water depth) located north of Kimolos Island (36°95.464'N, 24°06.354'E), as shown in Figure 1b. After splitting, the half core was stored as archival material, whereas the working half has been sampled for multiple analyses (micropaleontology, sedimentology, and geochemistry).

Fifty-eight samples were taken and used for paleontological (planktonic foraminifera and pteropods) and geochemical (Total Organic Carbon; TOC, stable oxygen and carbon isotopes; $\delta^{18}\text{O}$, $\delta^{13}\text{C}$) analyses between 196 cm and 4 cm. Samples were taken throughout the core but with different sampling resolutions. For the first gray interval corresponding to S1a, the sampling resolution was 1 cm; beyond these intervals the sampling was 2 cm, whereas the top 40 cm were sampled at a mean 8 cm resolution.

3.2. Micropaleontological Analyses

All samples were prepared following standard micropaleontological procedures. For the faunal analyses, approximately 3 cm³ of dried sediment was washed and sieved through a 63 μm screen, and residues were dried in an oven at 50 °C. Qualitative and quantitative analyses have been performed on both planktonic foraminiferal and pteropod assemblages for the >125 μm size fraction, split into aliquots, each one containing at least 300 specimens. It should be noted that the 125 μm fraction was selected since is the most common studied fraction in relevant investigations within the Aegean Sea, which analyze the Late Quaternary foraminiferal record [10,18,21,32,36], and implement a paleoclimatic analysis [6,15,20,72]. All shells were handpicked, identified following [73], counted in each sample, and then converted into percentages, based on the extrapolation of a counted split. Planktonic species with phylogenetic affinities and similar ecological characteristics [35,74] were counted together and grouped to better interpret distribution patterns. On this regard, all *Globigerinoides ruber* morphotypes (“Normal,” “Platys,” “Elongate,” and “Twin” types; [32]) were plotted together, distinguishing only the “alba” and “rosea” varieties due to their different ecological characteristics [75]. Furthermore, *Globigerina bulloides* group includes the species *G. bulloides* and *Globigerina falconensis*, the *Globigerinoides sacculifer* group includes *Globigerinoides trilobus* and *G. sacculifer*, and the *Globigerinella siphonifera* group includes the species *Globigerinella aequilateralis*, *Globigerina calida*, and *Globigerina digitata*. The species *Globigerinita glutinata* includes the morphotypes with and without bulla. Within the group of Neogloboquadriniids, two types were discerned: *Neogloboquadrina pachyderma* and *Neogloboquadrina dutertrei*.

3.3. Total Organic Carbon and Stable Isotopes

Total organic carbon (TOC) was determined based on the [76] methodology with the [77] adaptation at the Laboratory of the Hellenic Survey of Geology and Mineral Exploration (H.S.G.M.E.). For stable oxygen and carbon ($\delta^{18}\text{O}$, $\delta^{13}\text{C}$) isotope measurements, 30 specimens of the planktonic species *G. ruber* f. *alba* were picked from the 250–300 μm size fraction. In particular, we exclusively used the morphotype “Normal” of [32] (equivalent to *G. ruber sensu stricto* [75]) in order to minimize potential morphotype-specific differential responses in stable isotope compositions [24,78,79]. This narrow size fraction was used to minimize ontogenetic and growth rate effects on shell geochemistry [80]. The analyses were carried out at the Laboratory of Geology and Geophysics at Edinburgh University.

Foraminiferal $\delta^{18}\text{O}$ and $\delta^{13}\text{C}$ data were calibrated to National Bureau of Standards 19 (NBS19), and the isotope values are reported in ‰ relative to Vienna Pee Dee belemnite scale. The external standard errors of the stable carbon and oxygen isotope analyses are $<0.06\text{‰}$ and 0.08‰ , respectively.

3.4. Chronology

The chronology of the core KIM-2A is based on five accelerator mass spectroscopy radiocarbon (AMS ^{14}C) dates (on *G. ruber* tests at Beta Analytics laboratories), supplemented by tie-points which correspond to well-dated bio-litho-stratigraphic horizons (e.g., sapropel and planktonic foraminiferal biozone boundaries) from nearby Aegean cores (Table 1). Conventional ^{14}C ages were calibrated by means of the Calib version 7.0.2 software [81] and the Marine13 data set with a regional reservoir age correction (ΔR) of 139 ± 40 years for the S1 interval [82] and of 58 ± 85 years outside the sapropel S1 interval [83]. The chronology adopted in this study for core KIM-2A was derived from a polynomial fit through the calibrated dates and the chronostratigraphic control points' dating as shown in Table 1. Hereafter, ages in this study are reported in calibrated thousands of years before present, notated ka BP.

Table 1. Calibrated radiocarbon dates (AMS ^{14}C) and chronostratigraphic control points' dates.

AMS & Chronostratigraphic Control Points	Depth (cm)	Conventional Radiocarbon Age (BP)	Two Sigma Calibrated Age Range (BP)	Mean Calibrated Age (ka BP)	References
Beta—425634	14.5	4890+/-30	4845–5325	5.08	
Ia/Ib boundary	20			5.2	[84]
Beta—425635	28	5320+/-30	5444–5855	5.65	
S1b top	40			6.4	[7,16]
Beta—425636	50.25	6790+/-30	7036–7292	7.16	
S1b base	52.5			7.3	[7,16]
S1a top	65.5			7.9	[7,16]
Beta—425637	79.5	8320+/-30	8532–8883	8.71	
S1a base	89			10	[7,16]
Ic/II boundary	109			11.3	[84]
II/III boundary	153			15.5	[84]
$\delta^{18}\text{O}_{G. ruber}$ depletion	159			15.9	[52]
Beta—425638	195	18890+/-70	21962–22508	22.24	

3.5. Multivariate Statistical Analyses

Principal component analyses (PCA) is used to reduce the dimensionality of a multivariate data set to a few principal factors that determine the distributions of species. For this analysis all raw data for the totality of the samples and specimens were used. Raw data were processed using PAST (2.17) multivariate statistical software package of [85]. The resulting factor scores show the contribution of each factor in every sample, and therefore the down-core contribution of each factor. The total number of factors was defined by minimizing the remaining “random” variability, and by the possibility to relate the factors to modern hydrographic conditions and planktonic foraminiferal and pteropod ecology.

3.6. Paleoceanographic Indices

The planktonic foraminiferal relative distributions were used as a first-order estimate of sea-surface temperature (SST) variations. An index of the SST variations was constructed based on the down-core variation of planktonic foraminiferal abundances, referred to as planktonic paleoclimatic curve (PPC). The PPC was obtained by the formula $100 \times (w - c)/(w + c)$, where w represents the warm-water indicators (*G. ruber* f. *alba*, *G. ruber* f. *rosea*, *Orbulina universa*, *G. sacculifer* gr., *Globoturbotalita rubescens*, and *G. siphonifera* gr.), and c the cold-water indicators (*Globorotalia inflata*, *Globorotalia truncatulinoides*, *Turborotalita quinqueloba*, *G. glutinata*, and *Globorotalia scitula*). The eutrophication index (E-index; [7]) was

estimated using the sum of the eutrophic species (*N. pachyderma*, *N. dutertrei*, *G. bulloides*, *T. quinqueloba*, and *G. inflata*) versus the sum of the eutrophic plus oligotrophic species (*G. ruber alba*, *G. ruber rosea*, *G. rubescens*, *G. sacculifer*, *O. universa*, and *G. siphonifera*). The down-core ratio between *G. bulloides* and *G. ruber* was also estimated showing the degree of the stratification of the upper water column [86]. Following [7], this ratio is referred to as S-index, and its values reflect periods of strong summer stratification of the water column where oligotrophic taxa dominate (low values) and/or periods of strong winter mixing of the water column where eutrophic taxa dominate (high values).

4. Results

4.1. Lithological Description, Time Stratigraphic Framework, and Sedimentation Rates

Lithologically, the study core contains a distinct organic-rich dark interval, divided into two separate sub-units (S1a and S1b respectively), representing the regional expression of the most recent sapropel S1 [87,88] (Figure 2a). From the bottom up to 87.5 cm, light gray clay can be observed (Munsell soil color 5Y 7/1). The following 24 cm are of gray color (5Y 5/1) and correspond to the lower sub-unit (S1a) of the sapropel. Between 63.5 cm and 52 cm light gray clay (5Y 7/1) can be observed, indicative of the sapropel interruption (S1i). From 52 cm to 40 cm mud of gray color (5Y 5/2) characterizes the upper sapropel sub-unit (S1b). The clay continues up to 13.5 cm with a light gray clay (5Y 7/1) color. From this point to the top of the core watery clay of light-yellow color (5Y 7/4) can be observed (Figure 2a).

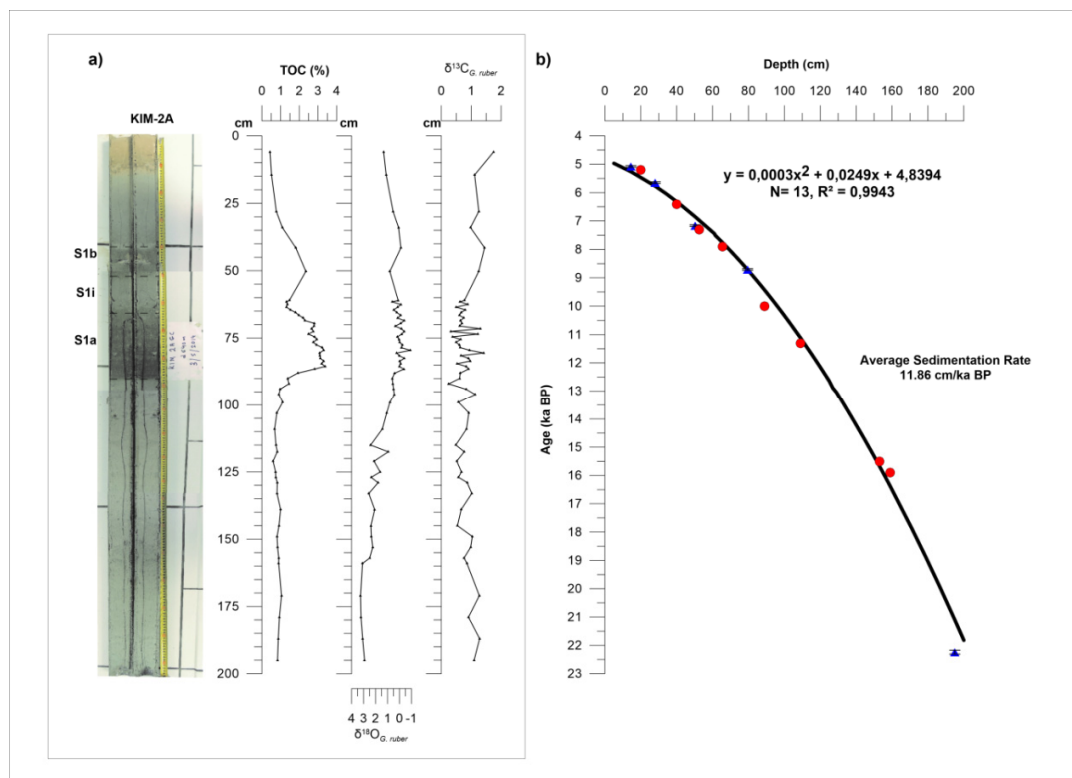


Figure 2. (a) Lithologic log of core KIM-2A along with the total organic carbon (TOC) concentration and $\delta^{18}\text{O}_{G. ruber}$ and $\delta^{13}\text{C}_{G. ruber}$ isotope values; (b) time stratigraphic framework of the study core; blue triangles represent AMS ^{14}C datings, whereas red dots represent control points and bio-litho-stratigraphic horizons used as stratigraphic markers. The errors of AMS ^{14}C datings are also shown.

Chronology adopted in this study for core KIM-2A derived from a polynomial fit through the five AMS ^{14}C datings mentioned above, and the time markers correlative to the start and end of sapropel

deposition, as well as the planktonic foraminiferal biozone Ia/Ib, Ib/Ic, Ic/II and II/III boundaries of [84] in the Mediterranean Sea (Table 1). The resulting age model is illustrated in Figure 2b and is consistent with the multi-proxy chronological framework of [37] for the Aegean sediment cores, thus supporting the robustness of our chronology. For the ages of the onset and termination of sapropel deposition, we have used the relevant ages from the nearby core NS-14 [7,16,17]. Additional control points related to the planktonic foraminiferal biozone boundaries were used for the age model construction, since they are useful chronologic standards for dating late Quaternary sequences in the central and eastern Mediterranean (including the Aegean Sea; [6,7,52,89] due to their Mediterranean-wide applicability and synchronicity [90–92].

Based on the relative abundances of the planktonic foraminifera species (Figure 3) the interval between 196 cm and 153 cm is characterized by the dominance of *N. pachyderma*, *T. quinqueloba*, *G. scitula* and *G. glutinata* with additional components the species *G. ruber* f. *alba* and *G. bulloides*. This glacial fauna corresponds to assemblage III and it has been recognized throughout the Mediterranean Sea (e.g., [6,52]). The interval between 153 cm and 109 cm corresponds to assemblage II and is characterized by high relative abundances of Neogloboquadrinids and *G. glutinata* and the presence of and *G. inflata*. In the lower part of this interval *G. ruber* f. *rosea* appears for the first time. Subzone Ic (109–40 cm) was identified by the warm subtropical species (*G. ruber* f. *rosea*, *G. siphonifera* gr. and *O. universa*). In addition it includes abundant *G. bulloides* and *G. rubescens* specimens. The sharp increase in the abundance of *G. inflata* at 41.5 cm is inferred to mark the onset of the Ib subzone. The Ia/Ib boundary (at 20 cm) is marked by the decrease of the latter species along with the decrease in the *N. pachyderma* abundance. In this core the Bioevent “Start of $\delta^{18}\text{O}_{\text{ruber}}$ depletion T1a” of [52], was also detected at 159 cm.

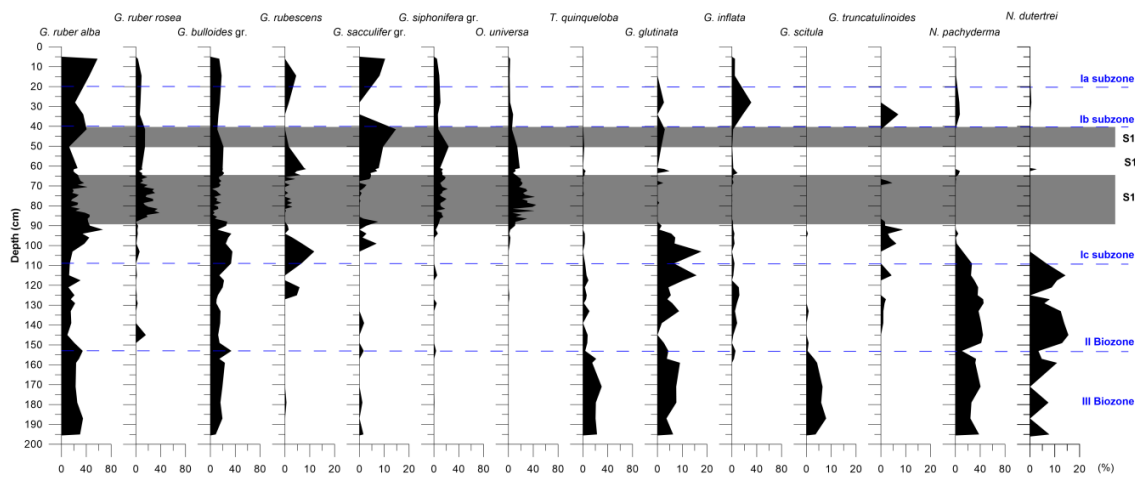


Figure 3. Frequency curves of the most indicative planktonic foraminiferal species in core KIM-2A. The dashed blue lines represent the Ia/Ib, Ib/Ic, Ic/II and II/III boundaries, whereas the gray bands the sapropel S1 sublayers respectively. X axes scales are of 80% and 20% corresponding to the high and low frequency abundances respectively.

According to our proposed age model (Figure 2b), the sedimentary horizons sampled in this study span the interval from the late glacial period, and the subsequent transition (Termination 1; T1) to the middle Holocene (Northgrippian stage) (i.e., ~5–22 ka BP). The average sedimentation rate is 11.86 cm/ka, and is in good agreement to those reported in the marginal Aegean basin [4,7,13,52]. These sedimentation rates were derived from the age model, assuming that the sediment accumulation has been moderately consistent throughout each interval. In particular, the average sedimentation rates are 8.10 cm/ka for the late glacial, 10.30 cm/ka for the Termination T1, and 16.46 cm/ka for the Holocene.

4.2. Planktonic Foraminifera Distribution Pattern

The qualitative analysis revealed 19 planktonic foraminiferal species lumped into 14 groups: *G. ruber* f. *alba*, *G. ruber* f. *rosea*, *G. sacculifer* group, *G. bulloides* group, *G. siphonifera* group, *G. scitula*, *G. truncatulinoidea*, *G. inflata*, *O. universa*, *T. quinqueloba*, *G. glutinata*, *G. rubescens*, *N. pachyderma*, *N. dutertrei*. The down-core stratigraphic distributions of their relative abundance are shown in Figure 3.

From the bottom of the core up to 153 cm, the fauna is characterized by high relative abundances of the species *G. ruber* f. *alba* (22–34%), *N. pachyderma* (10–40%), *T. quinqueloba* (3–30%), and *G. bulloides* gr. (8–33%). Additional components of the fauna are *N. dutertrei*, *G. glutinata*, and *G. scitula*. After the 153 cm, an abrupt decline in Neogloboquadrinids and *T. quinqueloba* can be observed, while *G. bulloides* follows an opposite trend with relative abundance of 33%. From that point up to 127 cm *N. pachyderma* and *N. dutertrei* reach their maximum abundances (45% and 15% respectively), whereas *T. quinqueloba* is still present but with low percentages (up to 10%). The relative abundance of *G. bulloides* does not exceed 16% and *G. ruber* f. *alba* is also present but with equally low frequency (lower than 20%). Between 127 cm and 100 cm the fauna is characterized by the dominance of *G. bulloides*, *N. pachyderma*, *N. dutertrei*, *G. ruber* f. *alba*, *G. glutinata*, and *G. rubescens*. Additional components, with lower percentages, are the species *T. quinqueloba* and *G. inflata*. The interval between 100 cm and 41.5 cm is characterized by a shift in fauna. Most of the species dominating the previous interval are decreasing or becoming absent (*T. quinqueloba*, Neogloboquadrinids, *G. glutinata* and *G. inflata*). Prevailing species of this interval are *O. universa* (44%), *G. ruber* f. *rosea* (38%), *G. bulloides* gr. (27%), *G. siphonifera* gr. (20%), and *G. sacculifer* gr. (14%). In the final segment of the core, from 41.5 cm to the top, the sampling presents poor resolution, but certain significant changes can be observed. The *G. ruber* f. *alba*, *G. inflata* and *G. truncatulinoidea* present a peak (57%, 31%, and 7% respectively) and the relative abundances of *G. ruber* f. *rosea*, *O. universa*, and *G. siphonifera* gr. are decreasing. *N. pachyderma*, *G. inflata*, and *G. glutinata* are re-appearing, but with low percentages.

4.3. Pteropod Distribution Pattern

All samples examined for foraminifera include significant amounts of aragonitic pteropods indicating excellent preservation (without any signals of dissolution) along with the strong carbonate preservation potential of the eastern Mediterranean basin [72,93]. A total of 12 species of Euthecosomata (*Heliconoides inflatus*, *Limacina trochiformis*, *Limacina bulimoides*, *Limacina retroversa*, *Creseis acicula*, *Creseis* sp., *Boasia chierchiae*, *Hyalocyclis striata*, *Styliola subula*, *Clio pyramidata* s.l., *Diacria trispinosa*, *Cavolinia* spp.) were identified. Adult specimens, when present, were fragmented (*Cavolinia* spp., *C. pyramidata*). The protoconchs (*Clio*, *Diacria* and *Cavolina*) made the identification of certain species and genera possible, as they were the only residue left. The down-core variation of their abundance is presented in Figure 4.

Within the basal part of the core sequence, the fauna is composed almost exclusively of the pteropod *L. retroversa*. An additional component is the species *C. pyramidata*, but with very low percentages (<3.5%). Between 153 cm to 127 cm the pteropodal fauna becomes more diverse with the species *H. inflatus*, *D. trispinosa*, *C. acicula*, and *B. chierchiae* appearing in the fauna. The relative abundance of *C. pyramidata* gradually increases (up to 45%), in contrast to the decline of *L. retroversa* (drops to ~40%). The latter disappears completely from the fauna at 105 cm. Between 109 cm and 85 cm the pteropod fauna consists mainly of *H. inflatus*, *C. acicula*, *C. pyramidata*, and *D. trispinosa*, with *L. bulimoides* appearing for the first time at 109 cm. The species *C. pyramidata* and *D. trispinosa* are exponentially decreasing until, and including, the top of the core sample. In the last 85 cm of the core, *Cavolinia* spp. appears in the fauna, reaching its maximum abundance (58%) at 41.25 cm and 85.5 cm, with the species *H. inflatus* and *B. chierchiae* (15–58% and 3–40% respectively) as additional components. At 65.5 cm, *L. trochiformis* presents a short occurrence and between 65 cm and 60 cm *Creseis* sp. presents its maximum relative abundance (36%). Towards the top of the core *L. trochiformis* and *S. subula* present their highest percentages (~6% and 15% respectively).

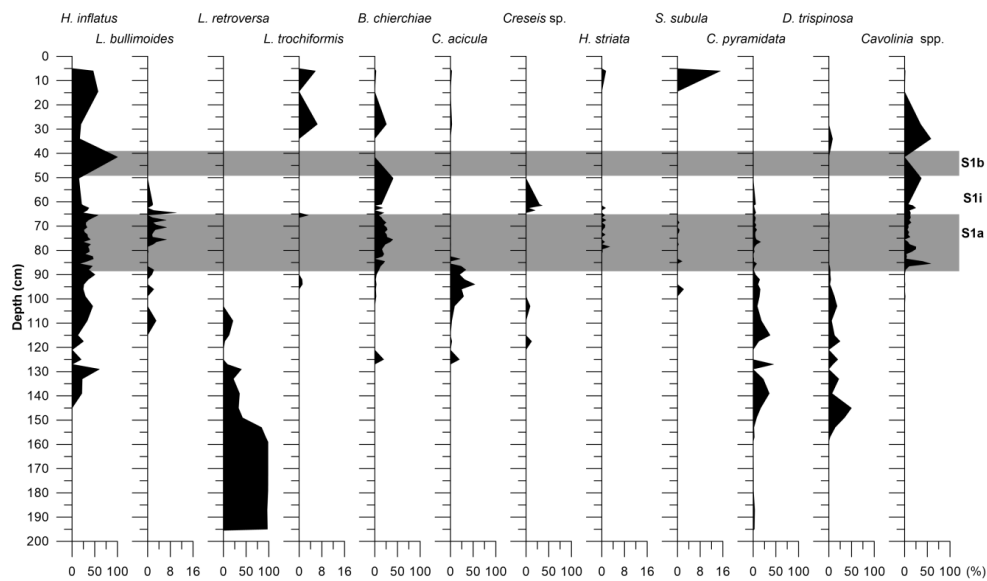


Figure 4. Frequency curves of the most indicative pteropods in core KIM-2A. Gray bands represent the sapropel S1 sublayers. X axes scales are of 100% and 16% corresponding to the high and low frequency abundances respectively.

4.4. Total Organic Carbon and Stable Isotopes

Total organic carbon (TOC) in KIM-2A generally exhibits values around 1%. This pattern is interrupted in two intervals related to the sapropel sub-units deposition. The first interval (S1a; 89–64 cm) is characterized by high TOC concentration, ranging from 1.5% to 3.4%, and in the second interval (S1b; 52.5–40 cm), TOC concentration ranges from 1.8% to 2.4% (Figure 2a). Thus, the deposition of S1 sapropel layer started at 89 cm and terminated at 40 cm. The interruption of sapropel S1 layer (S1i) is detected between 64 cm and 52.5 cm, as suggested by the TOC content (~1.3%).

As shown in Figure 2a, between 196 cm and 159 cm, $\delta^{18}\text{O}_{G. ruber}$ values range from +2.9 to +3.2‰. From 157 cm to 115 cm, a depletion in $\delta^{18}\text{O}_{G. ruber}$ values is observed (up to +0.9‰) and persists until the 34 cm with even lower values. More precisely, the depleted values were recorded from two intervals (88.5–65.5 cm and 50.25–34 cm) with an average value of −0.08‰ and +0.25‰ respectively. In the interval corresponding to 66.5–61 cm, slightly heavier $\delta^{18}\text{O}_{G. ruber}$ values were observed (+0.6 to −0.1‰). In the final unit of the core, from 28 cm until the top, a core enrichment in $\delta^{18}\text{O}_{G. ruber}$ is recorded. The $\delta^{13}\text{C}_{G. ruber}$ values of KIM-2A core exhibit more scatter than the $\delta^{18}\text{O}$ records. In the basal part of the core (200–88 cm) values range between +1.3 to +0.2‰. In the interval between 88 cm and 61 cm the $\delta^{13}\text{C}_{G. ruber}$ ranges between 0.3 and 0.9‰ with the exception of three high-positive peaks at 80.5 cm, 73.5 cm, and 71.5 cm with values of 1.4‰, 1.2‰, and 1.3‰ respectively. From 50.25 cm to the top of the core, $\delta^{13}\text{C}_{G. ruber}$ exhibits heavier values with an average of +1.29‰ (Figure 2a).

4.5. Principal Component Analysis

A standardized principal component analysis (PCA) was carried out on the total data set using the varimax method, in order to determine the impact of various environmental parameters on the planktonic distribution. The application of this statistical analysis yielded a three-factor model for both planktonic foraminiferal and pteropod communities (Supplementary Materials; including PCA scores and biplots). The interpretation of the three components in each case was based on the screen plots of eigen values, and the factor loadings of the planktonic foraminiferal and pteropod species respectively. The 3 distinguished factors were considered to account for 81.57% and 82.81% of the total variance in each category respectively (Tables 2 and 3), with their factor loadings showing the contribution of each factor in every sample and therefore the downcore contribution of each factor (Tables 4 and 5; Figure 5).

In the case of a bipolar factor, which has extremes of positive and negative loadings, high positive factor scores are related to the positive pole and high negative scores to the negative pole, respectively.

Table 2. Principle component analysis (PCA) factors based on planktonic foraminifera and their percentages of the total variability for core KIM-2A.

PCA Factors	Eigenvalue	% Variance	Cumulative % of the Total Variance
1	432.137	50.26	50.26
2	193.038	22.45	72.70
3	76.2131	8.86	81.57
4	53.3399	6.20	87.77
5	38.4841	4.47	92.25
6	24.4952	2.85	95.09
7	15.5611	1.81	96.90
8	7.97016	0.93	97.83
9	7.63218	0.89	98.72
10	5.03693	0.58	99.30
11	2.88765	0.33	99.64
12	2.25794	0.26	99.90
13	0.666282	0.08	99.98
14	0.159802	0.02	100.00

Table 3. PCA factors based on pteropods and their percentages of the total variability for core KIM-2A.

PCA	Eigenvalue	% Variance	Cumulative % of the Total Variance
1	1209.14	58.66	58.66
2	273.91	13.29	71.95
3	223.817	10.86	82.81
4	104.846	5.09	87.89
5	100.727	4.89	92.78
6	63.5077	3.08	95.87
7	53.2518	2.58	98.45
8	23.7844	1.15	99.60
9	4.32791	0.21	99.81
10	2.86233	0.14	99.95
11	0.755953	0.04	99.99
12	0.236728	0.01	100.00

Table 4. Ranking of the planktonic foraminiferal species and their factor loadings along the PCA factors in core KIM-2A. Bold data indicate the most important factor loadings in each factor.

Variables	Factor 1	Factor 2	Factor 3
<i>O. universa</i>	-0.511	0.363	0.194
<i>G. ruber</i> f. <i>alba</i>	-0.158	-0.776	0.443
<i>G. ruber</i> f. <i>rosea</i>	-0.375	0.302	0.101
<i>G. sacculifer</i> gr.	-0.028	-0.091	-0.122
<i>G. siphonifera</i> gr.	-0.251	0.099	-0.152
<i>G. inflata</i>	0.079	-0.020	-0.136
<i>G. bulloides</i> gr.	0.094	-0.199	-0.691
<i>G. rubescens</i>	0.008	-0.012	-0.209
<i>N. pachyderma</i>	0.643	0.320	0.305
<i>N. dutertrei</i>	0.155	0.100	0.051
<i>T. quinqueloba</i>	0.197	0.001	0.258
<i>G. truncatulinooides</i>	0.007	-0.060	0.004
<i>G. glutinata</i>	0.129	-0.014	-0.110
<i>G. scitula</i>	0.032	-0.009	0.064

Table 5. Ranking of the pteropod species and their factor loadings along the PCA factors in core KIM-2A. Bold data indicate the most important factor loadings in each factor.

Species	Factor 1	Factor 2	Factor 3
<i>H. inflatus</i>	-0.387	0.693	0.453
<i>L. bulimoides</i>	-0.015	-0.012	0.010
<i>L. retroversa</i>	0.895	0.175	0.304
<i>L. trochiformis</i>	-0.005	0.000	0.008
<i>B. chierchiaie</i>	-0.154	-0.334	0.286
<i>C. acicula</i>	-0.064	0.227	-0.328
<i>Creseis</i> sp.	-0.027	-0.031	-0.038
<i>H. striata</i>	-0.004	-0.002	0.008
<i>S. subula</i>	-0.006	0.015	0.004
<i>C. pyramidata</i>	0.009	-0.024	-0.437
<i>D. trispinosa</i>	0.051	-0.020	-0.420
<i>Cavolinia</i> sp.	-0.131	-0.570	0.380

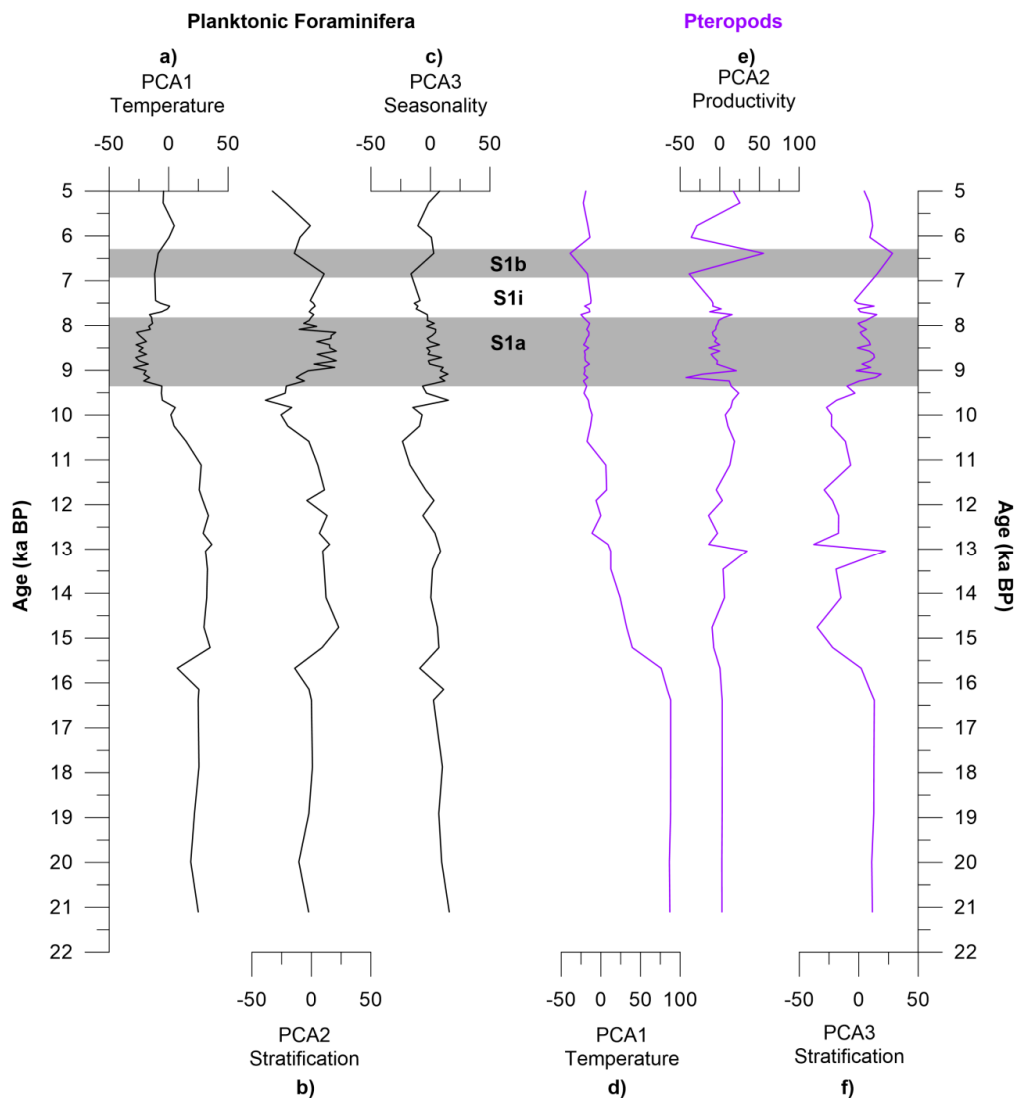


Figure 5. Environmental factors controlling planktonic foraminifera and pteropod distribution resulting from the PCA. (a) PCA1 of planktonic foraminifera as a temperature factor; (b) PCA2 of planktonic foraminifera as a stratification factor; (c) PCA3 of planktonic foraminifera as a seasonality factor; (d) PCA1 of pteropods as a temperature factor; (e) PCA2 of pteropods as a productivity factor; and (f) PCA3 of pteropods as a stratification factor.

4.5.1. Planktonic Foraminifera

The first varimax factor (PCA1; Figure 5a) accounts for 50.26% of the total variance (Table 2) and is interpreted as temperature indicator. Species with positive loadings (*N. pachyderma*, *T. quinqueloba*, *N. dutertrei*, *G. glutinata*, *G. inflata*, *G. bulloides*, and *G. scitula*; Table 4) thrive in cold–water masses, while the species with negative loadings (*O. universa*, *G. ruber* f. *rosea*, *G. siphonifera* gr., and *G. ruber* f. *alba*; Table 4) thrive in warm–water conditions. Factor PCA2 (Figure 5b) accounts for 22.5% of the total variance (Table 1), with the positive pole being expressed by species living in a highly stratified water column (*O. universa*, *G. ruber* f. *rosea* and Neogloboquadrinids) and negative pole by species typical of the weak development of these conditions (*G. ruber* f. *alba* and *G. bulloides* gr.). The third varimax factor (PCA3) describes 8.9% of the total variance (Table 2), and also display a bipolar character, with its positive pole to be represented mainly by *G. ruber* f. *alba* and *N. pachyderma* and the negative pole by *G. bulloides*. The above species that characterize the PCA3 factor are the main exponents of the seasonal contrasts governing planktonic foraminiferal assemblages in the Mediterranean Sea during the last glacial cycle [94–96]. Thus, the third varimax factor (PCA3; Figure 5c) is referred to as a seasonality factor.

4.5.2. Pteropods

The first varimax factor (PCA1; Figure 5e) accounts for 58.66% of the total variance (Table 3) and was interpreted as a temperature indicator. Negative loadings consist mainly of the warm–water species *H. inflatus*, whereas positive loadings consist mainly of the subarctic species *L. retroversa* (Table 5). The second factor (PCA2; Figure 5e) describes 13.29% of the total variance (Table 3) and was interpreted as a productivity factor, as its positive pole is represented mainly by the mesopelagic oligotrophic *H. inflatus*. The third varimax factor (PCA3; Figure 5f) explains 10.27% of the total variance (Table 3). The positively loading taxa expressed by the epipelagic *Cavolinia* sp., *L. retroversa* and *B. chierchiae*, as well as the mesopelagic and tolerant to low oxygen concentration *H. inflatus*, whereas the negatively loading taxa (mesopelagic *C. pyramidata* and *D. trispinosa*) prefer a well-ventilated water column (Table 5). Thus, the third factor (PCA3) can be regarded as a stratification factor.

5. Discussion

5.1. Factors Controlling Planktonic Fauna Distribution in the Aegean Sea

Of the oceanographic factors typically considered, SST shows the highest explanatory power for the distribution of the planktonic fauna during the Late Quaternary. This is in accordance with previously published studies showing temperature as the dominant factor controlling the biogeography of planktonic foraminifera and pteropods at both global and local scales [61,67,97]. However, the 2 remaining factors (PCA-2, PCA-3) exhibit a bipolar character and could be considered as indicators of the annual stability of the water column. For the planktonic foraminifera fauna, they show that the faunal composition in the south Aegean Sea was not only controlled by SST, but also seems to be affected by the degree of development and location of a permanent or seasonal thermocline/pycnocline. Its vertical placement in the water column is a direct consequence of changes in sea surface salinity (SSS) and productivity (SSP), which ultimately reflected the seasonal fluctuations of the periods of vertical mixing of water in the periods of intense stratification. The interpretation of the second axis focused on the appearance depths of pycnocline and deep chlorophyll maximum (DCM) and the thickness of mixed layer. The interpretation of the third axis focused on upwelling currents and/or river inputs (e.g., *G. bulloides*), parameters which primarily control the food availability and reproductive cycles of foraminifera [73] and are directly correlated to the seasonal fluctuations they present [94,98–100]. Therefore, a useful additional dimension of planktonic foraminifera ecology that is underlined by the PCA conducted in this study is the degree of vertical stratification of the water column and the way it is recorded (seasonal presence/absence pycnocline and DCM and upwellings and runoff), which are inextricably linked with the factors of primary productivity and seasonality.

Similarly, the second and third factor (PCA2, PCA3) of pteropods are focused on the hydrological conditions and the overall oxygenation of the water column. Particularly, the down-core scores of the second factor coincide with the $\delta^{13}\text{C}$ and E-index values, indicating that variations in primary productivity have an impact on pteropod abundances. Even though nutrient concentrations are not a limited factor for their distribution [67], our data suggest that fluctuations in nutrients and salinity due to the increased freshwater inputs during the sapropel deposition favor the flourishing of some species (*Cavolinia* spp., *B. chierchiae*; Figure 4). Additionally, the third factor suggests that oxygen concentration, and thus the intensity of the oxygen minimum zone (OMZ), are parameters that affect pteropod distribution and particularly the mesopelagic species [66].

5.2. Paleoceanographic Reconstruction

The results of the multivariate statistical analyses, in combination with paleoceanographic indices and isotopic data (Figure 6), reveal a succession of Late glacial to Holocene paleoclimatic and paleoceanographic changes. The evidence of these changes is interpreted and discussed in terms of the events that mainly accompanied the transition out of the late glacial period and the deposition of sapropel S1 during the Holocene Climatic Optimum (HCO).

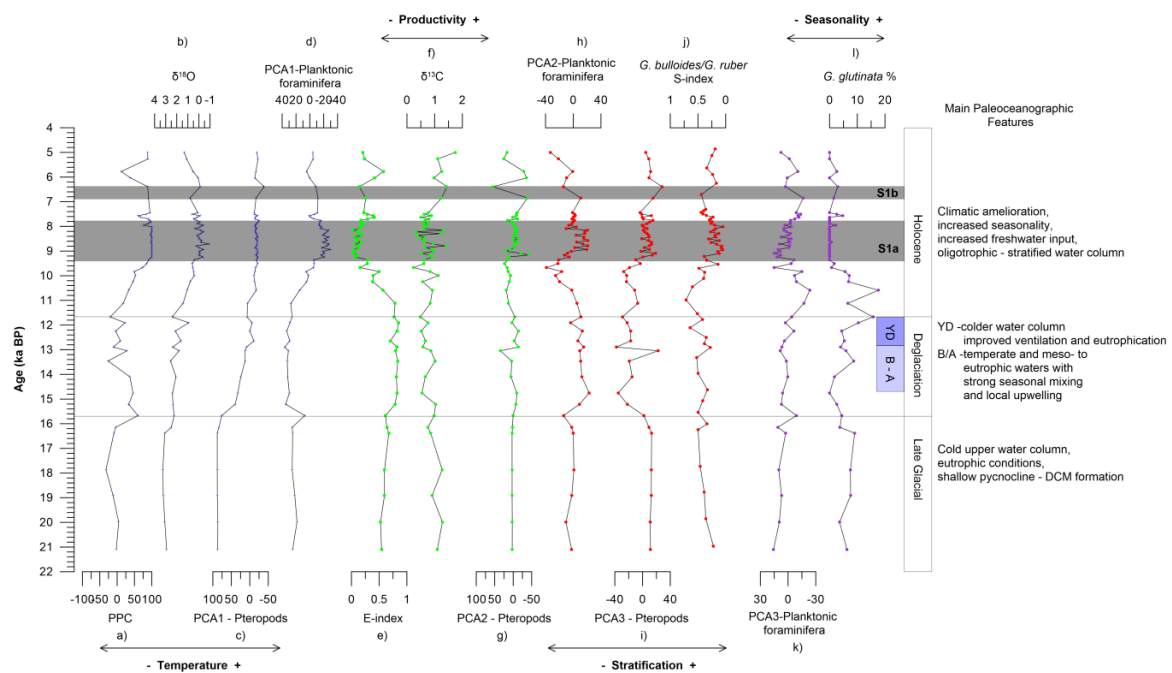


Figure 6. Comparison between down-core score plots of the factors revealed by PCA analysis, micropaleontological and geochemical results of core KIM-2A: (a) planktonic paleoclimatic curve (PPC); (b) oxygen isotope record ($\delta^{18}\text{O}_{G. ruber}$); (c) factor 1 of planktonic foraminifera (PCA1; temperature factor); (d) factor 1 of pteropods (PCA1; temperature indicator); (e) eutrophication index (E-index); (f) carbon isotope record ($\delta^{13}\text{C}_{G. ruber}$); (g) factor 2 of pteropods (PCA2; productivity factor); (h) factor 2 of planktonic foraminifera (PCA2; stratification factor); (i) factor 3 of pteropods (PCA3; stratification factor); (j) *G. bulloides/G. ruber* ratio (S-index); (k) factor 3 of planktonic foraminifera (PCA3; seasonality factor); and (l) *G. glutinata* %.

5.2.1. Late Glacial

During the late glacial period (21.1–15.7 ka BP), the heaviest $\delta^{18}\text{O}$ values (2.49–3.26‰), accompanied by relatively low PPC values (−32% to +4%), suggest a cold upper water column (Figure 6a,b). Particularly, this interval was characterized by high percentages of the cold water foraminifera species *T. quinqueloba* (~30%), accompanied by *G. glutinata* (9%), and *G. scitula* (8%), and significant percentages of the warm-water *G. ruber* f. *alba* (~34%), that are suggestive of milder

climate after the Last Glacial Maximum (LGM), which is in accordance with other records in the Mediterranean [101,102]. Pteropod fauna is composed mainly by the cold water species *L. retroversa* (98%) and the cold-tolerant mesopelagic *C. pyramidata* in very low percentages (3%) which is consistent with relevant late glacial Mediterranean records [33,61,103]. Eutrophic species are also abundant in this interval (*N. pachyderma*, *N. dutertrei*, *T. quinqueloba* and *G. bulloides*) and are associated with the high values of E-index (Figure 6e). Notably, the high abundance of *N. pachyderma* (26%) indicates shallowing of the pycnocline and the formation of a DCM layer. In addition, $\delta^{13}\text{C}$ values, around +1‰, and the trend to higher S-index values (Figure 6f,j), also support the development of eutrophicated waters. The moderate abundance of *G. bulloides* (5–17%; Figure 3) suggests little to no upwelling and/or runoff contribution in primary productivity. Therefore, the injection of nutrients into the euphotic zone can be attributed to the intensification and southward shift of westerly winds, as indicated by atmospheric circulation models for this time interval [104].

5.2.2. Deglaciation

At 15.7 ka BP an abrupt shift of PPC to positive values, accompanied by lighter $\delta^{18}\text{O}$ values (+2.2‰) (Figure 6a,b), are indicative of the climatic amelioration that occurred during the last deglaciation. These warmer conditions are also supported by the occurrence of the warm water species *H. inflatus* and *D. trispinosa* (up to 60% and 50% respectively), and the decrease in *L. retroversa* percentages (between 33% and 85%). This warming trend is in agreement with relevant paleoclimatic records from the eastern Mediterranean, and is attributed to the Bølling–Allerød (B-A) interstadial [7,13,14,105,106]. The increased SST and humidity are also recorded by the higher abundance of the terrestrial biomarkers in the south Aegean [17], and by a change in the benthic faunas from oxic to dysoxic indicator species [13]. In the beginning of this interval, Neogloboquadrinids were temporarily replaced by *G. bulloides* (26%), suggesting local upwelling. Though, later on the eutrophic *N. pachyderma* and *N. dutertrei* present their highest abundance (42% and 14% respectively). Additional components of this interval are *G. ruber* (both variants), *G. bulloides*, *T. quinqueloba*, and *G. inflata*, suggesting temperate and meso- to eutrophic waters, with strong seasonal mixing and local upwelling.

This state persisted until the onset of the Younger Dryas (YD) at about 12.9 ka BP, which is depicted in the abrupt decrease in PPC (from +28% to –10%) and in heavier values of $\delta^{18}\text{O}$ (1.0–2.5‰) (Figure 6a,b). The planktonic foraminiferal fauna shows an increase in cold water species (*N. pachyderma*, *T. quinqueloba*, *G. inflata* and *G. glutinata*). Pteropod fauna is composed mainly of the cold-water species epipelagic *L. retroversa* and the mesopelagic temperate to warm-water species *C. pyramidata* and *D. trispinosa*, while the warm-water *H. inflatus* presents a decreasing trend (Figure 3). This climate response of south Aegean depression to the YD event (12.9–11.7 ka BP) seems to be in accordance with relevant signals from other Aegean sub-basins [6,7]. Towards the end of YD (12.6–12.2 ka BP) the species *G. rubescens*, *C. acicula*, and *B. chierchiae* are added to the fauna suggesting that mild climatic conditions prevailed for a brief time interval of about 400 years within the YD event. This brief climatic amelioration in the mid YD, which has been attributed to the displacement of the polar front by a few degrees north [26], has been also observed in north-central Aegean marine records [7,106] and coincides with the pattern of GRIP and NGRIP ice-core records [107,108], pollen-based reconstructions from the Jura [109] and the Balkans [110], as well as chironomid-based reconstructions from North Italy [111]. The increases in the S-index and E-index at around 12.2 ka BP (Figure 6e,j) coincide with this amelioration, reflected by the improved ventilation and eutrophication of the water column.

5.2.3. Holocene

With the ending of the YD, a general climatic amelioration is seen in the records (increase in PPC, lighter values in $\delta^{18}\text{O}$, decline of temperature factors PCA1; Figure 6a–d) marking the beginning of the Holocene. Planktonic foraminifera fauna consists mainly by *G. ruber* f. *alba* that increases in abundance towards the onset of sapropel deposition, along with *G. bulloides* and *N. pachyderma*. The two latter species present an opposite trend, decreasing towards the onset of sapropel deposition. This trend

suggests the gradual development of stratified and oligotrophic surface waters. Pteropod fauna follows a similar pattern with the decreasing abundances of the species *D. trispinosa* and *C. pyramidata*, which are indicative of a well ventilated water column [112], and the increase in the epipelagic *B. chierchiae* and *C. acicula* (Figure 4). The reduction of E-index along with the values of $\delta^{13}\text{C}$ and the S-index (Figure 6e–j) are further evidence for the development of these conditions. The replacement of *G. inflata* by *G. glutinata* (Figure 3) may be tentatively explained in terms of increased seasonality, and of increased freshwater input, which reduced surface buoyancy loss and hence suppressed mixing during the beginning of the Holocene [7]. This was also enhanced by the presence of the epipelagic pteropods (*Creseis* spp.) that proliferate in low-salinity waters [113], and the seasonality factor (PCA3 of planktonic foraminifera; Figure 6k).

At around 9.4 ka BP, the deposition of sapropel S1 as witnessed by their high organic carbon content (C_{org} : 1.8–3.3%, Figure 2a), coincided with the start of the overall $\delta^{18}\text{O}$ depletion (+0.6‰ to –0.9‰; Figure 6b). The changes of the planktonic foraminifera fauna are characterized by an increase in *G. ruber* f. *rosea*, *G. ruber* f. *alba*, *G. siphonifera* and *O. universa* that are suggestive of extremely warm and stratified conditions (PPC ~100%; PCA1 low values; Figure 6b–d). The lower values of *G. bulloides*/*G. ruber* ratio in this interval are also indicative of strongly stratified water column and are in agreement with the stratification factor for both faunas (PCA2 of planktonic foraminifera and PCA3 of pteropod; Figure 6h–j). An increase in temperature and humidity around this time has been documented in all marine and terrestrial pollen records in the eastern Mediterranean region [6,7,14–16,114]. This paleoclimate change coincides with the Holocene summer precession-related insolation maximum in the Northern Hemisphere [115], and the monsoon intensification that resulted in a widespread increase in humidity over the Mediterranean region and concomitant increase of freshwater input to the Mediterranean Sea [116,117]. Pteropod fauna is characterized by the dominance of the warm oligotrophic *H. inflatus*, and the warm epipelagic *B. chierchiae*, *C. acicula*, and *Cavolinia* spp. (Figure 4). Mesopelagic species (*C. pyramidata* and *D. trispinosa*) are decreasing dramatically due to the enhanced stratification of the entire water column. Mesopelagic pteropods are affected by the OMZ alterations, which are climatically controlled [63,112]. In the humid and warmer conditions that persisted during the formation of S1, the subsequent stratification of the water column favored a strong and well developed OMZ that probably led to the reduction of mesopelagic species. The presence of the mesopelagic *H. inflatus* into the sapropel sublayers can be explained by its habitat. More explicitly, this species adopts a variable depth habitat during its growth stages, and it is more susceptible to the low oxygen concentration in the OMZ [63,118,119]. The presence of *L. bulimoides* in the upper part of S1a, with peaks at 8.4 ka BP, 8.1 ka BP, and 7.9 ka BP (~6%) and its absence in the S1b, suggest that during the end of S1a (8.6–7.7 ka BP) the conditions were more arid than during the onset of S1a (9.4–8.6 ka BP) and the interval of S1b (6.9–6.4 ka BP). In these two phases of S1a, $\delta^{13}\text{C}$ present a decreasing trend with an average value of +0.8‰ in the first phase and +0.6‰ in the second (Figure 6f).

The warm and stratified conditions favorable for the sapropel deposition were interrupted between 7.7 ka BP and 6.8 ka BP. This interval (S1i) is marked by the decrease in PPC (from 90% to 60%) and the heavier values of $\delta^{18}\text{O}$ (+0.5‰) and $\delta^{13}\text{C}$ (+0.8‰) as shown in Figure 6a,b,f. The subsequent cooling is also reflected in significant faunal changes, such as the increase in abundance of *G. inflata*, *T. quinqueloba*, *G. bulloides*, and *N. pachyderma* (Figure 3). These species are associated with relatively cold temperatures and increased food supply, suggesting high primary production and stronger mixing of the water column [46,52]. In addition, the pteropod *L. trochiformis*, which is related to the mixed layer of the water column and thrives in upwelling conditions [120–123], presents a peak at the beginning of S1i (Figure 4).

From 6.4 ka BP to the top of the core (~5.0 ka BP), a trend to heavier $\delta^{18}\text{O}$ values (from 0‰ to +1.3‰) and the drop of PPC (~60%) are recorded (Figure 6a,b). In planktonic foraminifera fauna an increase in *G. inflata*, *G. truncatulinoides* and *N. pachyderma* along with the reduction of *G. ruber* f. *rosea*, *G. siphonifera* gr. *O. universa* indicate lower SST, and stronger seafloor oxygenation due to vertical mixing. This latter is also suggested by the increase in the mesopelagic pteropod *D. trispinosa*.

The peak of *L. trochiformis* at 5.7 ka BP (Figure 4) is suggestive of upwelling conditions. At this point, and up to 5.0 ka BP, increased percentages of *G. bulloides* and *G. sacculifer* are indicative of increased productivity. This is also indicated by the high values of E-index, the heavy $\delta^{13}\text{C}$ (up to +1.7‰) and the PCA2 factor of pteropods (Figure 6e–g).

6. Conclusions

The results of the analysis of planktonic foraminifera and pteropods, combined with the results of principal component analysis and oxygen and carbon isotopic signals, describe the key factors controlling the formation of the micropaleontological assemblages, and therefore the paleoenvironmental and paleoclimatic changes during the last ~21 ka BP. Our data suggests that the sea surface temperature, stratification of the water column, seasonality, and productivity are the main controlling factors of the faunal distribution. During the Late Glacial, all the records indicate the occurrence of cold and eutrophicated waters. The time interval of 15.9–11.7 ka BP, corresponding to the deglaciation phase, was characterized by gradual climatic amelioration. During this interval, the warm interstadial Bølling–Allerød was identified, while low SST records at 12.9 ka BP revealed the onset of the YD. During this event, mild climate conditions were observed for around 400 years, and are attributed to the displacement of the polar front by a few degrees north. With the onset of the Holocene, a general climatic amelioration can be observed, with the gradual development of stratified oligotrophic surface waters. These conditions were intensified during the sapropel S1 deposition, which appears in two layers (S1a and S1b). The faunal and isotopic data suggest that conditions were more arid towards the end of S1a than at the onset of the S1a and the S1b. The interruption of sapropel deposition (S1i) and the post-sapropel interval are characterized by lower SST and stronger seafloor oxygenation due to vertical mixing.

Supplementary Materials: The following are available online at <http://www.mdpi.com/2077-1312/8/9/709/s1>, Figure S1: Planktonic foraminiferal PCA biplot of environmental factors of Temperature (Component 1) and Stratification (Component 2), Figure S2: Planktonic foraminiferal PCA biplot of environmental factors of Temperature (Component 1) and Seasonality (Component 3), Figure S3: Pteropods PCA biplot of environmental factors of Temperature (Component 1) and Productivity (Component 2), Figure S4: Pteropods PCA biplot of environmental factors of Temperature (Component 1) and Stratification (Component 3), Table S1: PCA scores based on planktonic foraminifera raw data, Table S2: PCA scores based on pteropods raw data.

Author Contributions: Conceptualization, C.G., G.K.; methodology, C.G., G.K., A.A.; software, C.G., G.K.; validation, C.G., G.K., A.A.; formal analysis, C.G., G.K., A.A.; investigation, C.G., G.K., C.I., A.A.; resources, C.G., C.I.; data curation, C.G., G.K.; writing—original draft preparation, C.G., G.K.; writing—review and editing, C.G., G.K., E.K., A.A.; visualization, C.G., G.K.; supervision, E.K., A.A.; project administration C.G., A.A.; funding acquisition, E.K., C.I. All authors have read and agreed to the published version of the manuscript.

Funding: This research was funded by EU/ESPA (NSRF; 2007–2013), YPOTHER project (351008) realized at the Institute of Geology and Mineral Exploration recent H.S.G.M.E. E.K. was funded by EU/ESPA (EPAnEK; 2014–2020), INNOVEXPO project (T1EDK-02363). The APC was funded by the Special Account for Research Grants, National and Kapodistrian University of Athens (Grant No. 16599).

Acknowledgments: We wish to thank the captain and crew of R/V Aegaeo (HCMR) for their technical assistance during the YPOTHER cruises, and N. Xirocostas and K. Vallianatou (H.S.G.M.E.) for the organic carbon analysis. We also thank M. Dagla for the English proofreading of the manuscript. Constructive comments by three anonymous reviewers have been essential in improving this manuscript and Victoria Li (Assistant Editor) is thanked for her editorial handling.

Conflicts of Interest: The authors declare no conflict of interest.

References

1. Zervakis, G.I.; Moncalvo, J.-M.; Vilgalys, R. Molecular phylogeny, biogeography and speciation of the mushroom species *Pleurotus cystidiosus* and allied taxa. *Microbiology* **2004**, *150*, 715–726. [[CrossRef](#)]
2. Giorgi, F.; Lionello, P. Climate change projections for the Mediterranean region. *Glob. Planet. Chang.* **2008**, *63*, 90–104. [[CrossRef](#)]
3. Rohling, E.J.; Grant, K.; Bolshaw, M.; Roberts, A.; Siddall, M.; Hemleben, C.; Kucera, M. Antarctic temperature and global sea level closely coupled over the past five glacial cycles. *Nat. Geosci.* **2009**. [[CrossRef](#)]

4. Aksu, A.E.; Yaşar, D.; Mudie, P.J. Paleoclimatic and paleoceanographic conditions leading to development of sapropel layer S1 in the Aegean Sea. *Palaeogeogr. Palaeoclim. Palaeoecol.* **1995**, *116*, 71–101. [[CrossRef](#)]
5. Roussakis, G.; Karageorgis, A.P.; Conispoliatis, N.; Lykousis, V. Last glacial–Holocene sediment sequences in N. Aegean basins: Structure, accumulation rates and clay mineral distribution. *Geo-Mar. Lett.* **2004**, *24*, 97–111. [[CrossRef](#)]
6. Geraga, M.; Ioakim, C.; Lykousis, V.; Tsaila-Monopolis, S.; Mylona, G. The high-resolution palaeoclimatic and palaeoceanographic history of the last 24,000 years in the central Aegean Sea, Greece. *Palaeogeogr. Palaeoclim. Palaeoecol.* **2010**, *287*, 101–115. [[CrossRef](#)]
7. Kontakiotis, G. Late Quaternary paleoenvironmental reconstruction and paleoclimatic implications of the Aegean Sea (eastern Mediterranean) based on paleoceanographic indexes and stable isotopes. *Quat. Int.* **2016**, *401*, 28–42. [[CrossRef](#)]
8. Lykousis, V.; Chronis, G.; Tselepidis, A.; Price, N.B.; Theocharis, A.; Siokou-Frangou, I.; Van Wambeke, F.; Danovaro, R.; Stavrakakis, S.; Duineveld, G.; et al. Major outputs of the recent multidisciplinary biogeochemical researches undertaken in the Aegean Sea. *J. Mar. Syst.* **2002**, *33–34*, 313–334. [[CrossRef](#)]
9. Poulos, S.E. The Mediterranean and Black Sea Marine System: An overview of its physico-geographic and oceanographic characteristics. *Earth Sci. Rev.* **2020**, *200*, 103004. [[CrossRef](#)]
10. Kontakiotis, G. Palaeoceanographic and Palaeoclimatic Study of Eastern Mediterranean During Late Quaternary, Based on Planktonic Foraminiferal Assemblages (in Greek, with English extended abstract). Ph.D. Thesis, National and Kapodistrian University of Athens, Athens, Greece, 2012.
11. Poulos, S.E.; Drakopoulos, P.G.; Collins, M.B. Seasonal variability in sea surface oceanographic conditions in the Aegean Sea (Eastern Mediterranean): An overview. *J. Mar. Syst.* **1997**, *13*, 225–244. [[CrossRef](#)]
12. Geraga, M.; Tsaila-Monopolis, S.; Ioakim, C.; Papatheodorou, G.; Ferentinos, G. Short-term climate changes in the southern Aegean Sea over the last 48,000 years. *Palaeogeogr. Palaeoclim. Palaeoecol.* **2005**, *220*, 311–332. [[CrossRef](#)]
13. Kuhnt, T.; Schmiedl, G.; Ehrmann, W.; Hamann, Y.; Hemleben, C. Deep-sea ecosystem variability of the Aegean Sea during the past 22 kyr as revealed by Benthic Foraminifera. *Mar. Micropaleontol.* **2007**, *64*, 141–162. [[CrossRef](#)]
14. Kotthoff, U.; Müller, U.C.; Pross, J.; Schmiedl, G.; Lawson, I.T.; van de Schootbrugge, B.; Schulz, H. Lateglacial and Holocene vegetation dynamics in the Aegean region: An integrated view based on pollen data from marine and terrestrial archives. *Holocene* **2008**, *18*, 1019–1032. [[CrossRef](#)]
15. Giamali, C.; Koskeridou, E.; Antonarakou, A.; Ioakim, C.; Kontakiotis, G.; Karageorgis, A.P.; Roussakis, G.; Karakitsios, V. Multiproxy ecosystem response of abrupt Holocene climatic changes in the northeastern Mediterranean sedimentary archive and hydrologic regime. *Quat. Res.* **2019**, *92*, 665–685. [[CrossRef](#)]
16. Triantaphyllou, M.V.; Ziveri, P.; Gogou, A.; Marino, G.; Lykousis, V.; Bouloubassi, I.; Emeis, K.-C.; Kouli, K.; Dimiza, M.; Rosell-Melé, A.; et al. Late Glacial–Holocene climate variability at the south-eastern margin of the Aegean Sea. *Mar. Geol.* **2009**, *266*, 182–197. [[CrossRef](#)]
17. Triantaphyllou, M.V.; Antonarakou, A.; Kouli, K.; Dimiza, M.; Kontakiotis, G.; Papanikolaou, M.D.; Ziveri, P.; Mortyn, P.G.; Lianou, V.; Lykousis, V.; et al. Late Glacial–Holocene ecostratigraphy of the south-eastern Aegean Sea, based on plankton and pollen assemblages. *Geo Mar. Lett.* **2009**, *29*, 249–267. [[CrossRef](#)]
18. Drinia, H.; Antonarakou, A.; Tsourou, T.; Kontakiotis, G.; Psychogiou, M.; Anastasakis, G. Foraminifera eco-biostratigraphy of the southern Evoikos outer shelf, central Aegean Sea, during MIS 5 to present. *Cont. Shelf Res.* **2016**, *126*. [[CrossRef](#)]
19. Koutrouli, A.; Anastasakis, G.; Kontakiotis, G.; Ballengee, S.; Kuehn, S.; Pe-Piper, G.; Piper, D.J.W. The early to mid-Holocene marine tephrostratigraphic record in the Nisyros-Yali-Kos volcanic center, SE Aegean Sea. *J. Volcanol. Geotherm. Res.* **2018**, *366*, 96–111. [[CrossRef](#)]
20. Antonarakou, A.; Kontakiotis, G.; Zarkogiannis, S.; Mortyn, P.G.; Drinia, H.; Koskeridou, E.; Anastasakis, G. Planktonic foraminiferal abnormalities in coastal and open marine eastern Mediterranean environments: A natural stress monitoring approach in recent and early Holocene marine systems. *J. Mar. Syst.* **2018**, *181*, 63–78. [[CrossRef](#)]
21. Louvari, M.A.; Drinia, H.; Kontakiotis, G.; Di Bella, L.; Antonarakou, A.; Anastasakis, G. Impact of latest-glacial to Holocene sea-level oscillations on central Aegean shelf ecosystems: A benthic foraminiferal palaeoenvironmental assessment of South Evoikos Gulf, Greece. *J. Mar. Syst.* **2019**, *199*, 103181. [[CrossRef](#)]

22. Kontakiotis, G.; Mortyn, P.G.; Antonarakou, A.; Martínez-Botí, M.A.; Triantaphyllou, M.V. Field-based validation of a diagenetic effect on *G. ruber* Mg/Ca paleothermometry: Core top results from the Aegean Sea (eastern Mediterranean). *Geochem. Geophys. Geosyst.* **2011**, *12*. [[CrossRef](#)]
23. Kontakiotis, G.; Karakitsios, V.; Mortyn, P.G.; Antonarakou, A.; Drinia, H.; Anastasakis, G.; Agiadi, K.; Kafousia, N.; De Rafelis, M. New insights into the early Pliocene hydrographic dynamics and their relationship to the climatic evolution of the Mediterranean Sea. *Palaeogeogr. Palaeoclim. Palaeoecol.* **2016**, *459*, 348–364. [[CrossRef](#)]
24. Antonarakou, A.; Kontakiotis, G.; Mortyn, P.G.; Drinia, H.; Sprovieri, M.; Besiou, E.; Tripsanas, E. Biotic and geochemical ($\delta^{18}\text{O}$, $\delta^{13}\text{C}$, Mg/Ca, Ba/Ca) responses of *Globigerinoides ruber* morphotypes to upper water column variations during the last deglaciation, Gulf of Mexico. *Geochim. Cosmochim. Acta* **2015**, *170*, 69–93. [[CrossRef](#)]
25. Le Houedec, S.; Mojtahid, M.; Bicchi, E.; de Lange, G.J.; Hennekam, R. Suborbital Hydrological Variability Inferred From Coupled Benthic and Planktic Foraminiferal-Based Proxies in the Southeastern Mediterranean During the Last 19 ka. *Paleoceanogr. Paleoclimatol.* **2020**, *35*, e2019PA003827. [[CrossRef](#)]
26. Cacho, I.; Grimalt, J.O.; Canals, M.; Saffi, L.; Shackleton, N.J.; Schönfeld, J.; Zahn, R. Variability of the western Mediterranean Sea surface temperature during the last 25,000 years and its connection with the Northern Hemisphere climatic changes. *Paleoceanography* **2001**, *16*, 40–52. [[CrossRef](#)]
27. Filippidi, A.; Triantaphyllou, M.; de Lange, G. Eastern-Mediterranean ventilation variability during sapropel S1 formation, evaluated at two sites influenced by deep-water formation from Adriatic and Aegean Seas. *Quat. Sci. Rev.* **2016**, *144*, 95–106. [[CrossRef](#)]
28. Kontakiotis, G.; Besiou, E.; Antonarakou, A.; Zarkogiannis, S.D.; Kostis, A.; Mortyn, P.G.; Moissette, P.; Cornée, J.J.; Schulbert, C.; Drinia, H.; et al. Decoding sea surface and paleoclimate conditions in the eastern Mediterranean over the Tortonian-Messinian Transition. *Palaeogeogr. Palaeoclim. Palaeoecol.* **2019**, *534*, 109312. [[CrossRef](#)]
29. Vasiliev, I.; Karakitsios, V.; Bouloubassi, I.; Agiadi, K.; Kontakiotis, G.; Antonarakou, A.; Triantaphyllou, M.; Gogou, A.; Kafousia, N.; de Rafélis, M.; et al. Large Sea Surface Temperature, Salinity, and Productivity-Preservation Changes Preceding the Onset of the Messinian Salinity Crisis in the Eastern Mediterranean Sea. *Paleoceanogr. Paleoclimatol.* **2019**, *34*, 182–202. [[CrossRef](#)]
30. Kontakiotis, G.; Mortyn, G.P.; Antonarakou, A.; Drinia, H. Assessing the reliability of foraminiferal Mg/Ca thermometry by comparing field-samples and culture experiments: A review. *Geol. Q.* **2016**, *60*, 547–560. [[CrossRef](#)]
31. Kontakiotis, G.; Karakitsios, V.; Cornée, J.-J.; Moissette, P.; Zarkogiannis, S.D.; Pasadakis, N.; Koskeridou, E.; Manoutsoglou, E.; Drinia, H.; Antonarakou, A. Preliminary results based on geochemical sedimentary constraints on the hydrocarbon potential and depositional environment of a Messinian sub-salt mixed siliciclastic-carbonate succession onshore Crete (Plouti section, eastern Mediterranean). *Mediterr. Geosci. Rev.* **2020**. [[CrossRef](#)]
32. Kontakiotis, G.; Antonarakou, A.; Mortyn, P.G.; Drinia, H.; Anastasakis, G.; Zarkogiannis, S.; Möbius, J. Morphological recognition of *Globigerinoides ruber* morphotypes and their susceptibility to diagenetic alteration in the eastern Mediterranean Sea. *J. Mar. Syst.* **2017**, *174*, 12–24. [[CrossRef](#)]
33. Wall-Palmer, D.; Smart, C.W.; Hart, M.B.; Leng, M.J.; Borghini, M.; Manini, E.; Aliani, S.; Conversi, A. Late Pleistocene pteropods, heteropods and planktonic foraminifera from the Caribbean Sea, Mediterranean Sea and Indian Ocean. *Micropaleontology* **2014**, *60*, 557–578.
34. Buccheri, G.; Capretto, G.; Di Donato, V.; Esposito, P.; Ferruzza, G.; Pescatore, T.; Russo Ermolli, E.; Senatore, M.R.; Sprovieri, M.; Bertoldo, M.; et al. A high resolution record of the last deglaciation in the southern Tyrrhenian Sea: Environmental and climatic evolution. *Mar. Geol.* **2002**, *186*, 447–470. [[CrossRef](#)]
35. Kontakiotis, G.; Antonarakou, A.; Zachariasse, W.J. Late Quaternary palaeoenvironmental changes in the Aegean Sea: Interrelations and interactions between north and south Aegean Sea. *Bull. Geol. Soc. Greece* **2013**, *47*, 167–177. [[CrossRef](#)]
36. Zarkogiannis, S.; Kontakiotis, G.; Antonarakou, A. Recent planktonic foraminifera population and size response to Eastern Mediterranean hydrography. *Rev. Micropaleontol.* **2020**, *69*, 100450. [[CrossRef](#)]
37. Casford, J.S.L.; Abu-Zied, R.; Rohling, E.J.; Cooke, S.; Fontanier, C.; Leng, M.; Millard, A.; Thomson, J. A stratigraphically controlled multiproxy chronostratigraphy for the eastern Mediterranean. *Paleoceanography* **2007**, *22*. [[CrossRef](#)]

38. Comeau, S.; Jeffree, R.; Teyssié, J.-L.; Gattuso, J.-P. Response of the Arctic Pteropod *Limacina helicina* to Projected Future Environmental Conditions. *PLoS ONE* **2010**, *5*, e11362. [[CrossRef](#)]
39. Lirer, F.; Sprovieri, M.; Vallefucio, M.; Ferraro, L.; Pelosi, N.; Giordano, L.; Capotondi, L. Planktonic foraminifera as bio-indicators for monitoring the climatic changes that have occurred over the past 2000 years in the southeastern Tyrrhenian Sea. *Integr. Zool.* **2014**, *9*, 542–554. [[CrossRef](#)]
40. Margaritelli, G.; Cisneros, M.; Cacho, I.; Capotondi, L.; Vallefucio, M.; Rettori, R.; Lirer, F. Climatic variability over the last 3000 years in the Central—Western Mediterranean Sea (Menorca Basin) detected by planktonic foraminifera and stable isotope records. *Glob. Planet. Chang.* **2018**, *169*, 179–187. [[CrossRef](#)]
41. Margaritelli, G.; Cacho, I.; Català, A.; Barra, M.; Bellucci, L.G.; Lubritto, C.; Rettori, R.; Lirer, F. Persistent warm Mediterranean surface waters during the Roman period. *Sci. Rep.* **2020**, *10*, 10431. [[CrossRef](#)]
42. Tsiolkakis, E.; Tsaila-Monopoli, S.; Kontakiotis, G.; Antonarakou, A.; Sprovieri, M.; Geraga, M.; Ferentinos, G.; Zissimos, A. Integrated paleohydrology reconstruction and Pliocene climate variability in Cyprus Island (eastern Mediterranean). *IOP Conf. Ser. Earth Environ. Sci.* **2019**, *362*, 012103. [[CrossRef](#)]
43. Zarkogiannis, S.; Kontakiotis, G.; Antonarakou, A.; Mortyn, P.; Drinia, H. Latitudinal Variation of Planktonic Foraminifera Shell Masses During Termination I. *IOP Conf. Ser. Earth Environ. Sci.* **2019**, *221*, 012052. [[CrossRef](#)]
44. Checa, H.; Margaritelli, G.; Pena, L.D.; Frigola, J.; Cacho, I.; Rettori, R.; Lirer, F. High resolution paleo-environmental changes during the Sapropel 1 in the North Ionian Sea, central Mediterranean. *Holocene* **2020**. [[CrossRef](#)]
45. Antonarakou, A.; Kontakiotis, G.; Karageorgis, A.P.; Besiou, E.; Zarkogiannis, S.; Drinia, H.; Mortyn, G.P.; Tripsanas, E. Eco-biostratigraphic advances on late Quaternary geochronology and palaeoclimate: The marginal Gulf of Mexico analogue. *Geol. Q.* **2019**, *63*. [[CrossRef](#)]
46. Pujol, C.; Grazzini, C. Distribution patterns of live planktic foraminifers as related to regional hydrology and productive systems of the Mediterranean Sea. *Mar. Micropaleontol.* **1995**, *25*, 187–217. [[CrossRef](#)]
47. Zarkogiannis, S.D.; Antonarakou, A.; Tripathi, A.; Kontakiotis, G.; Mortyn, P.G.; Drinia, H.; Greaves, M. Influence of surface ocean density on planktonic foraminifera calcification. *Sci. Rep.* **2019**, *9*, 533. [[CrossRef](#)]
48. Bazzicalupo, P.; Maiorano, P.; Giron, A.; Marino, M.; Combourieu-Nebout, N.; Pelosi, N.; Salueiro, E.; Incarbona, A. Holocene climate variability of the Western Mediterranean: Surface water dynamics inferred from calcareous plankton assemblages. *Holocene* **2020**, *30*, 691–708. [[CrossRef](#)]
49. Koskeridou, E.; Giamali, C.; Antonarakou, A.; Kontakiotis, G.; Karakitsios, V. Early Pliocene gastropod assemblages from the eastern Mediterranean (SW Peloponnese, Greece) and their palaeobiogeographic implications. *Geobios* **2017**, *50*, 267–277. [[CrossRef](#)]
50. Moissette, P.; Cornée, J.-J.; Antonarakou, A.; Kontakiotis, G.; Drinia, H.; Koskeridou, E.; Tsourou, T.; Agiadi, K.; Karakitsios, V. Palaeoenvironmental changes at the Tortonian/Messinian boundary: A deep-sea sedimentary record of the eastern Mediterranean Sea. *Palaeogeogr. Palaeoclim. Palaeoecol.* **2018**, *505*, 217–233. [[CrossRef](#)]
51. Karakitsios, V.; Roveri, M.; Lugli, S.; Manzi, V.; Gennari, R.; Antonarakou, A.; Triantaphyllou, M.; Agiadi, K.; Kontakiotis, G.; Kafousia, N.; et al. A record of the Messinian salinity crisis in the eastern Ionian tectonically active domain (Greece, eastern Mediterranean). *Basin Res.* **2017**, *29*, 203–233. [[CrossRef](#)]
52. Casford, J.S.L.; Rohling, E.J.; Abu-Zied, R.; Cooke, S.; Fontanier, C.; Leng, M.; Lykousis, V. Circulation changes and nutrient concentrations in the late Quaternary Aegean Sea: A nonsteady state concept for sapropel formation. *Paleoceanography* **2002**, *17*, 14–1–14–11. [[CrossRef](#)]
53. Casford, J.S.L.; Rohling, E.J.; Abu-Zied, R.H.; Fontanier, C.; Jorissen, F.J.; Leng, M.J.; Schmiedl, G.; Thomson, J. A dynamic concept for eastern Mediterranean circulation and oxygenation during sapropel formation. *Palaeogeogr. Palaeoclim. Palaeoecol.* **2003**, *190*, 103–119. [[CrossRef](#)]
54. Aksu, A.E.; Hiscott, R.; Isler, E. Late Quaternary chronostratigraphy of the Aegean Sea sediments: Special reference to the ages of sapropels S1–S5. *Turk. J. Earth Sci.* **2016**, *25*, 1–18. [[CrossRef](#)]
55. Howes, E.L.; Eagle, R.A.; Gattuso, J.-P.; Bijma, J. Comparison of Mediterranean Pteropod Shell Biometrics and Ultrastructure from Historical (1910 and 1921) and Present Day (2012) Samples Provides Baseline for Monitoring Effects of Global Change. *PLoS ONE* **2017**, *12*, e0167891. [[CrossRef](#)] [[PubMed](#)]
56. Lalli, C.M.; Gilmer, R.W. *Pelagic Snails: The Biology of Holoplanktonic Gastropod Mollusks*; Stanford University Press: Stanford, CA, USA, 1989.
57. Hunt, B.; Pakhomov, E.; Hosie, G.W.; Siegel, V.; Ward, P.; Bernard, K. Pteropods in Southern Ocean ecosystems. *Prog. Oceanogr.* **2008**, *78*, 193–221. [[CrossRef](#)]

58. Lochte, K.; Pfannkuche, O. Processes driven by the small sized organisms at the water-sediment interface. In *Ocean Margin Systems*; Wefer, G., Billet, D., Hebbeln, D., Jørgensen, B.B., Schluter, M., Weering, T.C., Eds.; Springer: Berlin/Heidelberg, Germany, 2003.
59. Vinogradov, M. Food sources for the deep water fauna. Speed of decomposition of dead Pteropoda. *Dokl. Akad. Nauk SSSR* **1961**, *138*, 1439–1442.
60. Herman, Y. Vertical and horizontal distribution of pteropods in Quaternary sequences. In *The Micropalaeontology of Oceans*; Funnell, B.M., Reidel, W.R., Eds.; Cambridge University Press: Cambridge, UK, 1971; pp. 463–486.
61. Buccheri, G. Pteropods as climatic indicators in Quaternary sequences: A Lower-Middle Pleistocene sequence outcropping in Cava Puleo (Ficarazzi, Palermo, Sicilia). *Palaeogeogr. Palaeoclim. Palaeoecol.* **1984**, *45*, 75–86. [[CrossRef](#)]
62. Almogi-Labin, A.; Hemleben, C.; Meischner, D.; Erlenkeuser, H. Paleoenvironmental events during the last 13,000 years in the central Red Sea as recorded by pteropoda. *Paleoceanography* **1991**, *6*, 83–98. [[CrossRef](#)]
63. Almogi-Labin, A.; Hemleben, C.; Meischner, D. Carbonate preservation and climatic changes in the central Red Sea during the last 380 kyr as recorded by pteropods. *Mar. Micropaleontol.* **1998**, *33*, 87–107. [[CrossRef](#)]
64. Almogi-Labin, A.; Bar-Matthews, M.; Shriki, D.; Kolosovsky, E.; Paterne, M.; Schilman, B.; Ayalon, A.; Aizenshtat, Z.; Matthews, A. Climatic variability during the last ~90 ka of the southern and northern Levantine Basin as evident from marine records and speleothems. *Quat. Sci. Rev.* **2009**, *28*, 2882–2896. [[CrossRef](#)]
65. Singh, A.D.; Nisha, N.R.; Joydas, T.V. Distribution patterns of Recent pteropods in surface sediments of the western continental shelf of India. *J. Micropalaeontol.* **2005**, *24*, 39. [[CrossRef](#)]
66. Almogi-Labin, A.; Edelman-Furstenberg, Y.; Hemleben, C. Variations in the biodiversity of thecosomatous pteropods during the Late Quaternary as a response to environmental changes in the Gulf of Aden—Red Sea—Gulf of Aqaba ecosystem. In *Aqaba—Eliat, the Improbable Gulf—Environment, Biodiversity and Preservation*; Por, F.D., Ed.; The Hebrew University Magnes Press: Jerusalem, Israel, 2008; pp. 31–48.
67. Johnson, R.; Manno, C.; Ziveri, P. Spring distribution of shelled pteropods across the Mediterranean Sea. *Biogeosci. Discuss.* **2020**, 1–23. [[CrossRef](#)]
68. Howes, E.L.; Stemann, L.; Assailly, C.; Irisson, J.O.; Dima, M.; Bijma, J.; Gattuso, J.P. Pteropod time series from the North Western Mediterranean (1967–2003): Impacts of pH and climate variability. *Mar. Ecol. Prog. Ser.* **2015**, *531*, 193–206. [[CrossRef](#)]
69. Lykousis, V. Subaqueous bedforms on the Cyclades Plateau (NE Mediterranean)—Evidence of Cretan Deep Water Formation? *Cont. Shelf Res.* **2001**, *21*, 495–507. [[CrossRef](#)]
70. Karageorgis, A.P.; Ioakim, C.; Rousakis, G.; Sakellariou, D.; Vougioukalakis, G.; Panagiotopoulos, I.P.; Zimianitis, E.; Koutsopoulou, E.; Kanellopoulos, T.; Papatrechas, C. Geomorphology, sedimentology and geochemistry in the marine area between Sifnos and Kimolos Islands, Greece. *Bull. Geol. Soc. Greece* **2016**, *50*, 334–344. [[CrossRef](#)]
71. Piper, D.; Perissoratis, C. Quaternary neotectonics of the South Aegean arc. *Mar. Geol.* **2003**, *198*, 259–288. [[CrossRef](#)]
72. Antonarakou, A.; Kontakiotis, G.; Vasilatos, C.; Besiou, E.; Zarkogiannis, S.; Drinia, H.; Mortyn, P.; Tsaparas, N.; Makri, P.; Karakitsios, V. Evaluating the Effect of Marine Diagenesis on Late Miocene Pre-Evaporitic Sedimentary Successions of Eastern Mediterranean Sea. *IOP Conf. Ser. Earth Environ. Sci.* **2019**, *221*, 012051. [[CrossRef](#)]
73. Hemleben, C.; Spindler, M.; Anderson, O. *Modern Planktic Foraminifera*; Springer-Verlag: New York, NY, USA, 1989; Volume 22.
74. Rohling, E.J.; Jorissen, F.; Grazzini, C.V.; Zachariasse, W.J. Northern Levantine and Adriatic Quaternary planktic foraminifera; Reconstruction of paleoenvironmental gradients. *Mar. Micropaleontol.* **1993**, *21*, 191–218. [[CrossRef](#)]
75. Aurahs, R.; Grimm, G.; Hemleben, V.; Hemleben, C.; Kucera, M. Geographical distribution of cryptic genetic types in the planktonic foraminifer *Globigerinoides ruber*. *Mol. Ecol.* **2009**, *18*, 1692–1706. [[CrossRef](#)]
76. Walkley, A.; Black, I.A. An examination of the Degtjareff Method for determining soil organic matter, and a proposed modification of the chromic acid titration method. *Soil Sci.* **1934**, *37*, 29–38. [[CrossRef](#)]
77. Angelova, V.; Akova, V.; Ivanov, K.; Licheva, P.A. Comparative study of titrimetric methods for determination of organic carbon in soils, compost and sludge. *J. Int. Sci. Publ. Ecol. Saf.* **2014**, *8*, 430–440. [[CrossRef](#)]

78. Wang, B.; Wu, R.; Fu, X. Pacific–East Asian Teleconnection: How Does ENSO Affect East Asian Climate? *J. Clim.* **2000**, *13*, 1517–1536. [[CrossRef](#)]
79. Löwemark, L.; Hong, W.-L.; Yui, T.-F.; Hugn, G.-W. A test of different factors influencing the isotopic signal of planktonic foraminifera in surface sediments from the northern South China Sea. *Mar. Micropaleontol.* **2005**, *55*, 49–62. [[CrossRef](#)]
80. Spero, H.J.; Mielke, K.M.; Kalve, E.M.; Lea, D.W.; Pak, D.K. Multispecies approach to reconstructing eastern equatorial Pacific thermocline hydrography during the past 360 kyr. *Paleoceanography* **2003**, *18*. [[CrossRef](#)]
81. Stuiver, M.; Reimer, P.J. Extended ^{14}C data base and revised CALIB 3.0 ^{14}C age calibration program. *Radiocarbon* **1993**, *35*, 215–320. [[CrossRef](#)]
82. Facorellis, Y.; Maniatis, Y. Apparent ^{14}C ages of marine mollusk shells from a Greek Island: Calculation of the marine reservoir effect in the Aegean Sea. *Radiocarbon* **1998**, *40*, 963–973. [[CrossRef](#)]
83. Reimer, P.; Bard, E.; Bayliss, A.; Beck, J.; Blackwell, P.; Ramsey, C.; Buck, C.; Cheng, H.; Edwards, R.; Friedrich, M.; et al. IntCal13 and MARINE13 radiocarbon age calibration curves 0–50,000 years cal BP. *Radiocarbon* **2013**, *55*, 1869–1887. [[CrossRef](#)]
84. Jorissen, F.J.; Asioli, A.; Borsetti, A.M.; Capotondi, L.; de Visser, J.P.; Hilgen, F.J.; Rohling, E.J.; van der Borg, K.; Vergnaud Grazzini, C.; Zachariasse, W.J. Late Quaternary central Mediterranean biochronology. *Mar. Micropaleontol.* **1993**, *21*, 169–189. [[CrossRef](#)]
85. Hammer, Ø.; Harper, D.A.T.; Ryan, P.D. PAST: Paleontological Statistics software package for education and data analysis. *Palaeontol. Electron.* **2001**, *4*, 9. Available online: http://palaeo-electronica.org/2001_1/past/issue1_01.htm (accessed on 21 June 2001).
86. Sbaffi, L.; Wezel, F.C.; Curzi, G.; Zoppi, U. Millennial- to centennial-scale palaeoclimatic variations during Termination I and the Holocene in the central Mediterranean Sea. *Global Planet. Change* **2004**, *40*, 201. [[CrossRef](#)]
87. Anastasakis, G.C.; Stanley, D.J. Sapropels and organic-rich variants in the Mediterranean: Sequence development and classification. *Geol. Soc. Spec. Publ.* **1984**, *15*, 497. [[CrossRef](#)]
88. Mercone, D.; Thomson, J.; Croudace, I.W.; Siani, G.; Paterne, M.; Troelstra, S. Duration of S1, the most recent sapropel in the eastern Mediterranean Sea, as indicated by accelerator mass spectrometry radiocarbon and geochemical evidence. *Paleoceanography* **2000**, *15*, 336–347. [[CrossRef](#)]
89. Zachariasse, W.; Jorissen, F.; Perissoratis, C.; Rohling, E.; Tsapralis, V. Late Quaternary foraminiferal changes and the nature of sapropel S1 in Skopelos Basin. In Proceedings of the 5th Hellenic Symposium of Oceanography and Fisheries, Kavala, Greece, 15–18 April 1997; pp. 391–394.
90. Capotondi, L.; Maria Borsetti, A.; Morigi, C. Foraminiferal ecozones, a high resolution proxy for the late Quaternary biochronology in the central Mediterranean Sea. *Mar. Geol.* **1999**, *153*, 253–274. [[CrossRef](#)]
91. Hayes, A.; Rohling, E.J.; De Rijk, S.; Kroon, D.; Zachariasse, W.J. Mediterranean planktonic foraminiferal faunas during the last glacial cycle. *Mar. Geol.* **1999**, *153*, 239–252. [[CrossRef](#)]
92. Casford, J.; Rohling, E.J.; Abu-Zied, R.; Cooke, S.; Boessenkool, K.P.; Brinkhuis, H.; Vries, C.; Wefer, G.; Geraga, M.; Papatheodorou, G.; et al. Mediterranean climate variability during the Holocene. *Mediterr. Mar. Sci.* **2001**, *2*, 45–55. [[CrossRef](#)]
93. Schneider, A.; Wallace, W.R.D.; Kortzinger, A. Alkalinity of the Mediterranean Sea. *Geophys. Res. Lett.* **2007**, *34*. [[CrossRef](#)]
94. Wilke, I.; Meggers, H.; Bickert, T. Depth habitats and seasonal distributions of recent planktic foraminifers in the Canary Islands region (29 °N) based on oxygen isotopes. *Deep Sea Res. Part I Oceanogr. Res. Pap.* **2009**, *56*, 89. [[CrossRef](#)]
95. Wit, J.C.; Reichert, G.-J.; Jung, S.J.A.; Kroon, D. Approaches to unravel seasonality in sea surface temperatures using paired single-specimen foraminiferal $\delta^{18}\text{O}$ and Mg/Ca analyses. *Paleoceanography* **2010**, *25*. [[CrossRef](#)]
96. Goudeau, M.L.S. Seasonality variations in the Central Mediterranean during climate change events in the Late Holocene. *Palaeogeogr. Palaeoclim. Palaeoecol.* **2015**, *418*, 304–318. [[CrossRef](#)]
97. Kucera, M.; Weinelt, M.; Kiefer, T.; Pflaumann, U.; Hayes, A.; Weinelt, M.; Chen, M.-T.; Mix, A.C.; Barrows, T.T.; Cortijo, E.; et al. Reconstruction of sea-surface temperatures from assemblages of planktonic foraminifera: Multi-technique approach based on geographically constrained calibration data sets and its application to glacial Atlantic and Pacific Oceans. *Quat. Sci. Rev.* **2005**, *24*, 951–998. [[CrossRef](#)]

98. Žarić, S.; Donner, B.; Fischer, G.; Mulitza, S.; Wefer, G. Sensitivity of planktic foraminifera to sea surface temperature and export production as derived from sediment trap data. *Mar. Micropaleontol.* **2005**, *55*, 75–105. [[CrossRef](#)]
99. Fraile, I.; Schulz, M.; Mulitza, S.; Kucera, M. Predicting the global distribution of planktonic foraminifera using a dynamic ecosystem model. *Biogeosciences* **2008**, *5*, 891–911. [[CrossRef](#)]
100. Fraile, I.; Mulitza, S.; Schulz, M. Modeling planktonic foraminiferal seasonality: Implications for sea-surface temperature reconstructions. *Mar. Micropaleontol.* **2009**, *72*, 1–9. [[CrossRef](#)]
101. Sprovieri, R.; Stefano, E.; Incarbona, A.; Gargano, M. A high-resolution record of the last deglaciation in the Sicily Channel based on foraminifera and calcareous nannofossil quantitative distribution. *Palaeogeogr. Palaeoclim. Palaeoecol.* **2003**, *202*, 119–142. [[CrossRef](#)]
102. Di Donato, V.; Esposito, P.; Russo-Ermolli, E.; Scarano, A.; Cheddadi, R. Coupled atmospheric and marine palaeoclimatic reconstruction for the last 35 ka in the Sele Plain—Gulf of Salerno area (southern Italy). *Quat. Int.* **2008**, *190*, 146–157. [[CrossRef](#)]
103. Biekart, W.J. Euthecosomatous pteropods as paleohydrological and paleoecological indicators in a Tyrrhenian deep-sea core. *Palaeogeogr. Palaeoclim. Palaeoecol.* **1989**, *71*, 205–224. [[CrossRef](#)]
104. Kutzbach, J.E.; Guetter, P.J. The Influence of Changing Orbital Parameters and Surface Boundary Conditions on Climate Simulations for the Past 18,000 Years. *J. Atmos. Sci.* **1986**, *43*, 1726–1759. [[CrossRef](#)]
105. Kotthoff, U.; Koutsodendris, A.; Pross, J.; Schmiedl, G.; Bornemann, A.; Kaul, C.; Marino, G.; Peyron, O.; Schiebel, R. Impact of Lateglacial cold events on the northern Aegean region reconstructed from marine and terrestrial proxy data. *J. Quat. Sci.* **2011**, *26*, 86–96. [[CrossRef](#)]
106. Dormoy, I.; Peyron, O.; Combourieu Nebout, N.; Goring, S.; Kotthoff, U.; Magny, M.; Pross, J. Terrestrial climate variability and seasonality changes in the Mediterranean region between 15,000 and 4000 years BP deduced from marine pollen records. *Clim. Past* **2009**, *5*, 615–632. [[CrossRef](#)]
107. Björck, S.; Walker, M.; Cwynar, L.; Johnsen, S.; Knudsen, K.; Lowe, J.; Wohlfarth, B. An event stratigraphy for the Last Termination in the North Atlantic region based on the Greenland ice-core record: A proposal by the INTIMATE group. *J. Quat. Sci.* **1998**, *13*, 283–292. [[CrossRef](#)]
108. Rasmussen, S.O.; Vinther, B.M.; Clausen, H.B.; Andersen, K.K. Early Holocene climate oscillations recorded in three Greenland ice cores. *Quat. Sci. Rev.* **2007**, *26*, 1907–1914. [[CrossRef](#)]
109. Peyron, O.; Bégeot, C.; Brewer, S.; Heiri, O.; Magny, M.; Millet, L.; Ruffaldi, P.; Campo, E.; Yu, G. Lateglacial climate in the Jura mountains (France) based on different quantitative reconstruction approaches from pollen, lake-levels, and chironomids. *Quat. Res.* **2005**, *64*, 197–211. [[CrossRef](#)]
110. Bordon, A.; Peyron, O.; Lezine, A.-M.; Brewer, S.; Fouache, E. Pollen-inferred Late-Glacial and Holocene climate in southern Balkans (Lake Maliq). *Quat. Int.* **2009**, *200*, 19–30. [[CrossRef](#)]
111. Larocque, I.; Finsinger, W. Late-glacial chironomid-based temperature reconstructions for Lago Piccolo di Avigliana in the southwestern Alps (Italy). *Palaeogeogr. Palaeoclim. Palaeoecol.* **2008**, *257*, 207–223. [[CrossRef](#)]
112. Sijinkumar, A.V.; Bejugam, N.; Guptha, M.V.S. Late Quaternary record of pteropod preservation from the Andaman Sea. *Mar. Geol.* **2010**, *275*. [[CrossRef](#)]
113. Rottman, M.L. Net tow and surface sediment distributions of pteropods in the South China Sea region: Comparison and oceanographic implications. *Mar. Micropaleontol.* **1980**, *5*, 71–110. [[CrossRef](#)]
114. Rossignol-Strick, M. Sea-land correlation of pollen records in the Eastern Mediterranean for the glacial-interglacial transition: Biostratigraphy versus radiometric time-scale. *Quat. Sci. Rev.* **1995**, *14*, 893. [[CrossRef](#)]
115. Laskar, J.; Robutel, P.; Joutel, F.; Gastineau, M.; Correia, A.C.M.; Levrard, B. A long-term numerical solution for the insolation quantities of the Earth. *A&A* **2004**, *428*, 261–285.
116. Rossignol-Strick, M. African monsoons, an immediate climate response to orbital insolation. *Nature* **1983**, *304*, 46–49. [[CrossRef](#)]
117. Rohling, E.J. Glacial conditions in the Red Sea. *Paleoceanography* **1994**, *9*, 653–660. [[CrossRef](#)]
118. Weikert, H.G.; Cederbaum, L.S. Particle-number-dependent theory of few-and many-body systems. *Few Body Syst.* **1987**, *2*, 33–51. [[CrossRef](#)]
119. Weikert, H. The vertical distribution of zooplankton in relation to habitat zones in the area of the Atlantis II Deep, central Red Sea. *Mar. Ecol. Prog. Ser.* **1982**, *8*, 129–143. [[CrossRef](#)]
120. Wormuth, J. Vertical distributions and diel migrations of Euthecosomata in the northwest Sargasso Sea. *Deep Sea Res. Part I Oceanogr. Res. Pap.* **1981**, *28*, 1493–1515. [[CrossRef](#)]

121. Bé, A.W.H.; Gilmer, R.W. A zoogeographic and taxonomic review of euthecosomatous Pteropoda. *Ocean. Micropaleontol.* **1977**, *1*, 733–808.
122. Sakthivel, M. A preliminary report on the distribution and relative abundance of Euthecosomata with a note on the seasonal variation of Limacina species in the Indian Ocean. *Bull. Nat. Inst. Sci. India* **1969**, *38*, 700–717.
123. Almogi-Labin, A.; Hemleben, C.; Deuser, W.G. Seasonal variation in the flux of euthecosomatous pteropods collected in a deep sediment trap in the Sargasso Sea. *Deep Sea Res. Part I Oceanogr. Res. Pap.* **1988**, *35*, 441–464. [[CrossRef](#)]



© 2020 by the authors. Licensee MDPI, Basel, Switzerland. This article is an open access article distributed under the terms and conditions of the Creative Commons Attribution (CC BY) license (<http://creativecommons.org/licenses/by/4.0/>).